Mixed Functionality Semiconductor Surfaces: Formation, Characterization, Interfacial Dynamics, and Applications

Leslie Esther O'Leary

In partial fulfillment of the requirements
for the degree of
Doctor of Philosophy
in Chemistry

California Institute of Technology
Pasadena, California
2012
(Defended May 9, 2012)

Dedication

This work is dedicated to Dennis O'Leary, whose support and encouragement will motivate and inspire me always.

Acknowledgements

Before I left the University of Minnesota to come to Caltech for graduate school Prof. Marc Hillmyer gave me a bit of advice; he said "Leslie, graduate school will go by faster than you think, and in the end you will only remember the good times, so have fun!" Looking back at my time at Caltech (granted, as I am writing this I have a few more weeks left), this is been overwhelmingly true, and I owe that to the wonderful people with whom I have worked, collaborated, talked science and become friends.

Of course whether or not the above statement can be true depends on the advisor. I cannot thank Nate Lewis enough for his guidance and mentorship. He gave me freedom in day-to-day research and always put bread on the table, but was there with a key suggestion or idea whenever asked. I arrived at Caltech an organic polymer chemist, but with Nate's wisdom, I am leaving a surface and semiconductor electrochemist. Beyond his depth of wisdom, I also have to thank Nate for his support throughout graduate school—sending me to conferences, backing me for the Link fellowship, aiding in my job search, not firing my SURF after she broke his ping-pong table, and helping me grow as a scientist and a person. Thank you Nate.

I was so lucky to have had the best committee Caltech has to offer. Perhaps it would have been improved with the addition of Harry Gray, but being limited in the number of members, I had the best committee. Bob Grubbs' adventurous spirit (inside and outside of lab) is an inspiration to me. I had the fantastic opportunity to learn more materials science through a collaboration with Julia Greer. Beyond a collaborator, Julia was also a source of support through her encouragement, advice and belief in my abilities. I thank Theo for serving as the chair of my committee and for always seeing the start point and the end point and believing in no obstacles.

Bruce Brunschwig, the director of the Molecular Materials Research Center, was our advisor while Nate was away/busy. Bruce was probably the most difficult to schedule on my committee, but his door was always open. His passion for science was contagious. Thank you Bruce!

Collaborations are a great thing in research. I thank Ryan Douglas Brown (UChicago), Clara Cho (Caltech), Yan Li (UC Davis), Gretchen Keller and Astrid Mueller (Caltech), Sergey Malyk (USC), and Brandon Giles and Kevin Ahn (Berkeley) for all those mornings I got into work with amazing results in my email in-box. I have learned so much from each of them about spectroscopy, photophysics, mechanical properties testing, He scattering, STM, computational chemistry, etc. It was really a pleasure to work with each of them.

I have to thank my undergraduate advisors, Marc Hillmyer and Bill Tolman, for preparing me for graduate school.

I overlapped with many people during my time in the Lewis group (forgive me if I missed anyone): Jordan Katz, Brendan Kayes, Todd Gingrich, Olivia Alley, Kimberly Papadantonakis,

Marc Woodka, Kate Plass, Steve Maldonado, Xiuling Li, Jim Maiolo, Tony Fitch, Anna Folinsky, Edgardo Garcia-Berrios, Jordan Theriot, Jeanne Peng (Penguin), Marisa Robles, Don Walker, David Knapp, David Gleason-Roher, Heather McCaig, Craig Wiggenhorn, Liz Santori, Emily Warren, James McKone, Joseph Beardslee, Shannon Boettcher, Erik Johansson, Tina Ding, Karla Reyes, Jacob Good, Matt Bierman, Michael Walter, Greg Kimball, Qixi Mi, Mike Rose, Bryce Sadtler, Nick Strandwitz, CX Xiang, Shane Ardo, Rob Coridan, Ron Grimm, Adam Pietrick, Adam Nichols-Nielander, Matt Shaner, Amanda Shing, Chris Roske, SangHee Park, Andrew Meng, Ruben Britto, Shu Hu, Fan Yang, Teddy Huang, Heather Audesirk, Nick Batara, Azhar Carim, Dennis Kim, Noah Plymale, Fadl Saadi, Prineha Narang, Victoria Tan, Marino Di Franco, and Suyeon Pyo. What I enjoyed most about my time with these people was watching the Lewis group change over time. The change driven, of course, by the wonderful individual personalities within the group.

Erik Johansson, Kate Plass, David Gleason-Roher, Judy Lattimer, Mike Rose, David Knapp, Tina Ding, Greg Kimball, Ron Grimm, Adam Nichols-Nielander, Chris Roske, Noah Plymale, Victoria Tan, and Suyeon Pyo have been my cohorts in surface chemistry. Kate introduced me to all of the techniques and got me started in lab. Tony, DK, Cinco, Judy, and Joseph kept the XPS instruments in tip-top shape. Greg Kimball was always excited and ready to talk about science and KRAH-A-TOS. Ron Grimm taught me so much, and his uncanny ability to remember names always put a smile on my face. I am most grateful to Ron for his patience in teaching me to code. Tina Ding was my first undergraduate student. Hi Tina!!! It was a weird and wonderful experience working with her. I miss the way she described her experiments as looking like 'Italy or something'. Tina had a large impact on the work presented here, and she will go far. Suyeon Pyo spent countless hours at the STM and AFM looking at our samples. She is dedicated and hard-working and everything we all hope for in a SURF. Thank you Chris, Noah, and Victoria for taking the surface chemistry torch.

Erik Johansson was my mentor through my 1st and 2nd years as a graduate student. Many of the creative ideas in this work came from our frequent coffee breaks. I loved talking science with Erik, I miss him, and I envy his students at Portland State. I owe him a huge thanks and acknowledgement for all the time he spent with me and all of the knowledge he passed on to me. Thank you Erik.

If I were to do a post-doc, I might choose Galen Stucky from what I have seen in Shannon Boettcher and Nick Strandwitz. Shannon and Nick were always happy to be talking about, thinking about, and doing science. Shannon taught me how to think and write like a scientist early in my career, and Nick was invaluable to my work on ALD later on.

The summer of post-docs happened between my 2nd and 3rd year. Mike Rose, Bryce Sadtler,

Matt Bierman, Nick Strandwitz, CX Xiang, Ron Grimm joined Mike Walter, Qixi Mi, and Karla Reyes were closely followed by Shane Ardo and Rob Coridan. This was an amazing and exciting time in our group. So many new branches of research took off around this time, and we applied for JCAP. For as absent as we all say Nate is, it was during this time I stood back and was taken aback by Nate's impeccable judge of character. Mike Rose was my partner in Heck chemistry. He taught me how to think like an inorganic chemist. Bryce Sadtler created an awesome light-driven material patterning project and filled me in on all of the yoga gossip. Matt Bierman was always positive and had a compassionate shoulder to lean on. I have not been to 6 a.m. kickboxing since he left. I look forward to working with him at Dow! JCAP is lucky to get such a great scientist as CX! Mike Walter taught me about conductive polymers. His enthusiasm and drive for outreach are inspirational. Shane Ardo helped me keep the midnight oil burning. Thanks late-night lab partner! Rob Coridan, a kind and gentle lab-mate, made my last Lewis group retreat one to remember.

James McKone, and Joseph Beardslee made up the 2008 class. James was my partner for SHArK for two years. James is also an amazing electrochemist. He was a role model and demonstration of 'doing everything' — great work, literature, outreach, mentoring, while still having time for his own life. I followed Joseph around offices. I hope I wasn't the one he was moving away from. Joseph is one of the funniest people I have ever met. There was no one else that could've filled Jim Maiolo's desk.

There were older students that left too early, and younger students I've only begun to get to know. Thank you Jim Maiolo, Josh Spurgeon, Marc Woodka, Edgardo Garcia-Berrios, Brendan Kayes, Steve Maldonado, and Kate Plass. Josh who sat next to me for 3 years and taught me the ideal of efficiency while at work. Marc who blew me away with his research. Brendan who was so modest and brilliant. Edgardo who took our group to athletic victory in soft-ball and tug-of-war in the same year. Go Cold Fusion! Steve, who is another example of rigor. Thank you Stag, Squirtle, Cub, and Real Ben. I never want to visit your apartment. Stag, thank you for teaching me about basketball and team spirit, and I expect you to take care of Robin. Shu became my foodie friend, 626! Amanda is full of energy and spunk. Matt Shaner brightened my day whenever he popped over to Noyes. As I am leaving there are a whole new set of amazing people starting: Fan, Noah, Victoria, Azhar, Teddy, Fadl, Nick B., and Heather A..

Of course I owe a great debt of gratitude to Barbara Miralles, Elyse Garlock, Paige Johnson, Nannette Pettis, and Amy Crown. These ladies helped get Nate's messages out to us, but also served to help get my messages through to Nate! They were so helpful in everything from my application for the Link Fellowship to management of grants and purchasing assistance to getting reimbursement and helping with travel. I will remember these ladies fondly, thank you for your

support, friendship, and most of all, all of your hard work!!!

Class of 2007 with Liz and Emily (and Rachel). Choosing a research group is difficult. Some of the group members you meet will be gone the next year, and all will be gone before you. The only thing you can be sure of, is that the people in your class will be there for nearly your entire time in graduate school, I am so happy I was with Liz and Emily. We learned to make electrodes and use a potentiostat together. We chose projects and took classes together. We went through candidacy together. We went on the job market together. I will look back at margaritas after candidacy, weekends spent preparing for BP, swapping resumes and cover letters, complaining about graduate school, worrying about the future, and many other memories in fondness. We will be lifelong friends. We will also take over the world after Emily has saved it, Rachel is a famous Professor, Liz controls federal science policy, and I still ride on their coat tails. Love you!

Of course the support and love from my friends and family outside of research was invaluable. Thank you Mom, my inspiration for loving and living life, for respecting and appreciating others, the rock of my family. Thank you Dad, racer of cars, builder of roller coasters, mover of stones — self-made, self-taught, and inspirational. Thank you Robin Tucker-Drob, my partner in life, for supporting me through the job search, props, graduation, and all the way to Michigan! My niece, Danica, whose picture decorated my computer screens through props and the writing of my thesis. My sisters Colleen and Shannon who are constantly amazing me and are caring, loving, and supportive. Their pictures decorated my desk throughout graduate school. Thank you Dave Klein and Laura O'Leary — 4 parents are greater than two! I will remember Scott Kelber, Mauricio Gonzalez, and Pheobe Delman from Classic Kickboxing forever. Angela Lewis-Dmello and Jen Plum, my best friends since childhood who always have the perfect bit of life advice. Rachel Klet, my best friend through graduate school, and Gretchen Keller the third of our trio. Love you all!

Of course I will only remember the good times of graduate school, every memory I have of graduate school, whether happy or sad, has these people in it to become joyful or bittersweet.

Abstract

The properties of any semiconductor device rely on the charge separation characteristics at interfaces within that device. The charge separation characteristics include relative energetics, interfacial electronic states, and the presence or absence of insulating layers. More importantly, the interfacial properties determine the maximum solar conversion efficiency for a photoelectrochemical or photovoltaic device. Solution-based halogenation/alkylation chemistry was used to functionalize Si surfaces. The chemistry was adapted to allow for the controlled formation of multicomponent molecular monolayers. Functional molecules were incorporated by the mixed monolayer approach, and lowered densities of surface electronic defect states and increased resistance toward the formation of deleterious Si oxides were observed. Heck coupling reactions were developed at thiophene-containing monolayers. Thiophene terminated Si(111) surfaces had defect frequencies of $>$ 1 defect per 1,000 surface atoms, too large for solar energy conversion applications, while multicomponent CH_3/thiophene monolayers had defect densities of $<$ 1 per 500,000 surface atoms. Robust secondary chemistry at Si(111) with facile charge transfer to covalently linked molecules with preservation of surface electronic properties was shown for the first time. Molecular adsorbates with interesting electronic dipoles, such as bromothiophene, were incorporated into mixed monolayers. The electron distribution across the surface dipole caused a shift in the work function of Si by $>$ 600 mV. The fundamental mechanism of W_f shift was elucidated by a combined ab initio and experimental study, and the dependence of Si band-edge positions on pH was relieved using Si-C bonds. Designer surface chemistry was used to covalently link Si microwires within a flexible PDMS matrix, and a direct correlation between the surface bonding mechanism and interfacial adhesion strength was unambiguously observed. The formation and electronic properties of Si/PEDOT junctions were studied, where PEDOT was covalently linked to the Si surface *via* electropolymerization initiation at a mixed molecular monolayer containing 2,2':5',2"-terthien-5"-yl- groups. Low-resistance, ohmic contacts were made at p-Si. Aldehyde groups were also incorporated into mixed monolayers. Facile, low-temperature atomic layer deposition (ALD) of Al_2O_3, MnO_2, and TiO_2 on aldehyde-functionalized Si was achieved. Neither surface oxidation nor surface electronic defects formed during ALD, which has not been shown previously.

Contents

List of Schemes

List of Figures

List of Tables

Chapter 1

Introduction and background of solution phase surface chemistry

The study of solution phase semiconductor surface chemistry, especially at Si surfaces, has enabled a range of device applications to fundamental surface studies. The H-terminated Si surface is the starting point for many Si-based devices.[1–5] In turn, the electronic and chemical properties of the H-terminated surface have been well studied. Halogenation of H-terminated Si surfaces has been studied as a reactive intermediate on the path to further functionalization. Added chemical functionality has increased utility of Si in chemical and biological sensor, molecular electronic, photoelectrochemical, and other optoelectronic device configurations. This thesis details work toward the end goal of functional, low electronic defect density, and air stable surface chemistries to be utilized by various applications. As such, Chapter 1 will introduce the state of the art with respect to chemical versatility and passivation, and surface electronic properties.

1.1 H-terminated Si surfaces

1.1.1 Synthesis of H-terminated Si surfaces

The H terminated Si surface can be formed by a variety of procedures, including vacuum techniques, electrochemical etching, and chemical etching.[6–16] H-terminated surfaces prepared by vacuum-cleavage of Si, followed by exposure to hydrogen, have been studied using high-resolution electron-energy loss spectroscopy (HREELS) and other ultrahigh vacuum techniques.[6,7] Low-energy electron diffraction (LEED) studies have indicated that the surface-order does not change upon exposure of a freshly cleaved surface to hydrogen.

Although such techniques enable investigation of the properties of very pure H-terminated surfaces, vacuum-cleavage of bulk crystals is not suitable for large-scale processing. A significant amount of effort has thus been devoted to elucidating the behavior of solution-based routes to H-terminated Si surfaces. The composition of the Si surface following HF-etching has been studied using multiple internal reflection Fourier transform infrared (MIR-FTIR) spectroscopy. The presence of IR-absorption bands ascribable to Si-H, Si-H_2, and Si-H_3 moieties indicated that aqueous HF-etching of Si(111) yielded microscopically rough surfaces, but line-width analysis suggested that the surfaces were locally ordered.[8,9,16]

The ability to create atomically flat Si(111) surfaces using a wet chemical approach (Figure 1.1) was discovered in 1989. The method built on the observation that HF-etching induced microscopic roughness to the Si(111) and Si(100) surfaces.[8,11] Following these studies, the effects of pH were examined to elucidate the effects of the HF(aq) concentration on Si surface quality.[10,11] Etching in buffered HF, where the pH was adjusted using either NH_4OH(aq) or HCl(aq), produced very different results than when the Si was etched in HF(aq) alone. Specifically, when the pH was greater than 4, a dramatic change occurred in the Si-H region of the FTIR spectra. A single, dominant peak, attributable to the Si-H stretching vibration, was produced with no peaks ascribable to the di-, and trihydride species that were observed on surfaces etched in acidic HF(aq) solutions.

In alkaline solution, the rate-determining step of the fluoride etch on Si is OH- attack. Simulations have shown that the relative reaction rates of OH- attack on features commonly encountered on a Si(111) surface, including kinks, dihydride, and monohydride steps, can differ by as much as eight orders of magnitude. The etch rates of single-crystal Si have been investigated as a function of crystallographic orientation (Table 1.1).[17] In all cases, the etch-rate of the (111)-oriented crystal face was considerably lower than the etch rates of the other faces, and a reaction scheme for the dissolution of (100) oriented Si is presented in Figure 1.2. The replacement of H atoms with -OH^- groups polarizes the Si back-bonds such that H_2O can attack. The (111) surfaces are much more stable because each surface atom has only one bond left to be OH-terminated. With only one -OH group, the back-bonds are less activated, and H_2O is less likely to attack. The anisotropy of the basic fluoride etch is significantly decreased by the introduction of trace metal, oxygen or other impurities into the etching-solution.[18,19] Introduction of O_2 into an NH_4F(aq) etching solution greatly reduces the fidelity of the resulting Si(111) surface, producing Si-H_2 and Si-H_3 surface-sites, as well as adding to the incorporation of O atoms into the Si-Si back bonds. Scanning tunneling microscopy (STM) images clearly show the effect of the presence of oxygen in the NH_4F(aq) etching solution. Without oxygen, the surface is dominated by large terraces of Si(111), whereas rough surfaces are produced by O_2-containing NH_4F(aq)

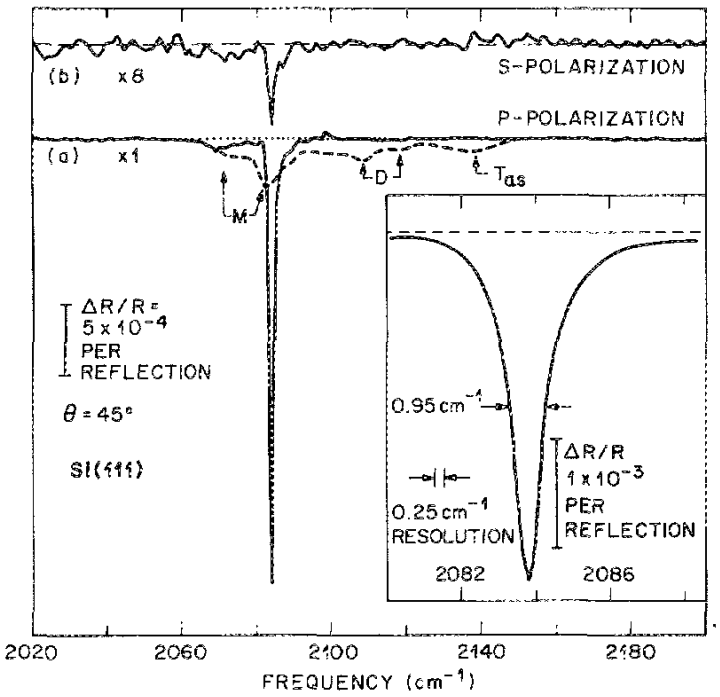

Figure 1.1. Internal reflection IR spectra of fluoride-etched Si(111)[10] Dashed line: surface etched in dilute, acidic HF solution (100:1 H_2O:HF). Solid line: surface etched in buffered HF (pH 9–10) probed under p-polarized light (a) and s-polarized light. Inset shows high-resolution spectrum of Si(111) etched in buffered HF.

etching solutions.[18,19]

Table 1.1. Orientation-dependent etch rates relative to (110) in mm/min as a function of [KOH] at 70 °C[17]

Crystallographic Orientation	KOH Concentration		
	30%	40%	50%
(100)	0.797 (0.548)	0.599 (0.463)	0.539 (0.619)
(110)	1.455 (1.000)	1.294 (1.000)	0.870 (1.000)
(210)	1.561 (1.072)	1.233 (0.953)	0.959 (1.103)
(211)	1.319 (0.906)	0.950 (0.734)	0.621 (0.714)
(221)	0.714 (0.491)	0.544 (0.420)	0.322 (0.371)
(310)	1.456 (1.000)	1.088 (0.841)	0.757 (0.871)
(311)	1.436 (0.987)	1.067 (0.824)	0.746 (0.858)
(320)	1.543 (1.060)	1.287 (0.995)	1.013 (1.165)
(331)	1.160 (0.797)	0.800 (0.619)	0.489 (0.563)
(530)	1.556 (1.069)	1.280 (0.989)	1.033 (1.188)
(540)	1.512 (1.039)	1.287 (0.994)	0.914 (1.051)

To further investigate the quality of the Si(111) surface, vacuum STM images and LEED patterns were obtained.[11] LEED-patterns suggested that both HF(aq) and NH_4F(aq) etching resulted in high-quality 1×1 surfaces with defect-densities of 0.5%. Vacuum STM data, however, showed clear differences in the surface morphology produced by HF(aq) *vs.* NH_4F(aq) etchants, consistent with the presence of Si monohydride, dihydride-, and trihydride peaks for HF(aq)-etched Si(111) surfaces, and consistent with only a sharp Si-H stretch in the IR spectrum of the NH_4F(aq)-etched surfaces. For NH_4F(aq)-etched surfaces, flat terraces extending thousands of Ångströms were observed with less than 1% surface contamination. The level of surface contamination seemed to not be intrinsic to the NH_4F(aq) etching procedure. XP spectra further confirmed that neither oxygen nor carbon constitute significant contaminants on surfaces prepared through the NH_4F(aq) etch.[19,20]

The techniques commonly used to characterize Si interfaces electronically were developed to study the Si/SiO_2 or Si/metal interface.[21] The formation of Si/SiO_2 structures and Si/metal junctions, however, rarely preserves the H-terminated Si surface. Consequently, almost all techniques used to study the H-Si surface are contact-less,[1,22] or form only soft contacts.[23–25] Using a contact-less device, the H-terminated Si has been shown to be very well passivated electronically. Measurements taken in HF(aq) or in other strong acids yielded minority-carrier lifetimes > 10 ms, suggesting that defect-densities were as low as 1 per 40 million surface atoms.[1] The possibility that measurements in various solvents yielded long minority-carrier lifetimes due to band-bending was investigated extensively, and it was found that one must proceed cautiously when correlating minority-carrier lifetimes to surface defect densities.[26–29] The highly ideal, flat, H-terminated Si(111) surface is attractive from an experimental point of view as it is a very well-defined system.

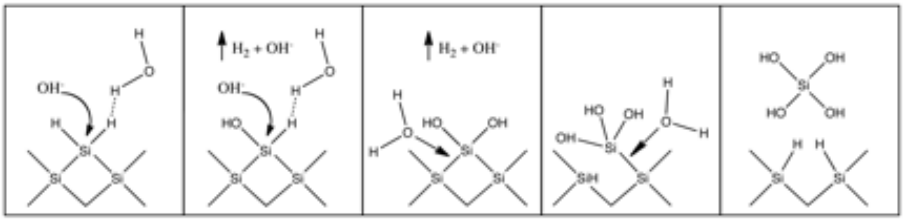

Figure 1.2. Proposed reaction scheme for the chemical dissolution of Si in basic media.[30]

1.1.2 Reactivity of H-terminated Si surfaces

Aqueous Acidic Media. The reactivity of H-Si with aqueous acidic media has been extensively evaluated.[30–33] Perhaps one of the most well-known examples of H-Si reacting with an aqueous acidic solution is the "SC-2 clean", where H-Si is reacted with an H_2O:H_2O_2:HCl mixture to ultimately yield a Si surface that is free of organic or inorganic contaminants. The chemistry of H-Si in aqueous acidic media is highly dependent on both the acid and on the presence of any additional reactants or reagents. Depending on the solution composition, H-Si surfaces are protected in some acidic media, oxidize in other media, and dissolve in yet others. In contrast to alkaline HF-etching, reactivity of Si in acidic media is highly isotropic.

In the absence of fluoride ions or oxidizing reagents, H-Si is stable in concentrated acids. This behavior is expected, because the high $[H^+]$ keeps the surface fully H-terminated. H-Si surfaces immersed in strong acids exhibit excellent electronic properties.[1] The lifetime of photogenerated minority carriers, as measured using a contact-less method wherein the carrier density was measured using an inductively coupled RF-bridge, was shown to be related to the electronic defect density on the surface. Low SRV values were observed in a number of strong acids, and the SRV was a function of acid molarity. Furthermore, changing the acid molarity induced reversible changes to the surface recombination velocity. From the dependence on $[H^+]$, it was suggested that H-Si surfaces contain a finite number of strained, or otherwise weak bonds, that act as recombination centers. The recombination centers resembled Lewis bases in an acid-base equilibrium with the surrounding solution, and the observed effect of acid molarity on SRV was ascribed to neutralization (H-termination) of these defect sites.

In contact with an acidic aqueous solution that contains oxidants, the near-surface layer of such H-terminated Si(111) surfaces is rapidly converted to 1–2 nm of SiO_x.[31] The SiO_x passivates the surfaces to further oxidation, because HF-free solutions that contain oxidizers do not etch SiO_x. As part of the Si cleaning procedure developed at RCA laboratories, oxidation of H-Si in $HCl(aq)/H_2O_2(aq)$ has been widely utilized.[32,34] The RCA cleaning procedure removes a variety of organic contaminants and leaves low levels of metal contaminants.

The incorporation of fluoride ions into acidic media causes etching of Si and of SiO_x. SiO_x

etches very quickly in HF(aq), however H-Si surfaces are more stable, etching at rates < 1 Å min^{-1}. The etch rate increases dramatically when oxidizers are added to the HF(aq) solution,[32] and numerous systems composed of H_2O, HF, and an oxidizer have been employed to rapidly etch Si.[35] Specifically, the HF(aq)/HNO_3(aq) system etch rate is measured in mm/min.[34]

Aqueous Basic Media. The H-terminated Si surface is unstable in alkaline media. The etching of Si in alkaline media has been studied extensively.[30] The alkaline etching of Si is anisotropic and, thus it proceeds very differently from etching in acidic, fluoride-containing, media.[33] The orientation-dependent etch rates were functions of [OH^-] and temperature. The alkaline etching of Si also depends on both [H_2O] and [OH^-]. In organic alkaline solutions the etch rate goes to zero as [H_2O] approaches zero. In alkaline aqueous solutions that contain an oxidizing-agent, hydrogen-terminated Si surfaces rapidly convert to Si covered with a thin overlayer of SiO_x. The conversion of H-Si to SiO_x has been studied extensively for RCA-2, $NH_4OH/H_2O/H_2O_2$.[32,34,35] The amount of oxidizer present in the alkaline aqueous solution determines whether a SiO_x overlayer will form and thus protect the Si from further alkaline etching. If only small amounts of oxidizer are present, the surface will be continuously etched by the hydroxide ions.

Oxygen-containing environments. Electronics must be robust in air, so the stability of HF-etched Si surfaces in oxygen-containing environments has been investigated quite thoroughly. The mechanism of the initial oxidation of H-Si surfaces is not fully understood, but many important aspects have been observed and described. The growth-rate of SiO_x on Si(100) was 0.2 nm/decade (hours), with a limiting oxide thickness of < 1.4 nm as determined using XPS.[36] Conflicting results exist as to the effect of microscopic roughness on the rates of initial oxidation, but recent data suggest that the oxidation rates depend on the surface roughness.[37,38]

Oxidation of H-terminated Si in the presence of O_2 has also been investigated for the special case of oxidation in a pure-oxygen, low-pressure (1–15 mTorr) environment at elevated temperatures (530-590 K). The reaction rate-constants between O_2 and various Si surface moieties, such as monohydrides and dihydrides present on various crystal phases, were quite different, differing as much as 20-fold. The monohydride-terminated surfaces were substantially more stable than the other surfaces. Si(111) surfaces oxidized signifinanctly slower than Si(100) surfaces, and dihydride-steps on Si(111) surfaces oxidized more rapidly than monohydride steps. Flat Si(111) surfaces were the most stable. It was suggested that neither O_2 nor H_2O alone could explain the rapid rates of native-oxide formation commonly observed, and perhaps radicals or other trace contaminants are responsible for the observed rate of oxide formation.[38] Curiously, the initial oxidation of H-Si surfaces proceeds without loss of atop Si-H bonds. Oxygen inserts into the Si back bonds without the formation of Si-OH species.[38,39]

Alcohols Alcohols are commonly used solvents for chemical reactions and cleaning-procedures,

thus their interaction with H-terminated Si is of great interest. The H-Si surface is stable in a number of solvents including acetonitrile,[40] toluene and mesitylene,[40] and diethyl ether,[41] however H-Si surfaces react with various alcohols.[29,40,42,43] Early investigations of reactions between H-Si and alcohols utilized porous Si, which provided for improved signal to noise in spectroscopic studies and allowed further investigation through its luminescence properties. Methanol was attached to porous Si through electrochemical processes involving partial dissolution of the Si substrate,[44] though simply exposing the H-Si to methanol has also been to be reported sufficient for CH_3O- attachment. Various studies have reported that attachment of alcohols to H-Si proceeds with partial oxidation of the underlying substrate,[45,46] while others have successfully formed Si-O-C bonds without oxidation of the substrate.[47,48] The reactivity between alcohols and H-Si was used to form ferrocene-modified Si electrodes. The ferrocene was covalently linked to H-Si(111) simply by immersion in a ferrocene derivative that contained a terminal OH-group. Immersion in other alcohols also yielded modified surfaces, although the bonding and surface quality was not thoroughly explored.[40] The Si-O-C bond is prone to hydrolytic cleavage, regenerating the original alcohol and leaving the surface Si-OH terminated, thus this approach is not generally used to effect subsequent modification of Si surfaces.

Protic and deuterated MeOH were used in a detailed study of Si-O-C formation on Si(111).[29,43] Partially methoxy-terminated Si surfaces were synthesized, with the remaining atop sites H-terminated and no observable incorporation of O atoms into the Si back-bonds. Prolonged exposure to methanol at room-temperature lead to some subsurface oxidation, while shorter exposures to methanol at 65 °C resulted in no detectable (less than 3%) subsurface oxidation. Approximately $^1/_3$ of the Si atop sites were methoxylated, in agreement with steric considerations (Figure 1.3). A likely reaction mechanism for the formation of methoxy-termination of Si(111) was suggested based on polarized FTIR spectra, Figure 1.4, however it was observed that upon exposure to CD_3OD, a Si-D species was present on the surface. The experimental data available did not allow for determining a likely reaction mechanism for the origin of the Si-D species.

The electronic effects of alcohol-termination of Si surfaces have also been investigated. The methoxylation of Si improved the anodic stability.[49] Exposure to methanol vapors affected both reversible and irreversible changes to H-terminated Si. Results from both capacitance-voltage and contact-potential measurements indicated that surface-methoxylation shifted the band-edge positions such that the electron affinity was decreased. The effects of methoxylation on the SRV were investigated as a function of the sample history, allowing for the separation of effects due to band-bending and passivation of the Si surface. Low effective SRV was observed due to band-bending, and it was demonstrated that care must be taken when using methanolic systems for characterization of Si surface properties.[26]

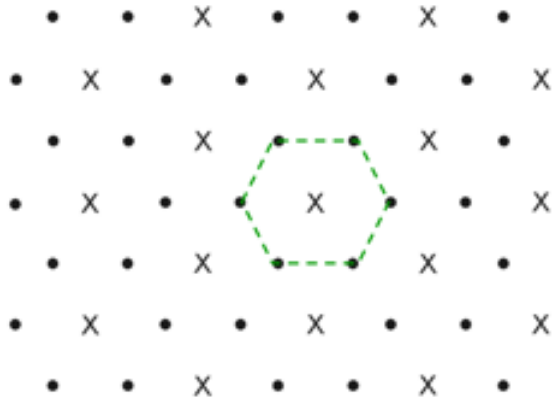

Figure 1.3. Si(111) with a saturation coverage of 66% Si-H (dots) and 33% Si-OCH_3 (crosses). The Si-OCH_3 groups block all nearest neighbor atoms (denoted by hexagon) by the 360° thermal rotation of the methyl group about the Si-O bond. Adapted from Ref. 29.

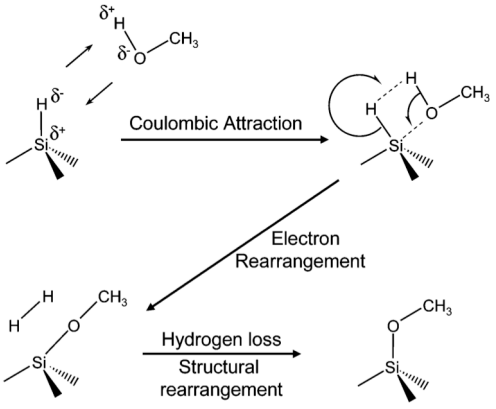

Figure 1.4. Proposed mechanism for the methoxylation of the H-Si(111) surface in neat methanol.[43] The mechanism produces H_2 and necessitates no free carriers from the bulk Si.

Metals Highly rectifying metal contacts on Si can be used as solar cells and photodiodes. Additionally, an understanding of the Si/metal interface is crucial to understanding the formation of Ohmic contacts to Si.[50] The ability to form Si/metal contacts without disrupting the H-termination of Si is also of great interest for nondestructive characterization of the interface, dopant densities, and surface quality across Si wafers. Unfortunately, the electronic properties of Si/metal junctions are, with a few exceptions, highly nonideal and are dominated by the junction properties rather than by the properties of the metal and the bulk Si. Ideally, the barrier height, Φ_m, of a Si/metal junction should be linearly dependent on the work-function, χ_m, of the contacting metal. However, for Si, the barrier height is only weakly dependent on χ_m.[21,51,52] This behavior has been ascribed to surface states, likely metal silicides, at the Si/metal interface. The barrier height can be correlated to metal work function, though the dependence is weak (Figure 1.5).

An important exception is the formation of Si/Hg junctions.[23,53–55] Si/Hg silicides do not form under ambient conditions, as has been shown via XPS.[53] Hense, the Si/Hg junction has proven to be an important tool for soft-contact, non-destructive, electrical characterization of Si surfaces. Impedance spectroscopy and current density vs voltage (J-V) data have shown that the Si/Hg junction is near ideal, in contrast to other metal/Si junction formation schemes.

1.2 Halogen-terminated Si surfaces

Halogen terminated silicon, *i.e.*, Cl-, Br- and I-Si, has been studied extensively because halogen etching and termination was, initially, integral to understanding the reconstructions of Si(111) and Si(100) surfaces.[56,57] This work was all performed under UHV conditions, with UHV-cleaned Si and molecular gases. Later it was discovered that Si surfaces in contact with Br_2/ROH or I_2/ROH solutions displayed very low surface recombination velocities.[26,58–60] While neither the surface-bound species nor mechanism for surface lifetime enhancement was known, this behavior sparked much interest, and motivated research in the field. Finally, more recent interest in halogenated silicon surfaces has been spurred because although the halogen-terminated surfaces are more reactive than H-terminated surfaces, they can nevertheless be handled briefly in ambient conditions.[61] Accordingly, the halogenated Si surfaces serve as convenient and scalable intermediates for the solution state-syntheses of bound organic monolayers,[62–66] and as a reactive surface for the deposition of inorganic films via atomic layer deposition (ALD).[67–71]

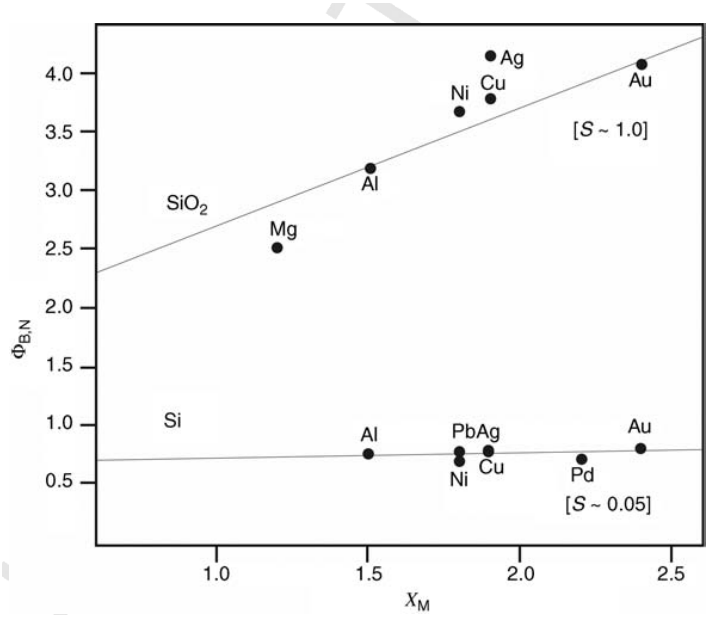

Figure 1.5. Barrier height, $\Phi_{\mathrm{B,N}}$, at Si/metal and SiO_2/metal junctions as a function of the metal electronegativity, χ_{M}. The slope, *S*, is inversely proportional to the extent of Fermi-level pinning, where an ideal junction would have *S* = 1.0. Adapted from Ref. 50.

1.2.1 Synthesis of Cl-terminated surfaces

Several methods allow for the synthesis of Cl-terminated Si surfaces, including gas-phase reactions with diatomic molecular halogens under UV irradiation,[66,72,73] elevated temperatures,[74–76] and room temperature,[72,77] in addition to solution-state methods like PCl_5 with a radical initiator.[62,72,78–82] These methods have been shown to result in nominally similar Si-Cl surface bonding, however, the coverage, homogeneity, and etch pit density vary for the different functionalization methods and for different crystal faces. The Van der Waals radius of Cl is 1.75 Å, so Cl atoms can terminate every atop site on an unreconstructed Si(111) surface.[83] SEXAFS showed that after exposure of Cl_2(g) to the reconstructed Si(111)-(7 × 7) surface, Si-Cl bonds were present and oriented normal to the surface.[84] Variable angle FTIR[72], STM[77] and HREELS[77] have also shown that the Si-Cl bonds are normal to the surface on Cl-Si(111) surfaces that have been synthesized from solution-phase or gas-phase reactions of the H-Si(111) surface, Figure 1.6 and Figure 1.7.

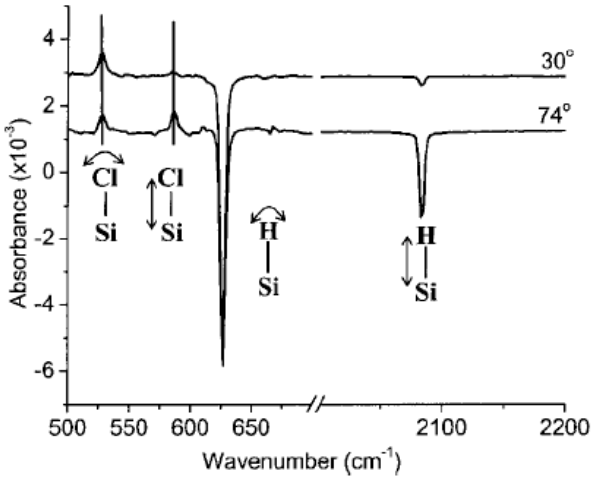

Figure 1.6. Transmission FTIR of the Cl-Si(111) surface (referenced to the H-Si(111) surface) produced using a wet chemical technique.[72] Si-Cl and Si-H (subtracted) bend modes are observed at both 30° and 74° off normal. The Si-Cl and Si-H stretch modes are polarization dependent and observed only at 74° off normal, indicating these modes are perpendicular to the surface.

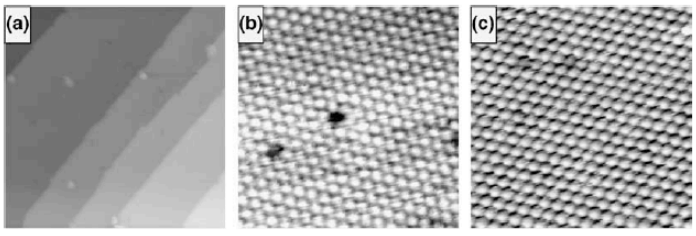

Figure 1.7. Constant-current STM images show full coverage halogenated Si(111) surfaces with little roughening. (a) Cl-Si(111), 50 × 50 nm^2, -1 V sample bias, 40 pA; (b) Cl-Si(111), 6.5 × 6.5 nm^2, -0.5 V, 50 pA; (c) Br-Si(111), 6.5 × 6.5 nm^2, 0.4 V, 400 pA.[77]

Detailed comparisons have been made between the properties of halogenated Si surfaces

prepared by gas-phase and solution-based methods. Room temperature gas-phase and solution-phase methods both produced Si-Cl bonds with a vibrational peak FWHM of 5 cm^{-1}, as observed *via* infrared absorption spectroscopy (IRAS).[72] This narrow peak width indicated extended regions of homogeneous Si-Cl termination. At short Cl_2 exposure times, partial Si-Cl coverage was observed without observable roughening of the surface.[83] The chemical shift of the Si-Cl stretching mode was dependent on the Si-Cl surface coverage. An STM study showed that the solution-state method, PCl_5 with benzoyl peroxide, was sensitive to the reaction temperature.[79] As the temperature of the reaction increased, so did the density of etch pits. Based on SXPS data, Si-Cl surfaces functionalized by the room-temperature gas-phase reaction gave comparable Si-Cl coverage to surfaces produced by a solution-state reaction pathway. While the solution-based method resulted in a higher amount of oxygen, 1.4 ± 0.6 ML as observed via XPS, no SiO_x was detectable in the SXPS spectra. The presence of oxygen was attributed to solvent work-up steps that were not necessary for the gas-phase reaction. IRAS is more sensitive for oxide detection, and based on integration of the 1080 cm^{-1} peak, gas-phase chlorination gave 3% of a ML of Si-O-Si, whereas the solution-phase chlorination produced $<$ 15% Si-O-Si coverage. In other IRAS studies, very low surface oxidation, 1.2%, or 0.15 ± 0.01 Å of subsurface oxide, was observed to form during the solution-phase chlorination reaction.[85] The observed differences in oxidation could thus be due to brief exposure of the surface to ambient air as opposed to the inherent properties of the reaction sequence. Based on vibrational shifts, the oxidation was presumed to be in isolated patches.[76] Despite the difference in etch pit density and initial SiO_x coverage, an SXPS study showed that the surfaces prepared by the room temperature gas-phase and solution-phase halogenation routes oxidized at comparable rates.[86] The initial oxide formation during the Cl-termination step did not affect the electronic trap-state density at the resulting Si-C terminated surfaces. In fact, CH_3CH_2-Si(111) surfaces formed from solution-functionalized Cl-Si(111) showed only a slightly higher oxidation after $>$ 3 days in air than surfaces made in gas-phase Si-Cl precursor surfaces, however, the SRV after 24 h in air was measured to be lower for surfaces made from the solution-phase route than for that of the CH_3CH_2-Si(111) surface formed from gas-phase-functionalized Cl-Si(111).

Differences in Si-Cl surface coverage, and surface roughness that resulted from various types of Cl_2(g) reactions, were found to be dependent on the reaction conditions. The photoinitiated chlorination of silicon led to broadening and a red shift of the Si-Cl vibrational peaks, suggesting that such Si(111) surfaces were not fully covered with Cl atoms.[72] A change in the temperature of chlorination of Si(100) with UV from 350 K to 423 K lead to an increase in surface roughness from 1.70 ± 0.54 Å to 7.9 ± 7.0 Å.[87] The initial H-terminated surface had a roughness of 1.61 ± 0.14 Å. Significant etching by Cl_2 occurred only above 350 K and 10 torr.

The temperature programmed desorption (TPD) analysis of Cl-Si(111) synthesized *via* a solution-based benzoyl-peroxide-initiated PCl_5 route closely matched that of high-coverage, gas-phase-functionalized Cl-Si(111), although some differences were observed in the high-temperature desorption.[62,78,88] TPD of high-coverage Si surfaces showed desorption of $SiCl_x$, where x = 2 and 3, beginning at 670 K, with some x = 4 and 2 desorbing at 850[62] or 950[88] K. At low Cl coverage, $SiCl_2$ was the main product, and desorbed at 950 K.[88] A recombinative desorption mechanism was proposed, in which Si-Cl + Cl $\rightarrow$ $SiCl_2$ and $SiCl_2$ + Cl $\rightarrow$ $SiCl_3$. The Cl-terminated Si surfaces were demonstrated to be stable for $>$ 12 h in inert atmosphere.[76,89]

Because halogen-terminated Si surfaces are a more reactive than H-terminated Si, the Cl-Si(111) and Cl-Si(100) surfaces have been used as starting surfaces for the ALD deposition of Al- and Hf-based dielectrics.[90] The resulting surfaces were fairly unreactive with water, however Si-M bonds were readily formed. After exposure to trimethyl aluminum (TMA), Al-CH_3 and Si-CH_3 modes were readily visible via IRAS. Pyridine has, nevertheless, been used as an accelerant in SiO_2 growth by ALD (Scheme 1.1).[91]

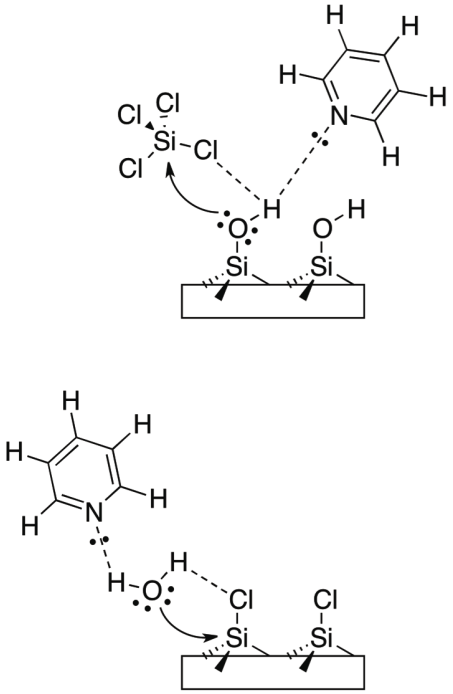

Scheme 1.1. Proposed mechanism of pyridine activation during the $SiCl_4$ (a) and H_2O (b) half-reactions of the ALD growth of SiO_2[70]

1.2.2 Synthesis of Br-terminated surfaces

Several methods, including Br_2(g) or Br_2(soln) and solution-based bromination reagents, such as NBS, have been used to obtain Br-terminated silicon surfaces.[65] It has been suggested that most of these functionalization methods proceed by the same mechanism. For example, it is

thought the NBS reaction generates *in situ*, small amounts of Br_2, which is presumed to be the actual brominating agent. Solution-based bromination has been achieved using NBS in DMF, with a radical initiator present, upon heating to 60 °C for 20 min. Bromochloroform can also be used both under thermolysis (80 °C for 30 min), photolysis (300 nm UV for 30 min), or radical initiation (benzoyl peroxide at 60 °C for 30 min) to produce Si-Br terminated Si surfaces.[65] All of these methods produced the same Si-Br shift in XPS, and showed C and O present on the surface, attributable to adventitious C and O sources.

1.2.3 Synthesis of I-terminated surfaces

Unlike Cl- and Br-terminated surfaces, iodine was not observed to terminate every atop site on Si(111), so such surfaces have always been found to be chemically inhomogeneous. Solution-state iodination of silicon surfaces has been accomplished through several methods. Si(001) surfaces functionalized by submersion in I_2/benzene gave 33% coverage of Si-atop sites.[64] Surfaces functionalized in this manner showed surface photovoltage effects suggesting the presence of midgap surface states. SEXAFS data of surfaces resulting from the reaction of I_2 with the reconstructed Si(111)-(7 × 7) surface showed that I binds in the same fashion as Cl-Si(111), forming Si-I bonds oriented normal to the Si surface.[84] Exposure of vacuum cleaned Si(100)-(2 × 1) surfaces to CH_3I resulted in mixed CH_3- and I-termination.[92–94] Approximately one CH_3I adsorbed per 2 Si atop atoms. The surface was characterized through a variety of techniques, including kinetic uptake measurements,[93] TPD,[93] Auger electron spectroscopy (AES),[93] HREELS,[92] and IRAS.[94]

1.2.4 Halogen etching

When clean, reconstructed Si surfaces or H-terminated Si surfaces are exposed to diatomic halogens, etching can occur, leaving a halogen-terminated surface.[56,57,67,72,89] Alternatively exchange of hydrogen for halogen termination on H-terminated Si surfaces occurs.[56,76,89] Both of these mechanisms result in a halogen-terminated Si surface, however, the choice of reaction conditions dictates whether the initial surface structure will be preserved. For example, Si is etched upon exposure to HCl in vacuum at high temperatures, but at lower temperatures, HCl exposure results in Si-Cl-termination.[75]

Solution-based Cl-termination of Si *via* radical-initiated PCl_5 ($\sim$ 0.7 M PCl_5 in chlorobenzene with a catalytic amount of benzoyl peroxide) results, by STM, in an increased density of etch pits relative to functionalization at room temperature with Cl_2(g).[79] The density of etch pits was dependent on the reaction temperature. IRAS was used to characterize surfaces functionalized *via* the solution method, and the Si-Cl stretch (586 cm^{-1}) and bend (626 cm^{-1}) were observed.[85]

1.3 Carbon terminated Si surfaces

The C-Si bond adds kinetic chemical stability to the Si surface. C-Si reactivity depends on roughness and crystal orientation, as does the reactivity of H-, Cl-, and Br-terminated Si surfaces. Additionally, for C-terminated Si surfaces, incomplete termination (*i.e.*, a mix of Si-C and Si-H terminated atop sites), and physical barriers imposed by large molecules also affect the surface reactivity. The fully methyl-terminated Si(111) (1 × 1) surface (CH_3-Si(111)) provides a unique opportunity to obtain detailed insight into the inherent chemical reactivity and electrical properties of the Si-C bond. A comparison between the atop Si atom spacing of 3.84 Å[50] and the van der Waals radius of the methyl group (∼2.5 Å) suggests that CH_3- is the only saturated hydrocarbon that can terminate every atop site on the unreconstructed Si(111) surface.[81,95,96] The conversion of atomically flat H-Si(111) to CH_3-Si(111), *via* the Cl-Si(111) surface, produces an atomically flat, CH_3-Si(111) surface with nominal unity coverage (Figure 1.8).[62,81,97] The CH_3-Si(111) surface can also be synthesized through the anodic addition of CH_3MgI to H-Si(111).[95] Because the smallest physical barrier to interacting with the Si-C bond is presented by the CH_3-Si(111) surface, its similarities to, and differences from, other C-terminated surfaces can be highlighted. Isolation of the stability introduced by a physical barrier to reactants is more difficult. Attempts at the deconvolution of the effects of a physical barrier and chemical stability have been attempted.[98] It is important to understand effects of a physical barrier on stability, as well as the consequences for common applications.

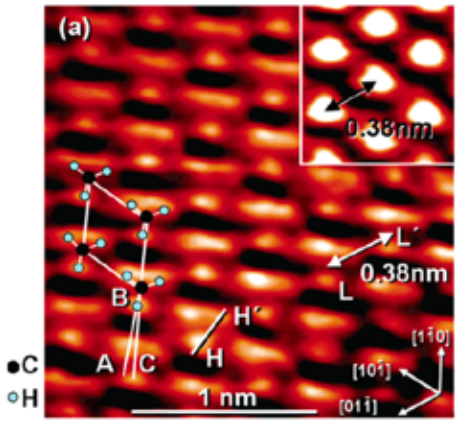

Figure 1.8. STM image of CH_3-Si(111) surface (4.7 K, sample bias V_s = -2.5 V, and constant current of 0.050 nA).[97] Center to center distance of the -CH_3 groups (L to L') is 0.38 nm. The low-index planes, denoted in the bottom right, were determined by x-ray crystallography. The surface unit cell is outlined by the parallelogram with -CH_3 groups superimposed at each vertex. The angle between A and C is 7 ± 3°. The inset (top right) is the same surface, image at 77 K.

1.3.1 Structural characterization of carbon-terminated Si

Two methods have been used to synthesize CH_3-Si(111) surfaces.[62,95] One is through anodic addition of CH_3MgI to H-terminated Si surfaces.[95] The other, more widely utilized approach,

is through surface halogenation followed by alkylation. In the later approach, highly reactive Si-Cl, or Si-Br surface is synthesized and then exposed to alkyl Grignard or organolithium reagents.[62] The resulting CH_3-Si(111) surface has been thoroughly characterized. The chlorination/alkylation procedure results in an unreconstructed Si(111) surface, as evidenced by LEED.[99] The absence of Si-H, Si-O, and Si-Cl stretching modes in the FTIR spectrum of CH_3-Si(111), along with the appearance of a polarization-dependent CH_3- umbrella mode, suggested that Si-C bonds terminated every atop Si atom on the unreconstructed Si(111) surface.[100] The polarization dependence of the methyl umbrella vibrational modes showed that the CH_3-group was attached normal to the Si(111) surfaces plane, and the Si-C bond has been directly observed through photoelectron spectroscopy (PES),[81,101] HREELS[78] and FTIR spectroscopy.[100] Surface-sensitive soft x-ray photoelectron spectroscopy (SXPS) and ultraviolet photoelectron spectroscopy (UPS), in conjunction with use of the substrate overlayer model, indicated a CH_3-group coverage of 1 monolayer.[81,101–103] Low-temperature STM images confirmed the high degree of order, and unity coverage, of the CH_3-Si(111) surfaces over large-area terraces.[97] Thus the CH_3-Si(111) surface is an ideal surface to understand the effects of kinetic stabilization of the Si-C bond without the confounding effects of the physical barrier imposed by a long chain alkane or by additional surface functionality.

A large body of literature describes the structural characterization of Si-C surfaces functionalized with groups other than methyl. The reactivities of all such surfaces, aside from CH_3-Si(111), are affected by a combination of Si-C site reactivity, non-Si-C-functionalized site reactivity, the physical barrier imposed by large molecules, and the terminating chain functionality. The fraction of saturated C-terminated Si atop sites is nominally unity only for the CH_3-Si(111) surface. For all other Si(111) surfaces functionalized with alkanes or alkenes, the Si-C coverage is less than unity, because of steric factors. For surfaces functionalized using the two-step reaction or hydrosilylation, the non-Si-C-terminated sites are most commonly terminated by Si-H bonds.[104–106] While the CH_3-Si(111) surface coverage was measured to be 100% termination of Si atop sites, the C_2H_5-Si(111) surface had a maximum of approximately 85% coverage.[82,107] As expected, the coverage decreased as the steric bulk of the alkyl group increased.[106] The maximum coverage of surfaces functionalized *via* hydrosilylation, which commonly employs large molecules, is approximately 50%.[96,105] Clearly, the CH_3-Si(111) surface is an attractive choice for the isolation and study of the Si-C bond.

The hydrosilylation reaction proceeds through a chain reaction on the surface, while for the two-step mechanism, each site-functionalization reaction is only influenced sterically by closely adjacent sites. The hydrosilylation surface chain-reaction therefore leads to patches of functionalization at low reaction conversion, (Figure 1.9).[108] In contrast, the two-step mechanism

is thought to give between random and self-avoiding coverage with bulky functional groups, because of the irreversibility, mechanistic independence, and steric considerations of each reaction event. This difference in mechanism, along with the tendency to proceed to higher coverage, implies that very few adjacent sites are not Si-C terminated on Si surfaces functionalized using the two-step halogenation/alkylation procedure.[82,85] A decreased rate of surface oxidation was observed on partially alkylated surfaces relative to that of Si-H surfaces.[86] It was suggested that if lateral SiO_x propagation proceeds through adjacent Si-H sites, the presence of even incomplete Si-C termination would retard the oxide growth. Although clear examples are lacking on the effect of adjacent site identity on surface stability, the degree and identity of non-C-terminated Si atop sites are likely to affect the reactivity of such surfaces.

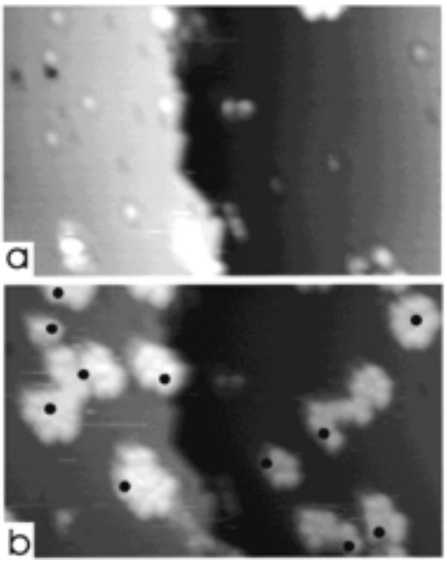

Figure 1.9. Occupied state STM images (215 Å × 215 Å, 22 pA) of a H-Si(111) surface with isolated dangling bonds created by desorption activated with the STM tip (a) before styrene addition and (b) after exposure of 12 L of styrene.[108] The black dots in (b) mark the initial dangling bonds showing these sites initiate hydrosilylation of styrene. Maximum height range is ∼5 Å (a) and ∼10 Å (b).

Despite a possible lower coverage of functionalized Si surface sites, an increase in the size of the surface-bound species can also produce a physical barrier on the surface. An increase in the monolayer thickness and density, but not in the total coverage of Si-C bonds on Si atop sites, has been obtained by chemical functionalization of ester-terminated alkane monolayers on Si.[98] This highly protected overlayer increased the stability of silicon toward oxidation under ambient conditions. The monolayer protected the underlying substrate not *via* kinetic stability of the Si-C bond, but primarily *via* physical separation between reactant and the silicon surface sites.

As the density of dangling bonds decreased, either because of surface roughness or due to the structure of specific crystal face, increased chemical stability has been observed for Si-H and Si-X terminated surfaces.[90,109] CH_3-Si(111) surfaces are better passivated towards oxidation in air than are CH_3-Si(100) surfaces.[106,110] The unreconstructed Si(100) surface has a higher density

of dangling bonds than does the Si(111)-(1 × 1) surface, 1.36×10^{15} compared to 7.83×10^{14} cm^{-3} on Si(111). Hence, on the Si(100) surface, the Si atop sites are more available for attack by oxidants, because sterically there is not enough space for CH_3- termination of every dangling bond.

Hydrosilylation proceeds to give nominally identical monolayers on Si(111) and Si(100) surfaces.[96,111] TPD results showed similar thermal stability on Si(100) compared to on Si(111), however increased disorder of the monolayer was observed *via* contact angle measurements. The observed behavior is consistent with the increased disorder of the initial H-Si(100) surface, which contained SiH, SiH_2, and SiH_3 moieties. Although a rigorous comparison of the stability of hydrosilylation-functionalized Si(100) and Si(111) surfaces has not been conducted, a large difference between the two crystal faces may not be present, because the dominant stabilization mechanism for hydrosilylation-functionalized surfaces is a physical barrier, which should be similar on both hydrosilylated crystal faces.

1.3.2 Electronic characterization of carbon-terminated Si

Surface recombination velocity. C-terminated Si surfaces can be prepared with very low electronic defect densities, and low electronic defect densities have been measured for surfaces synthesized *via* the two-step halogenation/alkylation reaction.[62,78] The CH_3-Si(111) surface exhibited stable SRV values of < 40 cm s^{-1} for > 30 days, in ambient air despite the growth of some SiO_x.[62,100,112] A combination of SXPS and UPS measurements indicated that the low SRV was due to low electronic defect-densities rather than due to band bending.[99] Even surfaces functionalized with bulky groups that are only capable of sparse coverage of the Si surface, showed SRV values > 100 cm s^{-1}.[106] These data thus showed that the Si-C bond efficiently passivated the Si surface, and that the electronic properties of these functionalized surfaces were stable in air over long periods of time, unlike the behavior of the Si-H terminated surfaces.

Surface dipole. The presence of an ~ 400 mV dipole, Figure Figure 1.10, at the CH_3-Si(111) surface has been observed *via* synchrotron photoemission spectroscopic measurements in UHV. The dipole has been attributed to the electronegativity difference between the C and H of the CH_3 groups.[99] Additionally, a comparison of the barrier height measurements made at n-Si-H/Hg and n-Si-CH_3/Hg contacts showed a ~ 0.55 eV dipole.[53,113] In the electrodeposition of Cd and Pb on H-Si *vs.* CH_3-Si, the dipole was manifested as the presence or absence of an oxidative stripping peak.[114]

Electronic Resistance. The presence of an insulating layer between two conducting phases presents a barrier to electron-transfer. Experimentally, such a barrier will appear as a series resistance, as has been observed for dense organic monolayers on Si and on other electrode

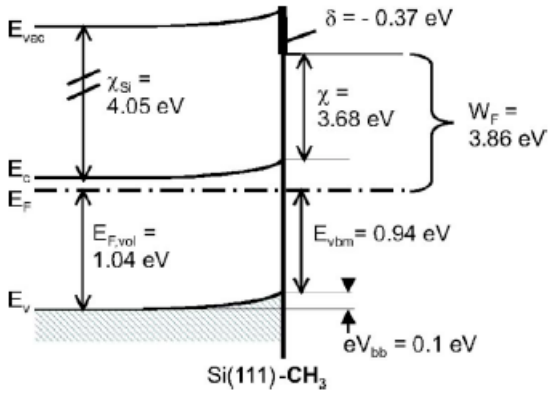

Figure 1.10. Surface energy band diagram of the CH_3-Si(111) surface.[99] The electron affinity, χ, of CH_3-Si(111) was measured at ∼3.7 eV *via* photoemission spectroscopic measurements, indicating the presence of a surface dipole, δ, of ∼400 mV. The Si is near flat-band conditions, $eV_{\rm bb} = 0.1 \pm 0.1$ eV, at the CH_3-Si(111)/vacuum interface.

surfaces.[115–118] If the dominant mechanism of electron transfer through a barrier is tunneling, the observed electron-transfer rate constant, k, should depend on the thickness of the barrier, as given by eqn.1.1

$$k = k_0 \exp\left[-\beta\left(d - d_0\right)\right] \tag{1.1}$$

where k_0 is the rate constant in the absence of a tunneling barrier, β is the materials-dependent electron tunneling constant (∼1.0 $Å^{-1}$ for saturated alkanes),[119–121] and $(d-d_0)$ is the thickness of the barrier. Interestingly, this relationship predicts that electron-transfer rates across Si-bound monolayers should also be highly dependent on the molecular identity.[53] A chain-length-dependent series resistance was observed for the photoelectrochemical systems Si(111) $C_xH_{2x+1}/Me_2Fc^{0/+}(CH_3OH)$ and Si(111)-$C_xH_{2x+1}/K_3Fe(CN)_6/K_4Fe(CN)_4$(aq) where x = 1-6.[122,123] Although the expected exponential dependence of the electron-transfer rate on chain length was not observed, it was thus suggested that solution redox couples could penetrate to some extent into the alkyl monolayers.[122] Low interfacial resistance is important for surface electrochemical stability, as well as for device efficiency. The branching ratio of Faradaic current associated with hole-transfer to Fe^{2+}, and that associated with oxidation of Si was altered by introducing a resistive interfacial element in the form of the alkylated overlayer. Ultimately, rapid anodic oxidation of the Si substrate was observed in the presence of very resistive monolayers.[122]

1.3.3 Reactivity of carbon-terminated Si

Functionalization of Si with the two-step halogenation/alkylation reaction, or through anodic deposition, can produce surfaces with short alkyl chains ($\leq C_4$). These two mechanisms, in addition to hydrosilylation and cathodic deposition of diazonium compounds, can also produce surfaces that have thicker organic monolayers. Electrochemical[122] and electro-less[86,106,110]

stability experiments with shorter chains suggest that higher coverage improves the resulting surface stability. However, electro-less experiments on longer alkyl chains ($\geq C_6$) showed that surfaces with a thicker organic monolayer are more stable.[98] These results seem contradictory, however, a higher degree of disorder is observed in short chain monolayers, such that small oxidizing agents, like water, could more easily penetrate such barriers. In this regime of oxidizing agents close to the surface, the total coverage of Si atop sites that have a kinetically stable Si-C bond is very important. On the other hand, with thicker organic monolayers, the long chain alkanes are more ordered, and are better at physically blocking oxidizing agents from the surface. These surfaces also all have nominally the same total coverage, so it is expected that the stability of such systems would increase with the overlayer thickness. A difference was also observed between stability in electrochemical and electro-less experiments. In experiments where Faradaic current is passed, the additional resistance that is imposed by an organic monolayer can affect the stability of the resulting surface.

Thermal Stability of Alkylated Silicon. The thermal decomposition mechanism, and thus the thermal stability of alkylated Si surfaces depends on the length of the alkyl chain. CH_3-Si(111) surfaces are stable up to at least 440 °C, but CH_3CH_2-Si(111) surfaces decompose at $<$ 300 °C under UHV conditions.[107,124] The thermal stability of C_xH_{2x+1}-Si(111) surfaces decreases with increasing chain length, but plateaus at $\geq C_6$.[124] Upon heating of surfaces functionalized with $\geq C_2$ to over 300 °C in UHV, Si-H moieties were observed. The suggested mechanisms of desorption included β-hydride elimination, to leave Si-H, and a minority reaction that results in C-C bond cleavage, to leave CH_3-Si.[107,124,125] These reactions were found to occur at 250-300 °C, while the subsequent desorption of the remaining CH_3-Si occurred at higher temperatures. These findings highlight the unique thermal stability of the CH_3-Si(111) surface. Under ambient pressure, heating without surface oxidation has proven difficult, and even in nominally reducing environments, Si in higher oxidation states is observed.[124]

Stability in Aqueous Conditions. When passing anodic currents across the Si/H_2O junction, a high concentration of electron-deficient sites (holes) is formed. This process, in the presence of good nucleophiles (H_2O, OH^-), leads to rapid SiO_x formation. Notably, under such conditions, Si-H terminated surfaces are extremely unstable, but Si-C terminated surfaces are remarkably stable.[122] Specifically n-CH_3-Si(111) and n-C_2H_5-Si(111) can sustain photoanodic current densities at 1 mA cm^{-2} for over 60 min in aqueous solutions with negligible change in open circuit voltage (V_{OC}) or fill factor, indicating negligible formation of surface states or SiO_x. For longer chains, $\geq C_4$, the photoelectrode performance decayed within the same 60 min time period, although the decay occurred much less rapidly than that of Si-H terminated surfaces. This behavior is consistent with the hypothesis that the additional resistance imposed by the

organic monolayer affected the branching ratio of productive to deleterious Faradaic processes, Figure 1.11. The Si-C termination not only passivated the Si surface toward oxidation, but also stabilized the band-edge positions as the pH was changed. A pH dependence of band-edge positions is a classic phenomenon observed for metal oxides in H_2O, and has also been reported for Si. It was suggested that the Si oxide protonation/deprotonation equilibrium shifts the Si band-edge positions, with pH however such shifts are minimal for Si-C terminated surfaces, and was shown to be correlated with the fraction of atop Si sites with C-termination. The reduction of $MV^{2+/\bullet+}$, a pH-independent and water soluble redox couple, at methyl terminated n-Si(111) surfaces was in fact shown to be essentially independent of pH.[126]

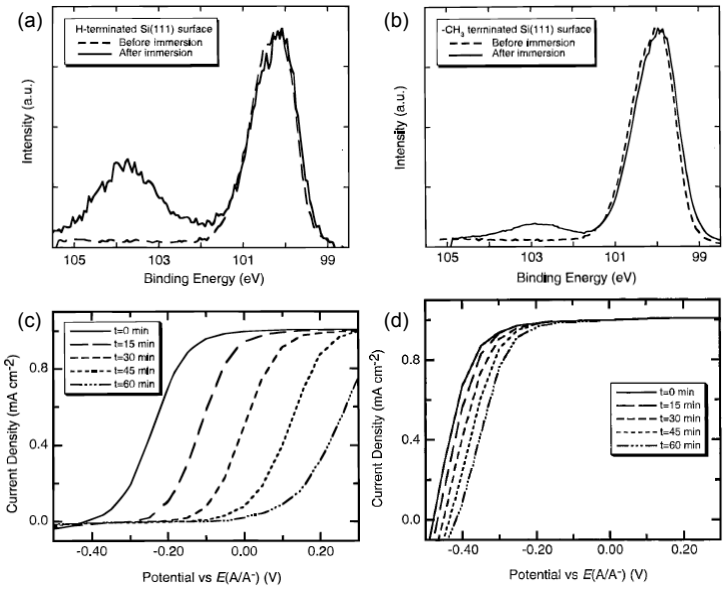

Figure 1.11. High-resolution XP spectra of the Si 2p region of H-Si(111) (a) and CH_3-Si(111) (b) surfaces before and after immersion in 0.35 M $K_4Fe(CN)_6$, 0.05 M $K_3Fe(CN)_6$ (aq) solution for 10 min.[122] the CH_3-Si(111) surface is better passivated toward SiO_x growth. Time-dependent *J-E* behavior of H-Si(111) (c) and CH_3-Si(111) (d) surfaces in contact with $Fe(CN)_6^{(3-/4-)}$ (aq) solution. *J-E* data were collected at a scan rate of 50 mV/s in a three-electrode configuration *vs* a Pt wire reference electrode poised at the Nernstian potential of the redox couple, $E(A/A^-)$.

Stability in acidic and basic aqueous conditions. Hydrogen-terminated Si is stable in concentrated acids, in the absence of oxidants.[2] C-terminated Si surfaces also exhibit good stability in aqueous acidic conditions. HREELS data has shown that surfaces functionalized with long alkyl chains *via* hydrosilylation remained intact after 7 h in 0.1 M H_2SO_4.[98] In fact, dilute solutions of acids, such as HCl(aq) and TFA in THF, are routinely used to clean Si surfaces after functionalization, or to carry out secondary functionalization reactions.[95,96,127] Organic monolayers have even been shown to stand up towards exposure to very concentrated and corrosive acids, like pH 2 H_2SO_4 for 2.5 h with no detectable oxide growth *via* XPS,[78] or boiling 2.5 M H_2SO_4 in 10% water in dioxane.[105] Additionally, the photoanodic performance of such Si surfaces was not affected by operation in pH 1.5.[126] Very concentrated acids have been observed to disrupt the Si-C monolayer. Immersion of CH_3-Si(111) surfaces in 36 M H_2SO_4, gave very low SRV while the

crystal was submerged, however, upon a second exposure to ambient air, the carrier lifetime decayed rapidly, suggesting that the monolayer had been damaged.[112]

Fluoride-containing aqueous acidic solutions are known to etch Si slowly, and have been shown to have little effect on oxide-free, Si-C terminated surfaces. The presence of silicon oxide species enabled partial removal of the Si-C monolayer, and fluoride-containing solutions were therefore used to quantify the oxidation of the silicon substrate.[78,105,115,128] Differences in monolayer characteristics have been studied by observing the effects of HF(aq) solutions on the Si substrate. C_{10}-Si(111)-functionalized surfaces synthesized *via* the chlorination/alkylation route or by photochemical hydrosilylation were more robust to immersion in NH_4F following 1 h in boiling water than those made *via* Lewis acid catalyzed hydrosilylation.[128] The increased stability was attributed to a higher surface coverage, giving denser organic monolayers in the more stable systems.

While concentrated acids are known to preserve the H-terminated Si surface, alkaline solutions are known to etch Si. Alkaline conditions have been used for secondary functionalization of Si-C surfaces, and a lack of reactivity towards OH^- was used as a means of deducing the presence of covalent linkages between alkyl groups and Si surfaces. For example, Si-C terminated surfaces have been subjected to aqueous 10% NH_4OH, to effect hydrolysis of ester-protected monolayers, without significant disruption of the surficial Si-C bond.[129] Several examples of Si-C terminated surfaces exhibiting a lack of reactivity towards base, with subsequent electronic and structural characterization detailing both the stability of the monolayer structure and the passivation of the Si surface toward oxidation, will be discussed below.

Cathodic biasing of H-terminated n-Si(111) surfaces in buffered pH 11 MV^{2+} solutions has been shown to lead to significant silicon oxide formation. In contrast, CH_3- terminated n-Si(111) surfaces displayed no electrochemical evidence of oxide-formation (Figure 1.12), and significantly less oxide formation was observed by XPS on Si-C terminated Si than on H-Si(111) surfaces.[126]

Hydrosilylated Si surfaces have shown stability to immersion in boiling 1 M NH_4OH in a 10% water/90% dioxane solution, but showed significant damage after 1 h in boiling 1 M NaOH in the same solvent mixture.[105] Organic monolayers synthesized *via* Grignard reagents or *via* photochemical hydrosilylation showed a 6% drop in the IR C-H stretching absorbtion intensity after 10 min in 2 M KOH.[128] XPS data on $C_{12}H_{25}$-Si(111) surfaces showed the growth of 0.5 ML of SiO_x after immersion in pH 13 KOH solutions, but showed almost no change in Si-C coverage, suggesting oxidation, but not etching, of the silicon.[78] An increased monolayer thickness resulted in an increase in monolayer stability in the presence of NaOH(aq). Although the monolayer remained intact after immersion in NaOH, the underlying Si was still subject to oxidation, although much less so than unprotected Si.[115] The passivating properties of Si-C

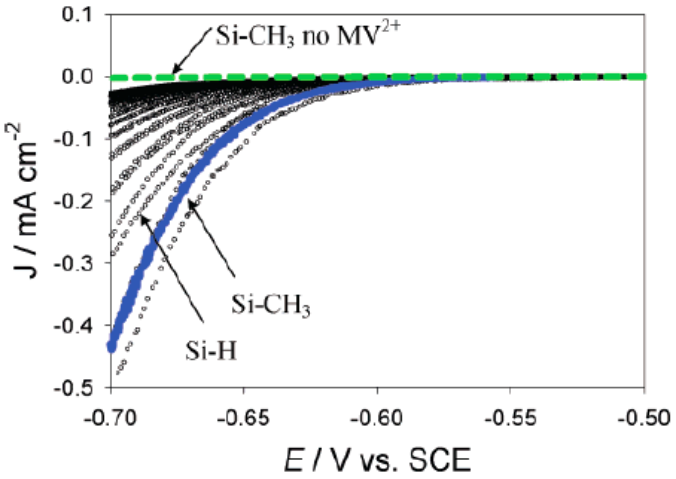

Figure 1.12. *J-E* behavior of H-Si(111) (open circles) and CH_3-Si(111) (filled circles) upon repeated cycling in the dark at 10 mV s^{-1} in contact with 10 mM $MV^{2+/\bullet+}$(aq) solution buffered at pH 11.0.[126] the dark *J-E* behavior of the CH_3-Si(111) surface in contact with aqueous solution with no MV^{2+} present is shown for comparison (dashed line).

termination also extend to porous silicon.[130] In summary, C-termination of Si atop sites impedes Si oxidation and dissolution in aqueous alkaline solutions, due to both the kinetic stability of the Si-C bond and the physical barrier presented by the monolayer.

Stability of Si-C Terminated Surfaces in Air. C-termination of Si surfaces significantly improves passivation toward SiO_x formation in ambient air compared to the behavior of H-terminated Si surfaces. For surfaces functionalized *via* a two-step chlorination/alkylation procedure, the rate of SiO_x formation correlated with increased steric bulk.[86] For example, after 12 h in air, CH_3-Si(111) surfaces had formed 0.08 ML of SiO_x, C_2H_5-Si(111) had formed 0.27 ML of SiO_x, and $C_6H_5CH_2$-Si(111) had formed 0.52 ML SiO_x. This was attributed to differences in the Si-C bond coverage on the various functionalized Si surfaces. Si-C termination has been shown to retard the rate of oxidation on a time scale of weeks.[86,110] The carrier lifetime at CH_3-Si(111) remained high, 300 ms, even after 1 month of exposure to air, despite the growth of some oxide.[112] A similar result was observed with surfaces functionalized by the reduction of aryl diazonium salts; with surfaces showing growth of 0.5 ML of SiO_x within 10 days, but no additional oxidation for greater than 6 months.[115,131] C_6H_{13}-Si(111) and C_6H_{13}-Si(100) surfaces, synthesized *via* hydrosilylation, were exposed to air for over 4 months without any detectable growth of silicon oxide *via* XPS, though the instrument sensitivity was not discussed.[132]

Multiple factors can act to impede oxide-growth. Oxidation in air has been shown to proceed inhomogeneously at surfaces functionalized via the two-step halogenation/alkylation reaction.[86] The observed oxide was mostly composed of Si^+ and Si^{3+}, with negligible presence of Si^{4+} moieties. Considerable Si^{4+} was detected at Si-H and Si-Cl surfaces within 1 day (Figure Figure 1.13). Propagation of oxidation has been hypothesized to proceed though adjacent Si-H or Si-Cl sites, so that even a moderate Si-C coverage would significantly impede long-term

oxidation to the Si^{4+} state. For surfaces functionalized with short chain alkanes, $< C_6$, it is unlikely that the resistance to oxidation in air is due to the physical blockage of oxidants or else the stability of C_2H_5-Si(111) would be improved over that of CH_3-Si(111). The disorder of short-chain monolayers, known to exist for C_2H_5-Si(111),[82] thus prevents the monolayers from acting as a significant physical barrier to reactants.

1.3.4 Silicon/organic monolayer/metal junctions

Metal silicides are produced at most metal/silicon contacts, and this holds true for most metal/CH_3-Si junctions as well. Evaporation of metals such as Au or Cu onto CH_3-Si(111) led to silicide formation and Fermi-level pinning, however, the CH_3-group slowed the formation of the silicides.[133] For Au evaporation onto a bare Si(111)-(7 × 7) surface, $SiAu_3$ formation was observed at any amount of evaporated Au. However, on CH_3-Si(111), silicide formation only occurred at $\geq$ 0.5 MLs of Au. Partial disruption of the CH_3-Si(111) monolayer was observed despite protection of the Si surface. Si/Au barrier heights remained unchanged from those observed on the pinned Si(111)-(7 × 7) surface. Very similar observations were made for Si/Cu junctions (Figure 1.14); Cu-silicide was observed on CH_3-Si(111) surfaces after $\geq$ 2 ML of Cu was deposited. Again, silicide formation was observed after any Cu deposition on the Si(111)-(7 × 7) surface. Evaporated Cu contacts on the CH_3-Si(111) surface also gave barrier heights that were identical to those of evaporated Cu on Si(111)-(7 × 7). One difference between Au and Cu evaporation was that the $SiCu_3$ remained buried at the Cu/Si interface, rather than floating atop the deposited metal film, as in the case of Au deposition.

There have been attempts to produce "softer", less destructive evaporated contacts on semiconductor surfaces. GaAs, which is also commonly limited by Fermi-level pinning, was contacted using indirect, collision-induced, cooled electron beam evaporation. This did not solve the problem of metal atom diffusion into the material, but did limit deleterious surface reactions with incoming metal atoms or clusters.[134] A second example of indirect metal evaporation on silicon was the lift-off, float-on (LOFO) technique, in which a metal film was evaporated on a glass slide. The film was under-cut through etching of the glass, to leave a very thin, floating metal film that was then transferred to a Si surface. This method could be used without apparent disruption of an octadecyl trichlorosilane self-assembled monolayer, although contact reproducibility was an issue.[135]

Hg/Si junction formation proceeds without interfacial silicide formation. Hg/H-Si(111) junctions showed barrier heights consistent with the electron affinity of Si and the work function of Hg: 0.3 eV at H-terminated n-Si(111) and 0.8 eV at H-terminated p-Si(111). Neither of these surfaces showed any evidence of reaction with Hg. Capacitance *vs.* voltage (*C*-*V*) and current-

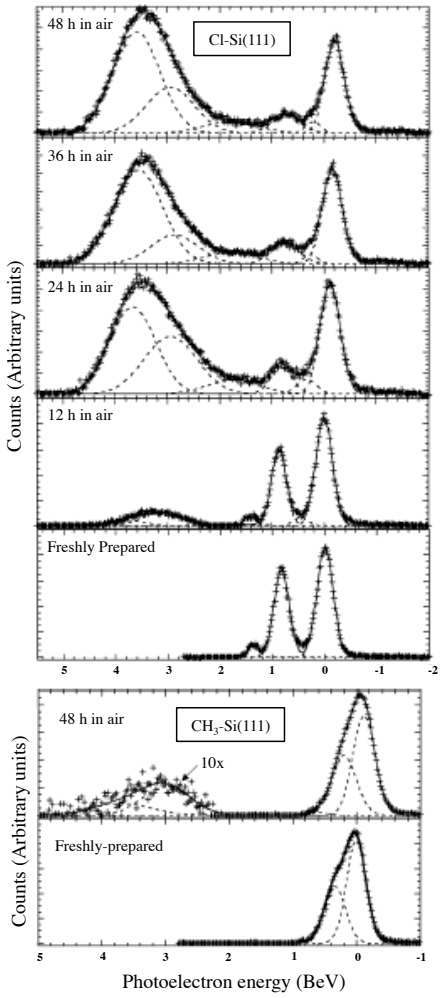

Figure 1.13. Time-dependent soft x-ray photoelectron spectra of Cl-Si(111) and CH_3-Si(111) surfaces with exposure to air.[86] Spectra are shown after background removal, spin-orbit stripping, and peak-fitting. Cross marks are raw data and dashed lines are fits. Note the appearance of oxidized Si signals after shorter exposures to lab air in the Cl-Si(111) spectra. In addition, higher oxides are observed at Cl-Si(111) surfaces than CH_3-Si(111) surfaces after exposure to air.

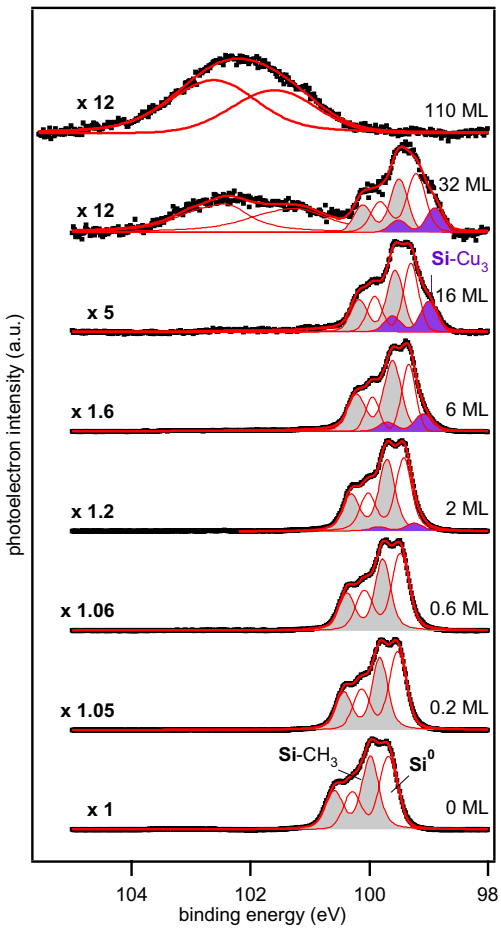

Figure 1.14. XP spectra (E_{ex} = 150 eV) of Cu deposition onto the CH_3-Si(111) surface.[133] Intensities have been scaled as indicated. Contributions from bulk Si^0, CH_3-bound surface components (CH_3-Si), and copper silicide ($SiCu_3$) are fit and noted.

density *vs.* voltage (*J*-*V*) measurements of CH_3-Si(111)/Hg junctions confirmed the presence of an interfacial dipole, of approximately 0.55 eV compared to that of H-Si(111), attributable to the CH_3-group. n-Si/Hg gave very high barrier heights of 0.91 eV, and p-Si gave practically Ohmic contacts.[53]

CH_3-termination of Si surfaces allows further freedom in Si/metal junction formation. High quality, unpinned Au/Si junctions were formed on CH_3-Si(111) surfaces though dispersion and sintering of butanethiol-capped Au nanoparticles. For H-Si, this scheme led to ill-defined interfacial reactions giving highly resistive barriers (Figure 1.15).[136] As previously mentioned, the electrodeposition of Cd and Pb on CH_3-Si(111) gave much higher solution/Si and metal/Si barrier heights, as evidenced by lowered oxidative stripping of the deposited metals. Additionally, much fewer nucleation sites are present at the CH_3-Si(111) surface relative to the H-Si(111) surface. Both Cd/Si and Pb/Si junctions formed by electrodeposition gave high barrier heights, of $\Phi_B \sim 0.8$ eV, at CH_3-n-Si(111), whereas at H-n-Si(111), the junctions gave $\Phi_B \leq 0.4$ and 0.59 eV, respectively.[114]

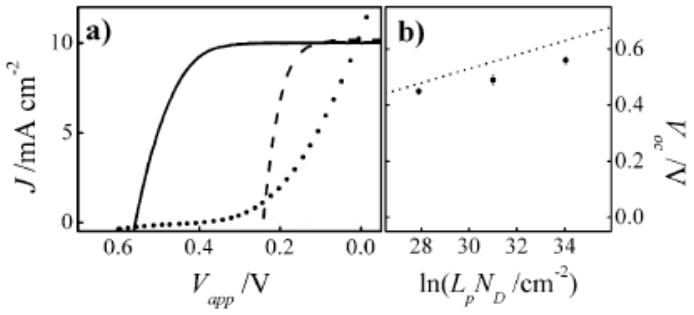

Figure 1.15. (a) *J-E* behavior for H-Si(111) (dotted line) and CH_3-Si(111) (solid line) in contact with sintered Au nanoparticles and H-Si(111) (dashed line) in contact with evaporated Au.[136]

1.4 Applications and strategies for functionalized Si surfaces

The previous three sections have explored the stability and reactivity of H-, halogen-, and C-terminated silicon surfaces. Compared to UHV-cleaned surfaces, functionalized Si surfaces exhibit remarkable stability. However, Si-based devices made today are expected to last for 10–20 years of operation in ambient conditions. Of the surfaces discussed, the only surface close to that sort of performance is the C-terminated Si surface. In this final section on Si, strategies to utilize organic monolayers on Si to further enhance the surface stability during device fabrication and operation will be discussed.

A very old technique for surface stabilization is the facilitation of charge transfer to turn over productive electrochemical events. This is the final of three surface stabilization techniques

presented in this chapter: kinetic stability of the Si-C bond, physical barrier to reactants, and facilitated charge transfer to effectively compete with surface oxidation. This section will deal with four methods to facilitate charge transfer, which in some cases, also utilizes the physical barrier method to protect against oxidation. The methods to be discussed include covalent attachment of redox active species, deposition of conductive or redox active polymers, deposition of metals, and deposition of other, nonmetallic inorganic films.

1.4.1 Tethered redox centers

Electrochemical oxidation of silicon occurs when deleterious oxidation events occur faster than the productive charge-transfer event. Facilitation of productive charge transfer can prevent electrical passivation of the Si. This behavior has been demonstrated by the tethering of a redox active center to n-type silicon. A ferrocene-derivatized silane was attached to n-Si(111), and the photoanodic performance was evaluated.[137–139] It was shown that charge transfer to $Ru(NH_3)_6^{2+/3+}$, $Fe(CN)_6^{4-/3-}$, and I^-/I_3^- could be facilitated by the bound ferrocene. Current-voltage cycling of the bound ferrocene produced nearly identical curves for 1000 cycles, whereas bare photoanodes could not produce even 1 reproducible voltage sweep. Furthermore, functionalized electrodes were stable, to within 10% of original photocurrent, for $>$ 5 h of continuous illumination with a turnover number of $> 10^5$. The photocurrent at bare electrodes decayed by $>$ 90% within 5 min of operation under anodic conditions.

In addition to bound individual redox-active species, stability enhancements have been demonstrated with polymeric-methyl-viologen-based derivatives.[140] When illuminated in solution with a redox reagent, $Fe(CN)_6^{4-}$, the poly(methyl viologen) coated n-Si electrodes exhibit enhanced stability. Coatings with a non-redox-active, but charged, backbone, derived from $(CH_3O)_3Si(CH_2)_3N^+(CH_3)_3$, also exhibited enhanced stability presumably because electrostatic binding interactions drew solution redox ions close to the electrode. In this fashion, direct charge transfer to the redox species was not inhibited, but a physical barrier blocked molecules that could undergo deleterious oxidation reactions with the underlying n-Si. In all cases, the photocurrent stability enhancement was a balance between physical barrier and charge-transport limitations.

1.4.2 Conductive polymer coatings

The previous section discussed the use of long-chain alkanes to form a physical barrier to chemical oxidants. While this could be extrapolated to longer and longer chains, it was also shown that these long chains introduce a detrimental effect on the photoelectrode efficiency, in the form of a series resistance. Therefore, thicker barriers must be conductive in order to efficiently pass charge across the interface.

The deposition of polypyrrole (PPy) on small band-gap semiconductors like n-GaAs, n-CdTe, n-CdSe, and n-CdS has resulted in improved stability under both cyclic voltammetric and continuous illumination photoanodic conditions.[141,142] Specifically, polypyrrole-coated GaAs has been shown to be stable for >100 h in methanol, whereas bare GaAs is stable under the same conditions for only a few minutes. Peeling of the polymer was a problem for these systems, and eventual oxidation was attributed to deleterious reactions at sites of peeling. The peeling was worse in water; PPy coated photoanodes were only stable for 10–20 min in water. Within that 10–20 min, an efficiency of 10.5% was achieved for the aqueous oxidation of $Fe(CN)^{3-/4-}$ under 170 mW cm^{-2} illumination.

In contact with various redox couples, PPy was also demonstrated to increase the stability of n-Si photoanodes that were coated with 5 Å of vacuum-evaporated Pt.[143,144] The initial photocurrent density was approximately 7% higher for n-Si/Pt photoanodes than for n-Si/PPy/Pt, but the performance of the surfaces that did not have a PPy coating decayed within 4 h.[143] PPy coated n-Si/Pt was continuously operated in an aqueous I^-/I_3^- cell for over 6 days, when the experiment was arbitrarily ended, Figure 1.16. Without the Pt, electrodes with PPy were stable for only a few min, and bare n-Si was stable for less than 1 min in this medium. The effects of metal deposition on stability are further discussed below. The V_{OC} observed for n-Si/Pt/PPy was 0.425 V, and varied by less than 100 mV for a change in redox potential of 1.25 eV. In contact with an acidic aqueous solution of $FeSO_4/FeNH_4(SO_4)_2$, the n-Si/PPy with no Pt was stable for 120 h, with a decline of $\sim$ 30% in photovoltage.[145] The stabilization effect has also been observed for PPy electrodeposited on amorphous, hydrogenated silicon.[146]

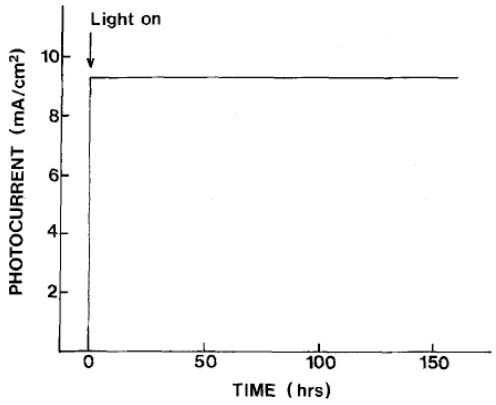

Figure 1.16. J_{SC} *vs.* time characteristics showing the photoanodic stability for n-Si/Pt/polypyrrole electrodes in contact with 0.1 M KI, 0.01 M I_2, 0.1 M KCl(aq), and illuminated at 75 mW cm^{-2} by a tungsten halogen lamp.[143] Polypyrrole was 250 monolayers thick.

Organic monolayers have been used to enhance the interfacial adhesion of PPy films on semiconductor surfaces. Electropolymerization of pyrrole was initiated at a pyrrole-functionalized silane self-assembled monolayer.[147] Films deposited onto this surface showed

enhanced stability in contact with an aqueous $FeCl_3/FeCl_2$/1 M HCl solution, and showed stable photocurrent densities of 7.8 mA cm^{-2} for $>$ 25 h. In contrast, films that were not covalently attached to the electrode surface showed a drop in photocurrent density from 6.5 to 1.8 mA cm^{-2} in less than 18 h. The increase in stability was attributed to a drastic decrease in the peeling of the films, Figure 1.17. This idea has been applied more recently to oxide-free semiconductor surfaces in which H-terminated Si surfaces were functionalized with an alkyllithium chain bearing a pyrrole. Polymer films electrodeposited at the pyrrole-functionalized surface were smoother than polymer films electrodeposited at an Si-H surface, as observed using AFM, and the diode quality factor dropped from 2.3 at noncovalently linked Si/PPy junctions to 1.5. The decrease in ideality factor is consistent with an increase in sites of contact between the Si and PPy.[148] Polythiophene derivatives have been electropolymerized at surfaces that were functionalized with a di(2-thienyl)carbinoyl obtained from the reaction of thienyl lithium with an acid-terminated organic monolayer that was formed via hydrosilylation.[148] Surface states that were suggested to dominate interfacial energetics were observed by capacitance *vs.* voltage methods. The maximum V_{OC} observed for the n-Si/polythiophene system was 390 mV. It was suggested that the low V_{OC} was attributable to film inhomogeneities, under which the current preferentially flowed through regions of low barrier height. Alternatively, adhesion and stability were improved by first depositing a Au film.[149]

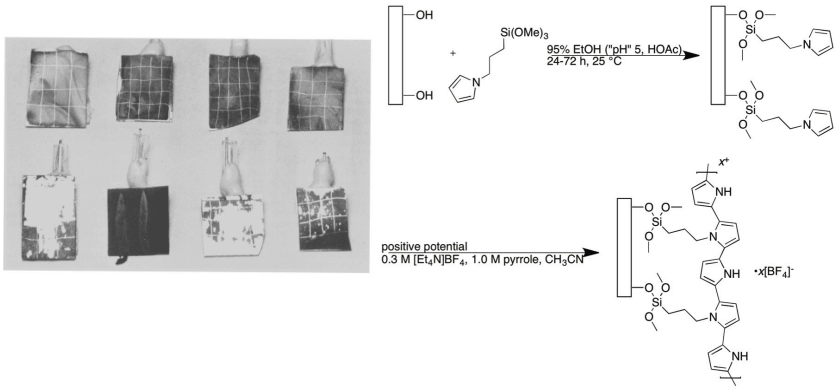

Figure 1.17. Comparison of peel-off of polypyrrole coated n-Si electrodes.[147] The top four electrodes were first modified with a pyrrole-functionalized silane (modification scheme shown at right), while polypyrrole was deposited on bare Si for the bottom four electrodes.

In addition to demonstration of enhanced photoanodic stability, conductive polymers can make highly rectifiying and Ohmic, non-Fermi-level-pinned contacts to both n- and p-Si.[150,151] Ring opening metathesis polymerization, ROMP, was used to make well-defined Si/polyacetylene (PA) junctions. PA can be doped with either K metal or I_2 to give n- and p-type PA, respectively. The exchange current density, J_0, was 6×10^{-7} and 2.4×10^{-8} A cm^{-2} at p-Si/$(CHK_{0.06})_x$ and n-Si/$(CHI_{0.17})_x$, respectively, whereas at most metals J_0 is typically on the order of 10^{-3} A cm^{-2}. Higher rectification was thus observed at Si/PA junctions than at metal/Si junctions.

n-Si/poly $(CH_3)_3$Si-COT contacts exhibited V_{OC} of up to 0.64 V.[150]

1.4.3 Metal films

Stability Enhancement. Improvement in the stability of Si and other small band-gap semiconductors has been achieved by facilitation of charge transfer through the deposition of metal overlayers on to the electrode surface.[152–154] Accordingly anodic and photoanodic stability at n-GaP, n-Si, p-Gap, and p-Si has been achieved by use of evaporated Au, Pd, or Ag films.[153,154] The devices exhibited very low V_{OC} and no dependence of V_{OC} on the redox potential of the solution, although, this could be avoided by depositing thinner metal layers without loss of the added stabilization.[152,154]

A combination of metallic and nonmetallic overlayers, such as Pt on a thin SiO_2, inhibits further electronic passivation.[152,155] At 10 Å deposition, the junction electrical properties were still determined by the contacting solution, however at 20 or 40 Å of film thickness, the interfacial energetics were dominated by the Si/Pt junction.

Deposition on Organic Monolayers. As discussed earlier, evaporation of metal, even on Si-C terminated silicon, leads to silicide formation and Fermi-level pinning at Si/metal junctions.[133] Evaporated metal penetrates -CH_3 terminated monolayers on Si.[156–159] In some cases, increasing the physical barrier to metal penetration, by increasing the monolayer chain length, has no effect.[156] Soft contacting techniques, such as sintered Au nanoparticles,[136] electrodeposition of Cd and Pb,[114] lift-off float-on (LOFO),[114] and polymer-assisted lift-off (PALO)[160] show some promise, however, recently, utilization of monolayer functionality for improved Si/metal junctions has been explored.

The morphology of evaporated films was observed to change with changes in the functionality of the monolayer.[161,162] Dithiodiacid and dithiodisilane reagents have been used to functionalize oxidized Al and Si surfaces, respectively. Evaporated Au films on treated surfaces were observed to be continuous at lower thicknesses than on bare surfaces, as determined *via* film resistivity measurements and TEM images. This behavior was attributed to interaction of incoming Au atoms with the terminating thiol groups.[161] E-beam evaporated Au films on oxidized Si surfaces treated with (3-mercaptopropyl)-trimethoxysilane exhibited a surface roughness factor of $\sim$ 2 Å over 1 mm^2 area.[162]

The interaction of terminal functionality with incoming metal atoms affords an opportunity to prevent metal penetration to the Si surface during the deposition step. ToF-SIMS has been a major tool in determination of metal penetration through monolayers *vs.* accumulation at the monolayer vacuum interface. ToF-SIMS data on Au evaporation onto CH_3 terminated monolayers on Au showed no change in the positive ion spectrum, even after deposition of 50

EL (equivalent layers or metal atoms/SAM molecule) of Au atoms.[159] Additionally, very little change was observed in the negative ion spectra, and no new ion peaks were observed. This behavior suggests that the monolayers float on top of the deposited Au.

An interaction between evaporation deposited Cu atoms and a monolayer organic functional endgroup (OFG), -C(O)OH, was observed by XPS.[163] High-resolution XP spectra of the O(1s) region showed peaks at 532.8 and 531.9 eV, representing the C(O)**O**H and C(**O**)OH peaks, respectively. After deposition of 1 nm of Cu, the region showed peaks at 531.6 and 530.8 eV, representing the C(**O**)OCu and C(O)**O**Cu, respectively.

Interactions between metal atoms and OFGs are specific. As the OFG identity is changed, the ratio of vacuum evaporated Au monolayer penetration and deposition at the monolayer vacuum interface also changes.[159] ToF-SIMS, AFM, and CPAFM have been used to analyze the extent to which monolayer penetration occurred in each system of interest. AFM images revealed that in the case of metal penetration, the structure of the Au(111) substrate was still clearly visible. If, however, the deposition occurred above the monolayer, mushroom like Au particles were observable, or a more disordered film was seen. CPAFM was used to show shorts, indicative of Au filaments spanning the monolayer with some deposition at the monolayer/vacuum interface. Less Au penetrated to the substrate when the OFG was changed from CH_3 to $C(O)OCH_3$ to C(O)OH to $C(O)O^-K^+$, Scheme 1.2. This is consistent with the expectations for the different physical barriers produced by the interactions between the metals and the different OFGs.

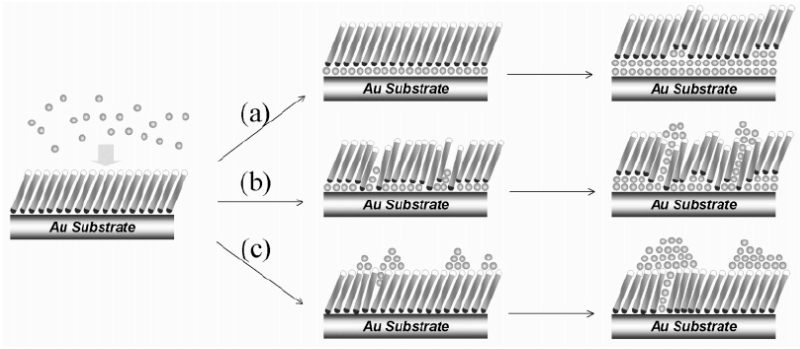

Scheme 1.2. Schematic illustration of Au behaviors on different self-assembled mono-layers (SAMs).[159] (a) Continuous, uniform penetration leading to smooth buried underlayers is seen for Au on the CH_3 and CO_2CH_3 SAMs; (b) penetration of Au to form conducting filaments with connected overlayer clusters, seen for Au on the CO_2H SAM; (c) high interaction of incoming Au with monolayer OFGs, as seen for Au on the K-modified CO_2CH_3 and CO_2H films, leads to nucleation of overlayer clusters with initial scattered penetration into the self-assembled monolayer and, at higher coverages, penetration leading to formation of scattered conducting filaments connected to overlayer clusters in mushroom-like overlayer deposits and contiguous overlayer islands.

Grazing incidence FTIR (GI-FTIR) has been used to observe the interactions between metal atoms and OFGs. Upon deposition of Au and Al onto thiol terminated SAMs, the monolayer peaks decreased in intensity, but neither a peak broadening nor a peak shift was observed, as would be expected upon disruption of the monolayer.[164] Deposition on the aryl-terminated monolayers resulted in a peak broadening and a peak shift, but without much change in

peak intensity. This behavior indicated penetration of metal atoms through the monolayer. Consistently, deposition of Ti destroyed all of the monolayers tested.

Al was observed to react with OH terminated monolayers to completion, rather than penetrating to the monolayer/substrate interface.[165] A dielectric Al layer was formed at low Al coverages. XP spectra at various deposition thicknesses showed a shift of the O binding energy, from 533.4 eV to a broadened peak at 532.6 eV, suggesting formation of an Al-O species. Additionally, at low deposition thicknesses, the Al peak was very broad, at 75.2 binding eV (BeV). At high Al thickness, a metallic peak was observed to grow in at 72.9 BeV, with retention of the nonmetallic Al-O species. IR spectra before and after deposition also showed changes in the C-O stretching frequency upon conversion from C-OH to C-OAl, and a peak assignable to Al-O species, at 850 cm^{-1}, appeared. By comparison, deposition on OCH_3 terminated monolayers showed penetration of the monolayer via observation of Al-S *via* XPS and ToF-SIMS. Interaction of different noble metals with the OCH_3 terminated monolayer was explored using ToF-SIMS, infrared reflection spectroscopy, and XPS.[157] Al penetrated the monolayer until the monolayer substrate interface was 1:1 Al/Au. In contrast, Cu and Ag continuously partitioned deposition through, and on top of, the monolayer. Au only deposited through the monolayer, and the monolayer was observed to float on top.

The J-V characteristics provide an additional indicator of the extent of monolayer penetration.[156,159] For example, Au has been evaporated onto CH_3 and SH terminated monolayers formed by hydrosilylation of Si.[159] *J-V* and capacitance-voltage measurements on the Au/monolayer/Si junctions showed similar effective barrier heights and built in potentials regardless of the nature of the OFG. Nanoscale electrical measurements *via* ballistic electron emission microscopy (BEEM) closely matched the macroscopic measurements, and threshold voltages were approximately the same across all of the samples, including evaporated films on H-terminated silicon. The current decreased by over 80% for functionalized samples, with a marked difference between CH_3 and SH terminated monolayers because of the difference in metal penetration. TEM showed much higher Au penetration for the -CH_3 OFGs, however, Au penetration of the monolayer was observed for all surface treatments.

Terminal functionality of monolayers has been utilized to facilitate other metal deposition techniques, such as transfer printing (TP) and nanotransfer printing (nTP).[166–168] These techniques utilize the interaction between a metal, for example, Au, and the terminal end of an organic monolayer, 1,8-octanedithiol on GaAs served as an early example to demonstrate transfer of an evaporated metal film.[167] By introduction of functionality to the organic monolayer, direct evaporation is avoided. Instead, the metal films are evaporated onto a treated PDMS stamp that has poor adhesion to the metal, and the films are then transferred to a surface

terminated with strongly interacting functional groups, to make the desired metal/organic monolayer/semiconductor structures. The use of TP to contact Si with Au yields a pure metal-insulator-semiconductor structure.[169] The tunneling through the monolayer was shown to be purely temperature-independent, in contrast to the behavior of Au evaporated on -SH monolayers. This method also readily forms nanoscale metal patterns with the master pattern being formed in the PDMS stamp, thus avoiding repetitive, costly lithography steps. SAMs of a thiol-terminated silane, $(CH_3)_3Si(CH_2)_3SH$, were formed on oxidized Si for the transfer of Au films to Si surfaces, Scheme 1.3.[167] nTP can make Cu contacts as well, with one additional processing step.[166]

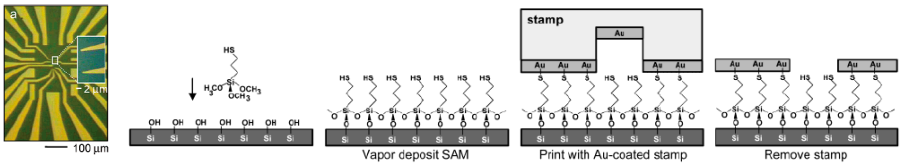

Scheme 1.3. (a) Optical micrograph of Au pattern formed by nanoscale transfer printing.[167] Scheme for creating nanoscale transfer printed Au pads on Si surfaces.

The stamp approach to contact patterning can also be used to pattern the initial monolayer.[170] In this method the stamp catalyzes hydrosilylation at the points of contact. Gold nanoparticles then deposited preferentially on the patterned monolayers. Pd nanoparticle-OFG interactions have been used to seed electro-less Ni deposition, however, the resulting junction properties very closely resembled those of evaporated Ni.[171]

Physical vapor deposition of metal on patterned monolayers consisting of more than one OFG has utilized the differential extent of monolayer penetration to pattern contacts.[158] In this method, the metal atoms deposit at the monolayer-substrate interface over a portion of the monolayer, and on top of the monolayer over the rest of the surface.

1.4.4 Semiconducting and nonmetallic coatings

Stability Enhancement. Nonmetallic coatings have been used frequently to stabilize Si under anodic or photoanodic conditions. ITO,[172,173] other doped SnO_2 films,[174] boron phosphide,[175] Thallium(III) oxide,[176] TiO_2,[177] Fe_2O_3,[178] and even silicides[179] have been used. These techniques yielded high-efficiency devices; for example, the n-Si/Thallium(III) oxide/ferricyanide electrochemical cell achieved 11.0% efficiency under natural light. An early problem was deposition of thick overlayers. For example, deposition of TiO_2 onto n-Si showed only the photoelectrochemical properties of the TiO_2.[177] Thus, methods such as ALD that can deposit thinner semiconducting films are desirable.

Deposition on by ALD. In addition to thin protective layers, ALD on Si is of interest for

transistors. The fundamental limitations on the use of SiO_2 as a dielectric in transistors cause problems for the future scale of electronics.[71] The thickness required, low k, and high leakage currents make SiO_2 not well suited for low-power applications or for the next stages of miniaturization of electronics. As low interfacial trap state densities are crucial, it would be hard create a more ideal interface than that of a well-prepared Si/SiO_2 interface, which has a typical midgap interface state density of 2×10^{10} states cm^{-2}. Most interfaces fabricated using ALD have between 1- and 2-orders-of-magnitude higher interfacial trap state density. In addition, these interfaces exhibit substantial flatband voltage shifts, in excess of 300 mV. For high-quality devices, no silicide or metal oxide phases should be at or near the channel interface, because silicide and most M-Si bonding will lead to leakage currents and low electron channel mobilities.

ALD is thus an attractive method to circumvent those difficulties with controlling the interfacial chemistry. Unfortunately, due to a lack of reactivity, ALD requires extreme conditions to yield film growth on Si-H.[180] ALD generally utilizes very high reactivity, but self-limiting, reactions for controlled material preparation. The Si-H surface simply does not have the inherent required reactivity. Long initial exposure times, of 3600 s, with H_2O, or an initial exposure to a metal precursor, TMA, for example, are thus necessary to initiate uniform growth on Si.[180] Si oxidation was observed to occur during this time, due to impurity M-OR species in the metal feed.[181] After metal binding, oxidation by H_2O was catalyzed. Oxidation during growth was more pronounced on the Si(100) face. One TMA exposure catalyzed the growth of 1.2 Å SiO_x.

Just as the evaporation of metal onto end-functionalized organic monolayers affected the extent of penetration to the substrate and the final metal film morphology, a similar effect occurs in ALD.[182,183] ALD of $Ti[N(CH_3)_2]_4$ at SAMs of alkyltrichlorosilanes with OH, -NH_2, and -CH_3 OFGs was studied as a step toward understanding the deposition of titanium nitride on organic monolayers.[183] The reaction proceeded at every temperature tested. Angle-resolved XPS was used to observe whether Ti deposition occurred at the SiO_2/SAM or SAM/vacuum interface. Deposition on CH_3 terminated monolayers penetrated to the SAM/SiO_2 interface, and partitioned to both interfaces at OH-functionalized SAMs. The NH_2 terminated SAM showed solely reactivity at the SAM/vacuum interface. Additionally, deposition rates at CH_3 terminated SAMs were severely attenuated, and islanding was observed using AFM.[96] Growth at OH and NH_2 surfaces was less attenuated, but growth was not uniform until thicker depositions were performed.

In situ and *ex situ* IR and XPS have been used to observe metal interactions with OFGs, during ALD of metallic Cu using $[Cu(sBu\text{-}amd)]_2$ as a precursor.[184] IR data showed that a carboxylic acid-terminated monolayer interacts with Cu atoms in a bidentate fashion without the formation of a SiO_x layer, Figure Figure 1.18. This work serves as a demonstration that high-

quality metallic contacts can be made to Si using ALD. Unlike deposition on H-terminated Si surfaces, Al_2O_3 can be deposited at COOH terminated monolayers on Si, without the formation of oxide.[185] TIR observation of Al_2O_3 growth showed formation of a high-quality film. The absence of any shifts or changes in the C-H region of the IR showed no disruption of the monolayer. Stringent conditions in monolayer preparation, and interaction of ALD reagents with the COOH rather than penetration to the SAM/Si interface, thus prevented formation of SiO_x species. Characteristic SiO_x vibrational modes only appeared upon heating to > 400 °C.

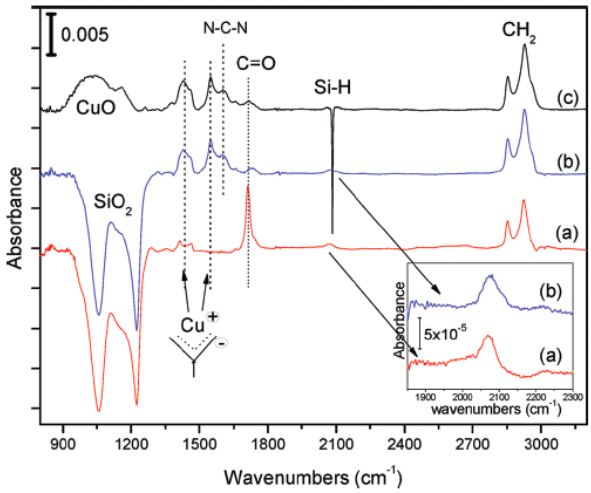

Figure 1.18. Absorption spectra of ALD deposition of Cu metal at a COOH-terminated SAM on Si.[184] (a) COOH-terminated SAM referenced to the Si native oxide; (b, c) COOH- terminated SAM with 20 Cu ALD cycles referenced to the native oxide and H-terminated surfaces, respectively.

1.5 Summary

Si-C termination renders Si surfaces much more stable to a larger range of working conditions than is observed for H- or halogen-terminated silicon surfaces. The increased stability stems from the kinetic stability of Si-C bonds and from the physical barrier imposed by a well-ordered organic film. Increased stability does not necessarily have to produce a loss of beneficial electronic properties. Beyond the stability imparted by the Si-C group, functional organic monolayers have great utility in the fabrication of advanced device structures. Classic problems with Si, including oxidation in air and Fermi-level pinning in contact with most metals, can be overcome by the clever use of organic monolayers. Global device issues such as high-cost patterning can be avoided by the use of cheaply patterned monolayers. A thorough understanding of the surface chemistry of Si thus enables the formation of well-defined, electronically preserved interfaces and, ultimately, more efficient devices in a variety of optoelectronic applications.

This thesis details the use of molecular monolayers on Si to increase stability in air and chemical functionality, and the effects of such molecular monolayers on the electronic properties

at semiconductor interfaces. Chapter 2 introduces the use of mixed alkyl monolayers on Si. Chapter 3 utilizes the mixed monolayer technique to add functionality for a surface-bound Heck C-coupling reaction. Chapter 4 explores the phenomenon of band-edge shift with surface functionality. Mixed monolayers are covalently linked to structural and conductive polymer matrices and used as ALD initiators in chapter 5.

Chapter 2

Synthesis and characterization of mixed monolayers on Si(111)

2.1 Introduction

Alkylated Si(111) surfaces have been widely investigated due to their desirable electrical properties and superior air stability relative to the H-terminated Si(111) surface.[67,186] In addition to several ultrahigh-vacuum techniques,[187,188] wet chemical methods for the formation of surficial Si-C bonds include radical-,[105,189] thermal-,[190] ultraviolet-[73] or white-light-initiated hydrosilylation;[191] metal-catalyzed hydrosilylation;[192] two-step halogenation/alkylation;[62] electrochemical;[193] and mechanochemical[194] processes. Hydrosilylation has been especially well developed,[148,195,196] facilitating incorporation of a wide range of functionalities of interest for catalysis and sensing,[195,196] as well as enabling the manipulation of surface properties and the covalent attachment of contacts.[148] Hydrosilylation cannot, however, make a surface terminated by a C_1, CH_3-Si(111), group.

The CH_3-Si(111) surface, which is readily prepared by a two-step halogenation/alkylation process, has been reported to exhibit exceptional passivation toward oxidation in ambient air,[99,112] essentially complete coverage of Si(111) atop sites,[97,197] low surface recombination velocity (S) values,[112] and a minimal barrier to electron tunneling.[53] However, due to the low reactivity of the -CH_3 moiety, facile secondary functionalization is difficult on the CH_3-Si(111) surface. Accordingly, the CH_2CHCH_2-Si(111) surface has been synthesized by a halogenation/alkylation procedure.[198–200] The CH_2CHCH_2-Si(111) surface has good passivation properties, but the total attainable coverage of functional groups is lower than that exhibited by the CH_3-Si(111) surface. Additionally, surface oxidation occurs more rapidly on the CH_2CHCH_2-

Si(111) surface than on the CH_3-Si(111) surface.[112,199] The CH_2CHCH_2-Si(111) surface does allow additional functionalization through the use of the Heck reaction or the olefin cross-metathesis reaction, but relatively low coverages of secondary functional groups are observed. For example, only $\sim 30\%$ functionalization is observed for the cross-metathesis reaction, presumably due to crowding of the allyl groups on the surface.

The use of mixed monolayers (MMs) can lead to functionalized surfaces that will undergo well-defined, high-yield, secondary functionalization reactions.[201] MMs on silicon have been produced by the attachment of long-chain hydrocarbons through hydrosilylation[124,127,202,203] and through the self-assembly of silanes on oxidized silicon surfaces.[204,205] Dilution of surface functional groups, to avoid crowding, has been achieved using both of these approaches.[124,201,204,206,207] For example, olefin cross-metathesis proceeded for only 10–15% of all surface-bound alkenes for a surface terminated with only alkenes,[207] whereas 50% of all alkenes reacted on an MM surface that consisted of a 1:1 ratio of alkenes to unreactive alkanes. Steric hindrance and cross-coupling of surface-bound species were presumed to contribute to the low amount of functionalization observed on the pure alkene monolayers.[201,206]

In this work, we describe the preparation and properties of mixed methyl/allyl monolayers on Si(111) surfaces (MM-Si(111)), Scheme 2.1. The formation of methyl/allyl MMs was confirmed using grazing-angle attenuated total reflectance infrared (GATR- IR) spectroscopy. The total surface coverage was investigated using x-ray photoelectron spectroscopy (XPS). The relative surface defect densities were investigated by surface recombination velocity measurements, and the surface oxidation over time was monitored using XPS. The goal was to prepare surfaces that had the desirable passivation and electrical properties of the CH_3-Si(111) surface while also enabling facile introduction of secondary functional groups at reasonably high coverages.

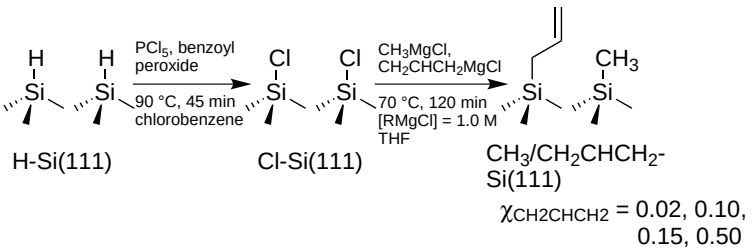

Scheme 2.1. Synthesis of mixed CH_3/CH_2CHCH_2-Si(111) surfaces by the two-step halogenation/alkylation reaction.

2.2 Experimental section

2.2.1 Materials and methods

All chemicals were used as received. Water was obtained from a Barnstead Nanopure system and had a resistivity of $\geq$ 18.2 MΩ cm. Float-zone grown n-type Si(111) wafers (Silicon Quest International, Santa Clara, CA), used for GATR, XPS, and transmission IR (TIR) were polished on both sides and had a resistivity of 63–77 Ω cm. Surface recombination velocity measurements were performed on double-side polished, high-purity, monocrystalline n-Si(111) wafers (Topsil, Santa Clara, CA) that had a resistivity of 4–8 kΩ cm. Surfaces were functionalized as described previously.[62,85,106,199]

1. Oxidation of and Removal of Organic Contaminants from Wafers. Si(111) wafers were cut to the appropriate size, 1 × 1 cm for XPS analysis and surface recombination velocity measurements, 1.5 × 1.5 cm for GATR-IR, and 1.5 × 3 cm for TIR, and were sequentially rinsed with water, methanol, acetone, methanol, and then water. The surfaces were then cleaned at 100 °C for 5 min in a piranha solution (1:3 by volume ratio of 10.1 M H_2O_2(aq): 18 M H_2SO_4). After the piranha treatment, the wafers were slowly cooled to room temperature and rinsed with water. Care was taken not to let the wafers dry during the cleaning procedure or prior to the hydrogen-termination steps.

2. Hydrogen Termination of Si(111) Samples. Atomically smooth H-Si(111) surfaces were obtained by use of one of the two following procedures: (A) The wafers were immersed for 45 s in a 6 M aqueous hydrofluoric acid (HF(aq)) solution that had been prepared by dilution of 49% HF(aq) (semiconductor grade, Transene Company, Inc., Danvers, MA). The Si(111) samples were then removed from the HF(aq), rinsed with H_2O, and immediately immersed for 10 min into 11 M NH_4F(aq) (semiconductor grade, Transene Company, Inc., Danvers, MA). The samples were removed from the NH_4F(aq) and then rinsed with water. (B) Wafers were submerged for 18 s in buffered HF(aq) (semiconductor grade, Transene Company, Inc., Danvers, MA). The samples were removed and immediately placed for 17 min in 11 M NH_4F(aq). The samples were then removed from the NH_4F(aq), rinsed with water, and quickly dried under a stream of N_2(g). In either procedure, A or B, the NH_4F solution was purged with ultrahigh purity Ar for at least 25 min prior to use. The NH_4F(aq) was continuously purged during the etching process, and agitation of the sample prevented the accumulation of bubbles on the surface of the wafer.

Both processes produced atomically flat H-terminated Si(111), as indicated by TIR spectroscopy.[10] After etching, the samples were immediately introduced into a N_2(g)-purged flush box that contained less than 10 ppm of O_2(g), unless the samples were to be investigated using TIR, in which case they were placed directly into a Fourier transform infrared (FTIR)

spectrometer.

3. Chlorination of H-Si(111). H-Si(111) samples were chlorinated by immersion into a saturated solution of PCl_5 (99.998% metal basis, Alfa Aesar) in chlorobenzene (Anhydrous, 99.8%, Sigma Aldrich) to which a small amount of benzoyl peroxide (Aldrich reagent grade, 97%, Sigma Aldrich) had been added. After heating to 90–95 °C for 45 min, the wafers were cooled to room temperature, removed from the chlorinating solution, and rinsed with chlorobenzene, followed by a rinse with tetrahydrofuran (THF).

4. Alkylation of Cl-Si(111) Samples. Immediately following chlorination, the samples were immersed in a 1.0 M alkylating solution (CH_3MgCl (diluted from 3.0 M in THF, Aldrich,), CH_2CHCH_2MgCl (diluted from 2.0 M in THF, Aldrich), or a mixture of the two) at 70–75 °C for 3 h. The alkylated samples were rinsed with THF, rinsed with methanol, brought out of the inert atmosphere box, and sonicated sequentially for 10 min each in THF, methanol, and water, or in methanol, acetonitrile, and then water. Regardless of the cleaning procedure, no Mg or Cl signals were observed on the surface by XPS.

5. Surface Oxidation. Samples used for the oxidation study (1 cm × 1 cm) were functionalized as described above. After the reaction workup, the samples were stored in lab air, in Fluoroware, in the dark. The samples were exposed to light only during transportation to the XPS chamber, which encompassed a total time of < 1 h, relative to the cumulative elapsed 4 weeks that the samples were exposed to air.

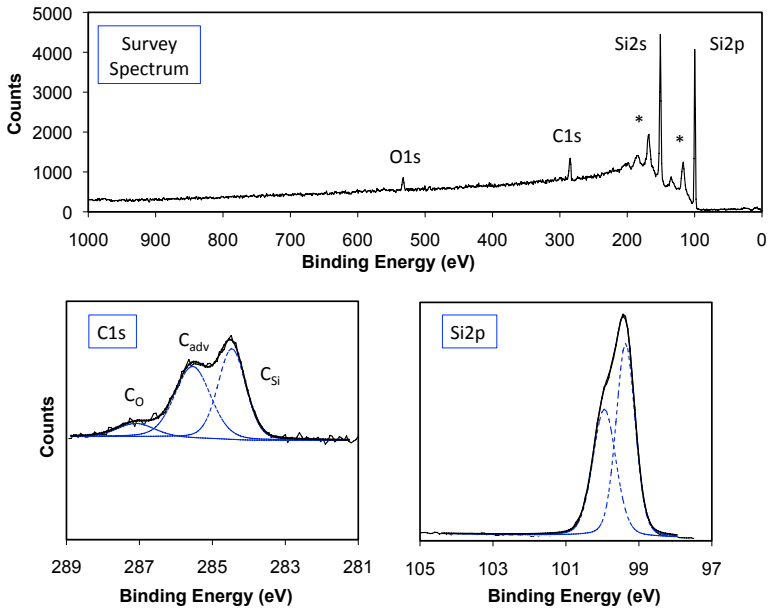

Figure 2.1. Typical M-Probe XP survey, C1s, and Si2p spectra of CH_3-Si(111). Peaks fit with a Shirley background. The C1s region was fit to C-O, adventitious C, and C-Si. The Si2p region was fit to bulk 2p($^1/_2$) and 2p($^3/_2$). No SiO_x was observed for any freshly prepared CH_3-Si(111), MM-Si(111), or CH_2CHCH_2-Si(111) surface within the resolution of the instrument. *Si phonon shake-down transitions.

2.2.2 Instrumentation

All FTIR spectra were collected using a Thermo Scientific Nicolet 6700 Optical Spectrometer that was equipped with a deuterated triglycine sulfate (DTGS) detector and a purified air purge. ATR spectra were recorded using the GATR accessory (Harrick Scientific Products, Inc.) in which samples were pressed against a hemispherical Ge crystal and illuminated at a fixed 65° incident angle. The aperture was maximized for 4 cm^{-1} resolution, and the throughput of the GATR accessory was 11.8% at 2500 cm^{-1}. Prior to mounting, the samples and the Ge crystal were cleaned with methyl ethyl ketone. The sample compartment was purged with purified air for at least 1 h before collection of spectra, and all spectra were averages of greater than 3000 consecutive scans. TIR spectra were collected by mounting the samples at a fixed 74° angle, as measured between the incident light and the surface normal. The sample chamber was purged with purified air for at least 1 h before collection of spectra. All of the reported TIR spectra represent averages of greater than 3000 consecutive scans.

XPS data were collected using a Surface Science Instruments M-Probe system that has been described previously.[78] Ejected electrons were collected at an angle of 35° from the surface normal, and the sample chamber was maintained at $< 5 \times 10^{-9}$ Torr. Survey scans from 0 to 1000 eV were performed to identify the elements present on the surface. High-resolution spectra were collected for the Si 2p and C 1s regions (Figure 2.1). The XPS data were analyzed using the ESCA Data Analysis Application (V2.01.01; Service Physics, Bend, OR). The monolayer (ML) thickness of oxidized Si was calculated as described previously.[106]

Photoconductivity decay measurements were made using a contact-less microwave conductivity apparatus.[112,199] Electron-hole pairs were generated with a 20 ns laser pulse at 905 nm using an OSRAM laser diode with an ETX-10A-93 driver. The lifetime of the excess charge carriers was monitored via the reflected microwave radiation that was detected by a PIN diode. Samples were tested immediately after workup as well as for several days after preparation. Samples were either stored in an N_2-filled glove box or in the dark in air. In both cases, the surface recombination velocity, S, stabilized over a few days, and reproducible trends were observed.

2.3 Results

Figure 2.2 depicts representative TIR spectra of the CH_3-Si(111) and CH_2CHCH_2-Si(111) surfaces. As observed previously, the CH_3-Si(111) surface exhibited a characteristic methyl umbrella mode at 1257 cm^{-1} and a CH_3 γ mode at 754 cm^{-1}, whereas the allyl-terminated Si(111) surface exhibited characteristic peaks at 3077 cm^{-1} (the =C-H stretching mode) and 1628 cm^{-1} (the C=C stretching mode).[199,202] A weak C=C-H bending mode is expected at 1420

cm^{-1}.

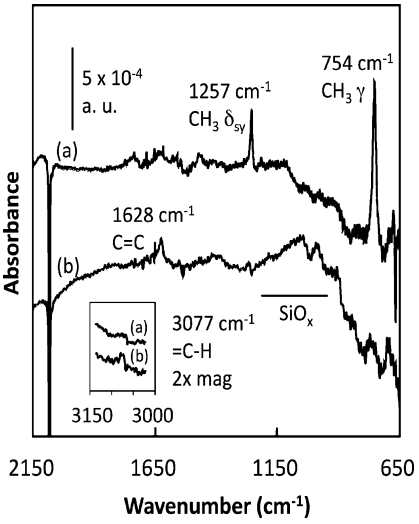

Figure 2.2. Transmission FTIR spectra of CH_3- and CH_2CHCH_2-Si(111) surfaces referenced to a H-Si(111) background. Characteristic CH_2CHCH_2- modes observed, including 3077 cm^{-1} (=C-H) and 1628 cm^{-1} (C=C) stretches. The 1257 cm^{-1} CH_3 δ_{sy} and 754 cm^{-1} CH_3 γ modes were characteristic of CH_3-Si.

2.3.1 GATR-FTIR spectroscopy

Qualitative information regarding the surface composition as a function of the composition of the reaction solution was obtained using GATR-FTIR spectroscopy. Figure 2.3 shows representative spectra of the mixed CH_3-/CH_2CHCH_2-Si(111) (MM-Si(111)) surfaces prepared from solutions that contained varying ratios of CH_3MgCl to CH_2CHCH_2MgCl, at a constant total Grignard reagent concentration of 1.0 M. The mole fraction of CH_2CHCH_2MgCl in the reaction solution, $\chi_{CH_2CHCH_2MgCl}$, was calculated as $\chi_{CH_2CHCH_2MgCl} = [CH_2CHCH_2MgCl]/([CH_2CHCH_2MgCl] + [CH_3MgCl])$. Peaks at 3077 cm^{-1} and 1628 cm^{-1}, previously assigned to the =C-H stretch and the C=C stretch of the allyl moiety, respectively,[199] were clearly observed for samples that were prepared using reaction solutions having $\chi_{CH_2CHCH_2MgCl}$ = 0.02, 0.10, 0.15, 0.25, 0.50, 0.75 and 1.00, but not for pure CH_3-Si(111) surfaces. The CH_3- umbrella mode, at 1257 cm^{-1}, was observed for CH_3-Si(111) samples, and was seen at reduced intensity for samples prepared using reactions solutions having $\chi_{CH_2CHCH_2MgCl}$ = 0.02, 0.10, 0.15, 0.25, and 0.50 (Figure 2.3). As expected, the CH_3 umbrella mode was not observed for surfaces prepared using only CH_2CHCH_2MgCl. While the absolute intensities in GATR-FTIR spectra are not useful for quantitative coverage determination, because the peak intensities are sensitive to the contact between the sample and the Ge crystal,[?] it is appears from the relative peak intensities of Figure 2.3 that the surface composition is not linearly dependent on reaction solution composition. Barring a large change in absorption cross section of the methyl and

allyl moieties with a change in surface composition, transmission FTIR spectroscopy should be useful for quantitative composition analysis. In this case, however, the vibrational modes characteristic of the allyl group are very weak. In addition, interference in the IR spectra caused by slight differences in Si wafer thickness when comparing CH_3-Si(111) to MM-Si(111) or CH_2CHCH_2-Si(111), and variation in final MM-Si(111) monolayer composition due to the variation in Grignard reagent concentrations, limited the precision with which weak signals could be quantitatively evaluated. Despite these limitations, the qualitative conclusion of transmission FTIR data (Figure 2.4) agrees with that of the GATR-FTIR data and shows that both CH_3- and CH_2CHCH_2- groups were present on the surface, and that the MM-Si(111) monolayer compositions were not linearly dependent on the solution composition.

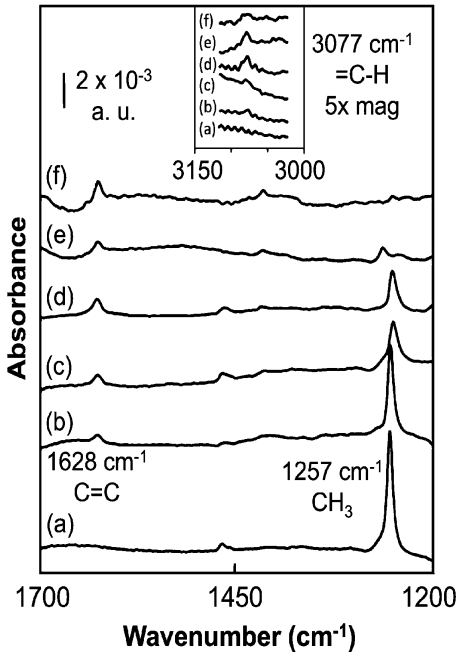

Figure 2.3. GATR-FTIR spectra of MM-Si(111) surfaces made from $\chi_{CH_2CHCH_2MgCl}$ = 0 (a), 0.02 (b), 0.10 (c), 0.15 (d), 0.50 (e), and 1.0 (f) referenced to a H-Si(111) background. CH_3- and CH_2CHCH_2- characteristic modes were observed on MM-Si(111) surfaces.

2.3.2 XPS surface-coverage measurements

Samples prepared using CH_3MgCl are known to produce a surface in which essentially all of the Si(111) atop sites are CH_3-terminated.[97] The fractional coverage of Si(111) atop sites terminated by C-bonds, θ_{C-Si}, was calculated as $\theta_{C-Si} = \Gamma_{C-Si}/\Gamma_{Si}$ where Γ_{C-Si} is the number of Si-C bonds per area unit, and Γ_{Si} is the number of Si atop sites per area unit. To calculate θ_{C-Si}, the area of the C 1s peak assignable to Si-bonded C was compared to that of a CH_3-Si(111) surface in the XPS spectra. To account for variations in absolute signal strength, all Si-bonded C signals were normalized by the Si 2p peak area observed for each sample.[106] Figure 2.5 and Table 2.1 display

$\theta_{\mathrm{C-Si}}$ obtained by this method, as a function of $\chi_{\mathrm{CH_2CHCH_2MgCl}}$. For monolayers prepared from $\mathrm{CH_2CHCH_2MgCl}$ alone, $\theta_{\mathrm{C-Si}}$ was approximately equal to 0.80. For the pure allyl surface, $\theta_{\mathrm{C-Si}}$ was, with 95% confidence, lower than that obtained for $\mathrm{CH_3}$-Si(111) or for MM-Si(111) surfaces that were prepared from Grignard solutions with $\chi_{\mathrm{CH_2CHCH_2MgCl}} \leq 0.10$. The errors in these measurements reflect a combination of differences in actual surface coverage and uncertainty in the measurements, hence for surfaces with high $\theta_{\mathrm{C-Si}}$ values the error bars may at times include values that exceed 100% coverage of Si atop sites.

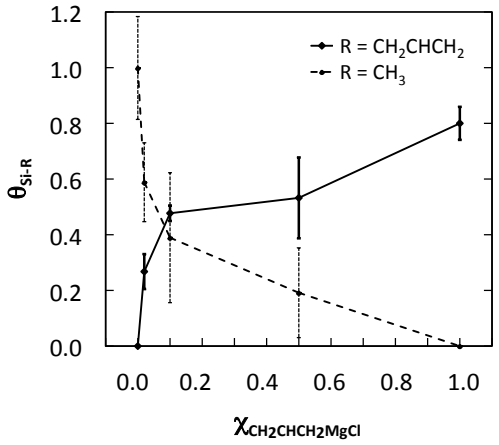

Figure 2.4. Surface composition, θ_{R} *vs* reaction solution composition, $\chi_{\mathrm{CH_2CHCH_2MgCl}}$. The fractional coverage of methyl groups, $\theta_{\mathrm{CH_3}}$, was determined by the half-peak areas of the 1257 $\mathrm{cm^{-1}}$ (δ_{sy} $\mathrm{CH_3}$ umbrella) and 754 $\mathrm{cm^{-1}}$ ($\mathrm{CH_3}$ γ) vibrational modes, and the fractional coverage of allyl groups, $\theta_{\mathrm{CH_2CHCH_2-Si}}$ = 0.8×(peak intensity MM-Si)/(peak intensity $\mathrm{CH_2CHCH_2}$-Si(111)), was determined using the 1628 $\mathrm{cm^{-1}}$(C=C) peak area. The error bars indicate ± 1 standard deviation.

Table 2.1. Summary of MM-Si(111) surface coverage.[a]

$\chi_{\mathrm{CH_2CHCH_2MgCl}}$[b]	$\theta_{\mathrm{C-Si}}$[c]
0	1.00±0.08
0.02	0.98±0.08
0.10	0.95±0.08
0.25	0.90±0.14
0.50	0.85±0.08
1.0	0.80±0.05

[a]Values ±1 standard deviation. [b]Total Grignard reagent concentration fixed at 1.0 M. [c]Quantified using XP spectroscopy with $\mathrm{CH_3}$-Si(111) as a standard of $\theta_{\mathrm{C-Si}} = 1.00$.

2.3.3 Surface recombination velocity measurements

Charge-carrier lifetimes were measured for the various MM surfaces, and the resulting lifetimes were then used to calculate surface recombination velocities and equivalent electronic defect

densities.[112] In this process, the measured excess charge-carrier density was fit to a single-exponential decay:

$$A = y_0 + ae^{-t/\tau} \tag{2.1}$$

The extracted lifetimes, τ, were converted to surface recombination velocities, S, using

$$\frac{1}{\tau} = \frac{1}{\tau_B} + \frac{2S}{d} \tag{2.2}$$

where τ and τ_B are the measured lifetime and the bulk lifetime, respectively, and d is the thickness of the Si wafer. Because τ is much less than τ_B, eq (2.2) can be simplified, yielding

$$S = \frac{d}{2\tau} \tag{2.3}$$

A consistent trend (Figure 2.6) was observed for S as a function of $\chi_{\mathrm{CH_2CHCH_2MgCl}}$. CH_3-Si(111) surfaces had consistently lower S values than CH_2CHCH_2-Si(111) surfaces, with MM-Si(111) samples having intermediate values of S.

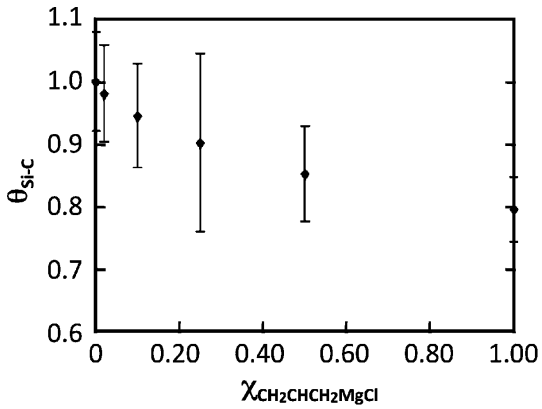

Figure 2.5. Fraction of C-terminated Si(111) atop sites, $\theta_{\mathrm{Si-C}}$, as a function of the reaction solution composition, $\chi_{\mathrm{CH_2CHCH_2MgCl}}$. Error bars represent $\pm$1 standard deviation over several ($\geq$ 4) samples.

2.3.4 Oxidation in air

The passivation toward oxidation of MM-Si(111) surfaces upon exposure to air was measured using XPS by monitoring the SiO_x peak at ∼102.5 eV. The air oxidation in the dark of MM-Si(111) surfaces was compared to that of CH_3-Si(111) and CH_2CHCH_2-Si(111) (Figure 5). After 4 weeks in air, the CH_2CHCH_2-Si(111) surface exhibited approximately 0.2 MLs of SiO_x, whereas after that same time period, the SiO_x peak observed on the CH_3-Si(111) was too small to be fit using the XPS analysis software. MM-Si(111) surfaces prepared from solutions having $\chi_{CH_2CHCH_2MgCl} = 0.02$ exhibited oxidation behavior that was essentially the same as that of the CH_3-Si(111) surface, whereas surfaces prepared from solutions having $\chi_{CH_2CHCH_2MgCl} = 0.10$ showed observable oxide after 2 weeks in air, and < 0.1 ML of SiO_x after 4 weeks in air.

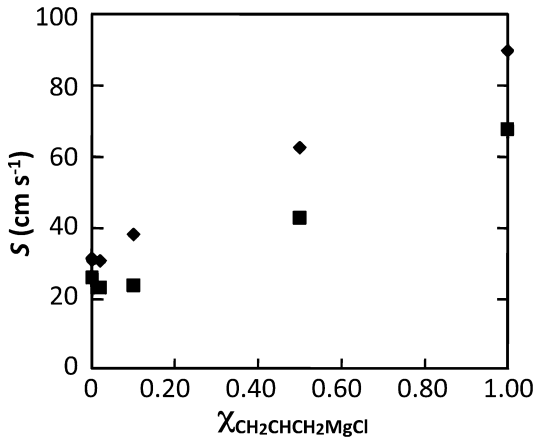

Figure 2.6. Surface recombination velocity *S vs* solution composition, $\chi_{CH_2CHCH_2MgCl}$. The value of *S* decreased with increased CH_3MgCl in the reaction solution. MM-Si(111) surfaces made from solutions having $\chi_{CH_2CHCH_2MgCl}$ = 0.02 exhibited *S* values indistinguishable from those of the CH_3-Si(111) surface although they also possessed $\theta_{CH_2CHCH_2-Si} \approx 0.30$.

2.4 Discussion

The formation of MM-Si(111) surfaces from reaction solutions having $\chi_{CH_2CH-\ CH_2MgCl} \leq 0.10$ resulted in an increase in θ_{C-Si} relative to that of the CH_2CHCH_2-Si(111) surface. On the basis of previous work, atop sites that were not terminated by an organic group are most likely to be H-terminated.[104,106]

The value of S increased approximately linearly with $\chi_{CH_2CHCH_2MgCl}$. Thus, the smallest values of S were observed for the pure methyl monolayer surfaces. However, the surface recombination velocities of the MM-Si(111) surfaces were also very low, and tended toward those of the pure CH_3-Si(111). None of the surface recombination velocities measured in this work would contribute significantly to electron-hole recombination in an actual device; however, the MM technique clearly produced surfaces with electrical recombination properties that closely resembled those of CH_3-Si(111), while allowing for incorporation of a functional group component in the monolayer. A second effect of the increase in θ_{C-Si} on the MM-Si(111) surfaces is the reduced rate of oxidation of these surfaces compared to the CH_2CHCH_2-Si(111) surface. One proposed mechanism for silicon oxidation involves H-Si(111) sites.[20?] In studies of the oxidation of alkylated Si(111) surfaces, Si-C bonds have been shown to be much more kinetically stable in air than Si-H bonds.[86] The MM-Si(111) surfaces made using solutions having $\chi_{CH_2CHCH_2MgCl} = 0.02$ showed θ_{C-Si} near 1. After 4 weeks in air, these MM-Si(111) surfaces ($\chi_{CH_2CHCH_2MgCl} = 0.02$) were indistinguishable from the CH_3-Si(111) surfaces in terms of SiO_x formation, despite having $\theta_{Si-CH_2CHCH_2} \approx 0.30$. We attribute this behavior to the higher θ_{C-Si} of the MM-Si(111) surface relative to the CH_2CHCH_2-Si(111) surface.

The composition of the MM-Si(111) surfaces obtained from the two-step chlorination/alkylation process is likely governed by the relative reaction kinetics of the CH_2CHCH_2MgCl and CH_3MgCl Grignard reagents with the Cl-Si(111) surface, rather than by steric or van der Waals interactions, or by diffusion kinetics to the surface. Both the GATR-FTIR spectra of Figure 2.3 and the transmission absorption trend of Figure 2.4 show that the surface composition is likely not linearly dependent on the composition of the reaction solution. Addition of the more bulky CH_2CHCH_2- group was observed to be preferred over that of the smaller CH_3- group, despite the higher surface strain induced by the CH_2CHCH_2- group.[197] This behavior is consistent with kinetic control of the surface composition due to the faster kinetics of the reaction of the surface with CH_2CHCH_2MgCl than with CH_3MgCl, assuming that once terminated by an organic group, Si sites are inert to exchange. Consistently, the reaction of CH_2CHCH_2MgCl with the Cl-Si(111) surface went to near completion in less than 10 min, while the reaction of CH_3MgCl with the same surface required < 30 min to approach completion.

MMs on silicon may thus exhibit benefits such as increased total surface coverage (θ_{C-Si}), superior passivation, decreased defect density, and, assuming a random distribution of functional groups, dilution of functional groups for higher-yielding secondary chemistry. A practical method to synthesize mixed allyl/ methyl monolayers with controlled composition has been demonstrated, and MM-Si(111) surfaces made from solutions having $\chi_{CH_2CHCH_2MgCl} < 0.20$ have a majority of atop sites terminated by methyl groups.

2.5 Conclusions

MMs consisting of methyl and allyl groups have been prepared on Si(111) surfaces. GATR-FTIR spectroscopy has been used to confirm the presence of both CH_3- and CH_2CHCH_2- groups on the resulting methyl/allyl-Si(111) surfaces. The total surface coverage (θ_{C-Si}), S values, and surface oxidation rates of MM-Si(111) surfaces were close to those of the CH_3-Si(111) surfaces, demonstrating that it is possible to preserve the beneficial properties of the CH_3-Si(111) while incorporating a significant fraction of functional groups to allow secondary reactivity. The procedure described herein allows for the synthesis of mixed molecular monolayers that have high total surface coverages, low surface recombination velocities, and the potential for secondary functionalization, while yielding surfaces that are not limited in composition to those based upon thermodynamic considerations from sterics alone.

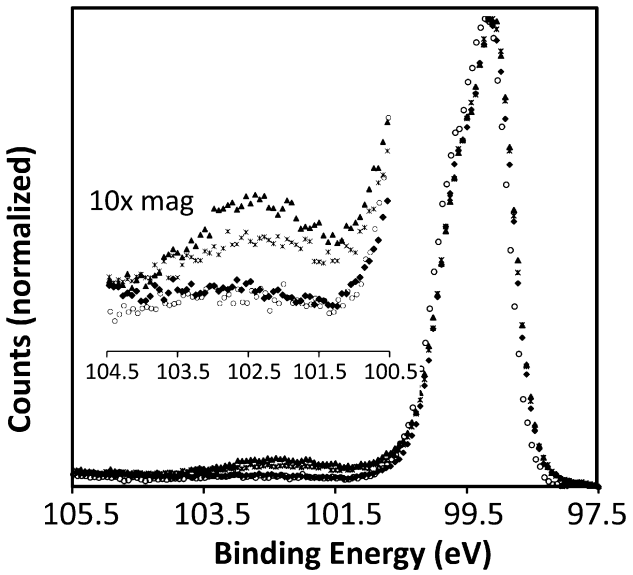

Figure 2.7. Si2p region of the XP spectrum for CH_3- (○), MM- (made from solutions with $\chi_{CH_2CHCH_2MgCl}$ = 0.02 (♦) and 0.10 (×)), and CH_2CHCH_2-Si(111) (▲) surfaces after 4 weeks exposure to ambient air. After 4 weeks, the CH_3-Si(111) surface and MM-Si(111) surfaces made from solutions having $\chi_{CH_2CHCH_2MgCl}$ = 0.02 were nearly identical with oxidation below the detection limit of the apparatus. The MM-Si(111) surface made from solutions having $\chi_{CH_2CHCH_2MgCl}$ = 0.10 exhibited less than one-third the oxidation observed on the CH_2CHCH_2-Si(111) surface.

Chapter 3

Coupling chemistry at thienyl-functionalized Si(111)

3.1 Introduction

Functionalized silicon surfaces are integral to microelectronics,[208–211] semiconductor photoelectrochemistry and photocatalysis,[123,212] and chemical and biochemical sensor technology.[196,213–215] The H-terminated Si(111) surface has a low electronic defect-state density and exhibits good interfacial electron-transfer properties in contact with liquid electrolytes that contain suitable one-electron, outer-sphere, redox couples.[1,216] However, the H-terminated Si(111) surface degrades electrically and chemically within minutes on exposure to air,[36–38,112] requires high overpotentials to effect the reduction of protons and/or of carbon dioxide at reasonable rates,[217,218] and possesses relatively little chemical selectivity, making it unsuitable for direct use in many device or sensing applications.[126,196,219,220]

Chemical modification of Si(111), specifically with methyl groups, can produce surfaces that have significantly improved properties relative to H-Si(111) surfaces.[112,123,126,136] For example, methyl-terminated Si(111) surfaces formed by a two-step halogenation/alkylation process or by an anodic functionalization route[221] exhibit superior chemical passivation properties to H-Si(111) surfaces, and also exhibit facile interfacial charge transfer and low electrical surface-state densities.[1,112] The behavior stems from the complete coverage of atop Si atoms by Si-C bonds as well as from the kinetic stability of Si-C bonds.[97,222] Methyl groups are small enough to terminate every Si(111) atop site on an unreconstructed Si(111) surface. Consistently, CH_3-Si(111) surfaces have been shown to exhibit atomically flat terraces > 200 nm in length, as evidenced by scanning tunneling microscopy (STM),[97] polarization-dependent transmission

Fourier transform infrared spectroscopy (FTIR),[100] and helium atom scattering (HAS).[222] x-ray photoelectron spectroscopy (XPS),[62,81] soft XPS,[99] scanning Auger microscopy,[86] scanning tunneling spectroscopy,[97] and surface lifetime measurements[112] have all revealed a high degree stability of the CH_3-Si(111) surface toward Si oxidation and a low density of electronic trap states over extended periods of time in air.

Although methyl groups are the only alkyl group that is sterically capable of terminating all of the Si(111) atop sites, in some applications, the presence of chemical functionality other than methyl groups would be desirable on Si(111) surfaces.[223,224] Hydrosilylation has been used to produce a wide variety of Si-C linked monolayers on H- terminated Si surfaces,[101,189] including ferrocene-functionalized electrodes,[225] layers that can support uniform atomic layer deposition,[184,185] and monolayers that enable a collection of transconduction-based chemical and biochemical sensors.[226] Hydrosilylation is a versatile method for functionalization of Si(111) surfaces, but hydrosilylation is limited to $\sim 50\%$ coverage of Si atop sites[105,132] and generally utilizes long, nonconjugated linkers. The hydrosilylation process is believed to proceed through a chain mechanism that likely leaves adjacent Si-H sites[108] susceptible to reactions that produce higher Si oxides.[86]

In more recent work, monolayers of more bulky, synthetically versatile groups have been mixed with CH_3 groups to obtain a higher total overall surface coverage of Si-C bonds.[110] In fact, mixed methyl/allyl monolayers have exhibited close to 100% atop site termination with Si-C bonds, as evidenced by independent FTIR and XPS analysis. The increased overall Si-C termination improved the oxidation resistance in air, and decreased the electrical defect state density at such surfaces. Furthermore, the higher surface coverage of Si-C bonds decreased the dependence of the Si band-edge positions on the environment, for example, on the pH of the solution.[227]

To combine the chemical inertness of complete Si-C atop site termination with the desired attribute of having versatile chemical groups on Si surfaces, one promising strategy is to perform secondary functionalization reactions on suitable mixed monolayers.[198,199] The Heck C-C bond-forming reaction[228] offers one potential approach to the preparation of such well-defined, functionalized, mixed monomolecular layers. The thienylated Si(111) surface, which has been synthesized previously and characterized via x-ray photoelectron spectroscopy (XPS), Auger spectroscopy, near-edge x-ray absorption fine structure (NEXAFS), and attenuated total reflectance Fourier transform infrared (ATR-FTIR) spectroscopy, can serve as a precursor for Heck chemistry, Scheme 3.1.[65] Previous work indicates that the Heck coupling chemistry can proceed readily on surfaces, including high-defect-density Si surfaces that have been functionalized by hydrosilylation[229,230] or self-assembled monolayers of thiols on Au

surfaces.[231–233] The remaining, non-thienyl-terminated sites on Si surfaces could in principle be terminated with Si-CH_3, to obtain the desired combination of Si-C coverage and chemical functionality. Accordingly, we describe herein the synthesis, reaction chemistry, and electronic properties of mixed CH_3/SC_4H_3 monolayers on Si(111). The aryl bromination, Pd addition, and Heck coupling reactions were monitored by XPS, and the properties of the resulting surfaces were characterized using microwave conductivity decay, grazing-angle attenuated total reflectance infrared (GATR-FTIR) spectroscopic, and electrochemical methods.

Heck coupling at mixed CH_3/SC_4H_3-Si(111) surfaces.

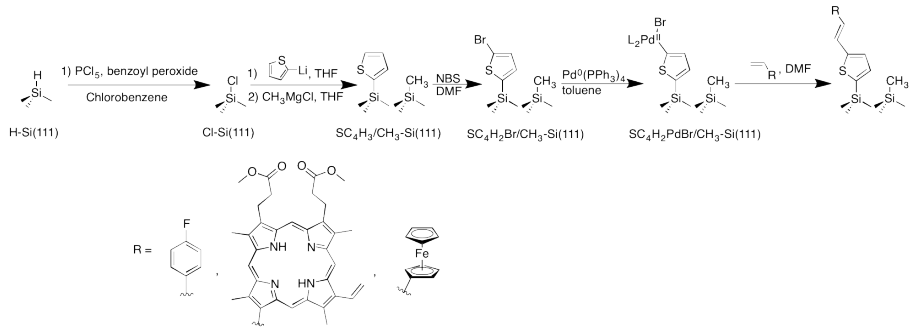

Scheme 3.1. Heck coupling at mixed CH_3/SC_4H_3-Si(111) surfaces

3.2 Experimental

3.2.1 Materials and methods

N-bromosuccinimide (NBS) was recrystallized in water, to obtain white crystals. All other chemicals were used as received. H_2O was obtained from a Barnstead Nanopure system, and had a resistivity of $\geq$ 18.2 MΩ cm. Unless specified, double-side polished, float-zone grown, n-Si samples (Silicon Quest International) had surfaces that were oriented to within $\pm$ 0.5° of <111> orientation. The samples had a resistivity of 63–77 Ω cm and a thickness of 440 $\pm$ 10 μm. Minority-carrier lifetimes were measured using high-purity, double-side polished, n-Si(111) that had a resistivity of 4–8 kΩ cm and bulk minority-carrier lifetimes, τ_{bulk}, of > 1–2 ms. Electrochemical data were obtained using single-side polished, 0.8 1.0 Ω cm resistivity, n-Si(111) samples.

1. Oxidation and removal of organic contaminants from Si surfaces. After cutting Si(111) wafers to the desired size, pieces of Si were rinsed sequentially with water, methanol, acetone, methanol, and then water. The pieces were then dried under a stream of N_2(g). Organic contaminants were removed by cleaning the Si in hot piranha acid (1:3 30% H_2O_2(aq): 18 M H_2SO_4 Caution! Piranha violently reacts with organics) followed by heating the solution to 90 °C for 10 min. The Si was then rinsed with copious amounts of water and dried (to near dryness) under a stream of

Table 3.1. Surface coverages before and after Heck coupling.

X-Si(111)	θ_{X}	Before Heck[a]		θ^{b}_{Pd}	After Heck[c]		
		$\theta_{\mathrm{Br-SC_4H_2}}$	$\theta_{\mathrm{Br-Si}}$		$\theta_{\mathrm{Br-SC_4H_2}}$	$\theta_{\mathrm{Br-Si}}$	$\theta_{\mathrm{FSty-SC_4H_2}}$
H-Si(111)	1.0	0[d]	0[d]	> 0.5	0[d]	0[d]	-[e]
Br-Si(111)	0.42±0.16	0[d]	0.42±0.16	0.06	0[d]	0.04	0.19
CH_3-Si(111)	1.0	0[d]	0.04±0.02	< 0.01	0[d]	0.03±0.02	< 0.01
CH_3/SC_4H_3-Si(111)	0.30±0.07[f]	0.15±0.03	0.05±0.01	0.12±0.02	0.06±0.02	0.03±0.01	0.11±0.03
SC_4H_3-Si(111)	0.55±0.08	0.26±0.03	0.03±0.02	0.12±0.02	0.11±0.03	0.02±0.02	0.11±0.02

[a] measured, using XPS, after exposure to NBS in DMF at 23 °C for 20 min, except for the H-Si(111) surface. [b] measured after exposure to $Pd(PPh_3)_4$ in toluene at 23 °C for 60 min. [c] measured after reaction with 4-fluorostyrene in DMF at 100 °C for 30 min. [d] species in question was not present on surface. [e] was not measured. [f] $\theta_{\mathrm{SC_4H_3}}$

N_2(g). The samples were etched (*vide infra*) immediately following cleaning with the Piranha solution.

2. Anisotropic etching to form atomically flat H-Si(111). To etch the surface, Si samples were submerged for 18 s in buffered HF(aq) (semiconductor grade, Transene Company, Inc., Danvers, MA). The solution was drained, and any excess HF(aq) was quickly rinsed away with water. The Si samples were then submerged for 9 min into an 11 M NH_4F(aq) solution that had been degassed by bubbling with Ar for $>$ 30 min. During submersion, the samples were occasionally agitated to remove bubbles from the surface of the Si. The Si samples were then removed from the NH_4F solution, rinsed with H_2O, and dried under a stream of N_2(g). Within 5 min of etching, the freshly etched Si surfaces were either placed under vacuum or introduced into a N_2(g)-purged container. A fresh buffered HF(aq) solution was used for every Si sample, and the NH_4F(aq) was replaced after $\sim$ 1 cm^2 of wafer had been etched in 5 ml of solution.

3. Chlorination of Si(111). H-terminated Si(111) surfaces were chlorinated using a saturated solution of PCl_5 (Alfa Aesar, 99.998% metal basis) in anhydrous chlorobenzene (Sigma Aldrich, 99.8%) with an initiating amount, $<$ 1 mg per 5 ml, of benzoyl peroxide (Sigma Aldrich, 97% reagent grade). The reaction solution was generally heated to 90 °C for 45 min, but the temperature and time did not exceed 95 °C and/or 60 min. The solution was then allowed to cool for 5–10 min. The Cl-terminated Si(111) samples were rinsed with chlorobenzene, followed by a rinse with anhydrous tetrahydrofuran (THF) (Sigma Aldrich).

4. Methylation and thiophenylation of Cl-Si(111). The Cl-Si(111) surfaces were alkylated at 5060 °C for $>$ 3 h in a 1.0 M solution in THF of either thienyllithium (Sigma Aldrich) or CH_3MgCl (Sigma Aldrich, diluted from 3.0 M). Mixed CH_3/SC_4H_3-Si(111) surfaces were prepared by submersion of Cl-Si(111) surfaces for 2 30 min in THF solutions of thienyllithium at 50 °C. The samples were rinsed thoroughly with THF, and then immersed into a THF solution of CH_3MgCl for $>$ 3 h at 60 °C. The composition of the mixed methyl/thienyl monolayer was controlled by varying the time of reaction, t_{rxn}, between the Cl-Si(111) surface and the thienyllithium solution. After completion of both reactions, the Si samples were rinsed thoroughly with THF and removed from the N_2(g)-purged glove box. Samples were sequentially sonicated for 10 min in each of THF, methanol, and water, and were then dried under a stream of N_2(g).

5. Bromination of surface-bound thiophene. To brominate the Si surfaces, the thiophene-functionalized surfaces (or the CH_3-terminated Si(111) surfaces in control experiments) were exposed for 20 min at room temperature to a solution of 20 mg of N-bromosuccinimide per ml of dimethylformamide (DMF). Care was taken to avoid exposing the reaction to light. After reaction, the samples were rinsed thoroughly with DMF and then with THF.

6. Pd addition and Heck coupling. To introduce Pd onto Si surfaces, Si(111) samples that had been functionalized with aryl bromides (*vide supra*) were exposed for 1 h at room temperature to a solution of 5 mg of $Pd(PPh_3)_4$ per ml of toluene. The Pd-activated samples were then rinsed thoroughly with toluene, followed by a rinse with DMF. The sample was then submerged into a 0.5 0.8 M solution of a terminal olefin in DMF. The reaction was sealed in a pressure vessel, wrapped in foil to prevent exposure to light, and heated to 100 °C for 30 min. The reaction was allowed to cool and then opened to air. The Si sample was rinsed sequentially with water, methanol, acetone, methanol, and water.

3.2.2 Characterization and electrochemistry

1. FTIR Spectroscopy. Fourier transform infrared (FTIR) spectra were collected using a Thermo Scientific Nicolet 6700 FT-IR Spectrometer that was equipped with a deuterated triglycine sulfate (DTGS) detector and a purified air purge. Attenuated total reflectance (ATR) spectra were recorded using a GATR accessory (Harrick Scientific Products, Inc.) in which samples were pressed against a hemispherical Ge crystal and illuminated at a fixed, 65°, angle of incidence. Instrument parameters were set for 4 cm^{-1} resolution. The throughput of the GATR accessory was 11.8% at 2500 cm^{-1}. Prior to acquisition of spectra, the samples were cleaned by rinsing sequentially with water, methanol, acetone, methanol, water, and trichloroethylene. The Ge crystal was cleaned with methyl ethyl ketone. All reported IR spectra represent averages of greater than 3000 consecutive scans.

2. X-ray Photoelectron Spectroscopy. X-ray photoelectron spectroscopy (XPS) data were collected using a Surface Science Instruments M-Probe system.[62] Ejected electrons were collected at an angle of 35° from horizontal, and the sample chamber was maintained at $< 5 \times 10^{-9}$ Torr. All XPS energies are reported herein as binding energies in eV. Survey scans from 0 to 1000 eV in binding energy were performed to identify the elements that were present on the surface. High-resolution XPS data were analyzed using the ESCA Data Analysis application (V2.01.01; Service Physics, Bend, OR). The thickness of a monolayer of oxidized Si was calculated as described previously.[106]

The fractional monolayer coverage, Φ_x, of a species of interest, x, was calculated using the fractional substrate-overlayer model (eqn 3.1):

$$\Phi_{ov} = \left[\frac{\lambda \sin\theta}{a_{ov}}\right]\left(\frac{SF_{Si}}{SF_{ov}}\right)\left(\frac{\rho_{Si}}{\rho_{ov}}\right)\left(\frac{I_{ov}}{I_{Si}}\right) \tag{3.1}$$

where λ is the escape depth of electrons through the overlayer, θ is the angle of electron collection from the surface (35°), a_{ov} is the atomic diameter of the atoms in the overlayer, SF_x

is the modified sensitivity factor, ρ_x is the density of species x, and I_x is the collected signal intensity. The value of a_{ov} was calculated from the density of the solid material of concern. Equation 3.1 holds when $\lambda_{ov} \approx \lambda_{Si}$. Total $\theta_{\mathrm{C-Si}}$ of CH_3-Si(111) surfaces was calculated using the intensity of the low-binding-energy C1s XP signal of C bonded to Si. $\theta_{\mathrm{C-Si}}$ of the mixed CH_3/SC_4H_3-Si(111) surfaces was calculated as the sum of the C bonded to Si C1s XP signal intensity and the S2s XP signal intensity.

The modified sensitivity factors were calculated as reported previously for the M-probe instrument used in this work.[234]

$$SF_m = SF_{\mathrm{scof}} \left[\frac{1486 - BE}{1486 - 284} \right]^{S_{\mathrm{exp}}} \tag{3.2}$$

where BE is the binding energy of the analyzed electron, 284 eV is the binding energy of C, and S_{exp} is the sensitivity exponent. For the instrument used in this work, $S_{\mathrm{exp}} = 0.6$ for high-resolution scans. Values of SF_x for other elements of interest were as follows: C 1s = 1.00, F 1s = 3.4, Br 3d = 2.84, S 2s = 1.85, Si 2p = 0.90 and Pd 3d($^5/_2$) = 9.02. The escape depths of photoelectrons were calculated from the empirical equation

$$\lambda = 0.41 a^{1.5} E^{0.5} \tag{3.3}$$

where E is the photoelectron kinetic energy in eV and a is the diameter of the overlayer atoms. The empirically determined value of $\lambda = 3.5$ nm for Si 2p electrons through long chain monolayers was used.[235–237] Using these values, $\lambda_{ov} \sim \lambda_{\mathrm{Si}}$ was a good approximation for C, S, Br, N, and Pd, but was not appropriate for F, Zn, Cu, and Co. Coverages were reported as fractions of a monolayer, θ_x, where $\theta_x = \Gamma_x \,/\, \Gamma_{\mathrm{Si(111)}}$, with Γ_x the number density of the species of interest (cm^{-2}) and $\Gamma_{\mathrm{Si(111)}}$ the number density of Si atop sites on an unreconstructed Si(111) surface, taken as $\Gamma_{\mathrm{Si(111)}} = 7.83 \times 10^{14}$ atoms cm^{-2}.

3. Photoconductivity decay measurements. Photoconductivity decay measurements were made using a contact-less microwave conductivity apparatus.[112,199] Electron-hole pairs were generated with a 20 ns laser pulse at 905 nm using an OSRAM laser diode with an ETX-10A-93 driver. The lifetime of the excess charge carriers was monitored via the reflected microwave radiation that was detected by a PIN diode. Samples were tested immediately after workup, as well as daily for several days after preparation. Between data collection, samples were stored in the dark, in air. The surface recombination velocity stabilized within a few days after preparation of the surface. For measurements taken at various reaction times, t_{rxn}, the reaction solutions were drained and the sample was rinsed with THF. Samples were then sealed in a Petri dish and removed from the glove box, to perform air-free carrier lifetime measurements.

4. Electrochemistry. Si electrodes were formed from ~ 1.5 cm^2 pieces of Si wafers. After surface functionalization, Ga-In eutectic was scratched into the back of the wafers, to produce Ohmic contacts. High-purity Ag paint (SPI supplies) was then used to fix the Si sample to a spool of tinned Cu wire. The wire was strung through a glass tube, and epoxy (Loctite 9460F) was used protect the tube entry, the wire, and the back and edges of the wafer from the solution. The epoxy was then allowed to cure in a desiccator for $>$ 24 h. Electrochemical experiments were performed in an Ar(g)-filled dry box that contained $<$ 0.3 ppm of O_2(g). Surface-bound redox species were characterized electrochemically using a Gamry Instruments Reference 600 potentiostat. A three-electrode set up was used, with a Pt mesh counter electrode, a $Ag/AgNO_3$ nonaqueous reference electrode (calibrated, 0.13 V *vs.* $Fc^{+/0}$), and a functionalized Si working electrode. The electrolyte was 1.0 M $LiClO_4$ (Sigma Aldrich, 99.99% metal basis, battery grade) in CH_3CN (passed over a column of activated Al_2O_3). Data were analyzed using the Gamry Framework version 5.61 software package.

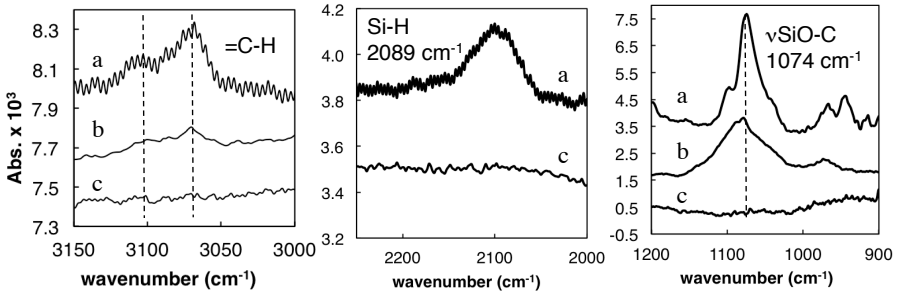

Figure 3.1. GATR-FTIR of T_3- (a) and mixed CH_3/SC_4H_3-Si(111) with $\theta_{SC_4H_3}$ = 0.54 (b) and 0.07 (c). Thienyl sp^2C-H stretching vibrations at 3067 and 3100 cm^{-1} were observed on mixed CH_3/SC_4H_3 surfaces with large $\theta_{SC_4H_3}$ and were observed yet more prominently on T_3- functionalized Si(111). Surfaces with low θ_{C-Si}, (a), showed Si-H stretching and Si-OC stretching modes, indicative of CH_3 addition during workup steps. Surfaces with high θ_{C-Si} and low $\theta_{SC_4H_3}$ did not show evidence of the methoxylation side reaction nor exhibited vibrations assignable to H-terminated Si sites.

3.3 Results

3.3.1 FTIR spectroscopy

Figure 3.1 shows the GATR-FTIR spectra of two compositionally different mixed CH_3/SC_4H_3-Si(111) surfaces, as well as the spectrum of a [2,2':5',2"-terthiophen]-5"-Si(111), T_3-Si(111), surface, all obtained *vs* a CH_3-Si(111) background. Vibrational modes characteristic of thiophene were observed in the GATR-FTIR spectra of T_3- and of high-coverage, $\theta_{SC_4H_3}$, mixed monolayer CH_3/SC_4H_3-Si(111) samples. The vibrational modes observed at 3060 and 3100 cm^{-1} are assignable to sp^2C-H stretching modes.

In addition to thiophene-derived modes, vibrational modes were observed at 1074 cm^{-1} (Si-OC stretch) and 2089 cm^{-1} (Si-H stretch). These modes (Figure 1a and b) were observed for

surfaces that had a low value of θ_{C-Si} by XPS (*vide infra*), but these peaks were not observed (Figure 3.1a) for surfaces that had high θ_{C-Si} values.

3.3.2 X-ray photoelectron spectroscopy

Figure 3.2 shows the XP survey spectra of CH_3/SC_4H_3-Si(111) surfaces through a progression of synthetic transformations of the surface functionality. The survey spectrum, as well as the high-resolution spectrum, of the CH_3/SC_4H_3-Si(111) surfaces showed signals that corresponded to the elements Si ($\sim$ 99, $\sim$ 150 eV), C ($\sim$ 284 eV), S ($\sim$ 163, $\sim$ 229 eV), and O ($\sim$ 532 eV). Br 3d peaks, at $\sim$ 70 eV, were present in spectra that were recorded after exposure of the functionalized Si surfaces to NBS. Pd 3d peaks, at $\sim$ 340 eV, were observed after exposure of brominated surfaces to the Pd(0) species. After heating the Pd-activated functionalized Si surface in a solution of fluorostyrene, the Pd signal was not detected, the Br signal was significantly diminished, and a new F peak at 687 eV was observed.

Values for $\theta_{SC_4H_3}$ were calculated from the high-resolution XPS data for all of the surfaces of interest, using the fractional substrate-overlayer model (Section 3.2.2). The reaction of thienyllithium with Cl-Si(111) reached a maximum coverage of $\theta_{SC_4H_3} = 0.55 \pm 0.08$ at 1 h reaction time. Reaction times of 2, 5, or 15 min at 50 °C produced surfaces that had $\theta_{SC_4H_3} =$ 0.05, 0.20, and 0.35, respectively.

Subsequent reaction of the thienylated Si(111) surfaces with CH_3MgCl for $>$ 3 h at 50 °C enabled the filling-in of nonfunctionalized Si surface sites with methyl groups. XPS analysis using the fractional substrate-overlayer model indicated that a high total surface coverage, $\theta_{C-Si} \geq$ 0.85, was obtained with $\theta_{SC_4H_3} \leq 0.20$.

Figure 3.3 shows the high-resolution Br 3d region of the XPS data on a variety of functionalized Si surfaces. Only low levels of Br were observed on the CH_3-Si(111) surface treated with NBS (Figure 3.3a). In contrast, NBS-exposed CH_3/SC_4H_3-Si(111) surfaces that had low (Figure 3.3b) and high (Figure 3.3c) values of $\theta_{SC_4H_3}$ and SC_4H_3-Si(111) surfaces (Figure 3.3d), exhibited Br signals that were composed of two doublets: a minor doublet that had the same binding energy as Br bound directly to Si (Figure 3.3e), and a major doublet that was shifted to higher binding energy, at 70.5 eV, indicative of an aryl bromide, as observed previously.[238] The maximum coverage of thienylbromide functionality was $\theta_{Br-SC_4H_2} \leq 0.26 \pm 0.03$. Analysis of the Br-Si signals showed that direct bromination of the Si atop sites proceeded to $\theta_{Br-Si} \leq$ 0.05 at CH_3/SC_4H_3- and SC_4H_3-Si(111). For surfaces that had $\theta_{C-Si} \geq 0.5$, control of the Br-Si side reaction was more sensitive to reaction conditions (solvent/NBS purity, exposure to light, reaction temperature) than it was dependent on θ_{C-Si}.

Figure 3.4 shows the high-resolution Pd 3d XP spectra. The high-resolution XP spectrum of

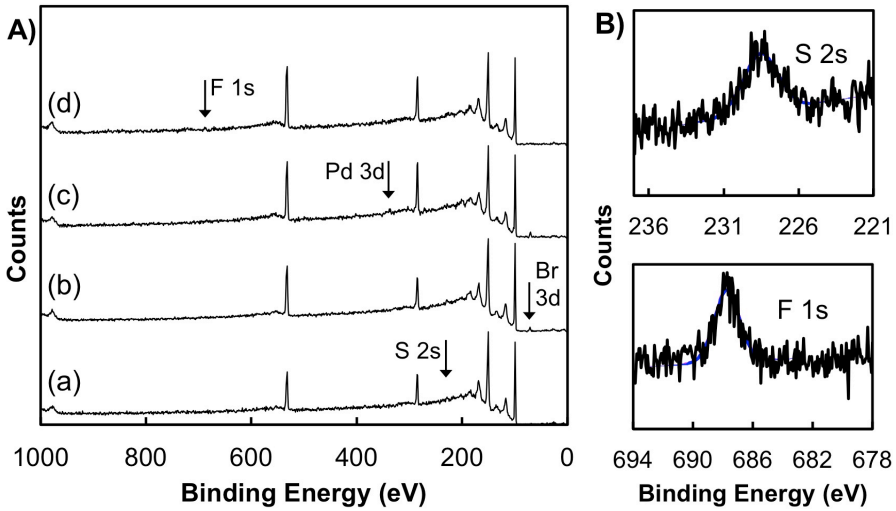

Figure 3.2. XP survey spectra of a series of CH_3/SC_4H_2X-Si(111) surfaces with $\theta_{SC_4H_3}$ = 0.24. Spectra are shown for (a) X = H; (b) X = Br, the NBS treated CH_3/SC_4H_3-Si(111) surface; (c) X = PdBr, the $Pd(PPh_3)_4$ treated CH_3/SC_4H_2Br-Si(111) surface; (d) X = FSty, Heck coupling of fluorostyrene to a CH_3/SC_4H_2PdBr-Si(111) surface. A Br 3d signal appeared at $\sim$ 70 eV for the CH_3/SC_4H_2Br-Si(111)surface, (b). The C 1s signal at 284 eV increased, and a Pd 3d signal appeared for the CH_3/SC_4H_2PdBr-Si(111) surface, (c). The C1s signal remained, a F 1s signal appeared at 689 eV, and, the Br 3d signal decreased after the complete Heck coupling of fluorostyrene to the CH_3/SC_4H_2PdBr-Si(111) surface to give the CH_3/SC_4H_2FSty-Si(111) surface, (d). (B) High-resolution S 2s and (C) F 1s spectra of the CH_3/SC_4H_2FSty-Si(111) surface are shown.

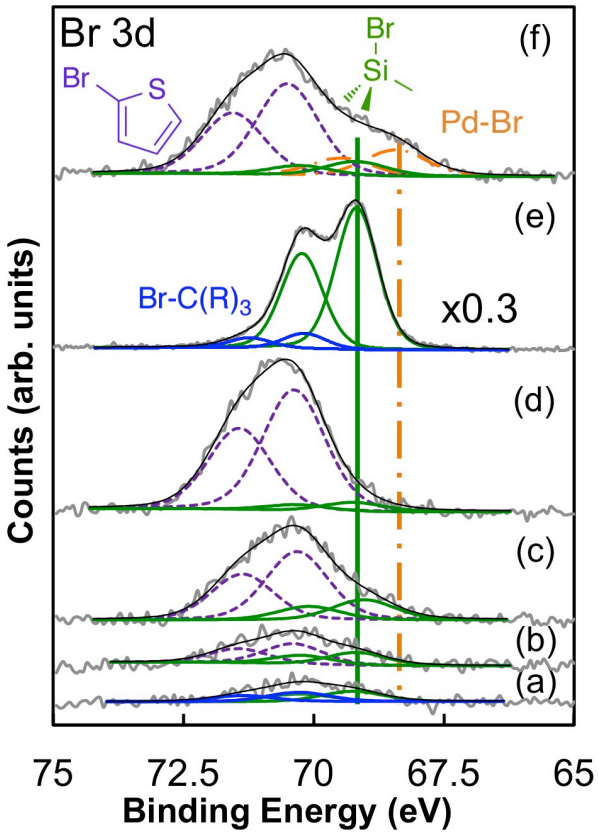

Figure 3.3. High-resolution Br 3d spectra of (a) CH_3-Si(111), (b) CH_3/SC_4H_3-Si(111) with $\theta_{SC_4H_3}$ = 0.06 and (c) with $\theta_{SC_4H_3}$ = 0.24, (d) SC_4H_3-Si(111), and (e) H-Si(111) all after bromination with NBS. The arylbromide appeared at a higher binding energy of $\sim$ 70.5 eV, as compared to Br-Si (scaled $\times$ 0.3), which exhibited a signal at a binding energy of $\sim$ 69.5 eV. With increasing $\theta_{SC_4H_3}$, the amount of arylbromide increased. Small amounts of another brominated C species were present at brominated H-Si(111) and CH_3-Si(111). (f) After addition of Pd, an electron-rich Br species appeared at a binding energy of 68.3 eV, with approximately the same coverage as Pd(II).

the Pd 3d region observed after exposure of surfaces that contained thienylbromide groups to a solution of $Pd(PPh_3)_4$ (Figure 3.4c) was consistent with expectations for oxidative addition of a Pd(0) into the aryl bromide bond yielding a surface-bound Pd(II) species, $\theta_{Pd(II)} = 0.12 \pm 0.02$. The Pd 3d binding energy of 338.2 eV is in accord with a Pd(II) oxidation state. Exposure of surfaces bearing thienylbromide groups to $Pd^{II}(PPh_3)_2Cl_2$ resulted in no detectable addition of Pd (Figure 3.4a).

Several Pd(0) sources bound nonspecifically to Si surfaces, so the choice of $Pd(PPh_3)_4$ was crucial to the subsequent Heck chemistry. Exposure of CH_3-Si(111) surfaces, before or after treatment with NBS, to a solution of $Pd(PPh_3)_4$ resulted in $\theta_{Pd(II)} < 0.01$ (Figure 3.4b). Exposure of Br-Si(111) to $Pd(PPh_3)_4$ produced spectra consistent with oxidative addition of Pd(II) (Figure 3.4e), whereas for H-Si(111), the observed Pd binding energies were indicative of Pd(0) deposition (Figure 3.4f).

After addition of Pd, the Heck reaction was used to effect the covalent attachment of 4-fluorostyrene, protoporphyrin-IX dimethyl ester, and vinylferrocene to the functionalized Si(111) surfaces. Figure 3.2 shows the high-resolution XPS data of the F 1s region of a $CH_3/FStySC_4H_2$-Si(111) surface after the coupling reaction had been performed, Table 3.1 includes a summary of coupling yields for SC_4H_3-Si(111), mixed CH_3/SC_4H_3-Si(111) with $\theta_{SC_4H_3} = 0.30$, and control surfaces. To provide a model ligand, protoporphyrin-IX dimethyl ester was coupled to mixed CH_3/SC_4H_2Br-Si(111) surfaces. Cu, Co, and Zn were also successfully coordinated to surface-bound porphyrins without excessive surface oxidation (Figure 3.5), yielding $\theta_{Cu-Por} = 0.03$, $\theta_{Co-Por} = 0.03$, and $\theta_{Zn-Por} = 0.09$ for surfaces with $\theta_{porph} = 0.04$, 0.04, and 0.09, respectively. The reactions all proceeded to completion as indicated by the lack of detectable residual Pd, as well as the observation that $\theta_{Pd} \sim \theta_{FSty}$.

3.3.3 Surface recombination velocity measurements

Surface carrier lifetimes were measured for CH_3/SC_4H_3-Si(111) surfaces that had a range of $\theta_{SC_4H_3}$, for SC_4H_3-Si(111) surfaces, and for $CH_3/FStySC_4H_2$-Si(111) surfaces that had been synthesized using the Heck coupling. The SC_4H_3-Si(111) surfaces displayed surface recombination velocity values, S, of 670 ± 190 cm s^{-1}. In contrast, CH_3/SC_4H_3-Si(111) surfaces with low $\theta_{SC_4H_3}$ values showed lower S values, with a much lower standard deviation of S, than did the SC_4H_3-Si(111) surfaces. For example, surfaces with $\theta_{SC_4H_3} \leq 0.35$ had $S < 100$ cm s^{-1} (Figure 3.7a). As $\theta_{SC_4H_3}$ increased to > 0.4, the magnitude and standard deviation of S also increased, however S remained below the values measured for SC_4H_3-Si(111) surfaces. The S values for Heck coupled $CH_3/FStySC_4H_2$-Si(111) surfaces were $S = 70 \pm 10$ cm s^{-1} (Figure 3.7b).

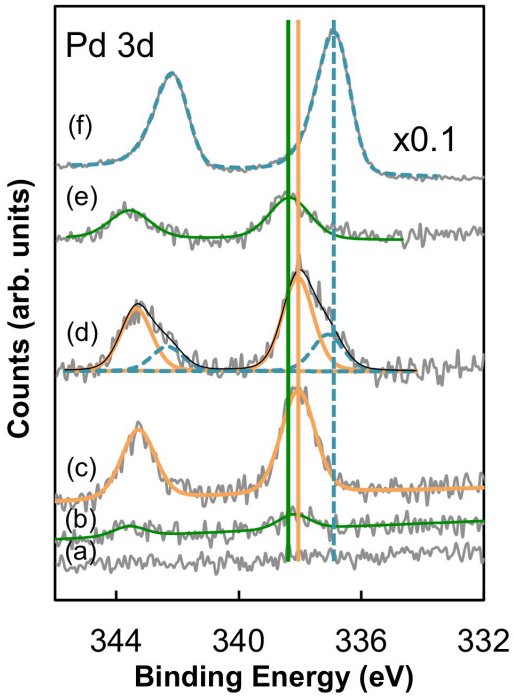

Figure 3.4. High-resolution Pd 3d XP spectra for exposure of the (a) CH_3/SC_4H_2Br-Si(111) surface to $Pd^{II}(PPh_3)_2Cl_2$, (b) CH_3-Si(111) surface to NBS followed by $Pd(PPh_3)_4$, (c) CH_3/SC_4H_2Br-Si(111) surfaces exposed to $Pd(PPh_3)_4$, (d) SC_4H_3-Si(111) surface to $Pd(PPh_3)_4$. Although treatment of the brominated thiophene surface, CH_3/SC_4H_2Br-Si(111), to Pd(II), $Pd^{II}(PPh_3)_2Cl_2$, (a) resulted in no detectable addition of Pd, treatment with Pd(0), $Pd(PPh_3)_4$, (c) yielded Pd(II) on the surface. The SC_4H_3-Si(111) surface treated with $Pd(PPh_3)_4$ (d) shows an asymmetric Pd peak indicative of Pd binding in a similar fashion to that observed on H-terminated Si(111) in (f). The addition of $Pd(PPh_3)_4$ to Br-Si(111) (e) terminated at $<$ 0.1 monolayer, whereas large, low binding-energy , Pd 3d signals were observed on H-terminated Si(111) surfaces (f).

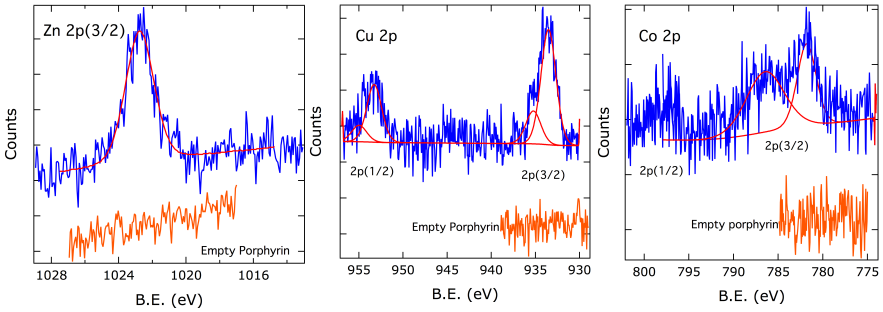

Figure 3.5. High-resolution XP spectra after metal complexation of surface-bound protoporphyrin-IX dimethyl ester, yielding θ_{M} = 0.09 Zn, 0.03 Cu, and 0.03 Co 2p($^3/_2$) with θ_{porph} = 0.09, 0.04, and 0.04, respectively.

For CH_3-MgCl and SC_4H_3-Li functionalization reactions at Cl-Si(111), air-free photogenerated carrier lifetimes were measured as a function of t_{rxn} (Figure 3.8). S increased rapidly, then slowly decreased with t_{rxn} for both CH_3- and SC_4H_3- functionalization. After completion of the reaction, t_{rxn} = 600 min, S continued to decrease for SC_4H_3-Si(111) surfaces for days after workup; however, S of CH_3-Si(111) surfaces remained consistent after reaction workup.

3.3.4 Electrochemistry of bound ferrocene

The reduction and oxidation of a ferrocene, bound to the Si surface *via* Heck chemistry, was investigated by cyclic voltammetry. Compared to the formal potential observed for dissolved ferrocenium/ferrocene (E = -0.13 *vs* $Ag/Ag^+(CH_3CN)$), the ferrocene-functionalized Si surfaces exhibited a redox wave at E = 0.05 V *vs* $Fc^{+/0}$, indicating that the thiophene linker had little effect on the electrochemical potential of the bound ferrocene species (Figure 3.6). Figure 3.9 shows the peak cathodic current at a ferrocene-functionalized n-Si(111) electrode *vs* both the scan rate and the square root of the scan rate in the cyclic voltammetry. The peak cathodic current was linear with the scan rate, indicative of a surface bound, rather than diffusing, redox-active species.

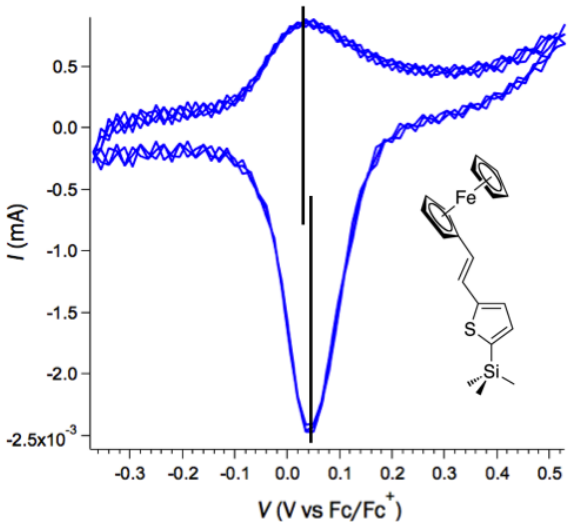

Figure 3.6. Cyclic voltammogram of vinyl ferrocene modified n-Si, θ_{Fc} = 0.12. 1.0 M $LiClO_4$ in acetonitrile, 2500 mV s^{-1}. The asymmetry is due to the electron transfer dynamics at nondegenerately doped semiconductor electrodes. The small splitting, 0.01 V, between the potentials where the cathodic and anodic currents exhibited peaks suggests facile electron transfer through the conjugated linker.

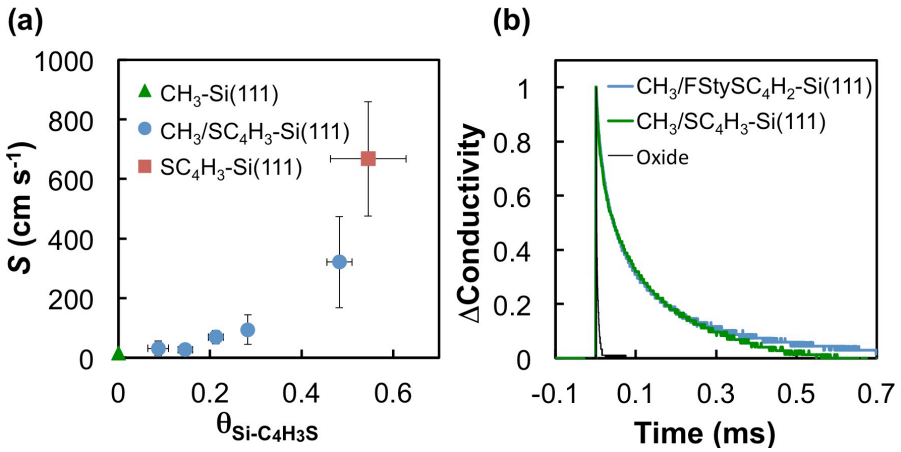

Figure 3.7. (a) Surface recombination velocity, *S*, as a function of thiophene coverage, $\theta_{SC_4H_3}$. The error bars presented represent $\pm$ 1 standard deviation. The value of *S* for $\theta_{SC_4H_3} < 0.2$ was indistinguishable from that for CH_3-Si(111), θ_{CH_3} = 1.0. As $\theta_{SC_4H_3}$ for the CH_3/SC_4H_3-Si(111) surface increased toward that of SC_4H_3-Si(111), *S* increased, as did the standard deviation. SC_4H_3-Si(111) surfaces exhibited large and variable *S* values. (b) Carrier lifetime decay curves for native oxide (black), CH_3/SC_4H_3-Si(111) with $\theta_{SC_4H_3}$ = 0.15 (green), and for the same surface after the coupling of fluorostyrene via the Heck reaction (blue), indicating little change in *S* values before and after this secondary chemistry was performed.

3.4 Discussion

3.4.1 Heck coupling at Si(111) surfaces

The data indicate that the Heck reaction can provide a robust, facile, and nondestructive method for the coupling of terminal olefins to aryl-bromide-functionalized Si(111). A small organic molecule (fluorostyrene), a larger heterocycle (protoporphyrin-IX dimethyl ester), and a redox active molecule (vinylferrocene) were all successfully coupled to Si(111) surfaces using this approach. Starting from a mixed monolayer CH_3/SC_4H_3-Si(111) surface, the aryl groups were brominated with NBS, a common brominating agent, followed by transmetallation using $Pd(PPh_3)_4$. Both the aryl-bromide-functionalized surface and the Pd-functionalized intermediate surface were stable, the Pd-catalyzed C-C bond formation proceeded to completion, and no trace Pd was observed by XPS after the coupling step.

The Heck-based secondary functionalization chemistry of Si(111) surfaces tolerated a broad scope of substrates, yielded clean reactions with no detectable residual Pd by XPS, and resulted in a functionalized Si surface that had a low electronic defect density. Unlike an olefin metathesis method, the Heck reaction does not have unproductive turnover events that could be a limiting factor in the attachment of large molecules at a surface.[199,239,240] Furthermore, the Heck chemistry allows for the possibility for complete conjugation from the electrode surface to a surface-bound, redox active species.

With an observed coverage of $\theta_{SC_4H_3} \geq 0.15$, and considering that the van der Waals radius of the olefinic substrate is less than that of the bound Pd species, Si-thienyl-$Pd(PPh_3)_nBr$, a generic terminal olefin C=C can thus be coupled to CH_3/SC_4H_3-Si(111) with maximum of $\theta_{C=C}$

= 0.15. This coverage compares favorably to the observed average coverage of $\theta_{C=C} = 0.11 \pm 0.02$, as shown in Table 3.1. The average coverage of protoporphyrin-IX dimethyl ester was lower than that of fluorostyrene or vinylferrocene, with $\theta_{porph} = 0.07 \pm 0.03$, likely due to its larger size.

Under the reported reaction conditions, the terminal olefin coupling step did not appear to proceed through hydrosilylation. Specifically, the coupling of olefins was not observed when CH_3/SC_4H_2Br-Si(111) surfaces were not first exposed to $Pd(PPh_3)_4$. Furthermore, the UV-initiated hydrosilylation of fluorostyrene at CH_3CH_2-Si(111) surfaces, which exhibited $\theta_{CH_3CH_2-Si} = 0.75$ and $S_{CH_3CH_2-Si} = 61$ cm s^{-1}, yielded a mixed CH_3CH_2/FSty-Si(111) that exhibited $S > 650$ cm s^{-1}. Additionally, $\theta_{FSty} \approx (\theta_{Br-SC_4H_2(Before)} \quad \theta_{Br-SC_4H_2(After)}) > \theta_{Br-Si}$.

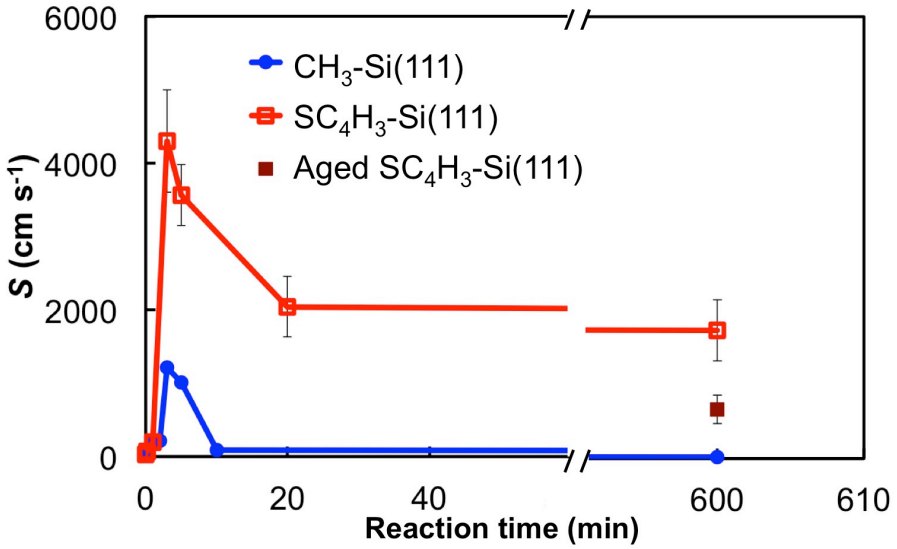

Figure 3.8. *S* emphvs t_{rxn} for the reaction of thienyllithium (red open squares) and CH_3MgCl (blue circles) with Cl-Si(111) surfaces as measured in an air-free, contact-less microwave conductivity apparatus. Initial Cl-Si(111) surfaces had $S < 50$ cm s^{-1}. The value of *S* rapidly increased at short t_{rxn}, then gradually decreased with reaction progress. The value of *S* of surfaces formed by reaction with thienyllithium were much higher than those formed by reaction with CH_3MgCl, even after completion of the reactions. The value of *S* of SC_4H_3-Si(111) surfaces further decreased after workup (filled red square).

3.4.2 Formation of surface-bound aryl bromide

NBS was used to transform surface-bound aryl groups to the synthetically versatile aryl halide groups. For CH_3/SC_4H_3-Si(111) mixed monolayers that had $\theta_{SC_4H_3} < 0.2$, nearly 100% yield of conversion of thiophene to bromothiophene was observed. A maximum of $\theta_{Br-SC_4H_2} = 0.26 \pm 0.03$ was obtained, on SC_4H_3-Si(111) surfaces.

NBS was required because direct attachment of bromothiophenes to H-Si(111) by use of 4-bromothienyllithium at room temperature and above led to formation of multilayers, and no reaction occurred at -77 °C. NBS has been used as a halogenating agent for H-Si(111),[65,241,242] but treatment of thiophene-functionalized surfaces with recrystallized NBS under rigorously

anhydrous conditions, in conjunction with exclusion of light and control of time and temperature (< 25 °C), limited the formation of Br-Si surface species to $\theta_{\mathrm{Br-Si}} < 0.05$. Specifically, after 20 min of reaction time with NBS, $\theta_{\mathrm{Br-SC_4H_2}}$ did not increase, but $\theta_{\mathrm{C-Si}}$ decreased and $\theta_{\mathrm{Br-Si}}$ increased, indicating the onset of side reactions.

3.4.3 Pd(II) intermediate and addition parameters

Transmetallation, resulting in a surface-bound Pd(II) species, proceeded readily at Si(111) surfaces that possessed bromothiophene groups. Accordingly, exposure of CH_3/SC_4H_2Br-Si(111) surfaces to a solution of $Pd(PPh_3)_4$ yielded a Pd-bound intermediate surface. The XPS data for the $BrL_nPd(II)$-SC_4H_2-Si(111) intermediate surface confirmed the Pd oxidation state as Pd(II), with Pd signals observed at a binding energy of 338.2 eV (Figure 3.3f). Further evidence of oxidative addition was the observation of a Br XP signal at 68.4 eV (Figure 3.4c), i.e., at a binding energy close to that of Br , and shifted from the 70.42 eV signal that is associated with Br bonded directly to the thiophene ring (Figure 3.3d). Toluene, THF, and CH_2Cl_2 were suitable solvents for the transmetallation. The P XPS signal of the PPh_3 ligands was obscured because the dominant P signals overlapped with the core-electron Si binding energies and with the Si phonon loss modes.

The success of the reaction steps depended significantly on the use of pure $Pd(PPh_3)_4$ as the Pd source. Other Pd sources, such as $Pd(dba)_2$ and $Pd_2(dba)_3$, or even low purity $Pd(PPh_3)_4$, added nonspecifically to the surface or resulted in uncontrolled Pd multilayer formation, even on CH_3-Si(111) surfaces.

In contrast to the oxidative addition observed for SC_4H_2Br-functionalized Si surfaces, SC_4H_3-Si(111) surfaces exhibited nonspecific binding of Pd(II). However, the Pd XP signal shape on such surfaces was distinct from the symmetric Voigt shape that was observed after the addition of Pd to surfaces that had arylbromide groups (Figure 3.4c). The asymmetric peak shape was well fitted by two Pd signals, one indicative of oxidative insertion of Pd at Si-H, and a second signal indicative of Pd(0) addition. The lower binding energy Pd XP signal, observed at both $Pd(PPh_3)_4$-exposed SC_4H_3-Si(111) (Figure 3.4c) and H-Si(111) (Figure 3.4f) surfaces, was shifted by -1.3 eV in binding energy from the main Pd signal. The data are consistent with a process in which Pd addition at SC_4H_3-Si(111) surfaces proceeded at the H-terminated Si sites in a similar fashion to reaction with the H-Si sites on a pure H-Si(111) surface. The absence of the lower binding energy Pd peak for Pd-treated SC_4H_2Br-Si(111) or mixed CH_3/SC_4H_2Br-Si(111) surfaces indicated that in such systems, the addition of Pd did not occur through the H-terminated sites.

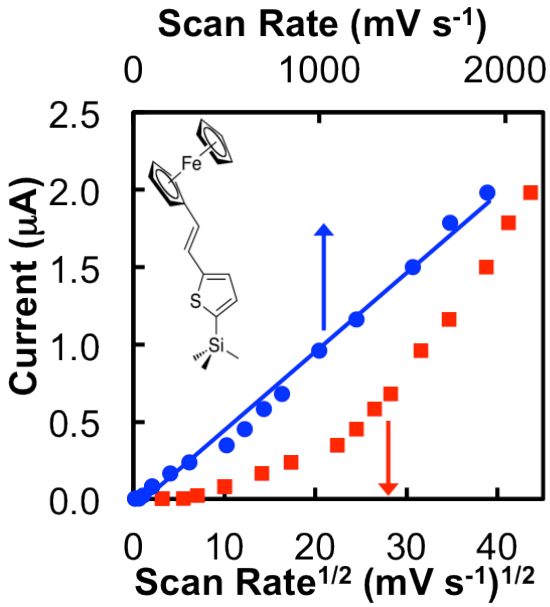

Figure 3.9. Current, $i_{p,c}$, *vs.* scan rate (blue circle) or scan rate$^{1/2}$ (red square) for ferrocene bound to Si(111) *via* the Heck reaction. The relation was linear with scan rate, not with the square root of the scan rate, confirming that the redox-active species was nondiffusive and thus bound to the surface.

3.4.4 Electronic defect density

The low S values for CH_3/SC_4H_3-Si(111) and for $CH_3/FStySC_4H_2$-terminated Si(111) surfaces that were synthesized *via* the Heck coupling process indicated that the synthetic transformations described herein did not result in significant trap states densities on the final functionalized Si surfaces. The surface electronic defect density that was observed before the Heck coupling depended strongly on the coverage and composition of the overlayer on the Si surface. SC_4H_3-Si(111) surfaces exhibited a low total Si-C coverage of $\theta_{SC_4H_3} = \theta_{C-Si} = 0.55 \pm 0.08$, and showed high, and largely variable, surface recombination velocities, with $S = 670 \pm 190$ cm s^{-1} (Figure 3.5). In contrast, mixed CH_3/SC_4H_3-Si(111) surfaces, which exhibited $\theta_{SC_4H_3} < 0.2$ and high $\theta_{C-Si} > 0.85$, showed $S = 27 \pm 9$ cm s^{-1}. The S values of mixed CH_3/SC_4H_3-Si(111) surfaces with $\theta_{SC_4H_3} < 0.2$ and $\theta_{C-Si} \geq 0.85$ were indistinguishable from those of the CH_3-Si(111) surface. The mixed monolayer technique therefore allows utilization of thiophene functionalization for photovoltaic or photoelectrochemical applications, despite the extremely low surface carrier lifetimes of SC_4H_3-Si(111) surfaces.

The effective trap state density, N_t, can be calculated from the surface recombination velocity, S, using the relation

$$S = \sigma \nu_{th} N_t \tag{3.4}$$

where $\sigma \approx 10$–15 cm^2 is the trap-state capture cross section, and $\nu_{th} \approx 10^7$ cm s^{-1} is the thermal velocity of charge carriers.[1] For a surface with $\theta_{SC_4H_3} = 0.1$, i.e., 1 thiophene per 10 surface

sites, and having a value of $S = 20$, the effective trap state density is $N_t = 2 \times 10^9$ cm^{-2}, i.e., 1 electronic trap site per 500,000 surface sites.

The chemical nature of the nonfunctionalized Si sites dictates the ability of those sites to act as electronic trap states, or to participate in further chemical reactions to produce electronic trap states. A high θ_{C-Si} thus correlated strongly in this work with surfaces that had low values of S.

However, t-butyl-functionalized Si(111) surfaces, with $\theta_{C-Si} = 0.42$, exhibit $S < 100$ cm s^{-1}.[106] The difference between S for the SC_4H_3-Si(111) surface and S for the t-butyl-terminated Si(111) surface, which exhibits similar θ_{C-Si},[106] could arise from differences between functionalization of Si with R-MgX relative to functionalization with R-Li. In small molecules, CH_3-Li is known to break Si-Si bonds,[243–245] and on a surface this process would initially produce dangling Si bonds. However, no change in S was observed for mixed CH_3/SC_4H_3-Si(111) surfaces that were synthesized with CH_3Li rather than with the CH_3-MgCl Grignard reagent.

At very short t_{rxn}, 0 sec $\leq t_{rxn} < 30$ sec, in the absence of exposure to air, the mixed Cl/CH_3-Si(111) surfaces and Cl/SC_4H_3-Si(111) surfaces both exhibited low S values (Figure 3.7). A large electronic trap state density has been observed at Cl-Si(111) surfaces,[79] however, a large field has also been shown to be present at the surface.[89] Because the surface field will separate photogenerated electrons and holes to preclude recombination, the low S value of the Cl-Si(111) surface is therefore expected, despite the large density of electronic trap states on such surfaces.

As the surface functionalization progressed, the value of S increased, consistent with a diminished surface field and incomplete passivation of the electronic trap states. As the reaction progressed, S quickly reached a maximum, and then slowly decreased. At completion of the reaction of CH_3MgCl with Cl-Si(111), 100% of the surface atop sites were terminated with Si-C bonds, and the CH_3-Si(111) surface exhibited a very low S. The S of SC_4H_3-Si(111) surfaces did not improve to that of CH_3-Si(111) because of the low filling fraction, $\theta_{C-Si} = 0.55 \pm 0.08$, as well as the presence of residual Cl-terminated sites. Unlike C_2H_5- and t-butyl-Si(111) surfaces with low S, some chlorinated sites remained on the SC_4H_3-Si(111) surfaces, as observed by XPS. The difference between the two types of surfaces is consistent with the observation of β-hydrogen transfer at aliphatic C_2H_5-Si(111) surfaces,[104] whereas similar H-atom abstraction is not likely to occur on the aromatic thiophene-functionalized surface. Hence, Si-Cl functionality, and ill-defined electronic trap sites, remained on SC_4H_3-Si(111) surfaces, likely contributing to the high observed S values.

3.4.5 Mixed CH_3/SC_4H_3- monolayers

In previous work, mixed monolayers were synthesized in one pot because the Grignard reagents, CH_2CHCH_2MgCl and CH_3MgCl, that were used in the competitive reaction had mutually similar reaction rates with the Si surface. The monolayer composition could therefore be controlled by changing the mole ratio of reactants in a single solution.[104,110] A sequential functionalization method was instead necessary to produce mixed CH_3/SC_4H_3-Si(111) surfaces. A solution composition of $< 1\%$ by mole CH_3Li produced 100% CH_3-Si(111) surfaces, indicating that the significantly higher reaction rates of CH_3Li with Si(111) surfaces precluded reaction of thienyllithium with Cl-Si(111) sites in one pot. Thienylation with thienylmagnesium bromide did not yield any detectable addition of thiophene. Because CH_3MgCl and thienyllithium are not mutually compatible, a two-step reaction sequence was therefore adopted in the work described herein.

The composition of the monolayer ($\theta_{SC_4H_3}$) was readily controlled by limiting the thienyl reaction time to between 2 min and 15 min, at 50 °C. The partial thienyl monolayer was then filled to completion by immersion of the Cl/SC_4H_3-Si(111) surface into a solution of CH_3MgCl. Surfaces with $0.05 < \theta_{SC_4H_3} < 0.55 \pm 0.08$ were formed using this approach. Mixed monolayers with a coverage of $\theta_{SC_4H_3} < 0.05$ are likely possible, but due to the broad nature of the S 2s XPS signal, the composition of such monolayers was difficult to quantify reliably.

Figure 3.1 shows the presence of Si-OC stretching modes, 1074 cm^{-1}, at [2,2':5',2"-terthiophen]-5"-Si(111), T_3-Si(111), and high $\theta_{SC_4H_3}$ CH_3/SC_4H_3-Si(111) surfaces. The formation of SiO-C bonds has been ascribed to THF ring opening or to methoxylation of non-functionalized sites during the reaction work-up steps.[85] To eliminate the possibility of THF ring opening, T_3-Si(111) was synthesized in diethyl ether. However, the T_3-Si(111) surfaces still exhibited the 1074 cm^{-1} Si-OC vibrational mode, indicating that this mode most likely appeared as a result of the addition of methanol during the work-up steps. Surfaces with higher total θ_{C-Si} are less susceptible to reaction with methanol, as evidenced by the absence of the 1074 cm^{-1} mode on CH_3/SC_4H_3-Si(111) with $\theta_{SC_4H_3} = 0.07$ and total $\theta_{C-Si} < 0.9$ (Figure 3.1c).

The presence of Si-H stretching modes, 2100 cm^{-1}, was also observed in the FTIR spectra of low total θ_{C-Si} Si(111) surfaces (Figure 3.1). Si-H has been observed previously on CH_3CH_2-Si(111), *t*-butyl-Si(111), and other functionalized Si surfaces.[100,104] Isotopic labeling experiments have shown that, in the presence of an $sp^3 - \beta$ hydride, the hydrogen atom comes from Si sites adjacent to those that form Si-H bonds. In the absence of an $sp^3 - \beta$ hydride, some Si-H sites are apparently still formed, while other non-Si-C terminated sites remain Si-Cl, so in such systems the H-termination presumably occurs through the solvent and/or through a separate mechanism.

3.5 Conclusions

A method for the robust secondary functionalization of Si(111) surfaces has been described that allows for the addition of organic or organometallic molecules or metal-binding ligands, with an average coverage of $\theta = 0.11 \pm 0.02$ and without the formation of electronic trap states at the surface. Formation of a synthetically versatile surface bound aryl bromide with coverage of $\theta_{Br-SC_4H_2} = 0.26 \pm 0.03$ is straightforward using the procedure described herein. The Heck reaction proceeded cleanly, and no residual surface-bound Pd was detected by XPS. Utilization of the mixed monolayer technique afforded surfaces having low electronic defect densities (roughly 1 in 500,000 sites), and exhibiting S values as low 27 ± 9 for CH_3/SC_4H_3-Si(111) with $\theta_{SC_4H_3} < 0.2$ before Heck functionalization, and $S = 70$ cm s^{-1} after the coupling reaction. The mixed-monolayer technique minimized residual Si-Cl electronic trap sites and deleterious secondary reactions, such as methoxylation of nonfunctionalized Si atop sites. An analysis of the peak voltammetric current *vs.* scan rate of the surface functionalized with vinyl-ferrocene confirmed that ferrocene had been covalently bound to the surface, and that the thiophene linker did not significantly shift the electrochemical potential of the bound redox species nor impede electron transfer processes significantly, on the time scale of the voltammetry.

Chapter 4

Controlling Si band-edge position by surface functionalization

4.1 Introduction

The efficiency of photoelectrochemical energy-conversion devices is dependent on proper alignment of the semiconductor band-edge energetics with the desired redox couple.[246] In many cases, materials with ideal band-gaps for solar-energy conversion are overlooked because of non-optimal band-edge positioning. For example, the potential of the conduction band-edge of n-TiO_2 surfaces is slightly positive of the H_2O/H_2 potential, precluding the use of n-TiO_2 for photoelectrochemical production of H_2 from water under standard conditions.[247] Similarly, the conduction band-edge of Fe_2O_3 surfaces is too positive to allow for production of H_2 from H_2O, even if efficient charge separation and collection could be achieved within the Fe_2O_3 photoanodes.[247,248] p-Si photocathodes are hindered by a similar problem, wherein the band-edge positions are too negative to allow for large photo voltages to be obtained for the reduction of H_2O to H_2.[249]

Surface functionalization with Si-C bonds has been shown to reduce surface oxidation, allows for secondary functionalization, and decreases surface electronic trap states. In addition, it provides a means to modify the electronic properties of silicon-based photoelectrochemical or photovoltaic devices, e.g., by modulating the band-edge energies. High-resolution photoelectron emission measurements of CH_3, and CH_3CH_2-terminated Si(111) compared with H-terminated Si(111) have found a difference of 0.50 V and 0.23 V in the electron affinity (EA), or equivalently their ionization potential (IP), respectively. A slightly larger difference of 0.7 eV was measured using differential capacitance techniques at the functionalized Si/Hg junction.

4.2 pH-dependent band-edge energies

One approach to achieving band-edge control involves changing the pH of the solution. For pH-dependent solution redox couples, for example, H_2O/H_2, the solution redox potential can be optimized for the material of interest, within reach of the Nernstian 59 mV / decade shift of the solution redox potential. However, a pH-dependent shift of the band-edge energies is expected for metal oxide electrodes in contact with aqueous solutions due to the protonation/deprotonation of surface OH-species.[250] Such surfaces do not show a change in energetics in contact with pH-dependent aqueous redox systems, because the H_2O/H_2 and O_2/H_2O redox potentials are also pH-dependent. In this case, the Nernstian shift in solution redox potential is cancelled out by a concomitant shift in band-edge potential, leaving the relative interfacial energetics of the system unchanged (Scheme 4.1).

In the case of a codependency of the band-edge energies and solution redox potential, an alternate approach to achieving band-edge control is necessary. Functionalization of the semiconductor surface in a fashion that eliminates pH-dependent surface sites allows for a concomitant change in the barrier height at the semiconductor/liquid interface with the pH-dependent change of half-reaction potential in solution. Surface functionalization can also introduce a controllable, fixed interfacial dipole to allow manipulation of the band-edge positions relative to a fixed reference potential. Provided that such surface functionalization can be performed in a fashion that allows for facile interfacial transfer of minority charge carriers with minimal surface recombination losses, control over the barrier height of such photo electrodes can provide an approach to optimization of the performance of such photo electrodes in half reactions of relevance to production of fuels, such as water splitting using sunlight. This is possible only if the semiconductor surface is free of electronic defects, which will otherwise limit the performance of such photoelectrodes.

We have evaluated the dependence of the open-circuit potential on pH of CH_3-, CH_2CHCH_2-, and mixed CH_3/CH_2CHCH_2-Si(111) photocathodes when in contact with an aqueous solution that contains a pH-independent redox-couple. The ability to efficiently suppress the pH-dependence of the Si band edges opens up the possibility to optimize the performance of Si photocathodes as outlined above (Scheme 4.1), by changing the pH of the solution. It is especially important to suppress the pH dependence for surfaces having functional moieties such as CH_2CHCH_2- groups, because such functional groups can be used to attach molecular catalysts to the Si surface with direct electrical contact. We have also studied the interfacial dipoles that are introduced by CH_3-, CH_2CHCH_2-, and mixed CH_3/CH_2CHCH_2-termination of Si(111) surfaces. Because of poor band-edge alignment, low photo voltages, and thus low energy-conversion efficiencies, are expected for Si photocathodes that are used for water

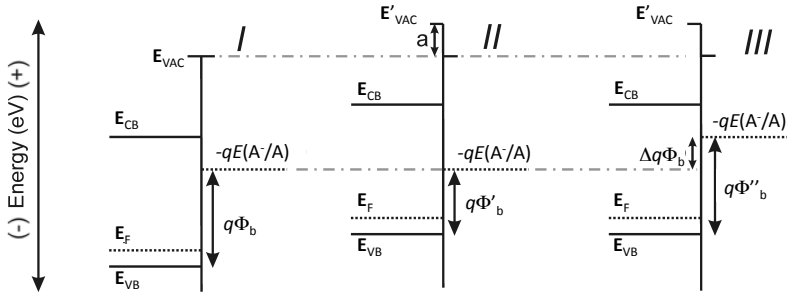

Scheme 4.1. Change in the energetics at flat-band conditions with increasing pH for a pH-sensitive semiconductor and pH-insensitive redox couple (*I* $\rightarrow$ *II*) and for both a pH sensitive semiconductor and redox couple (*I* $\rightarrow$ *III*). a represents the change in energy of passing an electron across an interfacial dipole. There is no effect observed on the interfacial energetics if both the solution redox couple and the interfacial dipole exhibit the same dependence on the solution pH; the barrier height ($q\Phi_{\rm b} = q\Phi_{\rm b}$") remains constant (*I* $\rightarrow$ *III*) as the pH is increased. The barrier height will change with pH for a semiconductor/liquid junction between a pH-insensitive redox couple and pH-sensitive semiconductor (*II*) or for a pH-sensitive redox couple and pH-insensitive semiconductor. In this later case, the barrier-height can be expressed as $q\Phi_{\rm b}" = q\Phi_{\rm b} + q\Delta\Phi_{\rm b}$. $\mathbf{E}_{\rm VAC}$ is the vacuum energy; $\mathbf{E}_{\rm CB}$ is the conduction band energy; $\mathbf{E}_{\rm VB}$ is the valence band energy; $-qE(A/A^-)$ is the solution redox energy; $\mathbf{E}_{\rm F}$ is the Si Fermi-energy.

reduction/hydrogen production. Successful band-edge control could be used to shift both the flat-band potential and the onset of photocurrent, thus increasing the energy-conversion efficiency of such systems.

Figure 4.1 displays representative *J-E* data for CH_3-, mixed CH_3/CH_2CH- CH_2-, CH_2CHCH_2-, and H-terminated p-Si(111) photo electrodes in solutions having pH values of 2.50, 6.75, or 11.0. The photocurrent was adjusted such that the limiting photocurrent density for all samples was within 15% of 1.0 mA cm^2. Furthermore, the photocurrent density for any electrode, measured in solutions of different pH, varied by less than 15%. Ideally, the dependence of V_{OC} on photocurrent, and thus on light intensity, is described by 4.1

$$V_{OC} \cong \left| \frac{AkT}{q} \ln\left(\frac{J_{ph}}{J_0}\right) \right| \tag{4.1}$$

where A is the diode quality factor (ideally 1.0), k is the Boltzmann constant, T is the temperature, q is the unsigned elementary charge, J_{ph} is the photocurrent density and J_0 is the exchange current density. A 15% difference in J_{ph} would therefore produce a 4 mV difference in the open-circuit voltage.

Table 4.1. Dependence of V_{OC} on solution pH for R-Si(111) electrodes in contact with $MV^{(2+/\bullet+)}$(aq)

R-	$\Delta V_{OC}/\Delta$pH	
	mean (mV/pH unit)	95% confidence interval (mV/pH unit)
CH_3-	-9	± 2
MM-	-17	± 1
CH_2CHCH_2-	-28	± 1
H-	-42	± 2

The open-circuit voltage, obtained from the *J-E* data by measurement of the voltage at which no current flowed, was observed to depend on the solution pH (Figure 4.1, Table 4.1). Because the redox potential of $MV^{(2+/\bullet+)}$ is independent of pH,[126] the observed shift in V_{OC} is due to changes at the semiconductor electrode. Over a pH range of 8.5 units (from pH 2.50 to pH 11.00), the V_{OC} shifted on average by -9, -17, -28, and -42 mV/ pH-unit for CH_3-, mixed CH_3-/CH_2CHCH_2-, CH_2CHCH_2-, and H-terminated Si(111) photocathodes, respectively, with the pH-dependence of the open-circuit voltage clearly increasing as the surface functionalization was changed from CH_3- to MM- to CH_2CHCH_2- to H-termination. For all surfaces, the pH dependence of V_{OC} was a function of the absolute pH of the solution, being greater at high pH values than at low pH values. The measured values of -9, -17, -28, and -42 mV/pH-unit for CH_3-, mixed CH_3-/CH_2CHCH_2-, CH_2CHCH_2-, and H-terminated Si(111) photocathodes, respectively, represent the average values over the entire pH-range of 8.5 units (from pH 2.50 to pH 11.00).

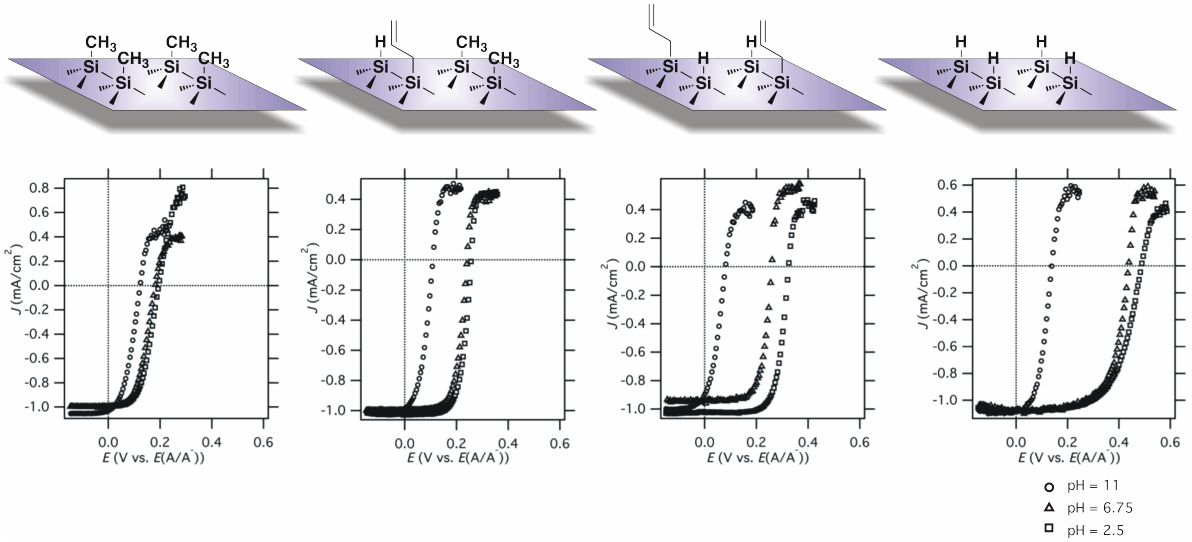

Figure 4.1. pH dependence of V_{OC} for CH_3-, mix CH_3/CH_2CHCH_2-, CH_2CHCH_2-, and H-terminated Si(111) surfaces in contact with $MV^{(2+/\bullet+)}$(aq).

$C_{\text{diff}} - V$ methods were utilized to measure the $\Phi_{\text{B,n}}$ at Hg/n-Si(111) junctions formed from either CH_3-, MM-, or CH_2CHCH_2-terminated n-Si- (111) surfaces. The differential capacitance, C_{diff}, was extracted by fitting the frequency-dependent impedance data to a simple test circuit that consisted of a resistor in series with a parallel capacitor and resistor. Bode plots of the log of the magnitude of the impedance *vs* frequency showed linear behavior with a slope of unity over a large frequency range, validating the use of the simplified equivalent circuit.

The semiconductor dopant density and the built-in voltage, V_{bi}, of Si for Hg/n-Si junctions were obtained from Mott-Schottky analysis by use of 4.2

$$\frac{1}{C_{\text{diff}}^2} = \frac{2}{q\epsilon\epsilon_0 N_D A_s^2}\left(V + V_{bi} - \frac{k_B T}{q}\right) \tag{4.2}$$

where ϵ and ϵ_0 are the dielectric constant of Si and the permittivity of vacuum, respectively, N_D is the dopant density, A_s is the junction area, and V_{bi} is the built in voltage of the Hg/n-Si junction. All junctions were largely defect-free, as shown by the dopant densities calculated from Mott-Schottky plots and by the values optioned from four-point probe measurements. The values of the dopant density calculated from the slope of the Mott-Schottky plots were in good agreement (less than 25% difference for all samples) with the dopant densities determined independently from four-point probe measurements. Built-in voltages were converted to barrier heights using 4.3

$$\Phi_{\text{B,n}} = V_{bi} - \frac{k_B T}{q}\ln\left(\frac{N_D}{N_C}\right) \tag{4.3}$$

where N_C is the effective density of states in the conduction band of Si (2.8×10^{19} cm^{-3}).[50] The measured barrier heights for the Hg/n-Si junctions were ~0.9 V, with no statistical difference observed between the barrier heights of the different types of alkylated Si(111) surfaces (Table 4.2).

Table 4.2. Dependence of V_{bi} and $\Phi_{\text{B,n}}$ on solution pH for R-Si(111) electrodes in contact with Hg

R-	V_{bi} (V)	$\Phi_{\text{B,n}}$ (V)	95% confidence interval (V)
CH_3-	0.69	0.94	± 0.06
MM-	0.68	0.92	± 0.02
CH_2CHCH_2-	0.64	0.89	± 0.12

Surface recombination velocities (S) of < 300 cm s^{-1} were measured in contact with acidic buffered solutions of pH 2.5. S values were observed to increase slowly during a 5 minute time period. $S < 25$ cm s^{-1} for H-Si(111) surfaces in contact with basic buffered solutions of pH 11.0. S was steady throughout the 5 min time period.

4.2.1 pH dependence of V_{OC} for Si(111) surfaces terminated by mixed methyl/allyl monolayers

The minimal pH-dependence of V_{OC} for CH_3-terminated p-Si(111)/$MV^{(2+/\bullet+)}$ junctions (Figure 4.1) is consistent with expectations for a system in which the flat-band potential of the photo electrode is largely independent of pH. This behavior is consistent with the expectations for a surface in which atop Si atoms are essentially fully terminated by a chemically inert Si-C linkage, thus rendering the energetics of such surfaces insensitive to changes in pH. In contrast, the CH_2CHCH_2-terminated p-Si(111) surfaces showed a significant dependence of V_{OC} on pH. Due to steric constraints, CH_2CHCH_2- groups terminate only $\sim 80\%$ of Si(111) atop sites with Si-C bonds. In the presence of even mild oxidants, such as MV^{2+}, the nonfunctionalized sites can oxidize to produce Si-OH and subsurface Si-oxide species. Thereby a mechanism for obtaining a pH dependence of E_{FB} for such surfaces is introduced, in accord with the observed change in V_{OC} with pH for such systems.

The classical model for insulators and non-degenerate semiconductor electrodes predicts that adsorption of a charged species (a proton, for example) will be accompanied by an accumulation of charge at the outer Helmholtz plane:

$$\text{Surface-A}+H^+ \leftrightharpoons \text{Surface-A}H^+$$

The Helmholtz double-layer voltage, that is, the difference in potential between the solid surface and the outer Helmholtz plane, is then predicted to have a Nerstian dependence on pH.[251] However, the chemical activity of the equilibrium species is likely to be a function of surface coverage consistent with observed pH-dependences of the interfacial dipole of < 59 mV/pH-unit.[252] For H-terminated Si in contact with aqueous solutions, the pH-dependence of the band-edges has been reported to range from linear (non-Nernstian),[253] to nonlinear,[254] to Nernstian.[255] The behavior of silica is informative because active surface groups on silica are Si-OH_2^+, Si-OH, and Si-O^-. The lowest concentration of charged species at the surface is expected at the pH for which silica is not charged, $pH_{pzc} \sim 2$.[256,257] The SiO_2 surface is terminated by an appreciable net surface charge-carrying species that is likely responsible for the interfacial dipole only when the pH of a solution contacting SiO_2 is sufficiently different from pH_{pzc}.[256,258]

For Si(111) surfaces that have been functionalized with dodecyl chains using hydrosilylation chemistry, the band-edge positions have been observed to be dependent on pH. For such surfaces, the flat-band potential varied by -25 mV/pH unit over the pH range 4–7, as determined by differential capacitance measurements.[256] The trend exhibited by all surfaces

investigated herein, with a pH dependence primarily observed in neutral to basic conditions, is consistent with expectations that the surface species is Si-OH, which can be deprotonated at higher pH to yield Si-O^-. Si(111) surfaces passivated by decal, carboxydecul, or mixed decal/carboxydecyl monolayers attached *via* hydrosilylation chemistry, and CH_3- groups attached using anodic decomposition of CH_3MgI, have been investigated using surface photo voltage, photoluminescence, capacitance, and FTIR measurements. Differences in experimental conditions (most notably the presence of dissolved oxygen in the solutions) preclude a more direct comparison to the data presented herein, but consistent agreement exists that the surfaces with lower Si-C coverage exhibit increased pH-sensitivity of the electronic properties of the resulting Si/solution junctions.[259]

The open circuit voltage is related to the barrier height of the semiconductor/liquid contact, but is also a function of surface- and bulk-recombination processes, and interfacial electron-transfer rates; hence, V_{OC} is an indirect measure of the barrier height. High-quality Si wafers of nominally identical quality and doping density were used for the photoelectrochemical studies, ensuring that the bulk recombination velocity did not affect changes in V_{OC}. The surface recombination velocities of CH_3-, MM-, and CH_2CHCH_2-, and H-Si(111) surfaces are similar to each other and are < 100 cm s^{-1}.[110] Accordingly, the electronic defect densities have been estimated to range from 1 in 40,000,000 to 1 in 100,000 effective surface recombination sites for H- and CH_2CHCH_2-terminated Si(111), respectively, with CH_3- and MM-terminated surfaces have intermediate S.[10,110,199] Hence, the surface recombination velocities of such systems are sufficiently low to not significantly affect the performance in typical device applications. The surface recombination velocity of H-Si(111) immersed in bufferd solutions (pH 2.50 to 11.0) was determined to ensure the interactions with the buffer did not result in high S values in the absence of inert Si-C termination. The surface recombination velocity was only weakly dependent on pH for H-Si(111) and was low enough that it would not significantly affect V_{OC}. Therefore, the shift in V_{OC} as a function of pH cannot be consistently ascribed to changes in surface-state density.

4.2.2 The effects of a permanent surface dipole on V_{OC}

A change in surface dipole for the various functionalized Si(111) systems could also produce different values of V_{OC} for each system. The CH_3- group has been shown to induce a surface dipole of -0.4 eV, as measured by XPS at the BESSY II synchrotron facility.[99] Similarly, the ethyl group has been shown to induce a surface dipole of -0.23 eV on Si(111).[107] Previous measurements of the barrier height of Hg/Si junctions in which the Si surface was functionalized with a variety of alkyl-chains, ranging in length from CH_3- groups to octyl-decane chains, has indicated that the barrier height is independent of the chain-length of the alkyl group. These

results suggest that the CH_3-, CH_2CHCH_2, and MM surface moieties used herein all introduce a mutually similar surface dipole.[53,113] While the photocathode data were obtained using p-Si, all Mott-Schottky data in this study were collected using n-Si, because alkyl-terminated p-Si forms very low barrier height junctions with Hg. The Mott-Schottky measurements yield the geometric average of the surface dipole, while V_{OC} measurements are more sensitive to regions of lower barrier-height. Furthermore, the V_{OC} measurements yield the photovoltage under a certain set of experimental conditions that are much different than those used for the Mott-Schottky measurements. the differences observed between these two measurements highlight their complementary nature.

Notably, the surface-dipole introduced by CH_3-, MM-, and CH_2CHCH_2-termination of Si(111) shifts the band-edges to more negative potentials than those observed for the H-Si(111) surface. This shift produces lower barrier height junctions on p-Si in the absence of Fermi-level pinning. Movement of the band-edge potentials more negative with respect to a fixed solution redox potential, by introduction of a permanent interfacial dipole, decreases the barrier height for p-type electrodes and thus decreases the maximum attainable V_{OC} for such junctions. For H_2O reduction to H_2, this shift can be overcome by use of a high solution pH. The band-edges are independent of the solution pH due to the permanent interfacial dipole, but the hydrogen reduction potential becomes more negative as the pH of the solution is increased, resulting in a higher barrier height. Alternately, in the case of a regenerative photoelectrochemical cell, a redox couple having a more negative potential could be used to produce a higher barrier-height interface. Alternatively, an opposite dipole would increase the barrier height by shifting band-edges to more positive potentials relative to the solution potential, thereby increasing the maximum attainable pH for a given solution.

4.2.3 Summary and lessons of decreasing pH-dependence of band-edge positions with Si-C bonds

H-terminated Si(111) surfaces in contact with $MV^{(2+/\bullet+)}$(aq) displayed a large dependence of the V_{OC} on pH, while CH_2CHCH_2-, MM-, and CH_3-terminated surfaces, having decreasing fractional coverage of Si-C bonds, displayed a consistently smaller pH-dependence. CH_3-, and MM-terminated Si(111) surfaces displayed significantly lower pH dependences than surfaces that were instead functionalized using a hydrosilylation process. The magnitude of the dependence of the band-edge positions on pH correlated with the percentage of Si(111) atop sites that were not terminated by Si-C bonds, suggesting that non-Si-C-termianted surface bonds reacted to produce groups such as Si-OH, that produced the observed pH dependence. CH_3-, MM-, and CH_2CHCH_2-termination of Si(111) surfaces all produced similar surface dipoles, as observed

using differential capacitance-voltage measurements on functionalized n-Si(111)/Hg contacts. It has been shown previously that the total coverage (defined as the fraction of Si atop sites terminated by a Si-C bond), surface recombination velocity, and rate of oxidation under ambient conditions are all correlated, and the surface recombination velocity, and rate of oxidation, increase monotonically with decreasing total coverage. Additionally, as has been shown in this chapter, functionalization can stabilize the band-edge positions of Si in contact with aqueous solutions of varying pH with the degree of stabilization highly dependent on the total Si-C coverage of such functionalized surfaces.

4.3 Understanding the direction and magnitude of fixed interfacial dipoles on Si(111) by ab initio methods

Section 4.2 detailed the efficacy of Si-C bonds to reduce the pH-dependence of band-edge position at high $\theta_{\mathrm{Si-C}}$. Additionally, the CH_3-termination imposed a positive dipole at the surface that shifted band edge positions to more positive potentials relative to a given contact potential. This increased barrier heights, $\Phi_{\mathrm{B,n}}$ for n-type Si, but decreased $\Phi_{\mathrm{B,p}}$ for p-type Si relative to H-Si(111) for a given junction (Figure 4.2). Such shifts of band-edges are directly associated with the surface dipole formed at the interface through the Helmholz equation

$$\Delta\phi = -4\pi\mu_z/S_0 \tag{4.4}$$

where $\mu_{\mathrm{z}} = \mu_{\mathrm{mol,z}} + \mu_{\mathrm{ind,z}}$ is the component of the surface dipole moment normal to the surface for a unit cell of area S_0, and μ_{mol} and μ_{ind} are the molecular dipole moment of the adsorbate and the induced dipole moment, respectively. $\phi = E_{\mathrm{vac}} - E_{\mathrm{F}}$ is the work function, which can be determined by the relative position of the Fermi level E_{F} to the valence band, E_{VB}, or conduction band, E_{CB}, edges at a specific doping density. In order to achieve control of the direction and magnitude of $\Delta\phi$, it is essential to understand and predict the formation of surface dipole moments at the adsorbate/silicon interface, and their dependence on the adsorbate type and surface coverage.

Previously, the Galli group at UC Davis explored electronic and spectroscopic properties of CH_3-functionalized Si(111) surfaces.[260,261] These calculations compared favorably with measured spectroscopic properties,[100] and were compared to scanning tunneling microscopy (STM) images and scanning tunneling spectroscopy (STS) data.[82,97] Building on this, Li, et al. carried out calculations of band-edge position of functionalized Si(111) surfaces, as a function of the adsorbate type and coverage. Density functional theory (DFT) and many-body perturbation

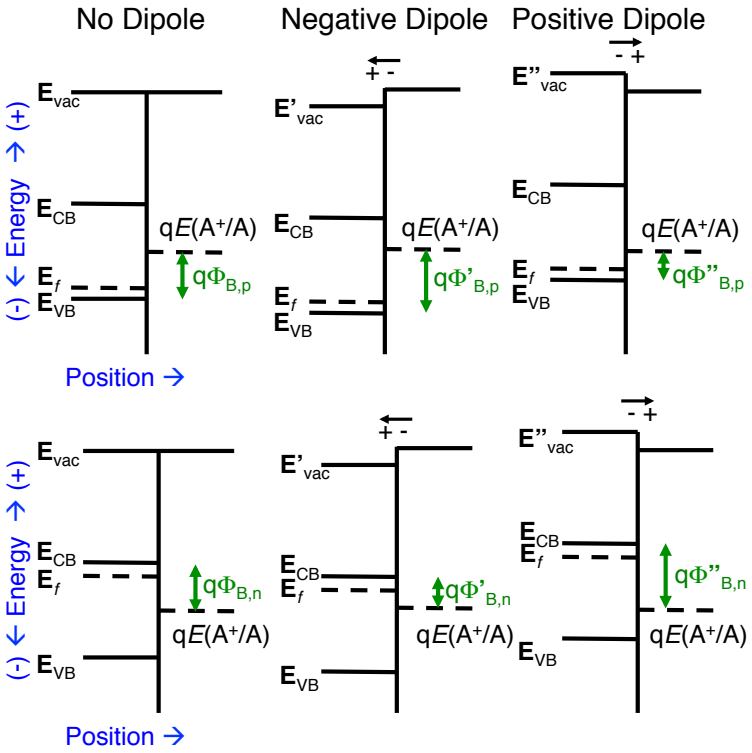

Figure 4.2. Flat-band energetics with a negative or positive fixed dipole across a generic p- or n-semiconductor/qE(A$^+$/A) junction. The maximum attainable V_{OC} for a given junction is dependent on Φ_B. For a p-type semiconductor, $q\Phi'_{B,p} > q\Phi_{B,p} > q\Phi''_{B,p}$ for a negative, symmetric, and positive fixed interfacial dipole, respectively. For a n-type semiconductor, $q\Phi''_{B,n} > q\Phi_{B,n} > q\Phi'_{B,n}$ for a positive, symmetric, and negative fixed interfacial dipole, respectively. Therefore, for a given Si/(A$^+$/A) junction, a positive dipole is desirable to increase V_{OC} at a given p-type semiconductor, and a negative dipole is desirable to increase V_{OC} at a given n-type semiconductor.

theory, in particular the G_0W_0 perturbative approach,[262] was used. Calculations show that the *absolute* positions of the valence band edges can be well described by the G_0W_0 self-energy corrections to DFT energy levels, while the *relative* work function shifts are in good agreement with experiment even at the DFT level. In particular, the sign and magnitude of surface dipole moments of different surface terminations follow a trend that may be explained by simple electronegativity rules.

4.3.1 Methods and materials

Computational Details The computational details are given in a forthcoming publication *"Controlling the work function of silicon by surface functionalization: a combined ab initio and photoemission study"* by Yan Li, Leslie O'Leary, Nathan Lewis, and Giulia Galli. Additionally, through this work, a fairly user-friendly computational template was set up. Therefore, the model may now be used by the Lewis group for predictive work. DFT calculations for geometry optimization and surface dipole evaluation were carried out with the plane-wave package QUANTUM ESPRESSO,[263] using norm-conserving pseudopotentials, local density (LDA) exchange and correlation functionals and plane wave basis sets with a kinetic energy cutoff of 50 Ry. Functionalized Si(111) surfaces were modeled by six-layer slabs at the experimental bulk equilibrium lattice constant (5.43 Å), with the bottom layer terminated by hydrogen atoms. A vacuum region of at least 10 Å between periodically repeated slabs was used to avoid spurious interactions between replicas. All atoms except the bottom hydrogen layer were relaxed during geometry optimizations until the maximum force is smaller than 0.03 eV $Å^{-1}$. A (1×1) unit cell and a $8 \times 8 \times 1$ k-grid were used for surfaces at full coverage; partial coverages at 25% was modeled by using a $(2 \times 2 \times 1)$ supercell with a $4 \times 4 \times 1$ k-grid, with the remaining atop Si sites terminated with hydrogen atoms. Dipole moments of gas phase molecules and radicals were computed using a simple cubic supercell of 30 bohr. In some cases, DFT calculations with local basis sets were performed with Gaussian 09[264] to compare with results from advanced quantum chemistry methods, such as coupled-cluster singles and doubles (CCSD) and second-order Møller-Plesset perturbation theory (MP2).

Many-body perturbation theory calculations within the G_0W_0 approximation were performed with the ABINIT code[265] using plane wave basis sets with a kinetic energy cutoff of 16 Ry, while the slab geometries were optimized at 50 Ry. To avoid the need for dipole corrections in G_0W_0 calculations, we used symmetric, doubly adsorbed slabs, with a vacuum region of 10 Å. We employed the plasmon-pole model proposed by Godby and Needs,[266] which has been shown[267] to have accuracy comparable to that of direct frequency integration techniques for bulk Si and H-

Si(111) slabs, in predicting both absolute and relative energy levels in the vicinity of the valence band maximum (E_v) and conduction band minimum (E_c). The absolute position of computed energy levels is sensitive to the slab thickness,[260,267] in contrast to geometric and vibrational properties which converge well for slabs of about 4–6 layers; therefore here we present DFT and G_0W_0 results for slabs of 12 layers.

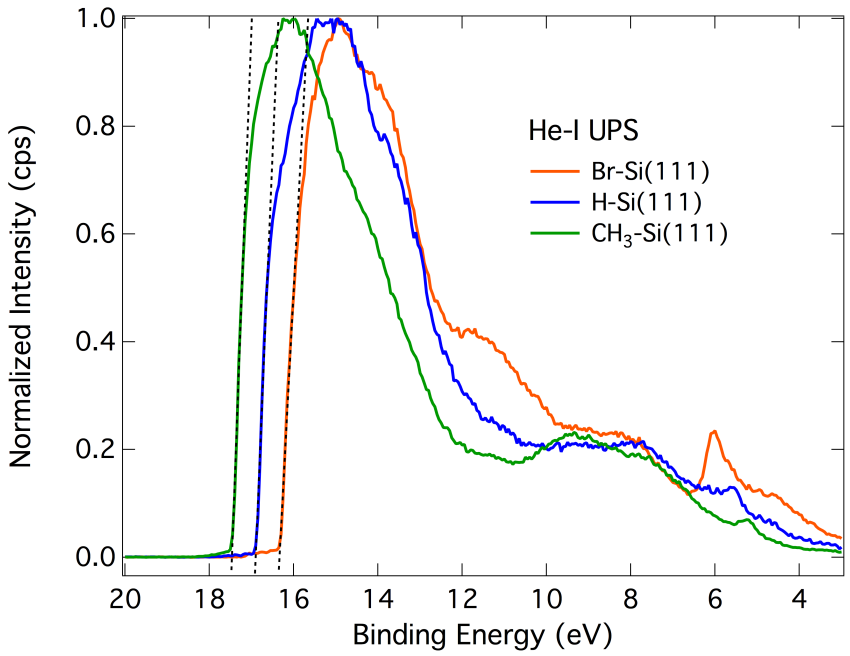

Figure 4.3. UPS measurement and W_f determination at Br- (orange), H- (blue), and CH_3- (green) terminated Si(111). W_f is determined by the extrapolation of the secondary electron cutoff. W_f shifts by $>$ +1 V upon going from a negative dipole, Br- group, to a positive dipole, CH_3- group.

Experimental Details. Cl-Si(111) samples were synthesized as previously described. In short, wafers 74.1 Ω cm resistivity n-Si(111), Silicon Quest Int. was used for UPS and 12.5 Ω cm resistivity n-Si(111), University Wafer was used for C_{diff}-V. Cl-Si(111) surfaces were immediately alkylated or transported, air-free, for UPS and XPS analysis.

Following anisotropic etching, *vide supra*, H-Si(111) surfaces were loaded into one side of a two-chamber glass Schlenk apparatus. Each chamber was isolated by a Kontes tap leading to a glass connection to the opposite chamber. The glass connection was additionally isolated from Ar/vacuum by a third Kontes tap. The chamber containing the H-Si(111) sample was immediately evacuated. Under static vacuum, degassed Br_2 was transferred from the second chamber to cover the H-terminated sample. A UV light was applied for 5 minutes. The Br_2 was removed *via* vacuum, and then the entire apparatus was sealed and transferred into an N_2 filled glove box for sample mounting and air-free transfer to the XPS/UPS system.

X-ray photoelectron spectroscopy (XPS) and ultraviolet photoelectron spectroscopy were

collected using a Kratos AXIS Ultra DLD with a magnetic immersion lens with a spherical mirror and concentric hemispherical analyzers with a delay-line detector (DLD). An Al kα (1.486 KeV) monochromatic x-ray excitation source was used. The He-I (21.2 eV) line was used for UV excitation. Ejected electrons were collected at an angle of 90° from horizontal. The sample chamber was maintained at $< 5 \times 10^{-9}$ Torr. XP survey scans from 0 to 1200 eV were performed to identify the elements that were present on the surface. Mg was not detected on any sample after workup. Si2p (104.5–97.5 eV), C1s (292–282 eV), Br3d (68–78 eV), and Cl2p (206–196 eV) high-resolution XPS data were taken. High-resolution XPS data were analyzed using Casa XPS v2.3.15. A simple substrate over layer model was used.

UPS data were exported and the low kinetic energy cut-off analyzed using IGOR to determine the sample work-function as

$$W_f = 21.2 - BE \tag{4.5}$$

where 21.2 eV = excitation energy, W_f is the sample work function, and BE is the secondary electron cutoff energy.

Table 4.3. Ionization potential and band gap of C_2H_5-, CH_3-, bulk, H-, Cl, and Br-Si(111) surfaces evaluated at $n_L = 12$; all energies are in eV

R-	LDA			G_0W_0			Exp.	
	E_g	IP	IP-IP_H	E_g	IP	IP-IP_H	IP	IP-IP_H
C_2H_5-[a]	0.72	3.83	-1.0	1.53	4.52	-0.9	4.94[a], 4.79[b]	-0.4[a],-0.7[b]
CH_3-	0.70	4.06	-0.8	1.50	4.76	-0.8	4.80[a], 4.76[b]	-0.5[a], -0.7[b]
bulk[b]	–	–	–	–	–	–	5.2	–
H-	0.73	4.83	–	1.53	5.46	–	5.29[c], 5.44[d]	–
Br-	0.62	5.59	0.8	1.44	6.27	0.8		0.53[e]
Cl-	0.65	5.89	1.1	1.46	6.56	1.1		1.2-1.5[f]

[a]Surface coverage of C_2H_5-Si(111) surface was estimated to be around 80% by STM experiments[?] , while a full coverage is assume in our calculations.

[b]$\mu = 0$, for comparison

[c]Refs.[99] and[107], estimated from high-resolution synchrotron photoelectron spectroscopy measurement.

[d]Ref.[53], estimated from measured barrier height of junctions between Hg and n-type Si(111) as: IP=WF^{Hg}-$q\Phi_{b,J-V}$+E_g, where WF^{Hg}=4.49 eV is the work function of Hg and E_g is assumed to be 1.12 eV.

[e]estimated from UPS measurement, this work

[f]Ref.[89], estimated from Kelvin probe measurements

4.3.2 Energy position of conduction and valence band-edges

Table 4.3 summarizes the ionization potentials (IP) and band gaps of the H-, CH_3-, C_2H_5-, Br-, and Cl-terminated Si(111) surfaces at full coverage computed within LDA and G_0W_0. Results for Br- and Cl-terminated Si(111) surfaces, show work function shifts which have the opposite sign due to the strong electron withdrawing character of the chemisorbed chlorine and bromine. At the LDA level, the band gaps are severely underestimated compared to $E_{g,bulk}^{exp.} = 1.12$ eV, and the computed IP values for the H-Si(111) and CH_3-Si(111) surfaces are underestimated by about 0.5–0.7 eV compared to those determined from photoelectron emission[99,107] and electrical

junction barrier measurements[53]. We note that in Ref. 107 and 53 the C_2H_5-Si(111) surfaces were terminated by both H− and C_2H_5− groups; therefore they are expected to have a larger IP than that of the computed C_2H_5-Si(111) surface at the full coverage. Overall, the observed trend is consistent with the fact that LDA usually tends to underestimate the band gap of semiconductors with the predicted valence band edge being too shallow.

Applying G_0W_0 selfenergy corrections to computed DFT/LDA levels significantly improves the absolute positions of E_v, however the band gaps now turn out to be overestimated by 0.3–0.4 eV with respect to $E_{g,bulk}$. This overestimate does not originate from theoretical approximations but rather from numerical approximations, in particular from the slow convergence with respect to the slab thickness[261]. For example, the G_0W_0-corrected band gap of the H-Si(111) surface, $E_{g,H}^{G_0W_0}$, is about 1.40 eV at $n_L = 24$, which is only slightly improved compared to the values of 1.53 eV at $n_L = 12$. From its value at n_L =6, 12, 18, 24, $E_{g,H}^{G_0W_0}$ can be roughly fitted to $E_{g,H}^{G_0W_0}(n_L) = E_{g,H}^{G_0W_0}(n_L \to \infty) + Constant \cdot n_L^{-1.6}$ with $E_{g,H}^{G_0W_0}(n_L \to \infty)$=1.3 eV, which is consistent with the computed of $\overline{E}_{g,bulk}^{G_0W_0} = 1.31$ eV from Γ to $\overline{M}$ for bulk Si. However, the computed relative band edge positions of different surfaces are already well converged even at n_L=6, both at the G_0W_0 and the DFT/LDA level. Therefore, despite the errors of DFT within local and semilocal approximations in predicting the *absolute* energy position of conduction and valence band edges, the computed DFT energy level *differences* are in satisfactory agreement with experiments and results from higher level of theory. Therefore we suggest that an accurate prediction of work functions of functionalized Si surfaces with different termination groups and/or coverages may be obtained by comparing computed DFT band edges with those of a reference surface, for example, H-Si(111) or CH_3-Si(111), whose absolute band edges are well characterized by experiments.

From Table 4.3, one observes that the measured and computed shift of IP values of functionalized Si(111) surfaces with respect to that of bulk Si, IP_{bulk}=5.2 eV, are consistent with the electronegativity difference of the Si atom and the adsorbate for adsorbate molecules whose dipole moment is zero or vanishing along the direction normal to the surface, i.e., $\chi_{Si}[= 1.9] < \chi_H[= 2.1] < \chi_{Br}[= 2.96] < \chi_{Cl}[= 3.16]$. In particular:

(1) Since $\chi_H > \chi_{Si}$, the total surface dipole of H-Si(111) is expected to be negative and all energy levels to move downward with respect to the vacuum level. Indeed, the measured and GW-corrected IP values of 5.3–5.5 eV are both slightly higher than IP_{bulk}.

(2) Since $0 > \chi_{Cl,Br} - \chi_{Si} \gg \chi_H - \chi_{Si}$, the surface dipoles of the Cl-Si(111) and Br-Si(111) surfaces are expected to be substantially more negative than that of H-Si(111). Indeed, an increase of IP or work function of 1.1 eV and 0.8 eV were estimated for the two

surfaces upon chlorination or bromination of the H-Si(111) surface, consistent with the experiments.[89]

In summary, the knowledge of atomic or molecular electronegativity values may be sufficient to predict the direction and magnitude of surface potential shifts for adsorbate molecules whose dipole moment is zero or vanishing along the direction normal to the surface, e.g. H, Cl, Br, etc. For polar adsorbate molecules, e.g., CH_3-, C_2H_5 or their derivatives, one also needs to know the molecular dipole moments, not only in the gas phase, but at the specific surface coverage (see below).

4.3.3 Surface dipole moment and work function shift

Next, we examine the work function shift of Si(111) surfaces terminated by additional types of functional groups. According to Eq. 4.4, the direction and magnitude of the work function shift can be controlled by varying the type and coverage of the terminal groups. Table 4.4 lists the computed surface dipole moments of Si(111) surfaces terminated by different functional groups at full coverage, or 1/4 coverage with the remaining atop Si atoms saturated by H. The bottom Si layer is always terminated by H atoms. Also presented is the work function difference measured from the top and bottom sides of the slab, $\Delta\phi$, which is equivalent to the work function difference between a fully saturated H-Si(111) surface and a Si(111) surface with terminal groups arranged as in the top layer of the simulated slab. Such work function difference can be directly estimated from photo-emission experiments or barrier height experiments.

As shown by Table 4.4, the relative magnitude of μ_z of different Si(111) surfaces at both coverages roughly follow the trend of $\mu_{\rm mol}$. However, the surface coverage of the adsorbate has a sizable impact on μ_z: polarizable terminal groups partially screen the electric field of neighboring, parallel dipole groups, thus effectively reducing μ_z with respect to the gas phase value $\mu_{\rm mol}$. Therefore, although the sign and magnitude of $\mu_{\rm mol}$ of the R-SiH_3 molecules give a rough estimate of work function shift for various R-Si(111) surfaces, the actual value of μ_z for the latter depends on the strength of intermolecular screening, which is a complex function of the molecular polarizability, orientation and surface coverage of the adsorbate. An accurate estimate of μ_z for a specific surface arrangement may be obtained by performing first-principle electronic structure calculations, as done in this work.

Because of the difficulty of applying advanced quantum chemistry (QC) methods (e.g., CCSD, MP2) or hybrid density functionals (e.g., B3LYP, PBE0) to large, periodic systems, we used DFT/LDA for functionalized Si(111) throughout the work. To examine the accuracy of dipole moments (and therefore work function shift) computed by DFT/LDA, we evaluated the dipole moments of a series of short-chain silanes, R-SiH_3 (R = CH_3, C_2H_5, C_3H_7, C_4H_9, C_2H_4CH and

Table 4.4. Computed surface dipole moment per terminal group (in Debye) normal to the surface and induced work function shift (in eV) for various terminal groups (R−) at 1/4 or full coverage. For comparison, dipole moments along the Si-C bond for R-SiH_3 are also listed

R−	R-SiH_3 $\theta = 1/4$		R-Si(111) $\theta = 1$		
	μ_z	μ_z	$\Delta\phi$	μ_z	$\Delta\phi$
CH_3-	0.87	0.41	-0.29	0.28	-0.79
CH_2CH_3-	0.90	0.50	-0.35	0.35	-0.99
$CH_3C{\equiv}C-$	1.71	1.41	-0.99	0.60	-1.69
Cl−	-1.21	-0.60	0.42	-0.38	1.06
Br−	-1.27	-0.60	0.42	-0.30	0.84

C_2H_3C, Br and Cl), using DFT with different exchange-correlation functionals and compared the results with those from advanced QC methods. All calculations were performed with the G09 package[264] using the cc-pvTz local basis set, with the geometry of the molecule fixed at the optimized geometry obtained using B3LYP/aug-cc-pVTz. The dipole moment (μ) is defined to be positive it it points from SiH_3 to the other half moiety.

Table 4.5 shows that μ has the largest values when computed by DFT with local and semi-local exchange-correlation functionals (LDA and PBE), and then it systematically decreases as one includes exact exchange contributions (B3LYP and HF). Further inclusion of correlation contributions beyond HF (MP2 and CCSD) slightly changes the value of μ. The molecular dipole moment predicted by LDA is overestimated compared with the CCSD values by about 0.1 Debye for all the alkyl-, alkenyl- and alkynyl-silanes studied here, whereas the relative errors decrease as the absolute value of μ increases, being largest for methylsilane ($\delta\mu \sim 14\%$). For the alkyl series, as the chain length increases, the dipole moment slightly increases, although a more definite trend should be determined by examining alkylsilanes of longer chains. On the other hand, as the degree of saturation decreases, e.g., from propyl- to propenyl- and propynyl-silane, the dipole moment substantially increases. For example, propynylsilane has a dipole moment almost twice as large as that of propylsilane. It has been shown experimentally that the propynyl group is oriented normal to the Si(111) surface plane and fully terminates the Si atop site.[268] This picture of full coverage, however, is not consistent with the huge difference in dipole moment between methylsilane and propynylsilane (see Table 4.4) and the fact that a similar barrier height was measured for the methyl- and propynyl-terminated Si(111) surface in contact with Hg.[53] A closer inspection of the latter experiment may be necessary to explain such a discrepancy.

Based on the comparison of LDA and experimental values of $\mu_{\rm mol}$, one may expect slightly overestimated values of μ_z for functionalized Si(111) surfaces from LDA calculations. For example, the IP difference between H-Si(111) and CH_3-Si(111) surfaces is estimated to be 0.8 eV from LDA, while a value of 0.5–0.7 was extracted from experiments.[99,107] The magnitude of

Table 4.5. The total dipole moment (in Debye) of R-SiH_3 computed using DFT and QC methods

R−	LDA	PBE	B3LYP	HF	MP2	CCSD	Exp.
CH_3-	0.84	0.84	0.79	0.75	0.75	0.74	0.73[269]
CH_3CH_2-	0.91	0.93	0.88	0.83	0.84	0.82	0.81[270]
$CH_3(CH_2)_2-$	0.92	0.93	0.88	0.83	0.84	0.82	
$CH_3(CH_2)_3-$	0.99	1.01	0.95	0.89	0.91	0.88	
$CH_3CH{=}CH-$	1.36	1.37	1.33	1.37	1.25	1.22	
$CH_3C{\equiv}C-$	1.61	1.63	1.58	1.60	1.50	1.53	
Cl−	-1.42	-1.34	-1.43	-1.61	-1.44	-1.45	-1.31[269]
Br−	-1.42	-1.32	-1.43	-1.67	-1.46	-1.46	-1.32[269]

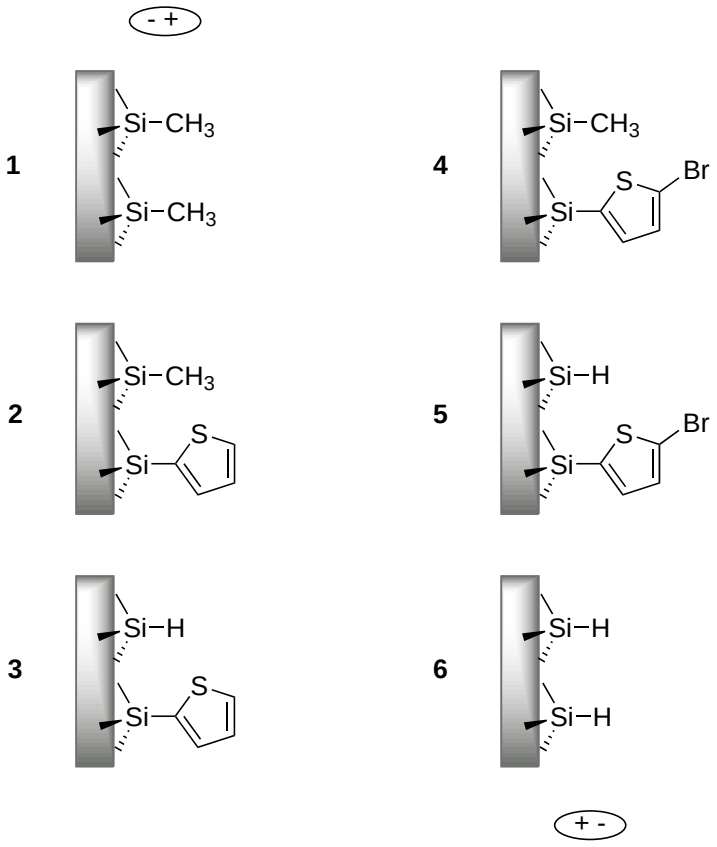

Scheme 4.2. List of functionalized Si(111) used for band-edge shift studies

LDA errors in μ_z, in general, may be similar or smaller than that in μ_{mol}, as LDA also tends to overestimate the intermolecular screening, which partially cancels the overestimate in the μ_{mol}, when the adsorbed functional groups form a closely packed monolayer.

4.4 Increasing $\Phi_{\mathrm{B,p}}$ at p-Si(111) junctions by surface functionalization with a positive adsorbate dipole

As discussed in the previous sections, surface-bound molecular dipoles can shift band-edge positions to adjust Φ_{B} at a given semiconductor heterojunction, Figure 4.2. The dipole can be a fixed, permanent dipole, as such is the case with CH_3-Si(111), or a modular dipole, as is the case with the pH-dependent set of species HO-Si(111). It was shown that band-edges could be stabilized using non-pH-sensitive Si-C bonds, and that that stabilization is dependent on the initial surface coverage of Si-C and Si-H bonds. The CH_3- group imposes a positive dipole at the Si(111) surface which decreases $\Phi_{\mathrm{B,p}}$ for a given heterojunction over that at the same H-terminated Si(111) heterojunction. In order to push the band-edge positions more positive in relation to the contact potential, *i.e.*, toward those of the H-Si(111) surface, a negative fixed dipole should be introduced at the surface. Where this dipole is imposed through Si-C bonds, one can gain the benefit of robust chemical passivation and low electronic defect density, as discussed in Chapters 1 and 2.

Scheme 4.2 shows the target surfaces for a study on band-edge shift with adsorbate molecular dipole. The CH_3-Si(111) surface, **1**, and the H-Si(111) surface, **6**, represent the two, well-characterized, end-points of the study. The mixed CH_3/SC_4H_3-Si(111), **2**, and the mixed CH_3/SC_4H_2Br-Si(111), **4**, surfaces were used in Chapter 3 as the initial and intermediate surfaces in the Heck coupling chemistry. Similarly, the reaction of Cl-Si(111) with SC_4H_3-Li can be run to completion to give the SC_4H_3-Si(111), **3**, and SC_4H_2Br-Si(111), **5**, with $\theta_{SC_4H_2X} = 0.55 \pm 0.08$. Alongside theoretical efforts, the band-edge shift with functionalization was studied for surfaces **1** - **6**.

4.4.1 Materials and methods

*1. Synthesis of surfaces **1** - **6**.* Synthesis of functionalized Si(111) was performed in similarly to that of Chapter 3. p-type Si(111) with a resistivity of 8.7 Ω cm or n-type Si(111) with a resistivity of 12.5 Ω cm was used for $C_{\mathrm{diff}} - V$ experiments. H-termination and Cl-termination were performed as described above. Table 4.6 shows the parameters used in the alkylation reactions of surfaces **1** - **5**. After alkylation, surfaces **2** and **3** were submerged into a solution of 20 mg / ml NBS in DMF, *vide supra*, with an initiating amount of $ZnCl_4$, $<$ 1 mg in a N_2

filled glove box with $<$ 1 ppm O_2. The NBS solution was drained, and samples were cleaned as described in Chapter 3.

Samples were removed from the N_2 filled glove box to make a back contact. To ensure contact with fresh Si, GaIn eutectic was scratched onto the back side of the samples. Samples were reintroduced to the N_2 filled glove box for $C_{\text{diff}} - V$ measurements.

Table 4.6. Alkylation parameters for surfaces **1 – 5**

Surface	SC_3H_3-Li[a] (min)	CH_3-MgCl[a] (min)
1	-	$>$ 60
2	15	$>$ 60
3	$>$ 60	-
4	15	$>$ 60
5	$>$ 60	-

[a] 1.0 M in THF, 60 °C

*2. Electronic characterization of surfaces **1** – **6**.* $J - V$ data was obtained before and after $C_{\text{diff}} - V$ measurement, using a Solartron 1287 using a sweep rate of 50 mV s^{-1}. $C_{\text{diff}} - V$ measurements were performed using a Schlumberger Model SI 1260 frequency response analyzer controlled by ZPlot software. A 10 mV amplitude sinusoidal signal was applied over the DC applied bias (0 to -0.5 V *vs.* counter) as the sinusoidal frequency was swept from 10 – 10^6 Hz. Data was selected from the frequency region with a phase angle of $\geq 85°$, and fit to a simple model of a parallel RC circuit in series with a resistance, R_s, Figure 4.5.

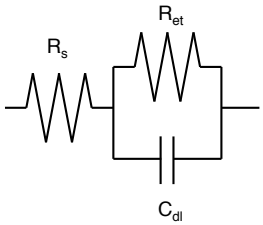

Figure 4.4. Model circuit

The impedance data were fit to the Mott-Schottky equation, eqn. 4.2, to obtain $\mathbf{E}_{\text{fb}}$. The $\Phi_{\text{B,n}}$ and $\Phi_{\text{B,p}}$ were calculated using eqn. 4.3 and 4.6, respectively.

$$\Phi_{\text{B,p}} = \frac{E_{\text{fb}}}{q} - \frac{k_{\text{B}}T}{q} \ln\left(\frac{N_D}{N_V}\right) \tag{4.6}$$

where N_D and N_V are the dopant density and the effective density of states in the valence band.

*3. Spectroscopic characterization of surfaces **1** – **6**.* Spectroscopic characterization was performed in a similar fashion to that of Chapter 3 and as described above. Samples were

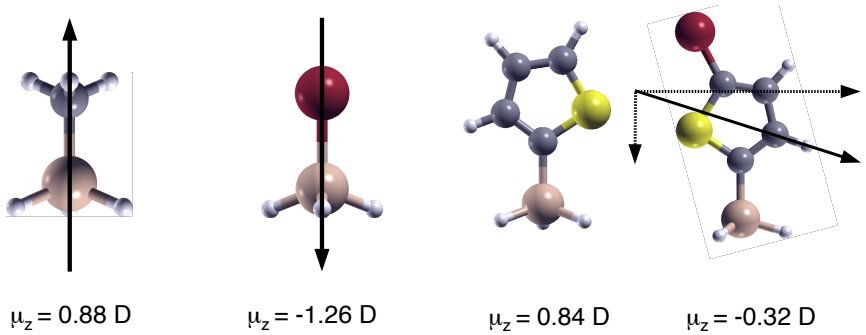

Figure 4.5. Calculated molecular dipole moments of CH_3-SiH_3, Br-SiH_3, SC_4H_3-Si_3, and SC_4H_2Br-SiH_3

measured using either a M-Probe XP spectrometer or Kratos AXIS Ultra DLD using the Al kα and He-I emission sources. Prior to Kratos XPS or UPS acquisition, samples were annealed at 175 °C for $>$ 1 h.

4.4.2 Theoretical ΔIP by Si(111) functionalization.

The ab initio model discussed in section 4.3 was used to predict the work function shift for surfaces **2**, **3**, **4**, and **5** upon functionalization. Figure 4.5 shows the molecular dipole moment of the gas phase silane molecules corresponding to **1**, Br-Si(111), **3**, and **5** with molecular dipole moments, μ_z, of 0.88 D, -1.26 D, 0.84 D, and -0.32 D, respectively. This suggests the SC_4H_2Br-group will form a negative surface dipole at SC_4H_2Br-functionalized Si(111).

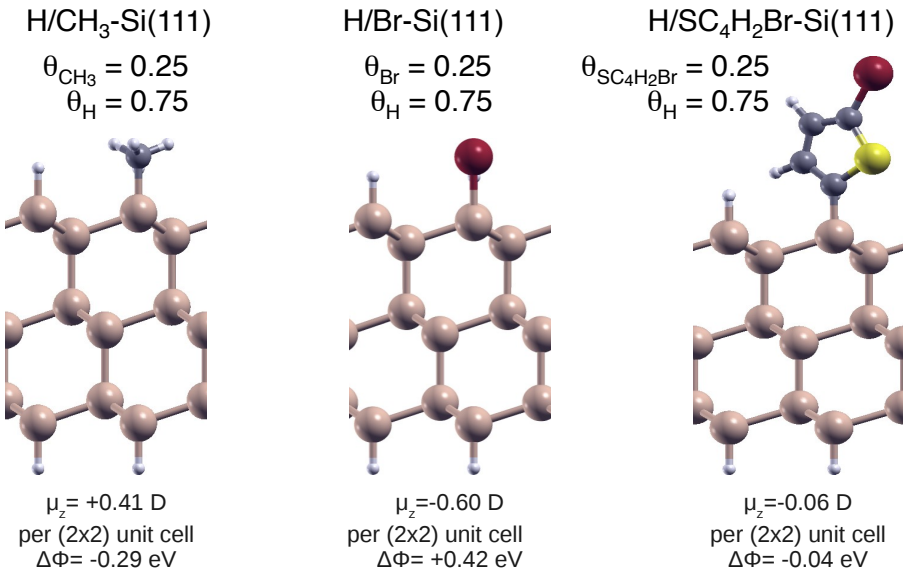

Figure 4.6. Calculated surface dipole moments of CH_3-Si(111), Br-Si(111), and SC_4H_2Br-Si(111).

The functionalized surfaces were modeled with 6-layer slabs. One surface was terminated with H-atoms and the other with the functionalization of interest. The DFT/LDA methods described previously were used to calculate $\Delta\phi = \phi_R - \phi_H$, where ϕ_R and ϕ_H are the work functions of the functionalized test surface and H-terminated surface, respectively. Figure 4.6

shows the (2 × 2) surface unit cell used in the model. The surfaces were modeled with partial functionalization of $\theta_{\mathrm{R}} = 0.25$, and with the remaining sites H-terminated, $\theta_{\mathrm{H}} = 0.75$.

Similarly, a (5 × 2) unit cell was used to model a mixed surface composition containing SC_4H_2-, CH_3, H-, and Br- groups, which would more realistically represent a synthetically attainable surface. A summary of the surface-functionalization induced work-function shifts, $\Delta\phi$ are given in Table 4.7. The $\Delta\phi$ show a typical mixed CH_3/SC_4H_2Br-terminated Si(111) surface will have intermediate band-edge positions compared to those of the CH_3- and H-terminated Si(111) surfaces.

Table 4.7. $\Delta\phi$ of Si(111) terminated with mixed molecular monolayers

R- =	SC_4H_2Br-	CH_3-	H-	Br-	$\Delta\phi^a$
$\theta_{\mathrm{R}} =$	0	1.0	0	0	-0.79[b]
	0.10	0.70	0.20	0	-0.56[c]
	0.10	0.70	0.10	0.10	-0.40[c,d]
	0.25	0	0.75	0	-0.04[b]
	0	0	1.0	0	0[b]

[a] $\Delta\phi = \phi_{\mathrm{R}} - \phi_{\mathrm{H}}$
[b] arranged in a (2 × 2) unit cell
[c] arranged in a (5 × 2) unit cell
[d] $-0.41 < \Delta\phi < -0.39$ depending on functional group arrangement.

The work function shift was shown to be monotonic, but nonlinear as the surface composition went from $\theta_{\mathrm{H}} = 1.0$ to $\theta_{\mathrm{H}} = 0$ and $\theta_{\mathrm{CH_3}} = 0$ to $\theta_{\mathrm{CH_3}} = 1.0$ (Figure 4.9). As the surface coverage of CH_3 groups increases, the intermolecular shielding slightly decreases the dipole moment / CH_3-group, resulting in the observed nonlinearity. Although the molecular dipoles of CH_3-Si_3 and SC_4H_3-SiH_3 are nearly identical (Figure 4.5), at a fixed θ_{H}, substitution of a CH_3-group for a SC_4H_3-group results in an increase of the total surface dipole moment and, thus, a larger reduction in the work function (Figure 4.9). The further reduction in the work function is attributed to a difference in charge exchange at the interface for the adsorbed CH_3-and SC_4H_3-groups.

4.4.3 Si(111) W_f shift with SC_4H_3- and SC_4H_2Br- functionalization

Figure 4.7 shows representative ultraviolet photoelectron spectra (UPS) of functionalized surfaces **1**, **3**, and **5**. The W_f, extrapolated from the secondary electron cut-off, was observed to increase by 200 mV on going from CH_3-functionalization, with $\theta_{\mathrm{C-Si}} = 1.0$, to SC_4H_3-functionalization, with $\theta_{\mathrm{C-Si}} = 0.55$ and $\theta_{\mathrm{H-Si}} \approx 0.45$. Upon bromination of the SC_4H_3- groups to SC_4H_2Br-groups, the W_f increases by a further 200 mV. The SC_4H_2Br-functionalized surface, **5**, was only 0.12 ± 0.05 mV lower than that of the H-terminated surface.

Similarly, an increase of W_f from surface **1** to **2** to **4** was observed. Interestingly, there was

not a large difference in W_f observed between surfaces **2** and **3**, nor was there a significant difference observed between surfaces **4** and **5**. Some adventitious carbon was present on SC_4H_3- and SC_4H_2Br- functionalized surfaces, despite a 175 °C anneal.

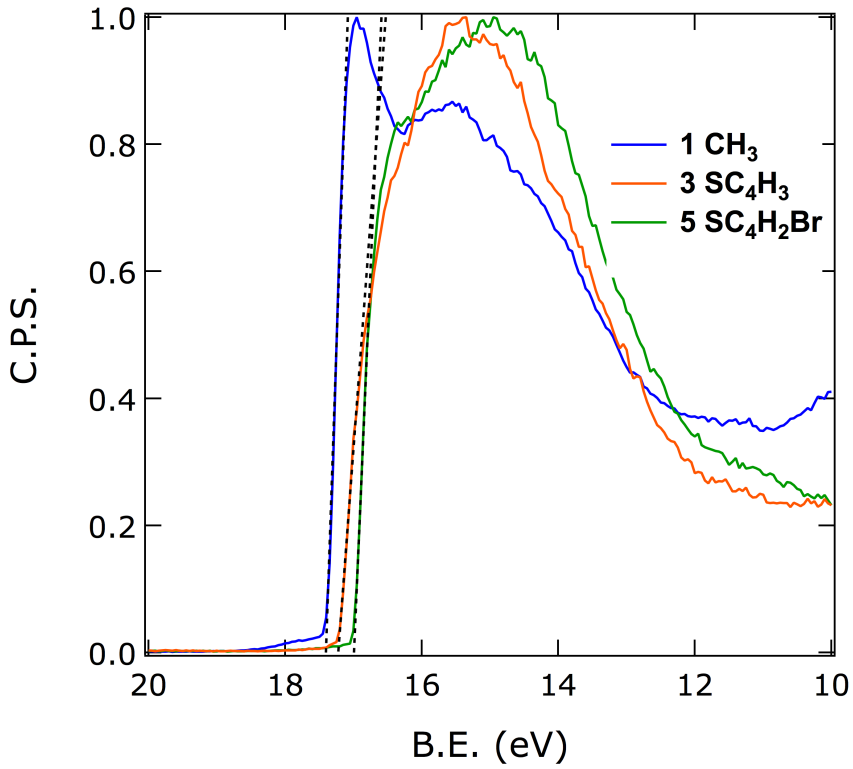

Figure 4.7. UP spectra of CH_3-, SC_4H_3-, and SC_4H_2Br-terminated Si(111) surfaces. Dashed lines show the extrapolation of the secondary electron cutoff. CH_3-Si(111) (blue, **1**) has the lowest W_f, with W_f increasing sequentially for SC_4H_3- (orange, **3**), and SC_4H_2Br- (green, **5**) terminated Si(111), in agreement with $C_{\text{diff}} - V$ measurements, and in partial agreement with theoretical predictions.

4.4.4 $\Phi_{B,p}$ and $\Phi_{B,n}$ of the functionalized Si(111)/Hg junction

$\Phi_{B,p}$ information was calculated using data from impedance measurements which were made at various functionalized p-Si(111)/Hg junctions. The surfaces were analyzed before and after impedance measurements. No evidence of monolayer degradation, Si surface oxidation, or reaction with Hg was evident as a result of the impedance measurements. As the W_f of Hg did not change, the variation in observed $\Delta\Phi_{B,p}$ or $\Delta\Phi_{B,n}$ was attributed to changes in the band-edge positions between samples. The compilation of experimental $C_{\text{diff}} - V$ of functionalized p-Si(111)/Hg data is summarized in Figure 4.8, Table 4.8, and Table 4.9.

Figure 4.8 shows the calculated barrier height at p-Si(111)/Hg Schottky junctions for surfaces **4**, **5**, and **6** determined from impedance data *vs.* the surface composition of SC_4H_2Br- groups, $\theta_{SC_4H_2Br}$. For comparison, $\Phi_{B,p}$ determined by J-V methods for **1** is included.[53] Table 4.8 compares the theoretical shift of the work function, $\Delta\phi$, with the measured shift in the barrier height at functionalized p-Si(111)/Hg Schottky junctions, $\Delta\Phi_{B,p}$. Where $\Delta\phi$ and $\Delta\Phi_{B,p}$ are the

theoretical and experimental shifts with respect to the H-terminated Si(111) surface, respectively.

$$\Delta\phi = \phi_{\mathrm{R}} - \phi_{\mathrm{H}} \tag{4.7}$$

$$\Delta\Phi_{\mathrm{B,p}} = \Phi_{\mathrm{R,B,p}} - \Phi_{\mathrm{H,B,p}} \tag{4.8}$$

As discussed earlier, even at the DFT level, $\Delta\phi$ and $\Delta\Phi_{\mathrm{B,p}}$ have very good agreement for the CH_3-terminated Si(111) surface, **1**. The mixed CH_3/SC_4H_2Br-Si(111) surface also shows very good agreement with theory. Additionally, the measured $\Delta\Phi_{\mathrm{B,p}} = -0.31$ eV and the theoretical $\Delta\phi = -0.40$ eV of surface **4** match very well. Finally, the measured $\Delta\Phi_{\mathrm{B,p}} = -0.09$ eV of surface **5** and the theoretical $\Delta\phi = -0.04$ eV of a surface with $\theta_{\mathrm{SC_4H_2Br}} = 0.25$ and $\theta_{\mathrm{H}} = 0.75$ are in good agreement.

The $C_{\mathrm{diff}} - V$ data suggest the band-edge positions of surface **5** with $\theta_{\mathrm{SC_4H_2Br}} = 0.10$, are very close to those of the H-Si(111) surface. Additionally, the band-edge positions of surface **4** are shifted to more positive potentials with respect to the CH_3-Si(111) surface, **1**, while the total $\theta_{\mathrm{Si-C}}$ is still very high, such that the pH-dependence of the band-edge positions is relieved and the surface is protected from oxidation.

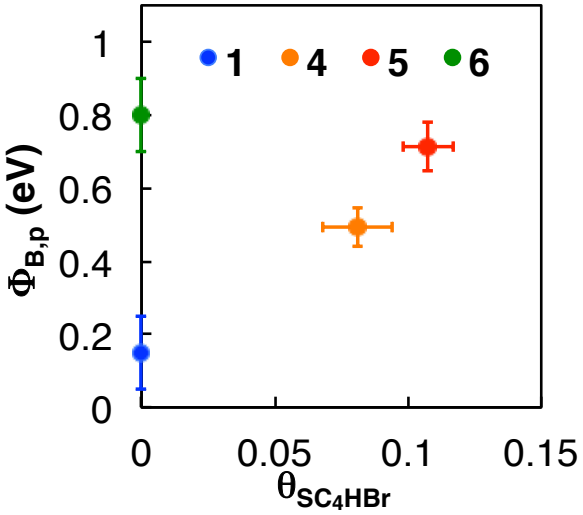

Figure 4.8. Change in work function with composition for mixed CH_3/SC_4H_2Br-Si(111) surfaces, experiment

DFT/LDA modeling suggests the surface dipole should increase with substitution of a CH_3-group with a SC_4H_3- group while keeping θ_{H} constant, Figure 4.9. The experimental $\Delta\Phi_{\mathrm{B,n}}$ results of impedance measurements at functionalized n-Si(111)/Hg surfaces are presented in Table 4.9. Theory predicts a monotonic increase in surface dipole with $\theta_{\mathrm{SC_4H_3}}$ or $\theta_{\mathrm{CH_3}}$, this is also observed in experiment. For example, Mott-Schottky analysis of the surface **3** shows $\Delta\Phi_{\mathrm{B,n}}$ = -0.40 eV, and the XP spectra show $\theta_{\mathrm{SC_4H_3}} = \theta_{\mathrm{C-Si}} = 0.55 \pm 0.08$. The surface **2** had $\Delta\Phi_{\mathrm{B,n}}$

Table 4.8. Experimental $\Delta\Phi_{B,p}$ and theoretical $\Delta\phi$ of SC_4H_2Br-functionalized p-Si(111)

R- =	SC_4H_2Br-	CH_3-	H-	Br-	$\Delta\Phi^a_{B,p}$ (eV)	$\Delta\phi^b$ (eV)
θ_R =	0	1.0	0	0	-0.65 ± 0.10	-0.79[c]
	0.10	0.70	0.10	0.10	-0.31 ± 0.05	-0.40[d,e]
	0.10	0.45[f]	0.40	0.05	-0.09 ± 0.07	-0.04[c,g]
	0	0	1.0	0	-	-[c]

[a] $\Delta\Phi_{B,p} = \Phi_{R,B,p} - \Phi_{H,B,p}$, experimental
[b] $\Delta\phi = \phi_R - \phi_H$, theoretical
[c] arranged in a (2×2) unit cell
[d] arranged in a (5×2) unit cell
[e] $-0.41 < \Delta\phi < -0.39$ depending on functional group arrangement.
[f] $\theta_{SC_4H_3}$
[g] theoretical for $\theta_{SC_4H_2Br} = 0.25$ and $\theta_H = 0.75$

Table 4.9. Experimental $\Delta\Phi_{B,n}$ and theoretical $\Delta\phi$ of SC_4H_3-functionalized n-Si(111)

R- =	SC_4H_3-	CH_3-	H-	$\Delta\Phi^a_{B,n}$	$\Delta\phi^b$
θ^c_R =	0	1.0	0	-0.65 ± 0.10	-0.79
	0.20	0.60	0.20	-0.59 ± 0.05	-0.90
	0.55	0	0.45	-0.40 ± 0.05	-0.89
	0	0	1.0	-	-

[a] $\Delta\Phi_{B,p} = \Phi_{R,B,p} - \Phi_{H,B,p}$, experimental
[b] $\Delta\phi = \phi_R - \phi_H$, theoretical, Figure 4.9
[c] estimated based on XPS data

= -0.59 eV and $\theta_{SC_4H_3} + \theta_{CH_3} = \theta_{C-Si} \approx 0.80$.

Theoretical results also suggest the SC_4H_3- groups should create a larger positive dipole on the Si(111) surface than the CH_3 groups, even though the silane derivative molecular dipoles are very similar (Figure 4.6). For example, at a constant θ_{C-Si}, substituting a CH_3 group for a SC_4H_3- group should increase the surface dipole and push the band-edge positions more negative, *i.e.*, further from the band-edges of the H-Si(111) surface (Figure 4.9). The magnitude of $\Delta\phi$ and difference between the increased dipole with SC_4H_3- over CH_3- functionalization is not observed. As observed in Figure 4.9, even at $\theta_{SC_4H_3} = 0.55$, surface **3** displays a more negative theoretical $\Delta\phi$ over surface **1** with $\theta_{CH_3} = 1.0$, and surface **2** with $\theta_{SC_4H_3} = 0.2$ and $\theta_{C-Si} \approx 0.8$ should also display a more negative $\Delta\phi$ than that of surface **1**.

Residual Si-Cl sites have been observed in the XP spectra of surface **3**. Additionally a rigorous study of $\Delta\Phi_B$ as a function of $\theta_{SC_4H_3}$ with constant θ_{C-Si} has not been conducted. In order to understand the discrepancy between the theoretical $\Delta\phi$ and the experimental $\Delta\Phi_B$, the Si-Cl sites must be removed from surface **3**. This might be done by an HF dip prior to $C_{diff} - V$ measurements.

4.4.5 Summary and outlook

While formation of Si-C bonds at Si(111) surfaces slow surface oxidation, passivate electronic defect states, and reduce the band-edge position dependence on pH, CH_3- and other alkyl

and unsaturated C chains impose a positive dipole that decreases the $\Phi_{B,p}$ at a given CH_3-terminated p-Si(111) heterojunction over that at the H-terminated surface. Si is more stable run cathodically, so increasing $\Phi_{B,p}$ is an important goal. Theoretical modeling of the SC_4H_2Br-functionalized Si(111) surface used for Heck couplings in Chapter 3, suggested the SC_4H_2Br-groups would impose a dipole very similar to that at the H-terminated Si(111) surface. Experimental studies at the SC_4H_2Br-functionalized mixed molecular surfaces **4** and **5** match theoretical predictions very well. Additionally, the band-edge positions appear to be very similar to those of the H-terminated Si(111) surface, so while the surface is protected by kinetically stable Si-C bonds, there is no functionalization-induced penalty in $\Phi_{B,p}$ at a given junction.

Adsorbates such as *para*-fluorophenyl- and perfluorophenyl-, and fluoro-substituted ethyl-groups should impose a larger negative dipole than SC_4H_2Br-. The issue with them is that they typically have low reactivity at the Cl-Si(111) surface. Perhaps anodic functionalization or higher temperature reactions can overcome the lack of reactivity. Initial results with mixed CH_3/*para*-fluorophenyl suggest at $\theta_{Fphen} \approx 0.1$, there is an increase in $\Phi_{B,p}$ at p-Si(111)/Hg heterojunctions over that at CH_3-Si(111).

Experimental results for positive dipoles do not match well with theory. While there may be some optimization needed on the computational side, there are some experiments which could be run on the experimental side to give clues into how far off the theory is. As described above, Cl-free and controlled constant θ_{C-Si} with variable $\theta_{SC_4H_3}$ can be preformed to understand how $\Delta\Phi_B$ changes with $\theta_{SC_4H_3}$. Furthermore, there are some limitations to $C_{diff} - V$ and UPS methods. Kelvin probe measurements should help in the understanding of the discrepancy between theory and experiment in the case of propynyl-terminated Si(111).

4.5 Conclusions

The dependence of band-edge position on surface dipole has been studied. Si, and many metal oxides, have pH-dependent band-edge energies. This is a drawback for Si photocathodes used for H_2O reduction to H_2 as $E(H_2O/H_2)$ is also pH-dependent, such that a change in $[H^+]$ cannot be used to change $\Phi_{B,p}$. CH_3-termination of an Si(111) surface stabilizes the band-edges with respect to pH by replacing H-Si sites, which convert to HO-Si sites, with stable C-Si bonds. Furthermore, the pH-dependence of the band-edges of Si(111) was also observed to be dependent on the coverage of C-Si sites, θ_{C-Si}. Therefore, while CH_3-Si(111), with $\theta_{C-Si} = 1.0$, mixed molecular monolayers are necessary in order to simultaneously introduce functional surface adsorbates, such as CH_2CHCH_2-, while imparting pH-stability to the band-edge positions.

CH_3-groups impose a positive dipole at the Si(111) surface. While the CH_3 groups add

oxidative stability and passivate electronic defect states, CH_3-termination lowers the $\Phi_{B,p}$ for a given heterojunction compared to the equivalent junction made with H-terminated Si(111). It is not immediately apparent that the dipole moment of the CH_3-terminated surface should be positive given the electronegativities of a CH_3 group and Si. Ab initio many-body perturbation theory and DFT calculations of ionization potential were performed for Cl-, Br-, H-, CH_3-, and CH_3CH_2-terminated Si(111) surfaces. The dipole at the CH_3-terminated surface is dominated by the CH_3- adsorbate, but is attenuated by the electronegativity difference between CH_3- and Si. The calculations were compared to UPS and $C_{\text{diff}} - V$ measurements, and were found to closely match the shift *vs.* H-Si(111) by more simple DFT/LDA approximations, and that the absolute IP matched well with G_0W_0 many body perturbation theory calculations. Calculations for the SC_4H_3- and SC_4H_2Br-terminated surfaces studied for Heck coupling chemistry were performed, with the prediction that the SC_4H_2Br-groups should impose a negative dipole at the surface. Indeed, the calculations also predict the SC_4H_2Br-groups should form a small negative dipole at the surface.

$C_{\text{diff}} - V$ and UPS measurements were performed on surfaces **1** - **6**. The $\Delta\Phi_{B,p}$ and experimental $\Delta\phi$ were compared with the theoretical $\Delta\phi$. Measurements for SC_4H_2Br-functionalized surfaces, **4** and **5**, matched predicted $\Delta\phi$ very well. Measurements for SC_4H_3-functionalized surfaces, **2** and **3**, followed some of the predicted trends, however, there was a discrepancy between experiment and theory on the magnitude of ΔIP and the difference between the surface dipole of adsorbed CH_3- and SC_4H_3- groups. Nevertheless, the band-edge positions of mixed CH_3/SC_4H_2Br-Si(111), surface **4** were pushed $\sim$ 340 mV positive of those at the CH_3-Si(111) surface, surface **1**. Furthermore, the band-edge positions of the mixed SC_4H_3/SC_4H_2Br-Si(111), surface **5**, were pushed $\sim$ 510 mV positive, nearly regaining the band-edge positions of H-terminated Si(111), surface **6**. Additionally, surfaces **4** and **5** have the added stability of surface termination with C-Si bonds.

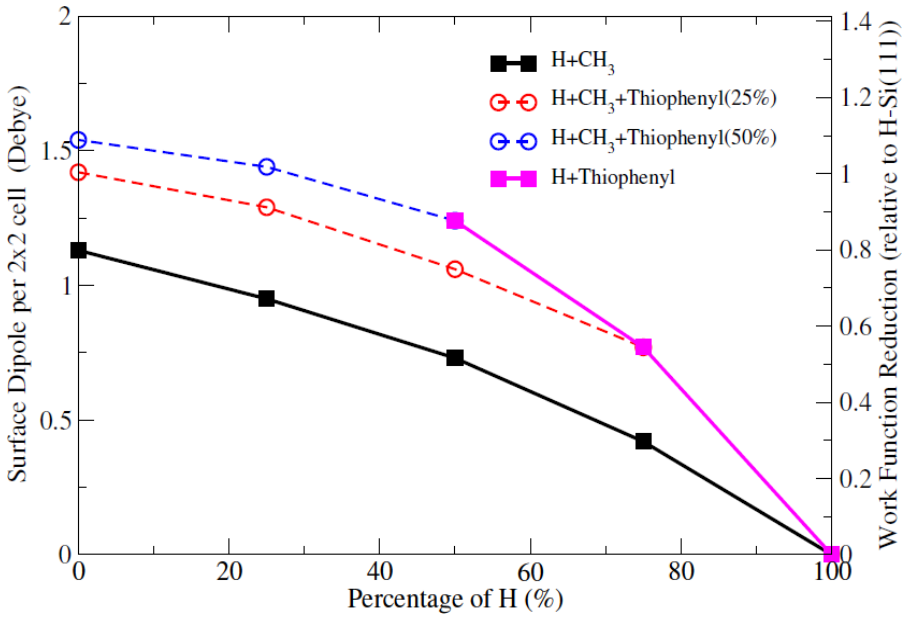

Figure 4.9. Change in work function as a function of composition for mixed CH_3/SC_4H_3-Si(111) surfaces, theory

Chapter 5

Surface-initiated polymerization and atomic layer deposition

In the previous chapters, the synthesis, and spectroscopic and electronic characterization of mixed molecular monolayers on Si(111) were studied. In the initial study of the utility of added functionality by this method, thiophene groups were bound to Si(111) surfaces, and subsequent Heck coupling chemistry was performed. In the initial section of this chapter, Section 5.1, we examine the addition of butenyl, $CH_2CHCH_2CH_2$-, groups into a mixed butenyl/CH_3- monolayer for the covalent bonding of Si microwires into a PDMS matrix. In Section 5.2 the use of mixed CH_3/2,2':5',2"-terthiophen-5"-yl- molecular monolayers was used to initiate covalently bound electropolymerization of EDOT at functionalized p- and n-type Si(111) surfaces. The electronic and adhesion interactions were studied. Finally, in Section 5.3, the utility of surface-bound aldehyde groups for atomic layer deposition, ALD, initiation of Al_2O_3, MnO_2, and TiO_2 at mixed CH_3/aldehyde molecular monolayers was investigated. The electronic properties of the surfaces before and after ALD were measured, and the degree of conformity and surface roughness were assessed.

5.1 Surface functionality mediated interfacial strength of Si microwire/PDMS composites

Single crystal semiconductor light absorbing materials have some of the highest solar energy conversion efficiencies. The single crystal substrates are expensive because a high purity is required to match the carrier diffusion length, L, with the optical penetration depth, α^{-1}. Furthermore, wafer sawing produces a lot of waste. The rigidity inherent in single crystal

semiconductors increases cost through expensive processing, heavy protective elements, and difficult installation. Semiconductor structuring allows for decreased single crystal growth cost because the structuring decouples the direction of light absorption, α^{-1}, from the direction of carrier collection, L.[271,272] Furthermore, that structured materials could be embedded in some flexible substrate making them amenable to roll-to-roll type processing.[273]

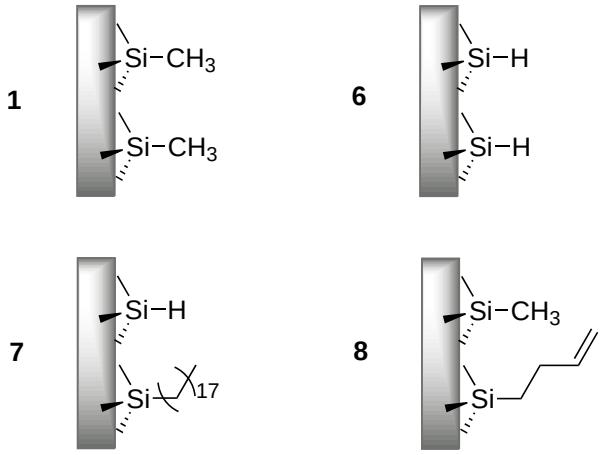

Scheme 5.1. Si-microwire surface functionalization for covalent and van der Waals bonding interactions with a PDMS matrix

Vapor-liquid-solid (VLS) grown Si microwires have been studied as inexpensive, high-efficiency, light-absorbing materials.[217,272,274–276] Removal of the wire array from the VLS growth substrate has been accomplished by embedding the Si-microwires in polydimethylsiloxane (PDMS).[273] The PDMS qualitatively showed improved interfacial adhesion compared to other polymers tested in that the crystallographic orientation of the Si-microwires was preserved, even after removal from the growth substrate. The array removal allowed for recycling of the single-crystal VLS growth wafer, thus significantly decreasing fabrication cost of crystalline Si microwire solar absorber arrays. Free standing, PDMS-embedded Si-microwire arrays have demonstrated efficiencies of 7.9% under AM1.5 illumination.

Because of the promise of this technology and the applicability to other applications and materials, we studied the Si-microwire/PDMS interfacial adhesion strength by single-wire pull-out tests.[277] The Si-microwire surface was decorated with H-, CH_3, $CH_3/CH_2CHCH_2CH_2$-, or $C_{18}H_{37}$- groups, Scheme 5.1, and the wire array was embedded into a PDMS matrix. *In situ* nanomechanical measurements of the interfacial shear strengths of wires with various surface functionalization, showed a direct connection between molecular-level chemistry and mechanical strength of the microwire/PDMS composite. Single-wire pull-out tests were performed in a custom built *in situ* nanomechanical instrument in Julia Greer's labs. The interfacial shear strength was based on the maximum applied load at the instance of debonding. An unambiguous correlation between surface functionality and interfacial shear strength was observed.

PDMS is an elastomeric material that crosslinks upon curing *via* hydrosilylation. Scheme 5.2 shows the chemical identity of part 1 (Base) and part 2 (Curing agent). A small amount of a Pt catalyst is included. Upon heating the, crosslinked PDMS matrix is formed by Pt catalyzed hydrosilylation between vinyl end groups of the base and the Si-H sites of the curing agent. We predicted that in the presence of curing PDMS, surfaces **6** and **8** would participate in the hydrosilylation reaction through the H-Si and CH_2=$CHCH_2CH_2$-Si sites, respectively, resulting in covalent linkages between the Si-microwires and the PDMS matrix. The mixed CH_3/CH_2=$CHCH_2CH_2$- surfaces were designed to avoid steric obstruction of the terminal olefin groups during the hydrosilylation reaction. The functional groups present at surfaces **1** and **7** would participate only in van der Waals interactions, therefore providing a comparison to the covalent bonding case, and allowing us to ascertain the effects of chain length.

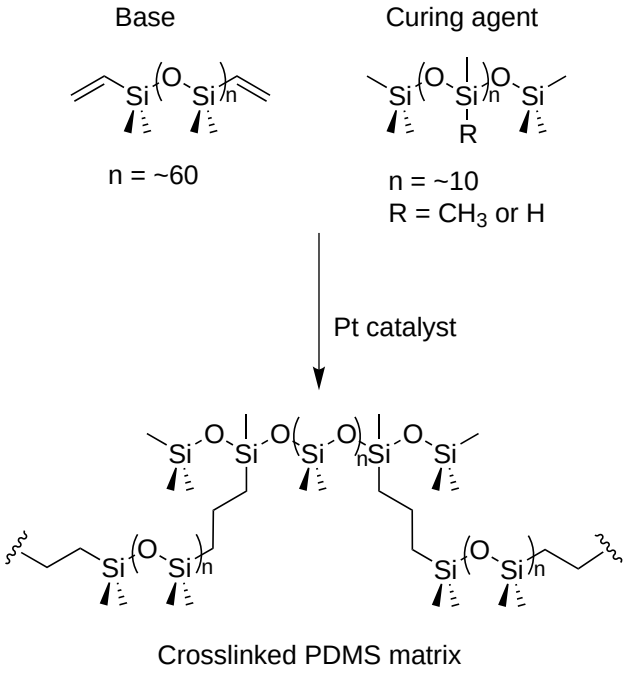

Scheme 5.2. Chemistry of PDMS components and crosslinking

Individual wire pull-out tests present a direct method for measurement of interfacial strength between the Si-microwires and the PDMS matrix.[278–280] Individual wire pull-out tests were performed in a custom-built *in situ* mechanical deformation instrument, SEMentor, comprised of Scanning Electron Microscope (SEM) and a nanomechanical module similar to a nanoindenter.[281]

An overview of the fabrication and processing steps is shown in Figure 5.1. In previous reports on Si-microwires, grown by same mechanism, Si(111) with a ± 4° miscut from <111> orientation was used at the growth wafer. In order to avoid convolution of torque forces within the composite with pure interfacial adhesion strength, a very low miscut angle wafer was used

as the growth wafer, step 1 of Figure 5.1. As reported previously,[272] after growth of a 100 nm thermal oxide, photolithography was used to expose 3 μm holes at a 7 μm pitch in a square pattern. The exposed SiO_2 over layer was etched in buffered HF through to the underlying Si(111) surface. Cu was evaporated on the sample, then the remaining photoresist and Cu deposited over the photoresist was removed, leaving 3 nm Cu particles confined in the oxide holes, step 2 of Figure 5.1. The sample was annealed, then microwires were grown from $SiCl_4$ and H_2 precursor gases. Wires were grown to 25–35 μm in length, step 3 of Figure 5.1.

After microwire growth, the Cu catalysts were removed with an RCA-II clean (5:1:1 H_2O: HCl: H_2O_2, 25 min, 70 °C), followed by buffered HF dip for 30 s. This was sometimes repeated to ensure full Cu removal. Surface functionalization was performed in a similar fashion to that described in previous chapters. After Cu removal, organic contaminants were removed from the wire arrays with a piranha clean (3:1 H_2SO_4:H_2O_2, 90 °C, 10 min). The piranha solution was drained, and the array was rinsed by sequential submersion in fresh 18 MΩ resistivity H_2O. The chemical oxide was removed with a 30 s dip in buffered HF. Residual buffered HF was rinsed from the sample by sequential submersion in 18 MΩ H_2O, and arrays were dried under a stream of N_2. Freshly etched arrays were immediately placed in a N_2 purged glove box with $<$ 10 ppm O_2.

Wire arrays were submerged in a saturated phosphorous(V) chloride (PCl_5, Alfa Aesar, 99.998% metal basis) in chlorobenzene (anhydrous, Sigma Aldrich, 98%) at 90 °C for 45 min. The solution was allowed to cool to near room temperature. The wire array was removed from solution and rinsed with chlorobenzene and THF (Anhydrous, Sigma Aldrich).

Cl-terminated wire arrays were alkylated at 60 °C for $>$ 3 h in a 0.5 M solution in THF of CH_3MgCl (Sigma Aldrich, diluted from 3.0 M in THF), 3-butenylMgCl (Sigma Aldrich, 0.5 M in THF), or octadecylMgCl (Sigma-Aldrich, 0.5 M in THF). Mixed CH_3/butenyl-terminated wire arrays were prepared by submersion of Cl-terminated wires for 10 min in 0.5 M 3-butenylMgCl in THF at 60 C. The mixed Cl/butenyl-terminated wire arrays were rinsed with copious amounts of THF, then submerged in 0.5 M CH_3MgCl for $>$ 3 h at 60 °C. After completion of both reactions, the Si samples were rinsed thoroughly with THF and removed from the N_2(g)-purged glove box. Samples were sequentially cleaned of residual Mg salts by repeated submersion in each of THF, methanol, and water. Finally, the arrays were dried under a stream of N_2(g).

A 10:1 ratio mix of PDMS base and curing agent (Sylgard 184, Dow Corning) was spin cast into Si wire array grown on Si wafer, which was cured at 120 °C for 2 h, step 4 of Figure 5.1. The PDMS embedded wire array was then peeled off from the substrate using a razor blade, flipped over, and bonded onto clean Si wafer using cyanoacrylate adhesive, step 5 of Figure 5.1.

Focused Ion Beam (FIB) with Ga^+ ion source was used to mill out the T-shaped top of the

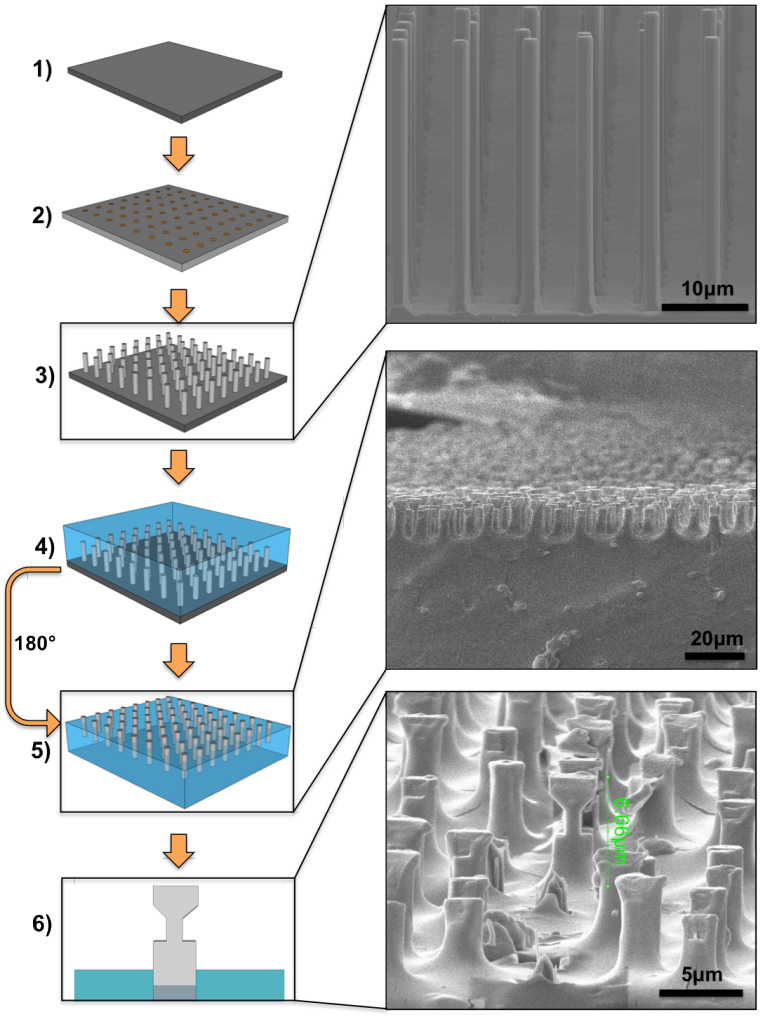

Figure 5.1. Schematic representation (left) and corresponding SEM images (right) of the fabrication and processing steps for the Si-microwire/PDMS composite. 1) 100 nm thermal oxide layer on Si(111) $\pm$ 0.1°. 2) Cu catalyst particles patterned into photolithographically defined 3 μm holes etched through the oxide overlayer. 3) (SEM image) VLS growth of Si-microwires using $SiCl_4$ and H_2 precursor gases. Wires grown to 25–35 μm in height. 4) Spin cast PDMS (Sylgard 184) over the array. 5) (SEM image) PDMS cure, and removal of embedded array from wafer. Flipped composite shows exposed wire bases. 6) (SEM image) The exposed wire end was milled into a T-shaped handle *via* FIB in preparation for mechanical testing.

wire to perform pullout test using diamond grip, step 6 of Figure 5.1. During the experiment, the sample stage was manually controlled to position the dog-bone shaped tip inside the FIB-machined diamond tension grips.

The pullout tests were performed by Clara Cho using *in situ* nanomechanical tester, SEMentor, at a constant displacement rate of 50 nm s^{-1}. Each wire was displace by 30 μm away from the surface, and most wires reached complete debonding from the matrix before reaching the displacement limit. 5–6 successful tests were carried out for each sample set. Load *vs* displacement curves were obtained from the experiment, from which we calculated interfacial shear stress by dividing by the surface area of the wires.

5.1.1 Results

Time-lapse SEM video frames with concurrent load *vs*. normalized displacement data generated by SEMentor during a typical pullout test are shown in Figure 5.2. Three distinct regions can be identified in the plot: Region 1 of Figure 5.2 corresponds to the initial elastic tensile loading of the composite with a fully bonded interface, as revealed by the corresponding SEM image. Wire debonding occurs at the onset of Region 2 of Figure 5.2 at the maximum load of 0.33 mN, followed by a marked ($\sim 3\times$) load drop over a short displacement of 1–2 μm. During this load drop, the prescribed displacement rate of 50 nm s^{-1} was difficult to maintain as the nanoindenter is inherently a load-controlled instrument, and the feedback loop requires time to adjust the displacement rate accurately. Consequently, the displacement rate during this debonding event is higher than prescribed, typically restoring to the latter in 2–3 seconds. During Region 3 of Figure 5.2, frictional stress between the debonded surface and the PDMS matrix dominates the load *vs*. displacement curve. The applied force gradually decreases as the microwire/PDMS interfacial area decreases. the matrix surrounding the wire in this region does not visibly deform as most of the stored elastic energy is presumably absorbed by friction. The underlying physical deformation mechanism after initial debonding varies depending on the type of surface functionalization: broken chemical bonds are irreparable in bonding-induced interactions, whereas in hydrogen- and nonbonding cases, the adjacent molecules can reconfigure themselves to keep the interface partially intact during frictional sliding.[282] Region 4 of Figure 5.2 is the point where the wire is completely removed from the PDMS matrix. At this point PDMS may be observed on the wire surface, which qualitatively indicates the degree to which debonding occurs within the PDMS matrix rather than at the PDMS/wire interface.

Figure 5.3 shows representative pull-out curves for the four functionalized Si wires, where the average interfacial shear stress (τ) is plotted against raw displacement normalized by the total wire length. Each image is vertically offset by one unit for clarity. The interfacial shear stress

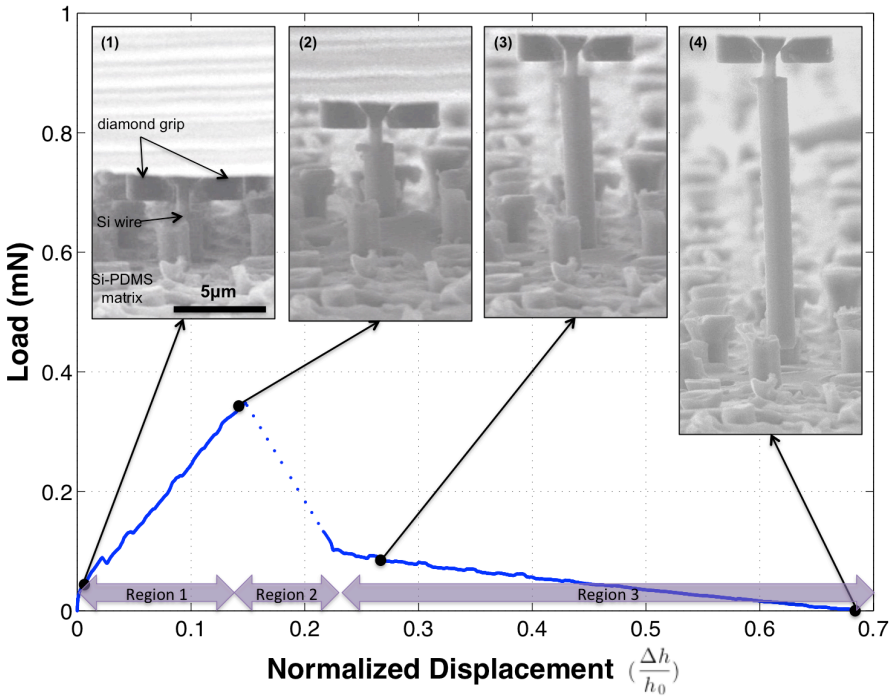

Figure 5.2. Sample load (mN) *vs.* normalized displacement $\left(\frac{\Delta h}{h_0}\right)$ behavior of a single PDMS embedded Si-microwire pull-out test. The displacement is normalized for wire height, h, and SEM images correspond to distinct regions: Region 1 — elastic loading of the Si/PDMS composite, Region 2 — interfacial debonding with partial removal of the wire from the PDMS matrix, Region 3 — frictional stress between the debonded wire surface and the PDMS matrix, and Region 4 - the completely removed wire with residual PDMS indicating failure did not occur entirely at PDMS/wire interface.

is calculated by dividing the applied axial load (F) by the interfacial contact area between the wire and PDMS

$$\tau = \frac{F}{2\pi r L} \tag{5.1}$$

where r and L are the radius and length of the wire, respectively. The overall interfacial shear strength is obtained by

$$\tau_{max} = \frac{F_{max}}{2\pi r L} \tag{5.2}$$

where F_{max} is the maximum applied axial load at the instance of debonding. Table 5.1 gives the average interfacial shear strengths and average normalized displacement at debonding for each sample type. Our results demonstrate that H-terminated Si nanowire surface exhibits the highest interfacial shear strength of 8 MPa, followed by methyl-terminated surface at 4.1 MPa, mixed butenyl-/methyl-terminated surface at 3.5 MPa, with the octadecyl-terminated surface having the lowest interfacial shear strength of 1.5 MPa. $\Gamma_{\mathrm{C-Si}}$ was determined from the substrate overlayer equation, as described in the previous chapters. The d_{ov} was assumed to be the same as that on the Si(111) surface. $\theta_{\mathrm{C-Si}}$ was calculated based on the number of atop atoms on a Si(011) surface, $\Gamma_{(011)} = 9.6 \times 10^{14}$.

SEM images of completely pulled out wires from each sample group, shown next to their respective stress-strain curves in Figure 5.3, reveal that samples with lower interfacial strengths retain their faceted, pristine surfaces while those with higher interfacial strengths have residual PDMS as a result of incomplete debonding during tensile loading. The adhered PDMS is also indicative of matrix cracking, implying that the work of fracture includes a significant amount of plastic dissipation, which can be estimated by calculating the work of adhesion at the wire-polymer interface (see reference 277).

5.1.2 Discussion

Table 5.1 shows the mean interfacial shear strengths of each functional group and the predicted adhesion interaction. The adhesion interaction correspond to a predicted bond strength of covalent bonds > van der Waals bonds. There is a larger predicted number density of covalent bonds for surface **6** than for surface **8**. There was a stronger predicted van der Waals interaction at surface **1** than **7** because the long octadecyl- groups at surface **7** are thought to hold the PDMS further from the Si surface than the CH_3- groups on surface **1**. A positive correlation is observed going from surface **7** to **1** to **6**. We expected partial covalent bonding for surface **8** through the terminal olefins, however, we actually observed a slightly lower interfacial shear strength compared with surface **1**. This is most likely due to the limited availability of H-Si sites to bind with the CH_2=$CHCH_2CH_2$-groups in the PDMS prepolymer. H-Si sites are limiting in the PDMS curing reaction, therefore, the butenyl- groups probably functioned to hold the curing PDMS far from the surface, similar to the octadecyl groups on surface **7**, such van der Waals interactions were also weakened over those at surface **1**.

A similar trend is observed for normalized displacement at the instance of debonding in Table 5.1. Stronger interfaces show greater strains-at-failure, with the covalently bonded interface (surface **6**) having normalized displacement of 0.57 before onset of debonding while for the fully nonbonded samples, (surface **7**) the failure occurs at the normalized displacement of only 0.14. Of note is the difference in the interfacial shear strength between methyl-terminated and octadecyl-terminated Si; as the latter appears to be 62% weaker than the former. This suggests that the adhesion mechanism in our system is not dominated by the entanglement of polymer chains with the long octadecyl- groups, as one might expect, because that would result in an increased interfacial shear strength with longer alkyl-chains.[282] Rather, it appears that chemical interaction is the dominant mechanism for adhesion in this system. The octadecyl-terminated Si shows lower interfacial shear strengths because the Si surface is densely covered with long, nonpolar C_{18}-chains, thereby preventing PDMS from interacting with the Si surface. Methyl-terminated Si surface, on the other hand, has only a C_1 chain covering the surface, and

Table 5.1. Summary of chemical functionalization and mechanical properties measured by single-wire pull-out tests

Surface Functionality	$\Gamma_{C\text{-}Si}$ (cm^{-2})	$\theta_{C\text{-}Si}$	Adhesion Interaction[a]	Interfacial shear strength (MPa)	Normalized displacement at debonding	Work at fracture ($J\ m^{-2}$)
H-Si(111) 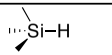	-	1[b]	Covalent bond	8	0.57	124
Mixed butenyl/ CH_3-Si(011) 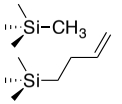	$5.0 \pm 0.2 \times 10^{14}$	0.52 ± 0.02[c]	Covalent bond	3.5	0.36	22
CH_3-Si(011) 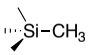	$6.8 \pm 0.2 \times 10^{14}$	0.71 ± 0.02[c]	vdW interaction	4.1	0.42	33
Octadecyl-Si(011) 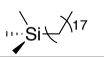	$2.7 \pm 0.3 \times 10^{14}$	0.28 ± 0.03[c]	vdW interaction	1.5	0.14	5

[a]Predicted adhesion interaction
[b]Reconstruction with mono-, di-, trihydrides
[c]$\theta_{C\text{-}Si} = \Gamma_{C\text{-}Si}/\Gamma_{Si(011)}$; as determined by XPS. Average ± standard deviation

therefore is less effective at shielding Si atoms from interacting with PDMS. This is further substantiated by XPS analysis of the Methyl-terminated Si (110) surface, which reveals that only 71 ± 2% of the surface was chemically functionalized, as shown in Table 5.1.

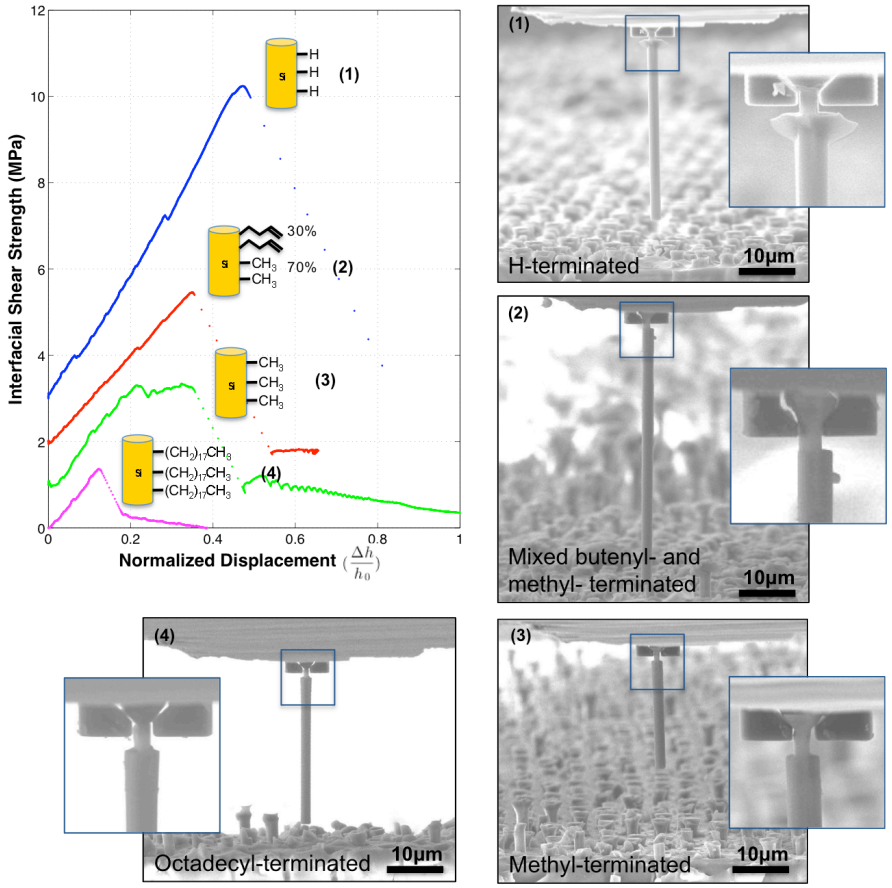

Figure 5.3. Interfacial shear strength *vs.* normalized axial displacement of H- (blue, 1), mixed CH_3/CH_2=$CHCH_2CH_2$- (red, 2), CH_3- (green, 3), and $C_{18}H_{37}$- (pink, 4) functionalized Si microwires from a PDMS matrix. The SEM images show the amount of residual PDMS at the wire surface.

5.1.3 Fracture analysis

The work of fracture was calculated by Clara Cho and Julia Greer and is based on the load *vs.* raw displacement curves, by utilizing the shear lag model for short wires embedded inside a matrix and performing an energy balance of the composite system, with the aim of expressing the interfacial shear stress at the instance of debonding.[279,280] Shear lag model developed by Cox in 1952 primarily describes the load transfer between the fiber and a soft matrix, since it assumes that the fiber carries all axial load in tension while the matrix only carries shear stress.[283] Since chemically functionalized surfaces contain only a very thin, atomic-level interface, it is reasonable to not treat this system as consisting a three-phase system with an interphase, as commonly done for traditional composites.

Debonding occurs when the rate of the elastic energy released by the composite (dU_c/dL) is

equal to the rate of surface energy increased due to debonding (dU_s/dL), plus the rate of elastic energy stored in the debonded wire (dU_{db}/dL)

$$\frac{dU_c}{dL} = \frac{dU_s}{dL} + \frac{dU_{db}}{dL} \tag{5.3}$$

By substituting the expression for the interfacial shear stress obtained from the shear lag model, the relationship between the work of fracture and interfacial shear stress is

$$G_i = \frac{\tau_i^2 r}{n^2 E_f} \tag{5.4}$$

where τ_i is the interfacial shear stress at debonding, E_f is the elastic modulus of the Si microwire (analogous to fiber), r is the microwire radius, and n is the dimensionless quantity

$$n^2 = \frac{E_m}{E_f\,(1+\nu_m)\ln\left(\frac{R}{r}\right)} \tag{5.5}$$

Details of this derivation are provided in ref 277.

Table 5.1 includes the average interfacial shear strengths, work of fracture (J m^{-2}), and microwire-normalized displacement at debonding for each surface functionality. We find that consistent with having the maximum interfacial shear strength of the functionalized samples tested, H-terminated Si (surface **6**) also has the highest work of fracture of 124 J m^{-2}. Comparing it with the predicted bond energy (around 1–5 J m^{-2}), correlated with the work of adhesion, H-terminated Si is expected to have significant plastic dissipation, which is consistent with the SEM image revealing substantial PDMS residue remaining on the wire post pull-out. The degree of such nonideal debonding, *i.e.*, resulting in some residual PDMS attached to the wire post pull-out, is indicative of PDMS cracking, as is clearly demonstrated by samples with a much lower contribution of plastic dissipation to the work of fracture term, having little or no residual PDMS attached to the pulled out wire.

We further demonstrate that the interfacial shear stress is unambiguously correlated to bond strength by estimating the bond energy based on the relative surface coverage as revealed by XPS analysis. We represent the facets of <111>-oriented Si wires *via* Wulff construction, which results in a hexagonal cross section with (110) facets.[284,285] We then prepared the planar controls, R-Si(110), for XPS analysis to estimate the percent coverage of these facets. Details of XPS calculations are given in previous chapters, and fractional coverage, $\theta_{\mathrm{C-Si}}$ is listed in Table 5.1. Based on these analyses, it is clear that the experimentally obtained work of fracture (G_i) correlates with the relative surface coverage of the particular ligand ($\theta_{\mathrm{C-Si}}$) Using the surface coverage of functionalized groups on the surface of (110) Si side facets and the radius of gyration of individual polymer chains, it is possible to estimate the total number of bonds formed at the

interface for all studied chemical functionalization types listed in Table 5.1, which would then enable bond energy calculations. These activities are currently ongoing and represent the scope of a separate publication.

5.1.4 Conclusions

In situ uniaxial tensile tests of individual Si nanowires embedded in a compliant PDMS matrix as a model toward flexible solar cell devices reveal that chemical functionalization of nanowire surfaces can be directly correlated with their interfacial adhesion strength. By using chemical reactions, four different functionalities spanning a range of bond energies, surface coverage, and alkyl chain, were covalently bonded to the Si-microwire facets, and the PDMS was allowed to cure in the presence of these functional groups. We find that covalent surface/matrix interactions, as with H-terminated Si, exhibited the highest interfacial shear strengths of 8 MPa, followed by mixed butenyl-/methyl-terminated and methyl-terminate Si forming predominantly van der Waals interactions (3–4 MPa), and then by octadecyl-terminated Si forming van der Waals interactions with greater separation (1–2 MPa). These results indicate that chemical functionalization can serve as an effective methodology for eliciting a wide range of interfacial adhesion between the rigid constituents and the soft polymer matrix, which in turn, can be quantifiably determined by the mechanical strength.

To further this research, a study on number of covalent bonds/area would be interesting, and a way to test a more simple model of the system. For example, mixed CH_3/H-functionalized Si-microwires with $\theta_{C-Si} = 0, 0.25, 0.50, 0.75$, and 1.0 could be used in the study. Another important experiment to suggest covalent bonding could be to return to the mixed CH_3/butenyl-functionalized surface, **8**, with a PDMS matrix with a majority Si-H sites rather than vinyl sites. There are fewer options for this experiment, however Silicon elastomer 9011 may work. It is a high molecular weight polymer with some Si-H sites. A UV cure after spin casting on surface **8** would covalently link the polymer to the surface.

5.2 Covalent linkage of PEDOT contacts at Si(111) surfaces

The success of 5.1 suggests surface chemistry can aid in the overall mechanical properties of a polymer embedded Si-microwire solar conversion device. A natural next step is to understand how to make covalent linkage to electronic contacts. Maintaining good electrical contact is important to photovoltaic efficiency, therefore, in order to gain the cost advantage of flexible modules, the electrical contact must also be robust to flexing. Conductive polymer coatings on

Si and other small band-gap semiconductors have been studied previously, predominantly as a stabilization layer.[141–147] Covalent bonding between Si and a conductive polymer was looked into as a method to improve adhesion.[147,148,286,287] The properties of Si/conductive polymer junctions have shown near-ideal junctions can be formed.[150,151,288]

Previous research has shown electrode surfaces functionalized with an oxidizable component, similar to the monomer species, will lead to increased adhesion between the electrode surface and an electropolymerized film.[148,286,287] AFM studies have shown an electropolymerized polymer film, deposited in the presence of surface-bound initiator groups leads to smoother films, and improved electrical properties compared to the same film deposited at a native oxide surface.[286,287]

The previously studied electropolymerization initiating surfaces are shown in Scheme 5.3. The drawback of surface **9** is the C_{11} chain separating the Si and PEDOT. This adds a large series resistance across the Si/PEDOT junction. Furthermore, the surface **9** was initially functionalized with undecylenate *via* UV-initiated hydrosilylation. Studies in our labs suggest UV-initiated hydrosilylation leaves surfaces with high electronic trap state densities.[80] High electronic trap state densities are observed even in a mixed monolayer with CH_3CH_2- groups, attached using the two-step alkylation, halogenation reaction, Table 5.2.

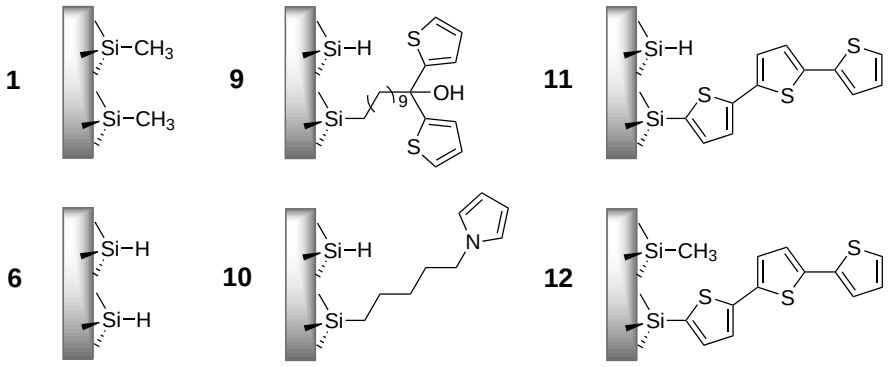

Scheme 5.3. Summary of surface functionalities explored for surface initiated electropolymerization. **1** and **6** used as control surfaces, **9**[148] and **10**[286,287] previously reported, and **11** and **12** studied in this work.

Surface **10** was synthesized by a reaction similar to the two-step halogenation/alkylation used in this work. Surface **10** was synthesized by the reaction of H-termianted Si(111), surface **6**, with a pyrrole-functionalized organolithium reagent, N-pyrrole-$(CH_2)_5$-Li. This is a common way to functionalize porous Si.[67,289] Infrared analysis spectroscopy showed evidence of pyrrole functionality, however, Si-H was still a significant, if not dominant species. Atomic force microscopy (AFM) showed lower rms roughness of films deposited at pyrrole-activated surfaces. Electronic properties across n-Si/pyrrole/polypyrrole and n-Si/native oxide/polypyrrole showed the barrier height, $\Phi_{B,n}$, did not change with surface functionalization, however, the diode quality factor did improve.

Table 5.2. Defect densities at Si(111) surfaces with mixed molecular monolayers synthesized from combined two-step/UV-initiated hydrosilylation reactions

Surface	S^a_{mix} (cm s^{-1})	$S^b_{\mathrm{mix,aged}}$ (cm s^{-1})	S^c_{cnt} (cm s^{-1})
CH_3/F-⌀-CH_2CH_2-[d]	400	61	28
CH_3CH_2/F-⌀-CH_2CH_2-[e]	660	> 600	61

[a]Measured within 1 h of hydrosilylation reaction work-up.
[b]Measured after 10 days in air.
[c]CH_3- or CH_3CH_2- functionalized surface after two-step halogenation/alkylation reaction. Synthesized in parallel with mixed monolayer surface.
[d]CH_3-Si(111) surface with $\theta_{\mathrm{C-Si}} = 1.0$, exposed to 4-fluorovinylbenzene under UV irradiation. $\theta_{\mathrm{F}} = 0$ as determined using XPS.
[e]CH_3CH_2-Si(111) surface with $\theta_{\mathrm{C-Si}} = 0.85$, exposed to 4-fluorovinylbenzene under UV irradiation. $\theta_{\mathrm{F}} = 0.1$ as determined using XPS.

Studies of PEDOT/PSS contacts with surface **1** showed a decreased majority carrier charge transfer velocity, ν_{n} than at an equivalent Si/Au heterojunction. This effectively decreases J_0, and therefore increases the maximum V_{OC}.[288] $V_{\mathrm{OC}} > 500$ mV were achieved at CH_3-terminated n-Si(111)/PEDOT:PSS junctions, whereas $V_{\mathrm{OC}} < 300$ mV were observed at the equivalent Si/Au junction.

Herein we use low electronic defect density terthiophene-functionalized Si(111) surfaces to initiate electropolymerization of EDOT. Surface recombination velocity measurements were performed at surfaces **1**, **11**, and **12**. X-ray photoelectron spectroscopy and grazing angle attenuated total reflectance FTIR spectroscopy were used to characterize surface coverage and composition. Dark, oxidative electropolymerization of EDOT was performed at p-type Si(111) surfaces **1**, **3**, **6**, **11**, and **12**. Subsequent $J - V$ properties of p-Si(111)/PEDOT surfaces show Ohmic contact. The tape test was used as a crude comparison of interfacial adhesion among the surface functionalities. Finally, oxide growth was assessed, postpolymerization for surfaces **6** and **1** by XPS after removal of the PEDOT by the Scotch tape method.

5.2.1 Materials and methods

*Synthesis of surfaces **1**, **3**, **6**, **11**, and **12**.* Electrochemical experiments were performed using single-side polished <111> oriented p-type Si wafers with resistivity of 2.3 Ω cm. Surface recombination velocity measurements were performed using double-side polished <111> oriented n-type Si wafers with resistivity of 4 – 6 kΩ cm. Degreasing, RCA-I and RCA-II cleaning were done as described in previous chapters. Immediately before functionalization, piranha cleaning and anisotropic etching in buffered HF and NH_4F(aq) was performed, as detailed in earlier

chapters. Surfaces **1**, **3**, and **6** were synthesized as described in Chapters 2 and 3. Surfaces **11** and **12** were synthesized by the two-step chlorination/alkylation reaction. Terthiophene functionalization was performed in a 0.1 – 0.3 M solution of 2-2',5'-2"-terthienyl-5"-Li in either hexanes (anhydrous, J. T. Baker), THF (anhydrous, Sigma Aldrich), or diethylether (anhydrous, dried over alumina columns). 0.9 equivalents of n-BuLi (Sigma Aldrich, 1.6 M in hexanes) was added to a 0.1 – 0.3 M solution of 2-2',5'-2"-terthiophene (Aldrich, 99%). The solution became a bright yellow/green solid slurry. Cl-terminated wafers were submerged in the terthienyllithium solution and heated to 60 °C (RT for diethylether reactions) for 10 – 120 min. The terthienyllithium solution was then drained and the surface was rinsed with hexanes (or THF or diethylether). The mixed Cl-/terthienyl-Si(111) surface was then submerged into a 1.0 M CH_3-MgCl solution for $>$ 1 h at 60 °C to produce surface **12**. Post-organolithium reaction work-up was performed as described in previous chapters.

Electropolymerization of EDOT at p-Si electrodes PEDOT films were deposited anodically from a solution of 10 mM 3,4-ethylenedioxythiophene (Sigma Aldrich, 97%) in acetonitrile (dried over alumina columns). Electrochemistry was carried out in an Ar filled glove box. 0.10 M lithium perchlorate (Sigma Aldrich, battery grade, dry, 99.99%) was used as the supporting electrolyte. The electropolymerization cell was set up as follows (Figure 5.4): A GaIn eutectic was scratched into the back of each sample as a back contact. The sample was placed on a stainless steel base with a Cu foil inserted between the sample and stainless steel to prevent reaction of the GaIn with the stainless steel. An o-ring was placed on top of the sample to make a seal between a teflon block and the sample. The teflon block was fastened to the stainless steel base *via* 4 screws. The area exposed to solution was determined by the o-ring. A glass tube screwed into a fitting in the teflon block directly over the sample. A $Ag/AgNO_3$ reference electrode ($\sim$ -230 mV *vs.* Fc^+/Fc, calibrated before each experiment) was used. A Pt mesh was used as a counter electrode. The sample surface, counter and reference electrodes were submerged in the EDOT solution. The potential was cycled from 0 V to 700 mV *vs.* reference 4 times (unless otherwise specified) at a rate of 50 mV / s. The deposition terminated at 700 mV. The solution was drained from the cell, the cell was disassembled, and the sample was rinsed well with fresh acetonitrile.

J-V *characterization.* The Si/PEDOT junction was probed by sweeping the potential in a two-electrode setup using a Solartron 1287 potentiostat. *J-V* characterization was performed in the same Ar filled glove box. The sample ('working') (with GaIn eutectic still making back contact) was placed on a Cu block. Contact to the PEDOT ('counter') was made by placing a Hg drop,

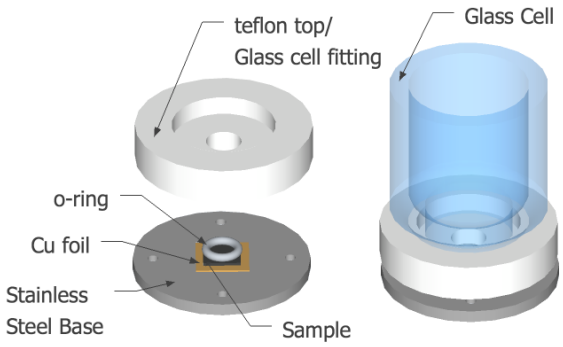

Figure 5.4. Teflon electropolymerization cell

confined within an o-ring, over the PEDOT layer. The potential was cycled from -0.5 to 0.5 V *vs.* counter at a rate of 50 mV s^{-1}.

Scotch® tape removal of PEDOT films. A "Scotch® tape peel-off test" was performed to test relative adhesion properties and remove PEDOT for XPS analysis. PEDOT surfaces were cleaned with acetonitrile and dried prior to the test. In air, a layer of 3M Scotch® tape was applied to the PEDOT and smoothed. The tape was peeled, by hand, 90° from the surface plane. A qualitative analysis of the amount of PEDOT remaining on the surface and the amount removed by the tape was noted.

Surface electronic trap-state density measurement. The electronic trap state density was measured as described in Chapter 2. Contact-less photogenerated carrier lifetimes were measured immediately after work-up and again after 1 day and 1 week in air.

Spectroscopic characterization. Grazing-angle attenuated total reflectance Fourier transform infrared (GATR-FTIR) spectroscopy was performed as detailed in Chapters 2 and 3. X-ray photoelectron spectroscopy (XPS) was performed as discussed in Chapters 3 and 4.3.1. Molecular coverages were determined by the substrate overlayer model as described previously.

5.2.2 Results

GATR-FTIR and XP spectroscopies. Figure 5.5 shows the GATR-FTIR spectrum of terthiophene-

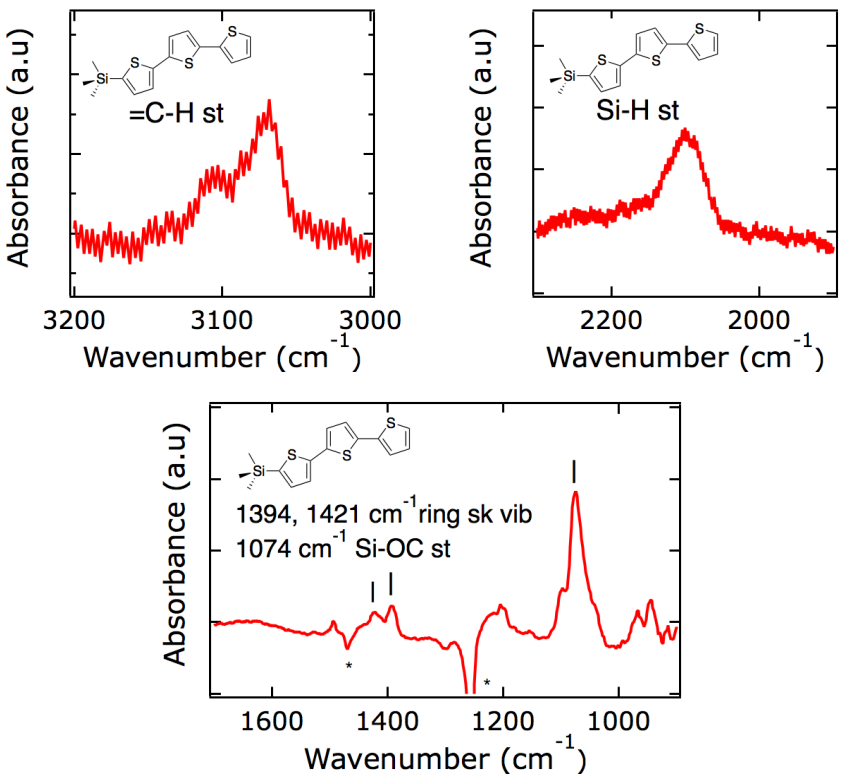

Figure 5.5. GATR-FTIR spectra of terthiophene-functionalized Si(111) with CH_3-Si(111) background subtraction, showing terthiophene vibrational modes at 3100 cm^{-1} and 3080 cm^{-1} (sp^2 =C-H stretch), and at 1394 cm^{-1} and 1421 cm^{-1} (ring skeletal vibrational modes). Signals at 2100 cm^{-1} and 1074 cm^{-1} are indicative of H- and CO-termination at non-terthiophene-functionalized sites, respectively.

terminated Si. Vibrational modes indicative of the terthiophene group were observed, including sp^2 =C-H stretching modes at 3100 and 3080 cm^{-1}. A multiplet of ring skeletal vibrational modes was observed with dominant peaks at 1394 and 1420 cm^{-1}. Peaks at 2100 cm^{-1}, Si-H stretch, and 1074 cm^{-1}, Si-OC stretch, were indicative of the identity of some non-Si-C terminated sites. Evidence for Si oxidation, beyond some Si-OC termination, was not apparent.

X-ray photoelectron spectroscopy data of the S 2s region indicated terthienyl termination with a maximum coverage of terthiophene groups of $\theta_{T_3} = 0.45 \pm 0.05$. In agreement with the GATR-FTIR data, here was no evidence for higher SiO_x in the high resolution Si 2p spectrum.

Photoconductivity decay measurements. Surface charge carrier lifetimes were measured for mixed CH_3/terthiophene-functionalized Si(111) (surface **12**), as well as the terthiophene-functionalized Si(111) surface (**11**), Figure 5.6. The surface carrier lifetime was compared to that at the native oxide terminated Si(111) surface. A summary of the observed S_{maj} values is given in Table 5.3. S_{maj} is calculated from the decay constant observed for the transition of the majority of the carriers, as double exponential decays were observed.

The terthiophene-functionalized surfaces showed improved S over the native oxide capped

Si(111) surface, however, $S_{T_3} > 400$ cm s^{-1}, Table 5.3. Incorporation of terthiophene into a multicomponent molecular monolayer containing $\theta_{T_3} = 0.10$ and $\theta_{CH_3} \approx 0.8$ decreased S to $\sim$ 30 cm s^{-1}.

Table 5.3. Surface carrier lifetime for terthiophene-functionalized Si(111)

Surface	S^a_{maj} (cm s^{-1})
CH_3-	25
CH_3/terthiophene-	31
terthiophene-	450
SiO_x	3400

[a]Conductivity decay fit as $y = y_0 + A_1 \exp(\frac{-t}{\tau_1}) + A_2 \exp(\frac{-x}{\tau_2})$ and $S = \frac{d}{2\tau_{maj}}$ where τ_{maj} is the decay constant for the path of the majority of carriers.

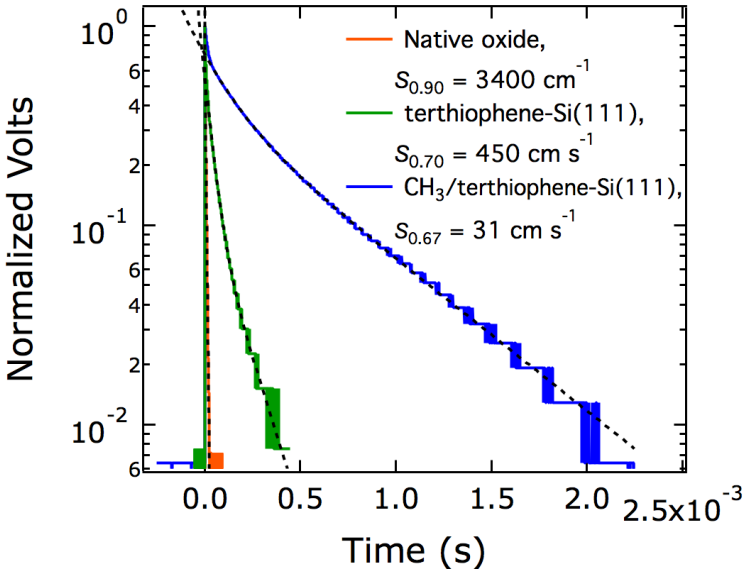

Figure 5.6. Photogenerated carrier decay profiles for native oxide, SiO_x capped and terthiophene and mixed CH_3/terthiophene-terminated Si(111)

J-V *analysis of p-Si/PEDOT junctions.* The Si/terthiophene/PEDOT junction was probed by making a soft Hg contact to the PEDOT. Dark J-V measurements were taken by scanning the potential of the Si from -0.5 to 0.5 *vs.* the PEDOT at a scan rate of 50 mV s^{-1}. Linear J-V behavior was observed for CH_3-, terthiophene-, and mixed CH_3/terthiophene-functionalized Si(111) electrodes (Figure 5.7), indicating Ohmic contact between the functionalized Si electrode and the PEDOT film. Surfaces containing a higher θ_{T_3} qualitatively displayed a lower total device resistance than those with lower θ_{T_3}.

Scotch® tape peel-off test. The relative interfacial adhesion strengths at Si/PEDOT interfaces were tested *via* the Scotch® tape test. PEDOT films were, by eye, completely removed from H-, CH_3- and SC_4H_3-functionalized electrodes (surfaces **6**, **1**, and **3**) *via* the tape test. By XPS, no remaining PEDOT was detected on CH_3- or H-terminated Si. The S 2s peak of the PEDOT was not sufficiently different from that of the SC_4H_3- groups on surface **3**. The tape test did not expose any polished Si and removed very little PEDOT from terthiophene-functionalized surfaces with $\theta_{T_3} < 0.1$. For surface **12** with $\theta_{T_3} < 0.1$, the tape test typically resulted in incomplete removal of the PEDOT film, and some of the underlying polished Si surface was exposed.

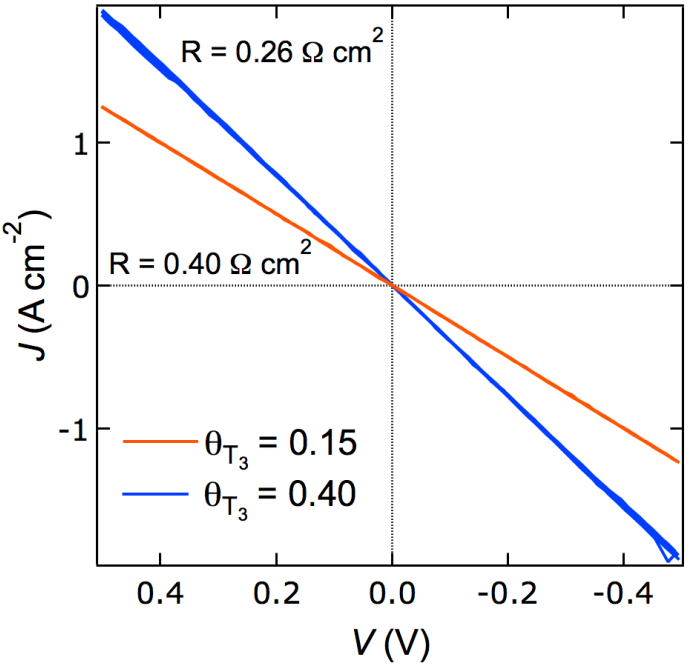

Figure 5.7. *J-V* characteristics of p-Si/terthiophene/PEDOT junctions with $\theta_{T_3} \approx 0.40$ and $\theta_{T_3} \approx 0.15$. PEDOT was electrochemically deposited directly onto terthiophene-functionalized p-Si(111) surfaces.

5.2.3 Discussion and future directions

Interfacial energetics across covalently linked Si/terthiophene/PEDOT junction. The p-Si/PEDOT:PSS, as formed by spin-coating of PEDOT:PSS onto surfaces **1** or **6**, contact has previously been found to be Ohmic, and an 840 mV barrier was observed at n-Si/CH_3/PEDOT:PSS junctions. The latter high barrier height junctions displayed $V_{OC} >$ 500 mV. The previous work is compared to the junction properties of covalently linked p-Si/terthiophene/PEDOT here. According to Chapter 4, the valence band levels of surfaces **11**

and **12** should fall between those of surfaces **1** and **6**, or according to theory, even more negative in potential than surface **1**. Therefore, if the Si/PEDOT:PSS junction is Ohmic and low resistivity at both H- and CH_3-terminated p-Si(111), it should also be Ohmic at p-Si/terthiophene/PEDOT junctions, given that the Fermi levels of PEDOT:PSS and the electrodeposited PEDOT are close.

As observed in Figure 5.7, the p-Si/terthiophene/PEDOT junction, as formed by surface initiated electropolymerization of EDOT at surface **12**, is ohmic. Furthermore, the contact resistance is lowered compared to that at the p-Si/PEDOT:PSS junctions, and seems to decrease with increasing θ_{T_3}. Therefore, the terthiophene linkage does not impede electron transfer across the interface, and may assist in electron transfer.

Surface electronic trap state densities at terthiophene-functionalized Si. Figure 5.6 shows the log conductivity decay profiles for a native oxide capped Si(111) surface, surface **11**, and the mixed composition surface **12**. Similar to the electronic defect state densities observed at thiophene-functionalized surface **3** *vs.* the mixed composition surface **2**, surface **11** displayed a much larger surface recombination velocity than surface **12**. For surfaces with $\theta_{T_3} < 0.20$, $S_{T_3} \approx S_{CH_3}$. A summary of S_{T_3} is given in Table 5.3.

Protection from surface oxidation during PEDOT deposition. Previous work[290] demonstrated the enhanced stability of Si/PEDOT devices with Si surface functionalization. Figure 5.8 clearly shows this. Both H- and CH_3-terminated p-Si/PEDOT:PSS junctions demonstrated low initial contact resistances. After 3 months aging, the CH_3-terminated interface displayed nearly identical contact resistance, while the H-terminated interface showed a large increase in contact resistance. The increase in contact resistance most likely is attributable to the inability of the PEDOT:PSS film to protect the H-terminated Si surface from slow oxidation.

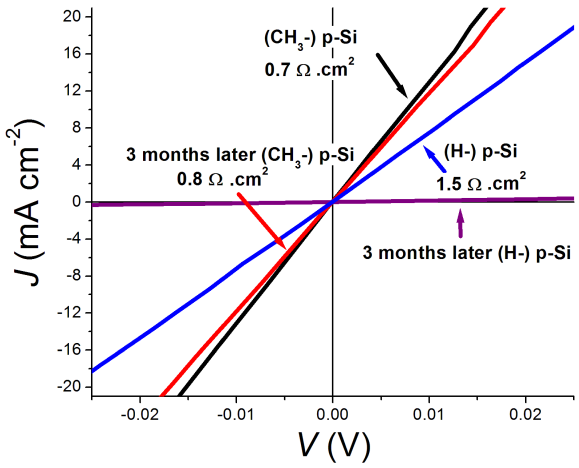

Figure 5.8. *J-V* characteristics of H- or CH_3-terminated p-Si(111)/PEDOT:PSS junctions, immediately after fabrication, and after aging

Oxide growth may occur under the anodic PEDOT deposition conditions as well. Figure 5.9 shows the high-resolution Si 2p XP spectra of surfaces **6** and **1** after anodic PEDOT deposition and PEDOT removal by tape test. Anodic electropolymerization of EDOT with $< {}^{1}/_{2}$ typical total charge passed at surface **6** resulted in 1.58 ± 0.05 ML SiO_x. Under the same conditions, CH_3-termination at surface **1**, limited SiO_x to 0.14 ± 0.04 ML SiO_x. In addition to formation of $>$ 1 magnitude greater thickness of SiO_x at surface **6** than at surface **1**, higher oxides were observed at surface **6**. Si^{3+} at 103.2 eV was the highes oxides observed after anodic electropolymerization at surface **1**, however, Si^{4+} was observed at 104.3 eV after electropolymerization at surface **6**. Scanning Auger spectroscopy previously showed that termination of Si with kinetically stable Si-C bonds blocks the oxidation of Si beyond the 3^+ state in air, while Cl- and H-termianted Si(111) quickly oxidized beyond Si^{3+} to Si^{4+} in air.[86]

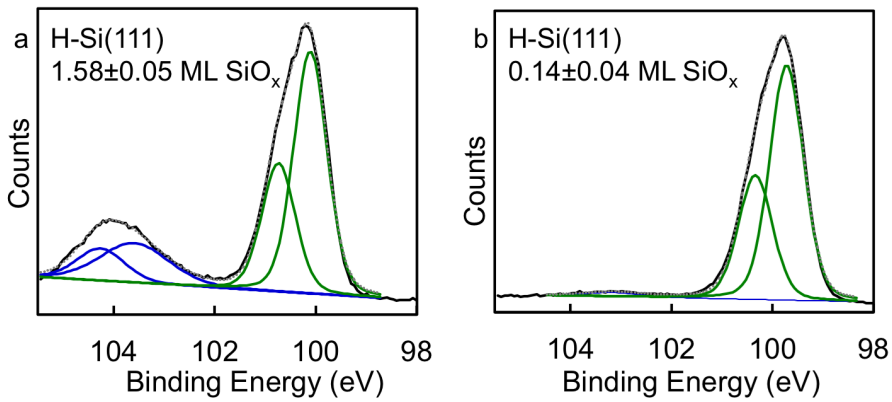

Figure 5.9. High-resolution Si 2p XP spectra of H- and CH_3-terminated Si(111) after anodic electropolymerization of EDOT and removal of deposited PEDOT by the Scotch® tape method. SiO_x thickness calculated *via* substrate overlayer model. Taken as average of 3 samples ± standard deviation.

Mechanical properties testing of covalent Si/thiophene/PEDOT junction. The Scotch® tape test was used to qualitatively compare the interfacial adhesion properties of anocially deposited PEDOT at surfaces **1**, **3**, **6**, **11**, and **12**. PEDOT was cleanly removed, to reveal the polished Si surface, from any surface not containing terthiophene groups. Only a small amount of polymer was removed from surfaces **11** and **12** with high θ_{T_3} *via* the tape test. The surface of the PEDOT was visibly roughened, and no polished Si was exposed. For surface **12** with low θ_{T_3}, more PEDOT was removed *via* the Scotch® tape, and patches of polished Si were exposed.

During the Scotch® tape test, interfacial failure can occur at the tape/PEDOT interface, within the PEDOT material, at the Si/PEDOT interface, or within the Si material. If the adhesion strength is comparable at multiple interfaces, a combined failure may be observed. The results of the tape test indicated that for surfaces **1**, **3**, and **6**, the adhesion failure occurred at

the Si/PEDOT interface. For surfaces **11** and **12** with large θ_{T_3}, the adhesion failure occurred within the PEDOT material. For surface **12** with low θ_{T_3}, the failure seemed to occur at a mixture of within the PEDOT and at the PEDOT/Si interface. The Scotch® tape test does not confirm covalent linkage, however, it suggests that there is a much greater adhesion strength at surfaces containing terthiophene groups. Additionally, that the interfacial adhesion with many terthiophene sites is larger than within the bulk PEDOT material.

5.2.4 Conclusions and future directions

PEDOT films were deposited through anodic electropolymerization of EDOT at functionalized p-Si(111) electrodes. Electrodes were functionalized with CH_3-, H-, SC_4H_3-, terthiophene, or mixed CH_3/terthiophene. The electronic defect density at surfaces with terthiophene containing monolayers decreased upon incorporation of CH_3- groups in a mixed molecular monolayer. Si-C termination decreased the thickness of SiO_x formation by greater than 1 order of magnitude, and prevented formation of high oxides, *i.e.*, Si^{4+}. The contact resistance of Si/PEDOT junctions decreased with terthiophene-functionalization, and seemed to be dependent on θ_{T_3}. The Scotch® tape test indicated the Si/terthiophene/PEDOT interfacial adhesion was greater than adhesion within the PEDOT film and at Si/R/PEDOT, where R = CH_3-, H-, or SC_4H_3-.

The continuation of this work should include, a more detailed dependence of R with θ_{T_3} at p-Si/terthiophene/PEDOT junctions. According to results at n-Si/CH_3/PEDOT junctions, the n-Si/terthiophene/PEDOT junction is promising as a mechanically robust, high V_{OC} junction. The collaboration with the Greer group should continue and include testing the robustness of the covalently linked electronic contact upon bending.

5.3 Surface-initiated atomic layer deposition

Atomic layer deposition (ALD) is an attractive method for depositing protective films or dielectric materials for transistors. Modern transistors are reaching a size scale where the SiO_2 must be replaced with a higher k dielectric materials. ALD progresses by sequential reactions of highly reactive gaseous precursors. The precursors react with surface sites, but not themselves, therefore, the reactions are self-limiting. ALD on Si has traditionally run upon three problems. The first is the lack of reactivity of the H-terminated Si sites. Long initiation times and additives are required to enhance reactivity. The second issue, is the concomitant formation of Si oxides with deposition of most metal oxide materials. The oxide changes the effective dielectric constant and required thickness of dielectric, as well as the interfacial properties. Finally, Si-M sites hold trapped charge. Therefore the interface is unsuitable for a transistor as it will lock the device in

the 'on' state. Similarly, the interface is unsuitable for a photoconversion interface as the Si-M sites form recombination centers.

Aldehyde terminated Si(111) surfaces were used for the initiation of ALD of Al_2O_3, MnO_2, and TiO_2. The surfaces used in this study are summarized in Scheme 5.4. CH_3- and H-terminated surfaces **1** and **6** were explored as 'nonreactive' surfaces. Propaldehyde groups were introduced to simultaneously protect Si surface sites while increasing general reactivity of the functionalized Si(111) toward ALD. Protected aldehyde functionalities were bound to the Si surface using (1,3-dioxan-2-ylethyl)magnesium chloride (Sigma-Aldrich, 0.5 M in THF), Scheme 5.5. The dioxanyl groups were removed in dilute, 0.004 M, aqueous HCl.

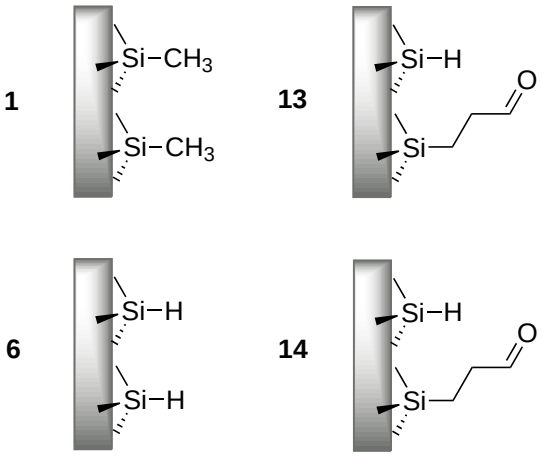

Scheme 5.4. Summary of surfaces used in atomic layer deposition studies

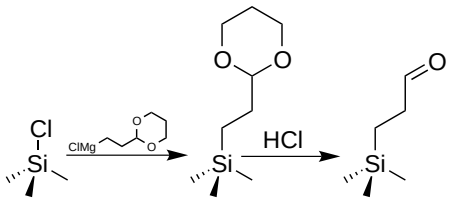

Scheme 5.5. Formation and deprotection of Si(111) surface bound aldehyde

Surfaces **1**, **6**, **13**, and **14** were used as substrates for ALD. It was hypothesized that deposition on surface **1** would occur simultaneously with Si-H oxidation, as was suggested previously, and deposition on surface **1** would proceed at defect sites and step edges. Alternatively, at aldehyde-functionalized surfaces, it was hypothesized that the chemistry would proceed by nucleophilic attack at the aldehyde carbon, then formation of O-M bond, as in Scheme 5.6.

XPS and transmission FTIR suggest aldehyde addition and deprotection proceed without formation of silicon oxide. Surfaces **1**, **13**, and **14** were cleaned prior to ALD. H-terminated surface **6** was used immediately after etching. The metal precursor was always pulsed first. Surfaces were exposed to $^1/_2$, 5, 10, or 20 cycles at the lowest reported temperatures for a given

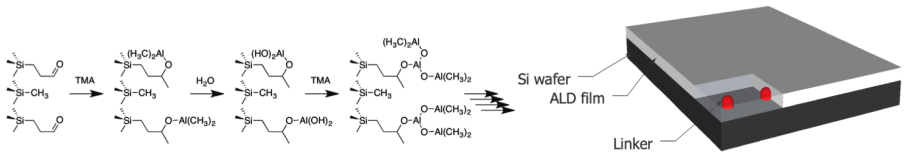

Scheme 5.6. ALD at aldehyde-functionalized Si(111) surfaces

material deposition.

XPS analysis showed Al_2O_3 deposition at surface **13** nearly equal to that at a freshly piranha cleaned surface. Deposition at H- and CH_3-terminated surfaces was sluggish for all depositions, however the greatest difference was observed with MnO_2. Very little Al_2O_3 was deposited on H-terminated Si until $\sim$ 5 cycles, at which point, deposition took off and deposition per cycle was nearly equal to that observed at the aldehyde terminated surface.

The surface recombination velocity was measured before deposition and after $^1/_2$, 5, 10, and 20 cycles. As expected the as-synthesized values for S of **13** were much higher than S of **14**. S values were not effected by the deprotection procedure.

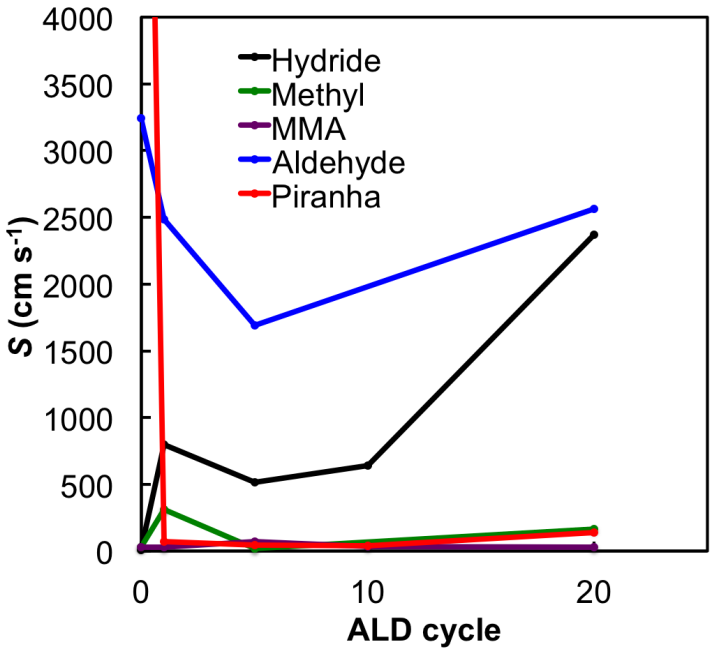

Figure 5.10. Surface recombination velocity, *S*, values for surfaces **6**, **1**, **14**, **13**, and piranha cleaned Si, as a function of Al_2O_3 deposition cycle. *S* calculated from low-level injection, contact-less photo-generated carrier lifetime measurements.

S of surface **1** was low, $S = 25$ cm^{-1}, and remained low, $S < 100$ cm s^{-1} after continuous ALD cycles. S of mixed CH_3/aldehyde-terminated surfaces, **14**, were very low, and remained lower than S measured at **1**. Interestingly, S of piranha cleaned surfaces was extremely large prior to ALD deposition, then dropped dramatically. The long observed carrier lifetimes could be due to trapped charge within the Al_2O_3 layer. This is not the case for all of the Al_2O_3 films

however, as high S were observed at all cycles for surface **13**, and increasing S was observed for H-terminated substrates. We believe the deposition is actually occurring at mixed CH_3/aldehyde-terminated surfaces without the formation of trapped charge or surface electronic defect densities, as suggested by the lack of trap charge induced S lowering with Al_2O_3 deposition at pure aldehyde monolayers, surface **13**. High level injection measurements could show this conclusively.

The roughness of the ALD films was measured using atomic force microscopy (Figure 5.11). For aldehyde and mixed CH_3/aldehyde-terminated surfaces, The crystal facets are observable, even after 20 deposition cycles. The AFM images of CH_3-terminated surface **1**, on the other hand, show a very rough surface. The substrate is not clearly visible under 2–4 nm tall clumps of Al_2O_3. The conformity of Al_2O_3 films deposited at aldehyde-activated substrates suggests ALD initiation occurred broadly across the substrate, rather than at single or patches of defects.

The use of aldehyde functionality on Si(111) surfaces increased ALD efficiency, and avoided SiO_x or electronic trap state formation. The depositions for Al_2O_3, MnO_2, and TiO_2 proceeded at the lowest reported temperature for each material without additives or long initiation times. the surface initiation led to smoother and more conformal films at short deposition times.

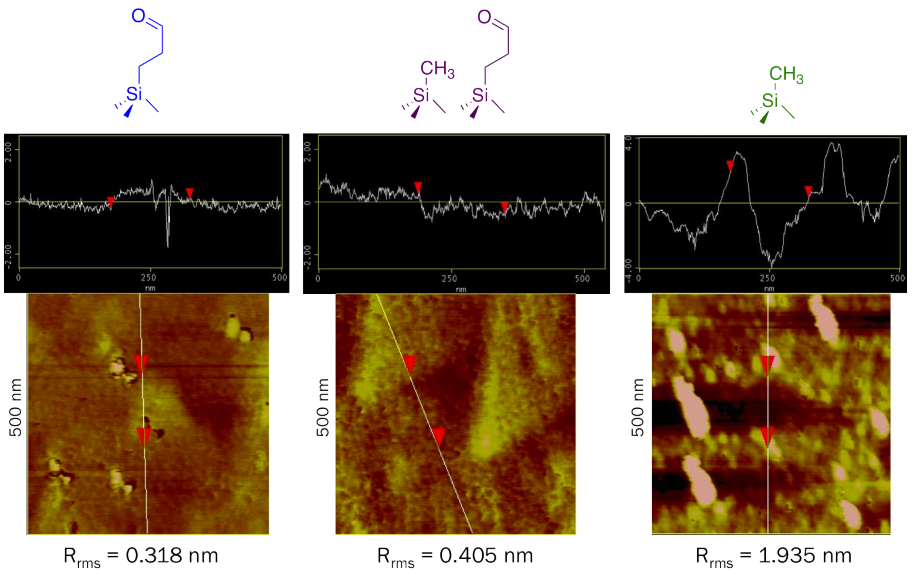

Figure 5.11. AFM images and height profile scans after 10 ALD cycles of Al_2O_3 deposited at aldehyde (**13**), mixed CH_3/aldehyde (**14**), and CH_3- (**1**) terminated Si(111). 500 × 500 nm scans. Height profiles from +2 to -2 nm for **13** and **14**, and +4 to -4 nm for **1**.

Bibliography

[1] E. Yablonovitch, D. L. Allara, C. C. Chang, T. Gmitter, and T. B. Bright. Unusually low surface-recombination velocity on silicon and germanium surfaces. *Physical Review Letters*, 57(2):249–252, 1986. Times Cited: 647.

[2] E. Yablonovitch and T. J. Gmitter. *Solid State Electronics*, 35:261–267, 1992.

[3] A. Heller. *Solar Energy*, 29:153–162, 1982.

[4] M. Grunder and H. Jacob. *Applied Physics A*, 39:73–82, 1986.

[5] F. J. Grunthaner and P. J. Grunthaner. *Materials Science & Engineering R-Reports*, 1:65–160, 1986.

[6] H. Ibach and J. E. Rowe. *Surface Science*, 43:481–492, 1974.

[7] T. M. Mayer and F. W. Lampe. *Journal of Physical Chemistry*, 78:2429–2433, 1974.

[8] V. A. Burrows, Y. J. Chabal, G. S. Higashi, K. Raghavachari, and S. B. Christman. *Applied Physics Letters*, 53:998–1000, 1988.

[9] Y. J. Chabal, G. S. Higashi, K. Raghavachari, and V. A. Burrows. Infrared-spectroscopy of si(111) and si(100) surfaces after hf treatment - hydrogen termination and surface-morphology. *Journal of Vacuum Science & Technology a-Vacuum Surfaces and Films*, 7(3):2104–2109, 1989. ISI Document Delivery No.: U7154 Times Cited: 545 Cited Reference Count: 23 AMER INST PHYSICS WOODBURY Part 2.

[10] G. S. Higashi, Y. J. Chabal, G. W. Trucks, and K. Raghavachari. Ideal hydrogen termination of the si-(111) surface. *Applied Physics Letters*, 56(7):656–658, 1990. Times Cited: 1092.

[11] G. S. Higashi, R. S. Becker, Y. J. Chabal, and A. J. Becker. *Applied Physics Letters*, 58:1656–1658, 1991.

[12] T. Bitzer, M. Gruyters, H. J. Lewerenz, and K. Jacobi. *Applied Physics Letters*, 63:397–399, 1993.

[13] J. Rappich, H. Jungblut, M. Aggour, and H. J. Lewerenz. *Journal of the Electrochemical Society*, 141:L99–L102, 1994.

[14] T. Dittrich, S. Rauscher, T. Bitzer, M. Aggour, H. Flietner, and H. J. Lewerenz. *Journal of the Electrochemical Society*, 142:2411–2413, 1995.

[15] J. Rappich and H. J. Lewerenz. *Journal of the Electrochemical Society*, 142:1233–1237, 1995.

[16] I. T. Clark, B. S. Aldinger, A. Gupta, and M. A. Hines. *Journal of Physical Chemistry C*, 114: 423–428, 2010.

[17] K. Sato, M. Shikida, Y. Matsushima, T. Yamashiro, K. Asaumi, Y. Iriye, and M. Yamamoto. *Sensors and Actuators a-Physical*, 64:87–93, 1998.

[18] C. P. Wade and C. E. D. Chidsey. *Applied Physics Letters*, 71:1679–1681, 1997.

[19] M. A. Hines. *Annual Review of Physical Chemistry*, 54:29–56, 2003.

[20] R. L. Cicero, M. R. Linford, and C. E. D. Chidsey. Photoreactivity of unsaturated compounds with hydrogen-terminated silicon(111). *Langmuir*, 16(13):5688–5695, 2000. Times Cited: 299.

[21] A. M. Cowley and S. M. Sze. Surface states and barrier height of metal-semiconductor systems. *Journal of Applied Physics*, 36(10):3212, 1965. Times Cited: 709.

[22] J. Linnros. *Journal of Applied Physics*, 84:275–283, 1998.

[23] M. Wittmer and J. L. Freeouf. *Physical Review Letters*, 69:2701–2704, 1992.

[24] M. Wittmer and J. L. Freeouf. *Physical Letters A*, 173:190–194, 1993.

[25] H. Angermann, K. Kliefoth, and H. Flietner. *Applied Surface Science*, 104:107–112, 1996.

[26] F. Gstrein, D. J. Michalak, W. J. Royea, and N. S. Lewis. Effects of interfacial energetics on the effective surface recombination velocity of si/liquid contacts. *Journal of Physical Chemistry B*, 106(11):2950–2961, 2002. Times Cited: 14.

[27] David J. Michalak, Florian Gstrein, and Nathan S. Lewis. Interfacial energetics of silicon in contact with 11 m nh4f(aq), buffered hf(aq), 27 m hf(aq), and 18 m h2so4. *Journal of Physical Chemistry C*, 111(44):16516–16532, 2007. Times Cited: 2.

[28] David J. Michalak, Florian Gstrein, and Nathan S. Lewis. The role of band bending in affecting the surface recombination velocities for si(111) in contact with aqueous acidic electrolytes. *Journal of Physical Chemistry C*, 112(15):5911–5921, 2008. Times Cited: 3.

[29] D. J. Michalak, S. R. Amy, A. Esteve, and Y. J. Chabal. *Journal of Physical Chemistry C*, 112: 11907–11919, 2008.

[30] V. Lehmann. *Electrochemistry of Silicon.* Wiley-VCH, Weinheim, 2002.

[31] R. C. Henderson. *Journal of the Electrochemical Society*, 119:772, 1972.

[32] W. Kern and D. A. Puotinen. *RCA Review*, 31:187–206, 1970.

[33] B. Tuck. *Journal of Materials Science*, 10:321–339, 1975.

[34] W. Kern. *Journal of the Electrochemical Society*, 137:1887–1892, 1990.

[35] W. Kern. *RCA Review*, 39:278–308, 1978.

[36] G. Mende, J. Finster, D. Flamm, and D. Schulze. Oxidation of etched silicon in air at room-temperature - measurements with ultrasoft x-ray photoelectron-spectroscopy (esca) and neutron-activation analysis. *Surface Science*, 128(1):169–175, 1983. Times Cited: 52.

[37] M. Niwano, J. Kageyama, K. Kurita, K. Kinashi, I. Takahashi, and N. Miyamoto. Infrared-spectroscopy study of initial-stages of oxidation of hydrogen-terminated si surfaces stored in air. *Journal of Applied Physics*, 76(4):2157–2163, 1994. Times Cited: 144.

[38] X. Zhang, E. Garfunkel, Y. J. Chabal, S. B. Christman, and E. E. Chaban. Stability of hf-etched si(100) surfaces in oxygen ambient. *Applied Physics Letters*, 79(24):4051–4053, 2001. Times Cited: 48.

[39] T. Yasaka, M. Takakura, K. Sawara, S. Uenaga, H. Uasutake, S. Miyazaki, and M. Hirose. *IEICE Trans. Electron.*, E75C(764-769), 1992.

[40] G. Cleland, B. R. Horrocks, and A. Houlton. *Journal of the Chemical Society, Faraday Transactions*, 91:4001–4003, 1995.

[41] Hua-Zhong Yu, S. Morin, D. D. M. Wayner, P. Allongue, and C. Henry de Villeneuve. *Journal of Physical Chemistry B*, 104:11157–11161, 2000.

[42] R. Boukherroub, S. Morin, P. Sharpe, D. D. M. Wayner, and P. Allongue. *Langmuir*, 16:7429–7434, 2000.

[43] D. J. Michalak, S. Rivillon, Y. J. Chabal, A. Esteve, and N. S. Lewis. Infrared spectroscopic investigation of the reaction of hydrogen-terminated, (111)-oriented, silicon surfaces with liquid methanol. *Journal of Physical Chemistry B*, 110(41):20426–20434, 2006. Times Cited: 15.

[44] M. Warntjes, C. Wieillard, F. Ozanam, and J.-N. Chazalviel. *Journal of the Electrochemical Society*, 142:4138–4142, 1995.

[45] J. E. Bateman, R. D. Eagling, B. R. Horrocks, and A. Houlton. *Journal of Physical Chemistry B*, 104:5557–5565, 2000.

[46] M. A. Hory, R. Herino, M. Ligeon, F. Muller, F. Gaspard, I. Mihalcescu, and J. C. Vial. *Thin Solid Films*, 255:200–203, 1995.

[47] J. E. Bateman, B. R. Horrocks, and A. Houlton. *Journal of the Chemical Society, Faraday Transactions*, 93:2427–2431, 1997.

[48] C. A. Hacker, K. A. Anderson, L. J. Richter, and C. A. Richter. *Langmuir*, 21:882–889, 2004.

[49] J.-N. Chazalviel. *Journal of the Electroanalytical Society*, 233:37–48, 1987.

[50] S. M. Sze. *The Physics of Semiconductor Devices*. Wiley, New York, 2 edition, 1981.

[51] T. U. Kampen and W. Monch. Lead contacts on si(111) - h-1 x-1 surfaces. *Surface Science*, 331: 490–495, 1995. Times Cited: 60 Part a 14th European Conference on Surface Science (ECOSS-14) SEP 19-23, 1994 LEIPZIG, GERMANY European Phys Soc; Int Union Vacuum Sci Tech & Applicat; Deut Phys Gesell; Deut Bunsengesell Phys Chem.

[52] T. U. Kampen, R. F. Schmitsdorf, and W. Monch. *Applied Physics Letters*, 60:391–394, 1995.

[53] S. Maldonado, K. E. Plass, D. Knapp, and N. S. Lewis. Electrical properties of junctions between hg and si(111) surfaces functionalized with short-chain alkyls. *Journal of Physical Chemistry C*, 111(48):17690–17699, 2007. Times Cited: 18.

[54] P. S. Schaffer and T. R. Lally. *Solid State Technology*, 26:229–233, 1983.

[55] P. J. Severin and G. J. Poodt. *Journal of the Electrochemical Society*, 119:1384, 1972.

[56] C. M. Aldao and J. H. Weaver. *Progress in Surface Science*, 68:306–309, 2001.

[57] J. S. Villarrubia and J. J. Boland. *Physical Review Letters*, 63:306–309, 1989.

[58] T. S. Horanyi, T. Pavelka, and P. Tutto. *Applied Surface Science*, 63:306–311, 1993.

[59] H. M'Saad, J. Michel, J. J. Lappe, and L. C. Kimerling. *Journal of Electronic Materials*, 23: 487–491, 1994.

[60] A. W. Stephens and M. A. Green. *Solar Energy Mareials for Solar Cells*, 45:255–265, 1997.

[61] R. J. Hamers. *Surface Science*, 600(3361-3362), 2006.

[62] A. Bansal, X. L. Li, I. Lauermann, N. S. Lewis, S. I. Yi, and W. H. Weinberg. Alkylation of si surfaces using a two-step halogenation grignard route. *Journal of the American Chemical Society*, 118(30):7225–7226, 1996. Times Cited: 233.

[63] W. F. Bergerson, V. Boiadjiev, J. A. Mulder, R. P. Hsung, and X. Y. Zhu. *Journal of the American Chemical Society*, 121:454–455, 1999.

[64] W. Cai, Z. Lin, T. Strother, L. M. Smith, and R. J. Hamers. *Journal of Physical Chemistry B*, 106:2656–2664, 2002.

[65] J. He, S. N. Patitsas, K. F. Preston, R. A. Wolkow, and D. D. M. Wayner. Covalent bonding of thiophenes to si(111) by a halogenation/thienylation route. *Chemical Physics Letters*, 286(5-6): 508–514, 1998.

[66] X. Y. Zhu, V. Boiadjiev, J. A. Mulder, R. P. Hsung, and R. C. Major. Molecular assemblies on silicon surfaces via si-o linkages. *Langmuir*, 16(17):6766–6772, 2000. Times Cited: 68.

[67] J. M. Buriak. Organometallic chemistry on silicon and germanium surfaces. *Chemical Reviews*, 102(5):1271–1308, 2002. Times Cited: 746.

[68] L. F. Edge, D. G. Schlom, R. T. Brewer, Y. J. Chabal, J. R. Williams, S. A. Chambers, C. Hinkle, G. Lucovsky, Y. Yang, S. Stemmer, M. Copel, B. Hollander, and J. Schubert. Suppression of subcutaneous oxidation during the deposition of amorphous lanthanum aluminate on silicon. *Applied Physics Letters*, 84(23):4629–4631, 2004. Times Cited: 64.

[69] S. Guha, E. Cartier, M. A. Gribelyuk, N. A. Bojarczuk, and M. C. Copel. Atomic beam deposition of lanthanum- and yttrium-based oxide thin films for gate dielectrics. *Applied Physics Letters*, 77 (17):2710–2712, 2000. Times Cited: 192.

[70] J. W. Klaus, O. Sneh, and S. M. George. Growth of sio2 at room temperature with the use of catalyzed sequential half-reactions. *Science*, 278(5345):1934–1936, 1997. Times Cited: 106.

[71] G. D. Wilk, R. M. Wallace, and J. M. Anthony. High-kappa gate dielectrics: Current status and materials properties considerations. *Journal of Applied Physics*, 89(10):5243–5275, 2001. Times Cited: 3149.

[72] S. Rivillon, Y. J. Chabal, L. J. Webb, D. J. Michalak, N. S. Lewis, M. D. Halls, and K. Raghavachari. Chlorination of hydrogen-terminated silicon(111) surfaces. *Journal of Vacuum Science & Technology A*, 23(4):1100–1106, 2005. Times Cited: 22 51st AVS International Symposium NOV 14-19, 2004 Anaheim, CA.

[73] J. Terry, R. Mo, C. Wigren, R. Cao, G. Mount, P. Pianetta, M. R. Linford, and C. E. D. Chidsey. *Nucl. Instrum. Methods Phys. Res. B*, 133:94, 1997.

[74] J. V. Florio and W. D. Robertson. Chlorine reactions on si(111) surface. *Surface Science*, 18(2): 398, 1969.

[75] Z. Li, T. I. Kamins, X. Li, and R. S. Williams. *Surface Science*, 554:L81–L86, 2004.

[76] S. Rivillon, F. Amy, Y. J. Chabal, and M. M. Frank. *Applied Physics Letters*, 85(2583-2585), 2004.

[77] B. J. Eves and G. P. Lopinski. *Surface Science*, 579:L89–L96, 2005.

[78] A. Bansal, X. L. Li, S. I. Yi, W. H. Weinberg, and N. S. Lewis. Spectroscopic studies of the modification of crystalline si(111) surfaces with covalently-attached alkyl chains using a chlorination/alkylation method. *Journal of Physical Chemistry B*, 105(42):10266–10277, 2001. Times Cited: 100.

[79] Peigen Cao, Hongbin Yu, and James R. Heath. Scanning tunneling microscopy and spectroscopy of wet-chemically prepared chlorinated si(111) surfaces. *Journal of Physical Chemistry B*, 110(47): 23615–23618, 2006. Times Cited: 5.

[80] L. J. Webb and N. S. Lewis. Comparison of the electrical properties and chemical stability of crystalline silicon(111) surfaces alkylated using grignard reagents or olefins with lewis acid catalysts. *Journal of Physical Chemistry B*, 107(23):5404–5412, 2003. Times Cited: 102.

[81] L. J. Webb, E. J. Nemanick, J. S. Biteen, D. W. Knapp, D. J. Michalak, M. C. Traub, A. S. Y. Chan, B. S. Brunschwig, and N. S. Lewis. High-resolution x-ray photoelectron spectroscopic studies of alkylated silicon(111) surfaces. *Journal of Physical Chemistry B*, 109(9):3930–3937, 2005. Times Cited: 46.

[82] H. B. Yu, L. J. Webb, S. D. Solares, P. G. Cao, W. A. Goddard, J. R. Heath, and N. S. Lewis. Scanning tunneling microscopy of ethylated si(111) surfaces prepared by a chlorination/alkylation process. *Journal of Physical Chemistry B*, 110(47):23898–23903, 2006. Times Cited: 13.

[83] G. A. Ferguson, S. Rivillon, Y. J. Chabal, and K. Raghavachari. *Journal of Physical Chemistry C*, 113:21713–21720, 2009.

[84] P. H. Citrin and J. E. Rowe. *Surface Science*, 132:205–211, 1983.

[85] S. R. Amy, D. J. Michalak, Y. J. Chabal, L. Wielunski, P. T. Hurley, and N. S. Lewis. Investigation of the reactions during alkylation of chlorine-terminated silicon (111) surfaces. *Journal of Physical Chemistry C*, 111(35):13053–13061, 2007. Times Cited: 9.

[86] L. J. Webb, D. J. Michalak, J. S. Biteen, B. S. Brunschwig, A. S. Y. Chan, D. W. Knapp, H. M. Meyer, E. J. Nemanick, M. C. Traub, and N. S. Lewis. High-resolution soft x-ray photoelectron spectroscopic studies and scanning auger microscopy studies of the air oxidation of alkylated silicon(111) surfaces. *Journal of Physical Chemistry B*, 110(46):23450–23459, 2006. Times Cited: 16.

[87] C. C. Finstad, A. G. Thorsness, and A. J. Muscat. *Surface Science*, 600:3363–3374, 2006.

[88] P. Gupta, P. A. Coon, B. G. Koehler, and S. M. George. *Surface Science*, (249), 1991.

[89] G. P. Lopinski, B. J. Eves, O. Hul'ko, C. Mark, S. N. Patitsas, R. Boukherroub, and T. R. Ward. *Physical Review B*, 71:125308, 2005.

[90] S. Rivillon, R. T. Brewer, and Y. J. Chabal. Water reaction with chlorine-terminated silicon (111) and (100) surfaces. *Applied Physics Letters*, 87(17), 2005. Times Cited: 7.

[91] J. W. Klaus, A. W. Ott, J. M. Johnson, and S. M. George. Atomic layer controlled growth of sio2 films using binary reaction sequence chemistry. *Applied Physics Letters*, 70(9):1092–1094, 1997. Times Cited: 58.

[92] M. L. Colaianni, P. J. Chen, H. Gutleben, and J. T. Yates. *Chemical Physics Letters*, 191:561–568, 1992.

[93] H. Gutleben, S. R. Lucas, C. C. Cheng, W. J. Choyke, and J. T. Yates. Thermal-stability of the methyl-group adsorbed on si(100) - ch3i surface-chemistry. *Surface Science*, 257:146–156, 1991.

[94] M. J. Kong, S. S. Lee, I. Lyubinetsky, and S. F. Bent. *Chemical Physics Letters*, 263:1–7, 1996.

[95] A. Fidelis, F. Ozanam, and J.-N. Chazalviel. *Surface Science*, 144:L7–L10, 2000.

[96] A. B. Sieval, B. van den Hout, H. Zuilhof, and E. J. R. Sudholter. *Langmuir*, 17:2172, 2001.

[97] H. B. Yu, L. J. Webb, R. S. Ries, S. D. Solares, W. A. Goddard, J. R. Heath, and N. S. Lewis. Low-temperature stm images of methyl-terminated si(111) surfaces. *Journal of Physical Chemistry B*, 109(2):671–674, 2005. Times Cited: 57.

[98] X. M. Bin, T. K. Mischki, C. Y. Fan, G. P. Lopinski, and D. D. M. Wayner. *Journal of Physical Chemistry C*, 111:13547–13553, 2007.

[99] R. Hunger, R. Fritsche, B. Jaeckel, W. Jaegermann, L. J. Webb, and N. S. Lewis. Chemical and electronic characterization of methyl-terminated si(111) surfaces by high-resolution synchrotron photoelectron spectroscopy. *Physical Review B*, 72, 2005. Times Cited: 31.

[100] L. J. Webb, S. Rivillon, D. J. Michalak, Y. J. Chabal, and N. S. Lewis. Transmission infrared spectroscopy of methyl- and ethyl-terminated silicon(111) surfaces. *Journal of Physical Chemistry B*, 110(14):7349–7356, 2006. Times Cited: 27.

[101] J. Terry, M. R. Linford, C. Wigren, R. Y. Cao, P. Pianetta, and C. E. D. Chidsey. Alkyl-terminated si(111) surfaces: A high-resolution, core level photoelectron spectroscopy study. *Journal of Applied Physics*, 85(1):213–221, 1999. Times Cited: 132.

[102] N. N. Greenwood and A. Earnshaw. *Chemistry of the Elements*. Reed Educational and Professional Publishing Ltd., Oxford, UK, 2 edition, 1997.

[103] F. J. Himpsel, F. R. McFeely, A. Talebibrahimi, J. A. Yarmoff, and G. Hollinger. *Physical Review B*, 38:6084–6096, 1988.

[104] E. Johansson, P. T. Hurley, B. S. Brunschwig, and N. S. Lewis. Infrared vibrational spectroscopy of isotopically labeled ethyl-terminated si(111) surfaces prepared using a two-step chlorination/alkylation procedure. *Journal of Physical Chemistry C*, 113(34):15239–15245, 2009. Times Cited: 2.

[105] M. R. Linford, P. Fenter, P. M. Eisenberger, and C. E. D. Chidsey. Alkyl monolayers on silicon prepared from 1-alkenes and hydrogen-terminated silicon. *Journal of the American Chemical Society*, 117(11):3145–3155, 1995. Times Cited: 767.

[106] E. J. Nemanick, P. T. Hurley, B. S. Brunschwig, and N. S. Lewis. Chemical and electrical passivation of silicon (111) surfaces through functionalization with sterically hindered alkyl groups. *Journal of Physical Chemistry B*, 110(30):14800–14808, 2006. Times Cited: 26.

[107] B. Jaeckel, R. Hunger, L. J. Webb, W. Jaegermann, and N. S. Lewis. High-resolution synchrotron photoemission studies of the electronic structure and thermal stability of ch3- and c2h5-functionalized si(111) surfaces. *Journal of Physical Chemistry C*, 111(49):18204–18213, 2007. Times Cited: 9.

[108] R. L. Cicero, C. E. D. Chidsey, G. P. Lopinski, D. D. M. Wayner, and R. A. Wolkow. Olefin additions on h-si(111): Evidence for a surface chain reaction initiated at isolated dangling bonds. *Langmuir*, 18(2):305–307, 2002.

[109] M. A. Gosalvez, K. Sato, A. S. Foster, R. M. Nieminen, and M. Tanaka. *Journal of Micromech. Microeng.*, 17:S1–S26, 2007.

[110] L. E. O'Leary, E. Johansson, B. S. Brunschwig, and N. S. Lewis. Synthesis and characterization of mixed methyl/allyl monolayers on si(111). *Journal of Physical Chemistry B*, 114(45):14298–14302, 2010. Times Cited: 0.

[111] Q. Y. Sun, L. C. de Smet, B. van Lagen, A. Wright, H. Zuilhof, and E. J. Sudholter. Covalently attached monolayers on hydrogen-terminated si(100): extremely mild attachment by visible light. *Angewandte Chemie*, 43(11):1352–5, 2004. Sun, Qiao-Yu de Smet, Louis C P M van Lagen, Barend Wright, Andrew Zuilhof, Han Sudholter, Ernst J R Germany International ed. in English Angew Chem Int Ed Engl. 2004 Mar 5;43(11):1352-5.

[112] W. J. Royea, A. Juang, and N. S. Lewis. Preparation of air-stable, low recombination velocity si(111) surfaces through alkyl termination. *Applied Physics Letters*, 77(13):1988–1990, 2000. Times Cited: 108.

[113] O. Yaffe, L. Scheres, S. R. Puniredd, N. Stein, A. Biller, R. H. Lavan, H. Shapisman, H. Zuilhof, H. Haick, D. Cahen, and A. Vilan. *Nano Letters*, 156:2390–2394, 2009.

[114] Stephen Maldonado and Nathan S. Lewis. Behavior of electrodeposited cd and pb schottky junctions on ch(3)-terminated n-si(111) surfaces. *Journal of the Electrochemical Society*, 156(2): H123–H128, 2009. Times Cited: 6.

[115] P. Allongue, C. H. de Villeneuve, J. Pinson, F. Ozanam, J.-N. Chazalviel, and X. Wallart. *Electrochimica Acta*, 43:2791–2798, 1998.

[116] T. Osaka, M. Matsunaga, S. Kudo, D. Niwa, Y. Shacham-Diamand, W. Jaegermann, and R. Hunger. *Journal of the Electrochemical Society*, 154:H919–H926, 2007.

[117] J. A. M. Sondag-Huethorst and L. G. Fokkink. *Langmuir*, 8:2560–2566, 1992.

[118] J. A. M. Sondag-Huethorst and L. G. Fokkink. *Journal of Electroanalytical Chemistry*, 367:49–57, 1994.

[119] A. M. Becka and C. J. Miller. *Journal of Physical Chemistry*, 96:2657–2668, 1992.

[120] C. E. D. Chidsey. *Science*, 251:919–922, 1991.

[121] S. B. Sachs, S. P. Dudek, R. P. Hsung, L. R. Sita, J. F. Smalley, M. D. Newton, S. W. Feldberg, and C. E. D. Chidsey. Rates of interfacial electron transfer through pi-conjugated spacers. *Journal of the American Chemical Society*, 119(43):10563–10564, 1997. Times Cited: 262.

[122] A. Bansal and N. S. Lewis. Stabilization of si photoanodes in aqueous electrolytes through surface alkylation. *Journal of Physical Chemistry B*, 102(21):4058–4060, 1998. Times Cited: 74.

[123] A. Bansal and N. S. Lewis. Electrochemical properties of (111)-oriented n-si surfaces derivatized with covalently-attached alkyl chains. *Journal of Physical Chemistry B*, 102(7):1067–1070, 1998. Times Cited: 93.

[124] A. Faucheux, F. Yang, P. Allongue, C. H. de Villeneuve, F. Ozanam, and J.-N. Chazalviel. *Applied Physics Letters*, 88:193123, 2006.

[125] M. M. Sung, G. J. Kluth, O. W. Yauw, and R. Maboudian. *Langmuir*, 13:6164–6168, 1997.

[126] T. W. Hamann and N. S. Lewis. Control of the stability, electron-transfer kinetics, and ph-dependent energetics of si/h2o interfaces through methyl termination of si(111) surfaces. *Journal of Physical Chemistry B*, 110(45):22291–22294, 2006. Times Cited: 7.

[127] R. Boukherroub and D. D. M. Wayner. *Journal of the American Chemical Society*, 121:11513–11515, 1999.

[128] R. Boukherroub, S. Morin, F. Bensebaa, and D. D. M. Wayner. *Langmuir*, 15:3831–3835, 1999.

[129] T. Bocking, A. Salomon, D. Cahen, and J. J. Gooding. *Langmuir*, 23:3236–3241, 2007.

[130] J. M. Buriak and M. J. Allen. *Journal of the American Chemical Society*, 120:1339–1340, 1998.

[131] P. Allongue, C. H. de Villeneuve, and J. Pinson. *Electrochimica Acta*, 45:3241–3248, 2000.

[132] A. B. Sieval, R. Linke, H. Zuilhof, and E. J. R. Sudholter. *Advanced Materials*, 12:1457–1460, 2000.

[133] R. Hunger, R. Fritsche, B. Jaeckel, L. J. Webb, W. Jaegermann, and N. S. Lewis. High-resolution photoemission studies of the interfacial reactivity and interfacial energetics of au and cu schottky barriers on methyl-terminated si(111) surfaces. *Surface Science*, 601:2896–2907, 2007. Times Cited: 7.

[134] H. Haick, O. Niitsoo, J. Ghabboun, and D. Cahen. *Journal of Physical Chemistry C*, 111:2318–2329, 2007.

[135] E. Moons, M. Bruening, A. Shanzer, J. Beier, and D. Cahen. *Synthetic Metals*, 76:245–248, 1996.

[136] Stephen Maldonado, David Knapp, and Nathan S. Lewis. Near-ideal photodiodes from sintered gold nanoparticle films on methyl-terminated si(111) surfaces. *Journal of the American Chemical Society*, 130(11):3300–+, 2008. Times Cited: 11.

[137] A. B. Bocarsly, E. G. Walton, M. G. Bradley, and M. S. Wrighton. *Electroanalytical Chemistry*, 100:283–306, 1979.

[138] A. B. Bocarsly, E. G. Walton, and M. S. Wrighton. *Journal of the American Chemical Society*, 102:3390–3398, 1980.

[139] J. M. Bolts, A. B. Bocarsly, M. C. Palazzotto, E. G. Walton, N. S. Lewis, and M. S. Wrighton. *Journal of the American Chemical Society*, 100:1378–1385, 1979.

[140] M. D. Rosenblum and N. S. Lewis. *Journal of Physical Chemistry*, 88:3103–3107, 1984.

[141] R. Noufi, D. Tench, and L. F. Warren. *Journal of the Electrochemical Society*, 127:2310–2311, 1980.

[142] R. Noufi, D. Tench, and L. F. Warren. *Journal of the Electrochemical Society*, 128:2596–2599, 1981.

[143] T. Skotheim, I. Lundstrom, and J. Prejza. *Journal of the Electrochemical Society*, 128:1625–1626, 1981.

[144] T. Skotheim, L.-G. Petersson, O. Inganas, and I. Lundstrom. *Journal of the Electrochemical Society*, 129:1849–1850, 1982.

[145] R. Noufi, A. J. Frank, and A. J. Nozik. *Journal of the American Chemical Society*, 103:1849–1850, 1981.

[146] T. Skotheim, I. Lundstrom, A. E. Delahoy, F. J. Kampas, and P. E. Vanier. *Applied Physics Letters*, 40:281–284, 1982.

[147] R. A. Simon, A. J. Ricco, and M. S. Wrighton. *Journal of the American Chemical Society*, 104: 2031–2034, 1982.

[148] Bruno Fabre, G. P. Lopinski, and D. D. M. Wayner. *Journal of Physical Chemistry B*, 107: 14326–14335, 2003.

[149] F.-R. F. Fan, B. L. Wheeler, A. J. Bard, and R. Noufi. *Journal of the Electrochemical Society*, 128:2042–2025, 1981.

[150] M. J. Sailor, E. J. Ginsburg, C. B. Gorman, A. Kumar, R. H. Grubbs, and N. S. Lewis. *Science*, 249:1146–1149, 1990.

[151] M. J. Sailor, F. L. Klavetter, R. H. Grubbs, and N. S. Lewis. *Nature*, 74:155–157, 1990.

[152] R. T. Howe, R. T. Hawkins II, and T. H. Fleisch. *Journal of the Electrochemical Society*, 133: 1369–1375, 1986.

[153] S. Menezes, A. Heller, and B. Miller. *Journal of the Electrochemical Society*, 127:1268–1273, 1980.

[154] Y. Nakato, T. Ohnishi, and H. Tsubomura. *Chemistry Letters*, 19(883-886), 1975.

[155] A. Q. Contractor and J. O. M. Bockris. *Electrochimica Acta*, 29:1427–1434, 1984.

[156] M. A. Kuikka, W. Li, K. L. Kavanagh, and H.-Z. Yu. *Journal of Physical Chemistry C*, 112: 9081–9088, 2008.

[157] A. V. Walker, T. B. Tighe, O. M. Cabarcos, M. D. Reinard, B. C. Haynie, S. Uppili, N. Winograd, and D. L. Allara. *Journal of the American Chemical Society*, 126:3954–3963, 2004.

[158] C. Zhou, G. Nagy, and A. V. Walker. *Journal of the American Chemical Society*, 127:12160–12161, 2005.

[159] Z. Zhu, T. A. Daniel, M. Maitani, O. M. Cabarcos, D. L. Allara, and N. Winograd. *Journal of the American Chemical Society*, 128:13710–13719, 2006.

[160] K. T. Shimizu, J. D. Fabbri, J. J. Jelincic, and N. A. Melosh. *Advanced Materials*, 18:1499–1504, 2006.

[161] D. L. Allara, A. F. Hebard, F. J. Padden, R. G. Nuzzo, and D. R. Falcone. *Journal of Vacuum Science & Technology A*, 1:376–382, 1983.

[162] A. K. Mahapatro, A. Scott, A. Manning, and D. B. Janes. *Applied Physics Letters*, 88:151917–151919, 2006.

[163] A. W. Czanderna, D. E. King, and D. Spaulding. *Journal of Vacuum Science & Technology A*, 9: 2607–2613, 1991.

[164] B. de Boer, M. M. Frank, Y. J. Chabal, W. Jiang, E. Garfunkel, and Z. Bao. *Langmuir*, (1539-1542), 2004.

[165] G. L. Fisher, A. V. Walker, A. Hooper, T. B. Tighe, K. B. Bahnck, H. T. Skriba, M. D. Reinard, B. C. Haynie, R. L. Opila, N. Winograd, and D. L. Allara. *Journal of the American Chemical Society*, 124:5528–5541, 2002.

[166] K. Felmet, Y.-L. Loo, and Y. Sun. *Applied Physics Letters*, 85:3316–3318, 2004.

[167] Y.-L. Loo, R. L. Willett, K. W. Baldwin, and J. A. Rogers. *Journal of the American Chemical Society*, 124:7654–7655, 2002.

[168] Y.-L. Loo, D. V. Lang, J. A. Rogers, and J. W. P. Hsu. *Nano Letters*, 3:913–917, 2003.

[169] D. Guerin, C. Merckling, S. Lenfant, X. Wallart, S. Pleutin, and D. Vuillaume. *Journal of Physical Chemistry C*, 111:7947–7956, 2007.

[170] H. Mizuno and J. M. Buriak. *Journal of the American Chemical Society*, 130:17656–17657, 2008.

[171] J. E. Lynch, P. E. Pehrsson, D. N. Leonard, and J. M. Calvert. *Journal of the Electrochemical Society*, 144:1698–1703, 1997.

[172] G. Hode, T. J. Dubow, and K. J. Rajeshwar. *Journal of the American Chemical Society*, 105: 324–330, 1983.

[173] L. Thompson, T. J. Dubow, and K. J. Rajeshwar. *Journal of the Electrochemical Society*, 129: 1934–1935, 1982.

[174] F. Decker, M. Fracastoro-Decker, W. Badawy, K. Doblhofer, and H. Gerischer. *Journal of the Electrochemical Society*, 130:2173–2179, 1983.

[175] D. S. Ginley, R. J. Baughman, and M. A. Butler. *Journal of the Electrochemical Society*, 130: 1999–2002, 1983.

[176] J. A. Switzer. *Journal of the Electrochemical Society*, 133:722–728, 1986.

[177] P. A. Kohl, S. N. Frank, and A. J. Bard. *Journal of the Electrochemical Society*, 124:225–229, 1977.

[178] H. Morisaki, H. Ono, H. Dohkoshi, and K. Yazawa. *Japanese Journal of Applied Physics*, 19: L148–L150, 1980.

[179] F.-R. F. Fan, R. G. Keil, and A. J. Bard. *Journal of the American Chemical Society*, 105:220–224, 1983.

[180] M. M. Frank, Y. J. Chabal, M. L. Green, A. Delabie, B. Brijs, G. D. Wilk, M. Y. Ho, E. B. O. da Rosa, I. J. R. Baumvol, and F. C. Stedile. Enhanced initial growth of atomic-layer-deposited metal oxides on hydrogen-terminated silicon. *Applied Physics Letters*, 83(4):740–742, 2003. Times Cited: 70.

[181] M. M. Frank, Y. J. Chabal, and G. D. Wilk. Nucleation and interface formation mechanisms in atomic layer deposition of gate oxides. *Applied Physics Letters*, 82(26):4758–4760, 2003. Times Cited: 77.

[182] Abhishek Dube, Manish Sharma, Paul F. Ma, Peter A. Ercius, David A. Muller, and J. R. Engstrom. Effects of interfacial organic layers on nucleation, growth, and morphological evolution in atomic layer thin film deposition. *Journal of Physical Chemistry C*, 111(29):11045–11058, 2007. Times Cited: 9.

[183] A. S. Killampalli, P. F. Ma, and J. R. Engstrom. The reaction of tetrakis(dimethylamido)titanium with self-assembled alkyltrichlorosilane monolayers possessing -oh, -nh2, and -ch3 terminal groups. *Journal of the American Chemical Society*, 127(17):6300–6310, 2005. Times Cited: 39.

[184] Oliver Seitz, Min Dai, F. S. Aguirre-Tostado, Robert M. Wallace, and Yves J. Chabal. Copper-metal deposition on self assembled monolayer for making top contacts in molecular electronic devices. *Journal of the American Chemical Society*, 131(50):18159–18167, 2009. Times Cited: 11.

[185] Meng Li, Min Dai, and Yves J. Chabal. Atomic layer deposition of aluminum oxide on carboxylic acid-terminated self-assembled monolayers. *Langmuir*, 25(4):1911–1914, 2009. Times Cited: 4.

[186] J. M. Buriak. *Chemical Communications*, pages 1051–1060, 1999.

[187] Andrew V. Teplyakov, M. J. Kong, and S. F. Bent. *Journal of the American Chemical Society*, 119:11100–11101, 1997.

[188] J. T. Yates. *Science*, 279:335–336, 1998.

[189] M. R. Linford and C. E. D. Chidsey. Alkyl monolayers covalently bonded to silicon surfaces. *Journal of the American Chemical Society*, 115(26):12631–12632, 1993. Times Cited: 396.

[190] A. B. Sieval, A. L. Demirel, J. W. M. Nissink, M. R. Linford, J. H. van der Maas, H. de Jeu, W. H. Zuilhof, and E. J. R. Sudholter. *Langmuir*, 14:1759–1768, 1998.

[191] M. P. Stewart and J. M. Buriak. *Angewandte Chemie-International Edition*, 37:3257–3260, 1998.

[192] N. S. Lewis. *Journal of the American Chemical Society*, 112:5998–6004, 1990.

[193] P. Allongue, M. Delamar, B. Desbat, O. Fagebaume, R. Hitmi, J. Pinson, and J. M. Saveant. *Journal of the American Chemical Society*, (201-207), 1997.

[194] T. L. Niederhauser, G. L. Jiang, Y. Y. Lua, M. J. Dorff, A. T. Woolley, M. C. Asplund, D. A. Berges, and M. R. Linford. *Langmuir*, 17:5889–5900, 2001.

[195] A. R. Pike, L. H. Lie, R. A. Eagling, L. C. Ryder, S. N. Patole, B. A. Connolly, B. R. Horrocks, and A. Houlton. *Angewandte Chemie-International Edition*, 41:615–617, 2002.

[196] T. Strother, W. Cai, X. S. Zhao, R. J. Hamers, and L. M. Smith. Synthesis and characterization of dna-modified silicon (111) surfaces. *Journal of the American Chemical Society*, 122(6):1205–1209, 2000. Times Cited: 323.

[197] E. J. Nemanick, S. D. Solares, W. A. Goddard, and N. S. Lewis. Quantum mechanics calculations of the thermodynamically controlled coverage and structure of alkyl monolayers on si(111) surfaces. *Journal of Physical Chemistry B*, 110(30):14842–14848, 2006. Times Cited: 12.

[198] A. Juang, O. A. Scherman, R. H. Grubbs, and N. S. Lewis. Formation of covalently attached polymer overlayers on si(111) surfaces using ring-opening metathesis polymerization methods. *Langmuir*, 17(5):1321–1323, 2001. Times Cited: 85.

[199] K. E. Plass, X. L. Liu, B. S. Brunschwig, and N. S. Lewis. Passivation and secondary functionalization of allyl-terminated si(111) surfaces. *Chemistry of Materials*, 20(6):2228–2233, 2008. Times Cited: 9.

[200] R. D. Rohde, H. D. Agnew, W. S. Yeo, R. C. Bailey, and J. R. Heath. *Journal of the American Chemical Society*, 128:9518–9525, 2006.

[201] S. Dutta, M. Perring, S. Barrett, M. Mitchell, P. J. A. Kenis, and N. B. Bowden. *Langmuir*, 22: 2146–2155, 2006.

[202] Y. J. Liu, N. M. Navasero, and H. Z. Yu. *Langmuir*, 20:4039–4050, 2004.

[203] Q. Y. Sun, L. C. de Smet, B. van Lagen, M. Giesbers, P. C. Thune, J. van Engelenburg, F. A. de Wolf, H. Zuilhof, and E. J. R. Sudholter. *Journal of the American Chemical Society*, 127: 2514–2523, 2005.

[204] K. Mathauer and C. W Frank. *Langmuir*, 9:3002–3008, 1993.

[205] D. A. Offord and J. H. Griffin. *Langmuir*, 9(3015-3025), 1993.

[206] B. Fabre and F. Hauquier. *Journal of Physical Chemistry B*, 110:6848–6855, 2006.

[207] A. Heise, M. Stamm, M. Rauscher, H. Duschner, and H. Menzel. *Thin Solid Films*, 327:199–203, 1998.

[208] W. R. Ashurst, C. Yau, C. Carraro, C. Lee, G. J. Kluth, R. T. Howe, and R. Maboudian. Alkene based monolayer films as anti-stiction coatings for polysilicon mems. *Sensors and Actuators a-Physical*, 91(3):239–248, 2001. Times Cited: 102 Solid-State Sensors and Actuators Workshop JUN 04-08, 2000 HILTON HEAD ISL, SOUTH CAROLINA.

[209] P. G. Clem, N. L. Jeon, R. G. Nuzzo, and D. A. Payne. Monolayer-mediated deposition of tantalum(v) oxide thin film structures from solution precursors. *Journal of the American Ceramic Society*, 80(11):2821–2827, 1997. Times Cited: 51.

[210] H. Ko, S. Peleshanko, and V. V. Tsukruk. Combing and bending of carbon nanotube arrays with confined microfluidic flow on patterned surfaces. *Journal of Physical Chemistry B*, 108(14): 4385–4393, 2004. Times Cited: 59.

[211] U. Srinivasan, M. R. Houston, R. T. Howe, and R. Maboudian. Alkyltrichlorosilane-based self-assembled monolayer films for stiction reduction in silicon micromachines. *Journal of Microelectromechanical Systems*, 7(2):252–260, 1998. Times Cited: 259.

[212] N. S. Lewis. Frontiers of research in photoelectrochemical solar energy conversion. *Journal of Electroanalytical Chemistry*, 508(1-2):1–10, 2001. Times Cited: 31.

[213] S. F. Bent. Organic functionalization of group iv semiconductor surfaces: principles, examples, applications, and prospects. *Surface Science*, 500(1-3):879–903, 2002. Times Cited: 364.

[214] V. S. Y. Lin, K. Motesharei, K. P. S. Dancil, M. J. Sailor, and M. R. Ghadiri. A porous silicon-based optical interferometric biosensor. *Science*, 278(5339):840–843, 1997. Times Cited: 585.

[215] J. W. Parce, J. C. Owicki, K. M. Kercso, G. B. Sigal, H. G. Wada, V. C. Muir, L. J. Bousse, K. L. Ross, B. I. Sikic, and H. M. McConnell. Detection of cell-affecting agents with a silicon biosensor. *Science*, 246(4927):243–247, 1989. Times Cited: 219.

[216] M. X. Tan and N. S. Lewis. Charge transfer rate constants for the reduction of cobaltocenium at accumulated n-si electrodes. *Inorganica Chimica Acta*, 242(1-2):311–321, 1996. Times Cited: 10.

[217] Shannon W. Boettcher, Emily L. Warren, Morgan C. Putnam, Elizabeth A. Santori, Daniel Turner-Evans, Michael D. Kelzenberg, Michael G. Walter, James R. McKone, Bruce S. Brunschwig, Harry A. Atwater, and Nathan S. Lewis. Photoelectrochemical hydrogen evolution using si microwire arrays. *Journal of the American Chemical Society*, 133(5):1216–1219, 2011. Times Cited: 8.

[218] R. N. Dominey, N. S. Lewis, J. A. Bruce, D. C. Bookbinder, and M. S. Wrighton. Improvement of photo-electrochemical hydrogen generation by surface modification of p-type silicon semiconductor photo-cathodes. *Journal of the American Chemical Society*, 104(2):467–482, 1982. Times Cited: 194.

[219] W. Cai, J. R. Peck, D. W. van der Weide, and R. J. Hamers. Direct electrical detection of hybridization at dna-modified silicon surfaces. *Biosensors & Bioelectronics*, 19(9):1013–1019, 2004. ISI Document Delivery No.: 804CF Times Cited: 101 Cited Reference Count: 30 Cai, W Peck, JR van der Weide, DW Hamers, RJ ELSEVIER ADVANCED TECHNOLOGY OXFORD.

[220] X. Y. Wang, E. C. Landis, R. Franking, and R. J. Hamers. Surface chemistry for stable and smart molecular and biomolecular interfaces via photochemical grafting of alkenes. *Accounts of Chemical Research*, 43(9):1205–1215, 2010. ISI Document Delivery No.: 652WM Times Cited: 7 Cited Reference Count: 51 Wang, Xiaoyu Landis, Elizabeth C. Franking, Ryan Hamers, Robert J. National Science Foundation[CHE0314618, CHE0613010, CHE0911543, DMR-0210806, DMR-0706559] The work described here was supported in part by the National Science Foundation Grants CHE0314618, CHE0613010, CHE0911543, DMR-0210806, and DMR-0706559. The authors wish to acknowledge Drs. Wensha Yang, Tami L Clare, Paula L. Colavita, Beth M. Nichols, Jeremy A. Streifer, and the many others who made significant contributions to the work described in this manuscript. The authors acknowledge fruitful collaborations and interactions with Dr. James Butler and Professor Lloyd M. Smith. AMER CHEMICAL SOC WASHINGTON.

[221] A. Teyssot, S. Fellah, F. Ozanam, and J.-N. Chazalviel. *Electrochimica Acta*, 47:2565, 2002.

[222] J. S. Becker, R. D. Brown, E. Johansson, N. S. Lewis, and S. J. Sibener. Helium atom diffraction measurements of the surface structure and vibrational dynamics of ch3-si(111) and cd3-si(111) surfaces. *Journal of Chemical Physics*, 133(10), 2010. Becker, James S. Brown, Ryan D. Johansson, Erik Lewis, Nathan S. Sibener, S. J.

[223] R. Chen, H. Kim, P. C. McIntyre, D. W. Porter, and S. F. Bent. Achieving area-selective atomic layer deposition on patterned substrates by selective surface modification. *Applied Physics Letters*, 86(19), 2005. Times Cited: 27.

[224] M. A. Filler and S. F. Bent. The surface as molecular reagent: organic chemistry at the semiconductor interface. *Progress in Surface Science*, 73(1-3):1–56, 2003. Times Cited: 208.

[225] Bruno Fabre. Ferrocene-terminated monolayers covalently bound to hydrogen-terminated silicon surfaces. toward the development of charge storage and communication devices. *Accounts of Chemical Research*, 43(12):1509–1518, 2010. Times Cited: 14.

[226] S. Ciampi, J. B. Harper, and J. J. Gooding. Wet chemical routes to the assembly of organic monolayers on silicon surfaces via the formation of si-c bonds: surface preparation, passivation

and functionalization. *Chemical Society reviews*, 39(6):2158–83, 2010. Ciampi, Simone Harper, Jason B Gooding, J Justin England Chem Soc Rev. 2010 Jun;39(6):2158-83. Epub 2010 Apr 14.

[227] Erik Johansson, Shannon W. Boettcher, Leslie E. O'Leary, Andrey D. Poletayev, Stephen Maldonado, Bruce S. Brunschwig, and Nathan S. Lewis. Control of the ph-dependence of the band edges of si(111) surfaces using mixed methyl/allyl monolayers. *Journal of Physical Chemistry C*, 115(17):8594–8601, 2011. Times Cited: 0.

[228] R. F. Heck and J. P. Nolley. Palladium-catalyzed vinylic hydrogen substitution reactions with aryl, benzyl, and styryl halides. *Journal of Organic Chemistry*, 37(14):2320, 1972. ISI Document Delivery No.: M9625 Times Cited: 770 Cited Reference Count: 6 HECK, RF NOLLEY, JP AMER CHEMICAL SOC WASHINGTON.

[229] Mengnan Qua, Yuan Zhang, Jinmei He, Xiaoping Cao, and Junyan Zhang. Pd-catalyzed coupling reaction on the organic monolayer: Sonogashira reaction on the silicon (111) surfaces. *Applied Surface Science*, 255(5):2608–2612, 2008. Times Cited: 1.

[230] C. M. Yam, J. Cho, and C. Z. Cai. Preparation and heck reaction of multidentate carbosilane films derived from focally functionalized and allyl-terminated dendrons on hydrogen-terminated silicon(111) surfaces. *Langmuir*, 20(4):1228–1233, 2004. Times Cited: 14.

[231] Jason J. Davis, Claire B. Bagshaw, Katerina L. Busuttil, Yuki Hanyu, and Karl S. Coleman. Spatially controlled suzuki and heck catalytic molecular coupling. *Journal of the American Chemical Society*, 128(43):14135–14141, 2006. Times Cited: 18.

[232] Jason J. Davis and Yuki Hanyu. Mechanistic studies of afm probe-driven suzuki and heck molecular coupling. *Nanotechnology*, 21(26), 2010. Times Cited: 1.

[233] D. Munao, J. W. M. van Erven, M. Valvo, E. Garcia-Tamayo, and E. M. Kelder. Role of the binder on the failure mechanism of si nano-composite electrodes for li-ion batteries. *Journal of Power Sources*, 196(16):6695–6702, 2011. Times Cited: 2 SI.

[234] J. A. Haber, I. Lauermann, D. Michalak, T. P. Vaid, and N. S. Lewis. Electrochemical and electrical behavior of (111)-oriented si surfaces alkoxylated through oxidative activation of si-h bonds. *Journal of Physical Chemistry B*, 104(43):9947–9950, 2000. Times Cited: 36.

[235] J. A. Haber and N. S. Lewis. Infrared and x-ray photoelectron spectroscopic studies of the reactions of hydrogen-terminated crystalline si(111) and si(100) surfaces with br-2, i-2, and ferrocenium in alcohol solvents. *Journal of Physical Chemistry B*, 106(14):3639–3656, 2002. Times Cited: 51.

[236] P. E. Laibinis, C. D. Bain, and G. M. Whitesides. *Journal of Physical Chemistry*, 95:7017–7021, 1991.

[237] B. J. Tufts, Amit Kumar, A. Bansal, and N. S. Lewis. *Journal of Physical Chemistry*, 96:4581, 1992.

[238] R. Basu, C. R. Kinser, J. D. Tovar, and M. C. Hersam. Bromine functionalized molecular adlayers on hydrogen passivated silicon surfaces. *Chemical Physics*, 326(1):144–150, 2006. Times Cited: 14.

[239] Ian C. Stewart, Christopher J. Douglas, and Robert H. Grubbs. Increased efficiency in cross-metathesis reactions of sterically hindered olefins. *Organic Letters*, 10(3):441–444, 2008. Times Cited: 55.

[240] Ian C. Stewart, Benjamin K. Keitz, Kevin M. Kuhn, Renee M. Thomas, and Robert H. Grubbs. Nonproductive events in ring-closing metathesis using ruthenium catalysts. *Journal of the American Chemical Society*, 132(25):8534–+, 2010. Times Cited: 10.

[241] P. B. Gansle, B. C. Gruber, J. T. Jarvis, A. Slaitas, S. M. DeJesus, and K. DeJesus. The selective monohalogenation of dihydro- and trihydrosilanes. *Microchemical Journal*, 55(2):222–234, 1997. Gansle, PB Gruber, BC Jarvis, JT Slaitas, A DeJesus, SM DeJesus, K.

[242] K. Tamao, T. Hayashi, and Y. Ito. Silicon-carbon bond-cleavage of pentacoordinate anionic silicates by n-bromosuccinimide. *Bulletin De La Societe Chimique De France*, 132(5-6):556–558, 1995. TAMAO, K HAYASHI, T ITO, Y.

[243] L. Hevesi, M. Dehon, R. Crutzen, and A. LazarescuGrigore. Kinetic control in the cleavage of unsymmetrical disilanes. *Journal of Organic Chemistry*, 62(7):2011–2017, 1997. Times Cited: 6.

[244] W. C. Still. Conjugate addition of trimethylsilyllithium - preparation of 3-silyl ketones. *Journal of Organic Chemistry*, 41(18):3063–3064, 1976. Times Cited: 209.

[245] W. C. Still and A. Mitra. 1,2 and 1,4 addition of group-iva anions to 2-cyclohexenones - kinetic and thermodynamic product control. *Tetrahedron Letters*, (30):2659–2662, 1978. Times Cited: 57.

[246] A. J. Bard and L. R. Faulkner. *Electrochemical methods: fundamentals and applications*. John Wiley & Sons, Inc., New York, 2nd edition, 2001.

[247] A. J. Nozik and R. Memming. *Journal of Physical Chemistry*, 100:13061–13078, 1996.

[248] Y. Xu and M. A. A. Schoonen. *American Mineralogy*, 85:543–556, 2000.

[249] M. X. Tan, P. E. Laibinis, SonBinh T. Nguyen, J. M. Kesselman, C. E. Stanton, and N. S. Lewis. *Progress in Inorganic Chemistry*, 41:21–144, 1994.

[250] T. W. Hamann, F. Gstrein, B. S. Brunschwig, and N. S. Lewis. *Chemical Physics*, 326:15–23, 2006.

[251] S. R. Morrison. *Electrochemistry at Semiconductor and Oxidized Metal Electrodes*. Plenum Press, New York, 1980.

[252] H. Gerischer. *Electrochimica Acta*, 34:1005–1009, 1989.

[253] M. J. Madou, B. H. Loo, K. W. Frese, and S. R. Morrison. *Surface Science*, 108:135–152, 1981.

[254] Y. Nakato, T. Ueda, Y. Egi, and H. Tsubomura. *Journal of the Electrochemical Society*, 134: 353–358, 1987.

[255] G. Schlichthorl and L. M. Peter. *Journal of the Electrochemical Society*, 141:L171–L173, 1994.

[256] E. J. Faber, W. Sparreboom, W. Groenveld, L. C. de Smet, J. Bomer, W. Olthuis, H. Zuilhof, E. J. R. Sudholter, P. Bergveld, and A van der Berg. *ChemPhysChem*, 8:101–112, 2007.

[257] D. A. Sverjensky. *Geochim. Cosmochim. Ac.*, 69:225–257, 2005.

[258] J. A. Schwarz, C. T. Driscoll, and A. K. Bhanot. *Journal of Colloid and Interface Science*, 97: 55–61, 1984.

[259] D. Aureau, J. Rappich, A. Moraillon, P. Allongue, F. Ozanam, and J.-N. Chazalviel. *Journal of Electroanalytical Chemistry*, 646(33-42), 2010.

[260] A. Aliano, Y. Li, G. Cicero, and G. Galli. *Journal of Physical Chemistry C*, 114:11898–11902, 2010.

[261] Y. Li and G. Galli. *Physical Review B*, 82:045321, 2010.

[262] L. Hedin. *Physical Review*, 139:A796–A823, 1965.

[263] P. Giannozzi and other. *Journal of Physics-Condensed Matter*, 21:395502, 2009.

[264] M. J. Frisch. *Gaussian 09 Revision A.1.* Gaussian Inc., Wallingford, CT, 2009.

[265] X. Gonze. *Comput. Mater. Sci.*, 25:478–492, 2002.

[266] R. W. Godby and R. J. Needs. *Physical Review Letters*, 62:1169–1172, 1989.

[267] Y. Li, D. Lu, H.-V. Nguyen, and G. Galli. *Journal of Physical Chemistry A*, 114:1944–1952, 2010.

[268] P. T. Hurley, E. J. Nemanick, B. S. Brunschwig, and N. S. Lewis. Covalent attachment of acetylene and methylacetylene functionality to si(111) surfaces: Scaffolds for organic surface functionalization while retaining si-c passivation of si(111) surface sites. *Journal of the American Chemical Society*, 128(31):9990–9991, 2006. Times Cited: 36.

[269] Dipole moments. In W. M. Haynes, editor, *Handbook of Chemistry and Physics*. CRC Press/Taylor and Francis, Boca Raton, FL, 92nd edition, 2012.

[270] Y. Niide and M. Hayashi. *Journal of Molecular Spectroscopy*, 216:52–60, 2002.

[271] B. M. Kayes, H. A. Atwater, and N. S. Lewis. Comparison of the device physics principles of planar and radial p-n junction nanorod solar cells. *Journal of Applied Physics*, 97(11), 2005. Times Cited: 128.

[272] Brendan M. Kayes, Michael A. Filler, Morgan C. Putnam, Michael D. Kelzenberg, Nathan S. Lewis, and Harry A. Atwater. Growth of vertically aligned si wire arrays over large areas (¿ 1 cm(2)) with au and cu catalysts. *Applied Physics Letters*, 91(10), 2007. Times Cited: 73.

[273] K. E. Plass, Michael A. Filler, Joshua M. Spurgeon, Brendan M. Kayes, Stephen Maldonado, Bruce S. Brunschwig, Harry A. Atwater, and Nathan S. Lewis. Flexible polymer-embedded si wire arrays. *Advanced Materials*, 21:325–328, 2009.

[274] Shannon W. Boettcher, Joshua M. Spurgeon, Morgan C. Putnam, Emily L. Warren, Daniel B. Turner-Evans, Michael D. Kelzenberg, James R. Maiolo, Harry A. Atwater, and Nathan S. Lewis. Energy-conversion properties of vapor-liquid-solid-grown silicon wire-array photocathodes. *Science*, 327(5962):185–187, 2010. Times Cited: 86.

[275] Michael D. Kelzenberg, Daniel B. Turner-Evans, Morgan C. Putnam, Shannon W. Boettcher, Ryan M. Briggs, Jae Y. Baek, Nathan S. Lewis, and Harry A. Atwater. High-performance si microwire photovoltaics. *Energy & Environmental Science*, 4:866–871, 2011.

[276] Morgan C. Putnam, Shannon W. Boettcher, Michael D. Kelzenberg, Daniel B. Turner-Evans, Joshua M. Spurgeon, Emily L. Warren, Ryan M. Briggs, Nathan S. Lewis, and Harry A. Atwater. Si microwire-array solar cells. *Energy & Environmental Science*, 3:1037–1041, 2010.

[277] Clara J. Cho, Leslie E. O'Leary, Nathan S. Lewis, and J. R. Greer. Interfacial strength of chemically functionalized si microwires in flexible solar cells as revealed by in-situ nano-mecahnical testing. *submitted*, 2012.

[278] C. Hsueh. *Materials Science and Engineering: A*, 123:1–11, 1990.

[279] M. Piggott. *Composites science and Technology*, 42:57–76, 1991.

[280] M. Piggott. *Load Bearing Fiber Composites*. 2002.

[281] J.-Y. Kim and J. R. Greer. *Acta Materialia*, 57:5245–5253, 2009.

[282] T. Wang, A. B. Dalton, and J. L. Keddie. *Macromolecules*, 41:7656–7661, 2008.

[283] H. Cox. *British Journal of Applied Physics*, 3:72, 1952.

[284] D. B. Migas and V. E. Borisenko. *Journal of Applied Physics*, 105:104316, 2009.

[285] V. Schmidt, J. V. Wittemann, and U. Goesele. Growth, thermodynamics, and electrical properties of silicon nanowires. *Chemical Reviews*, 110(1):361–388, 2010. Times Cited: 46.

[286] N. Y. Kim and P. E. Laibinis. Improved polypyrrole/silicon junctions by surfacial modification of hydrogen-terminated silicon using organolithium reagents. *Journal of the American Chemical Society*, 121:7162–7163, 1999.

[287] I. E. Vermeir, N. Y. Kim, and P. E. Laibinis. Electrical properties of covalently linked silicon/polypyrrole junctions. *Applied Physics Letters*, 74:3860–3862, 1999.

[288] J. Price, Michelle, Justin M. Foley, Robert A. May, and Stephen Maldonado. Comparison of majority carrier charge transfer velocities at si/polymer and si/metal photovoltaic heterojunctions. *Applied Physics Letters*, 97:083503, 2010.

[289] J. H. Song and M. J. Sailor. Reaction of photoluminescent porous silicon surfaces with lithium reagents to form silicon-carbon bound surface species. *Inorganic Chemistry*, 38:1498–1503, 1999.

[290] Michael G. Walter, X. L. Liu, Leslie E. O'Leary, Bruce S. Brunschwig, and Nathan S. Lewis. Conductive polymer (pedot) contacts on n-, p-, and n+-si: The effects of polymer solvent treatment and silicon surface functionalization on the electronic and photovoltaic junction behavior. *In preparation*, 2012.